U.PORTO

FEUP FACULDADE DE ENGENHARIA
UNIVERSIDADE DO PORTO

EXPERIMENTAL STUDY OF LOCAL SCOUR AROUND COMPLEX BRIDGE PIERS

MARIO ENRIQUE MORENO CASTIBLANCO

Thesis submitted for the fulfilment of the requirements for the degree of

Doctoral Program in Civil Engineering

Supervisor: Professor Doctor Rodrigo Jorge Fonseca de Oliveira Maia

---

Co-Supervisor: Doctor Lúcia Teixeira Couto

JULY 2016

ACKNOWLEDGEMENTS

Since I started working as an undergraduate student in the area of water resources and hydraulics at Los Andes University in Colombia 14 years ago, I decided that the ultimate goal of my educational process should be to pursue a Ph.D. in Civil Engineering. This document includes the results of the Ph.D. research project that I conducted during the last six years in Portugal. This period of time was some of the richest and most exciting years of my life. In this big journey, literally from South America to Europe, I met many people with whom I learned a lot and who I will never forget. The following lines are dedicated to thank the ones that in one way or another contributed to my stay in Portugal as well as in the completion of this research.

First I would like to thank my supervisors, Professor Rodrigo Maia and Dr. Lúcia Couto, for their unconditional support and encouragement throughout my research work. I must also acknowledge all their availability, dedication, guidance and feedback on the papers, for conferences and journals, which we co-authored with other colleagues during my Ph.D. studies. I also appreciate their availability in reviewing this document. I also thank Professor Maia for his guidance and supervision of the tests performed at the hydraulics laboratory of the Faculty of Engineering of the University of Porto (FEUP). I appreciate the discussion moments we have about the political and economic situation of Colombia and the success of soccer Colombian players in the Porto team. Chiefly, I cherish the friendship that has grown among us through these years. I want to thank his for providing comfortable conditions at FEUP during the last two years of my Ph.D. studies. I also owe a debt of gratitude to Mrs. Lúcia, for her constant support, great advice and comments, direction and assistance during the performance of the experimental campaign performed at the National Laboratory for Civil Engineering (LNEC). I appreciate her experience in physical modelling of hydraulic structures as it allowed discussing and decision making regarding the experimental results obtained in this research. I want to thank her specially for providing all necessary conditions at LNEC so I could work comfortably during the first four years of my Ph.D. studies. She definitely played a very important role in my adaptation to this new country (*e.g.* culture, customs and food). Sometimes, her personal advice, recommendations and protective attitude reminded me of my mom.

I would also like to thank my committee members, professor Vitor Abrantes Almeida, professor Francesco Ballio, professor António H. Cardoso, professor Fernando Veloso Gomes and professor Francisco Taveira Pinto for serving as my committee members. I also want to thank you for letting my defence be an enjoyable moment, and for your brilliant comments and suggestions, thanks to you.

I also met other inspiring people working as part of the research project denominated "Experimental study of local scour at complex bridge piers" with which I had the pleasure to participate in enriching discussions as well as had their valuable feedback on my own research project. I also want to thank Professors João P. Pêgo, Cristina Fael and Rui Lança, senior researcher João Rocha and also to the consultants Roger Bettess, Juan P. Martín-Vide, Roberto Gaudio and Luís Texeira; each one, in their own way, helped me to pursue and to refine my research goals. I am grateful for all the discussion to clarify the physics underlying scouring process at bridge piers. I also would like to thank João Manuel and his team for the adequacy and preparation of the experimental facility at LNEC, as well as António Muralha for the help in some measurements of tests performed at LNEC. I am also grateful to students Luís Brito and Pedro Ramos for assisting me with the test measurements carried out at FEUP; and to Cristina Silva for the continuous support in the affairs of the university.

During the four years that I was at LNEC, I had the opportunity and pleasure to meet other researchers that made my experience even more enriching. I want to thank my colleagues of the Department of

Hydraulics and Environment Teresa Viseu, Elsa Alves, Ana Estela Barbosa, José Melo, Leandro Valente, Mateus Mendoça, Natália Lopes, João Fernandes, Sílvia Amaral, Rute Viera, Gonçalo Jesus, Adelaide Gonçalves, Ricardo Rossato, Fernando Pereira, Pedro Massa, Ana Mendoça, Diogo Neves, Lourenço Sasseti, Paula García, Ricardo Jónatas, João Rogeiro, João Gomes, João Pedro, Inês Reis and Jorge Gadelho for welcoming a foreigner. I will always remember the interesting discussions we usually had at lunch time as well as the meetings and activities outside of LNEC with some of you.

I acknowledge those days I worked in the same office at LNEC with Ricardo, my first Italian friend. I want to thank him for all the good moments we spent together and to introduce me to his friends, Italians of course, who are now my new friends. During the four years that I was in Lisbon I met a little more than 200 Italians that I hope to see again in Italy or anywhere in the world. I would like to express my special appreciation to my Italian housemates Federico, Chiara, Silvia, Beatrice, Giorgio, Ylenia, Consuelo and Teo for their friendship and support in my Ph.D. I will always remember the good dinners at our house as well as at Ti Natércia restaurant - Tina thanks for being my favourite chef. I also regard the many visits of Lavinia. Besides, I want to thank them for the good times both in Portugal and in Italy. Grazie mille amici!

In life, it is always good to find people with similar interests; Ruben Silva "my new brother" is one of them. Besides sharing a house during my first year in Lisbon we both are sports fans. I remember the good times when we attended to different sport competitions in Portugal (*e.g.*, MotoGP race, Le Mans Series race, Tennis tournament, Surf championship, Cycling race) and of course a lot of soccer matches at different stadiums of the country (supporting Porto, Benfica, Sporting and the National team). I will never forget our big trip to Barcelona to celebrate the fifth Champions League won by the Barcelona team as well as our weekend trips to explore amazing places found in Portugal. I would like to express my special appreciation to him for his friendship during these six years and I am very grateful for letting me share four Christmas with his family. Até breve meu caro amigo!

It was a pleasure to meet other Ph.D. students in Portugal with whom I could share experiences and support to finish my thesis. I want to thank Ana Ricardo, Helena Nogeira, Sebastián Guillén and David Ferrás for his friendship and advice. I want to thank my compatriot Diana Díaz by ringing a visit to Lisbon and for the good times we had together at December of 2013. I also want to thank my old Colombian friends Jenny, Susana, Santana, Chicho and Gustavo for their continuous support.

I would also like to express my sincere gratitude to my two mentors at Los Andes University, Professors Juan Saldarriaga and José "Pepe" Rengifo, for the unconditional support in my academic and research activities in Colombia: they were the ones that encouraged me to make this journey. I owe Juan a debt of gratitude for motivating me as well as providing an immense knowledge that was conveyed to me when we worked together for nine years at the Aqueduct and Sewage Research Centre at the Universidad de Los Andes. A special thanks to Pepe, who I consider my grandfather, for his enthusiasm, motivation, patience and advice during the last fourteen years of my life.

Por último, quiero dedicar esta tesis a mi familia, lo más valioso de mi vida! Mis padres, Mario y Elvira, merecen una mención especial por su inseparable apoyo, paciencia y amor. Les transmito un reconocimiento especial a mi hermano, Maicol, y su señora, Maritza, por su continuo apoyo. Me gustaría agradecer inmensamente el apoyo amoroso de mis encantadoras sobrinas, a pesar de la distancia, Mabelita, la más bella violinista, y Manuelita, loquilla preciosa. También agradezco a mis otros dos hermanos, Maher y Marlon, por su continuo ánimo y apoyo. Agradezco inmensamente los buenos deseos de mis abuelos, tíos, primos y demás familiares.

This research was supported by the Portuguese Foundation for Science and Technology with the research grant SFRH/BD/76396/2011 and the research project PTDC/ECM/101353/2008.

ABSTRACT

Due to physical, geotechnical and economic considerations, bridges are frequently built with foundations of complex geometries. Currently, two types of pier-foundations are used in new large-span bridges: (1) common complex piers (also named as pile-supported piers), which consist of a column founded on a pile cap supported by an array of piles; and (2) special complex piers, which are characterized by non-conventional column and pile-cap geometries (*e.g.*, pile-supported piers with multi-columns). In this study, the term "complex piers" applies to pier geometries characterized by a column founded on a pile cap supported by an array of piles.

Local scour is a complex phenomenon involving three-dimensional flow structures, typically developed around piers and bridge abutments founded in movable bed rivers. Local scour can lead to partial failure or to collapse of bridge piers and decks. The cost of large bridges, with common and/or special complex piers, justifies carrying out an accurate prediction of scour depth, for both economic and safety reasons, which in turn leads to the interest of hydraulic engineers in predicting the equilibrium scour depth at complex piers. However, it is known that, despite the studies conducted in the past for pile-supported piers, the scour predictors do not reproduce adequately the measured scour values, as suggested by Ferraro *et al*. (2013). This derives from the fact that there are many factors influencing the phenomenon. Presently, three methods to predict equilibrium scour depth at complex piers can be considered as consolidated: the Auckland method (Coleman, 2005), the FDOT method (Sheppard and Renna, 2010) and the HEC-18 method (Arneson *et al*., 2012).

The present study develops an extensive research to systematically map equilibrium scour at complex piers and relate the observations with the characteristic variables of the tests. A total of eighty-four long-duration tests with seven complex pier models, aligned with the approach flow under clear-water flow conditions, were performed. Six of the complex piers models were analysed at the flume of the Hydraulics and Environment Department, National Laboratory for Civil Engineering (LNEC) while the remaining one was evaluated at the flume of the Faculty of Engineering of the University of Porto (FEUP).

Forty-eight out of the total number of tests were used to quantify the influence of the complex-pier position and geometry on the scour depth time evolution. The following combined effects were analysed: (1) the relative column width, D_c/D_{pc} ($D_c =$ column width; $D_{pc} =$ pile-cap width), and the relative pile-cap position, H_c/h ($H_c =$ distance from the initial bed level to the top surface of the pile cap; $h =$ approach flow depth); (2) the relative pile-cap thickness, T/h ($T =$ pile-cap thickness), and H_c/h; and (3) the pile-group configuration (characterized by the number of alignments in the group, n) and H_c/h. The experimental results were classified according to three pile-cap situations: (i) Situation 1, characterized by the bottom of the pile cap being above the initial bed level; (ii) Situation 2, characterized by the pile cap being partially buried in the initial bed configuration; and (iii) Situation 3, characterized by the pile cap being initially completely buried in the bed. The common criterion to stop experimental tests on complex piers was analysed, and a new criterion was introduced. In these forty-eight tests, the equilibrium scour depth was calculated by extrapolation of data series. The results are used to evaluate the three specified influences (D_c/D_{pc} and H_c/h; T/h and H_c/h; n and H_c/h) on the equilibrium scour depth for the three mentioned situations. The analysis includes the definition of the pile-cap position at which the maximum equilibrium scour depth occurs.

Some of the methods most commonly used to predict equilibrium scour depth around complex piers are based on tests carried out, separately, for their individual components: the column, the pile cap and the pile group. In some of those methods, the scour depth at complex piers is estimated by adding the

contributions of the isolated components, ignoring the non-linear interaction between them. In the present study, a new, physically sounder approach to experimentally assess the contribution of complex piers' components to scouring is presented and discussed. The new approach takes into account the interactions of the different aspects of the flow field and their impact on the local scour depth. Seventy out of the total number of tests performed in this study were used to estimate the complex pier components' contributions on equilibrium scour depth according to the new approach. Results showed that the contribution of each component is highly dependent on its position (relative to the initial bed level), and also depends on: (1) D_c/D_{pc}; (2) T/h; and (3) f_c/D_p ($f_c =$ longitudinal extension of the pile cap out from the upstream pile front; $D_p =$ pile width). A comparison of the results of this approach with the corresponding contributions based on tests with isolated components was also performed.

Finally, forty-eight out of the total number of tests carried out in this study were used to evaluate the performance of the three mentioned predictors, concluding that: (1) the Auckland predictor gives more acceptable values of equilibrium scour depth; (2) the FDOT predictor gives conservative values of the equilibrium scour depth; and (3) the HEC-18 predictor systematically tends to underestimate equilibrium scour depth values. Based on the experimental results of the present study and on the conceptual approaches of Auckland and FDOT methods, an alternative formulation for a predictor of equilibrium scour depth at complex piers is suggested and validated. This new formulation performed better than the other three methods (in terms of accuracy).

KEYWORDS

Local scour, complex pier, bridge foundations, equilibrium scour depth, laboratory tests.

RESUMO

Considerações de ordem física, geotécnica e económica têm levado a que, cada vez mais, as fundações de pontes sejam construídas com geometrias complexas. Atualmente, dois tipos de pilar-fundação são usados nos novos projetos de grandes pontes: (1) pilares complexos comuns (igualmente designados por pilares suportados por estacas), constituídos por uma coluna fundada em um maciço de encabeçamento e suportado por um grupo de estacas; e (2) pilares complexos especiais, que são caracterizados por geometrias não convencionais do pilar e do maciço de encabeçamento. Em este estudo, o termo "pilares complexos" aplica-se a geometrias constituídas por colunas fundadas em maciços de encabeçamento suportados por estacas.

As erosões localizadas podem ser entendidas como processos complexos associados a estruturas tridimensionais do escoamento que se observam junto de obstruções ao mesmo. De entre essas obstruções destaca-se os pilares (simples ou complexos) ou encontros de pontes, atentas as correspondentes erosões localizadas, que podem conduzir à rotura parcial ou ao colapso de pontes. O custo de grandes pontes, com pilares complexos comuns e/ou especiais, justifica uma previsão rigorosa das profundidades de erosão, tanto por razões económicas como de segurança. Porém, é sabido que, apesar dos numerosos estudos conduzidos no passado, ainda não se atingiu sucesso pleno nas propostas e métodos para prever a profundidade máxima das cavidades de erosão, como sugere Ferraro *et al*. (2013). Nos últimos anos têm vindo a ser considerados, como referência, três métodos de previsão da profundidade de equilíbrio desenvolvida junto de pilares complexos: método de Auckland (Coleman, 2005), método do FDOT (Sheppard and Renna, 2010) e método do HEC-18 (Arneson *et al*., 2012).

O presente estudo apresenta uma extensa campanha experimental que caracteriza sistematicamente as profundidades de equilíbrio da cavidade de erosão em pilares complexos, relacionando as observações com as variáveis características dos ensaios. Um total de oitenta e quatro ensaios de longa duração foi realizado com sete modelos de pilares complexos, alinhados com o escoamento de aproximação em condições de escoamento sem transporte sólido generalizado. Seis dos modelos de pilares complexos foram analisados no canal do Departamento de Hidráulica e Ambiente, Laboratório Nacional de Engenharia Civil (LNEC) enquanto o restante modelo foi analisado no canal da Faculdade de Engenharia da Universidade do Porto (FEUP).

Quarenta e oito do número total de ensaios realizados neste estudo foram usados para quantificar a influência da posição e geometria do pilar complexo na evolução temporal da profundidade de erosão. Os seguintes efeitos combinados foram analisados: (1) a largura relativa da coluna, D_c/D_{pc} ($D_c =$ largura da coluna; $D_{pc} =$ largura do maciço), e a posição relativa do maciço, H_c/h ($H_c =$ distância desde o nível inicial do leito à parte superior do maciço; $h =$ profundidade do escoamento de aproximação); (2) a espessura relativa do maciço, T/h ($T =$ espessura do maciço), e H_c/h; e (3) a configuração do grupo de estacas (caracterizada pelo número de alinhamentos no grupo, n) e H_c/h. Os resultados experimentais foram enquadráveis em três situações tipificadas: (i) Situação 1, caracterizada pelo facto de o maciço estar acima do nível inicial do leito; (ii) Situação 2, caracterizada pelo facto de o maciço se encontrar parcialmente enterrado no leito inicial; e (iii) Situação 3, caracterizada pelo facto de o maciço estar completamente enterrado no leito inicial. Os ensaios conduzidos permitiram também avaliar o critério comumente usado para estimar o tempo de duração adequado para pilares complexos. Foi introduzido um critério para finalizar os ensaios de pilares complexos. Nestes quarenta e oito ensaios, as profundidades de equilíbrio da cavidade de erosão foram calculadas por extrapolação de cada uma das séries de dados. Os resultados são utilizados para avaliar

as três referidas influências (D_c/D_{pc} e H_c/h; T/h e H_c/h; n e H_c/h) nas profundidades de erosão de equilíbrio para as três situações mencionadas. A análise inclui a definição da posição do maciço em que ocorre a máxima profundidade de erosão de equilíbrio.

Alguns dos métodos consolidados para prever a profundidade de erosão de equilíbrio juto de pilares complexos foram desenvolvidos com base em diferentes tipos de ensaios experimentais, entre os quais se destacam, ensaios com colunas suspensas no escoamento, ensaios com maciços de encabeçamento suspensos no escoamento e ensaios com grupos de estacas submersos. Em alguns desses métodos, as profundidades de erosão individuais de cada componente podem somar-se para obter a previsão da profundidade de erosão da estrutura completa, ignorando a interação não-linear entre elas. No presente estudo, uma nova abordagem, fisicamente mais sólida, para avaliar a contribuição dos diferentes componentes estruturais do pilar complexo na profundidade máxima de erosão é apresentada e discutida. De acordo com a nova abordagem, a profundidade de erosão em um determinado componente é calculada subtraindo a profundidade de erosão em dois componentes do pilar contíguos da profundidade de erosão no correspondente pilar complexo completo, mantendo desta forma as interações predominantes. Setenta do número total de ensaios realizados neste estudo foram utilizados para estimar as contribuições das componentes do pilar complexo na profundidade de erosão de equilíbrio de acordo com a nova abordagem. Os resultados mostraram que a contribuição de cada componente é altamente dependente da sua posição (em relação ao nível do leito inicial), e também depende de: (1) D_c/D_{pc}; (2) T/h; e (3) f_c/D_p (f_c = extensão longitudinal do maciço para fora a partir da frente da estaca de montante; D_p = largura da estaca). Foi também realizada uma comparação dos resultados desta abordagem com as correspondentes contribuições baseadas em ensaios com componentes isolados.

Finalmente, quarenta e oito do número total de ensaios realizados neste estudo foram utilizados para avaliar o desempenho dos três modelos de previsão antes mencionados, concluindo que: (1) o método de Auckland fornece uma aceitável estimativa da profundidade de erosão de equilíbrio; (2) o método do FDOT fornece previsões conservadoras da profundidade de erosão de equilíbrio; e (3) o método do HEC-18 fornece sistematicamente subestimação dos valores da profundidade de erosão de equilíbrio. Com base nos resultados experimentais do presente estudo e nas abordagens conceptuais dos métodos de Auckland e do FDOT, uma formulação alternativa para prever a profundidade de erosão de equilíbrio em pilares complexos é sugerida e validada. Esta nova formulação de previsão tem um desempenho melhor do que os outros três métodos analisados.

PALAVRAS-CHAVE

Erosão localizada, pilares complexos, fundações de pontes, profundidade de erosão de equilíbrio, ensaios laboratoriais.

TABLE OF CONTENTS

1. INTRODUCTION 1

1.1. BACKGROUND 1
1.2. OBJECTIVES 4
1.3. LIST OF PUBLICATIONS WITH RESULTS FROM THE PRESENT STUDY 5
1.4. THESIS STRUCTURE 6

2. LITERATURE REVIEW 9

2.1. INTRODUCTION 9
2.2. LOCAL SCOUR AROUND SINGLE PIERS 10
2.2.1 Flow structure 10
2.2.2 Dimensional analysis 13
2.2.3 Time evolution of scour depth 15
2.2.4 Equilibrium scour depth in laboratory tests 18
2.2.5 Effects of specific parameters on maximum local scour depth 19
2.2.6 Methods for estimation of local scour depths 27
2.3. LOCAL SCOUR AROUND COMPLEX PIERS 31
2.3.1 Flow structure 31
2.3.2 Dimensional analysis 33
2.3.3 Time evolution of scour depth 35
2.3.4 Equilibrium scour depth in laboratory tests 38
2.3.5 Effects of specific parameters on maximum local scour depth 38
2.3.6 Methods for estimation of local scour depths 45

3. EXPERIMENTAL SETUP 59

3.1. INTRODUCTION 59
3.2. EXPERIMENTAL CAMPAIGN 60
3.2.1 Complex pier models 60
3.2.2 Experimental conditions 61
3.2.3 Tests 62
3.3. LNEC'S FLUME 64
3.3.1 Hydraulic circuit 64
3.3.2 Tilting Flume 66
3.4. FEUP'S FLUME 67
3.5. EXPERIMENTAL PROCEDURES 69
3.5.1 Complex piers preparation and fixation 69
3.5.2 Preparation of the sand bed 70
3.5.3 Flow-discharge and flow-depth stabilization 71
3.5.4 Scour depth measurement 72
3.5.5 End of the experiment 73

4. TEMPORAL EVOLUTION OF THE SCOUR DEPTH AT COMPLEX PIERS 75

4.1. INTRODUCTION 75
4.2. SCOUR DEPTH TIME EVOLUTION IN TESTS WITH MODELS 1 TO 6 (LNEC'S MODELS) 76
4.2.1 General approach 76

4.2.2 Influence of relative column width and position 78
4.2.3 Influence of pile-cap thickness and position 81
4.2.4 Maximum scour depths 84
4.3. SCOUR DEPTH TIME EVOLUTION IN TESTS WITH MODEL 7 (FEUP'S MODEL) 85
4.3.1 Influence of the pile-cap position 85
4.3.2 Maximum scour depths 87
4.4. CRITERION TO STOP LABORATORY EXPERIMENTS 87
4.5. CONCLUSIONS 90

5. EFFECT OF COMPLEX PIER GEOMETRY ON EQUILIBRIUM SCOUR DEPTH 91

5.1. INTRODUCTION 91
5.2. EQUILIBRIUM SCOUR DEPTHS 92
5.3. COMBINED EFFECTS OF RELATIVE COLUMN WIDTH AND POSITION 93
5.4. COMBINED EFFECTS OF RELATIVE PILE-CAP THICKNESS AND RELATIVE COLUMN POSITION 97
5.5. EFFECT OF PILE-GROUP CONFIGURATION 98
5.6. COMPARISON OF THE PRESENT EXPERIMENTAL STUDY WITH RESULTS REPORTED IN LITERATURE 100
5.6.1 Assessment of experimental data 100
5.6.2 Comparison in Situation 1 102
5.6.3 Comparison in Situation 2 102
5.6.4 Comparison in Situation 3 104
5.7. CONCLUSIONS 105

6. COMPLEX PIER COMPONENTS CONTRIBUTIONS ON THE EQUILIBRIUM SCOUR DEPTH 107

6.1. INTRODUCTION 107
6.2. EXPERIMENTAL DATA PRESENTATION 110
6.3. TEMPORAL EVOLUTION OF THE SCOUR DEPTH (CONFIGURATIONS C2 AND C3) 111
6.4. CONTRIBUTIONS OF COMPLEX PIER COMPONENTS TO THE EQUILIBRIUM SCOUR DEPTH BY A SUBTRACTION APPROACH 113
6.5. COMPARISON OF SUBTRACTION AND SUPERPOSITION APPROACHES 118
6.5.1 Experimental data from studies with isolated components 118
6.5.2 Comparison of the contributions of complex pier components from both approaches 120
6.6. FURTHER DISCUSSION 123
6.7. CONCLUSIONS 124

7. PREDICTION OF EQUILIBRIUM SCOUR DEPTH AROUND COMPLEX PIERS 127

7.1. INTRODUCTION 127
7.2. APPLICABILITY OF AVAILABLE SCOUR DEPTH PREDICTORS 127
7.3. PROPOSAL OF A REVISED PREDICTOR 129
7.4. VALIDATION OF THE PROPOSED PREDICTOR 135
7.5. CONCLUSIONS 138

8. CONCLUSIONS AND FUTURE RESEARCH 139

8.1. CONCLUSIONS 139
8.1.1 General approach 139
8.1.2 Temporal evolution of the scour depth at complex piers 140
8.1.3 Effects of complex pier geometry on the equilibrium scour depth 140
8.1.4 Complex pier components contribution on the equilibrium scour depth 141

8.1.5 Prediction of equilibrium scour depth around complex piers 142
8.2. FUTURE RESEARCH 143
REFERENCES 145
APPENDIX: EXPERIMENTAL DATA 155

LIST OF FIGURES

Figure 1.1 – Ancient bridges in: (a) England, (b) China and (c) Italy 1

Figure 1.2 – (a) scheme of basic bridge structure and (b) photographs of common complex piers 2

Figure 1.3 – Examples of bridge failures in Portugal: (a) Penacova bridge, (b) EN122 bridge, (c) Gafanha bridge and (d) Hintze Ribeiro bridge (photos a to c by J. Rocha) 3

Figure 1.4 – Photographs of local scour experiments at (a) single piers (Sheppard, 2003), (b) pile groups (Lança, 2013) and (c) complex piers (Sousa, 2007) 4

Figure 2.1 – Streamline plots of the flow at various times, adapted from Unger and Hager (2007) 11

Figure 2.2 – (a) visualization of the vortex system inside the scour hole, adapted from Kirkil *et al*. (2008), (b) visualization of transverse section of the vorticity map, adapted from Nogueira *et al*. (2008) and (c) visualization of the horseshoe vortex system in a transversal section, adapted from Zhao and Huhe (2006) 11

Figure 2.3 – Visualization of wake vortices at downstream of the pier made by: (a) Rao *et al*. (2004), (b) Ettema *et al*. (2006), (c) Sadeque *et al*. (2008) and (d) Kirkil *et al*. (2008) 12

Figure 2.4 – Flow structure around cylindrical bridge piers 12

Figure 2.5 – Set of variables describing the scour process with influence in the scour depth at a single pier 13

Figure 2.6 – Evolution of scour depth with time under: (a) clear-water condition (adapted from Sheppard *et al*., 2004) and (b) live-bed condition (adapted from Sheppard and Miller, 2006) 16

Figure 2.7 – Phases of the scouring process under clear-water condition, adapted from Lança *et al*. (2010) 17

Figure 2.8 – Equilibrium scour depth as a function of velocity, for comparatively coarse uniform bed sediment 20

Figure 2.9 – Equilibrium scour depth as a function of the geometric standard deviation of sediment sizes for tests under: (a) clear-water conditions and (b) live-bed conditions 21

Figure 2.10 – Equilibrium scour depth as a function of bed material size 22

Figure 2.11 – The influence of flow shallowness on equilibrium scour depth 23

Figure 2.12 – Equilibrium scour depth as a function of the sediment Reynolds number 24

Figure 2.13 – Scour holes around different pier shapes: (a) cylindrical pier (adapted from Rey and Raikar, 2007) and (b) square pier (adapted from Raikar and Dey, 2008) 25

Figure 2.14 – Shape factor (K_S) as a function of L/D for: (a) rectangular piers, (b) rectangular round-nose or oblong piers, (c) lenticular piers and (b) elliptic piers 25

Figure 2.15 – Schemes of the scour hole in relation with the pier alignment angle 26

Figure 2.16 – Diagrams of scour hole around rectangular piers oriented in different angles to flow direction 26

Figure 2.17 – Local scour depth variation with pier alignment (rectangular piers) 27

Figure 2.18 – Scheme of flow structure and local scour around pile groups 32

Figure 2.19 – Flow structure around: (a) a rectangular debris cluster (adapted from Pagliara and Carnacina 2011) and (b) pier with caisson (adapted from Veerappadevaru *et al*. 2011) 32

Figure 2.20 – Scheme of the flow structure around complex piers 33

Figure 2.21 – Scheme of complex pier geometry 34

Figure 2.22 – Complex pier situations as a function of the relative pile-cap position 35

Figure 2.23 – Temporal evolution of scour depth at pile groups, adapted from Lança *et al*. (2013a) 36

Figure 2.24 – Temporal variation of scour depth at complex piers in position (3), adapted from Sousa (2007) 36

Figure 2.25 – Scour depth time evolution at complex piers in position (4), adapted from Ferraro *et al*. (2013) 37

Figure 2.26 – Scour depth time evolution at complex piers in position (6), adapted from Ferraro *et al*. (2013) 37

Figure 2.27 – Dimensions of complex pier models used in the five studies from literature 39

Figure 2.28 – Scour depth as function of the relative column position 41

Figure 2.29 – Effect of the relative column width on scour depth as function of the relative column position, based on Melville and Raudkivi (1996) data 42

Figure 2.30 – Effect of the pile-cap thickness on scour depth: (a) complex pier models and (b) scour depth variation as function of the relative column position, adapted from Ferraro *et al*. (2013) 43

Figure 2.31 – Effect of the relative pile spacing on the relative scour depth for pile groups with: (a) a single row (m = 1) and (b) a single column (n = 1) 44

Figure 2.32 – (a) variation of d_{spg}/d_s with S_p/D_p and θ, adapted from Lança *et al*. (2013a) and (b) system of wake vortices at an alignment of piles, adapted from Lança *et al*. (2012) 45

Figure 2.33 – Conceptual variation of equivalent diameter with column position, adapted from Coleman (2005) 46

Figure 2.34 – Conceptual hypothesis for superimposing scour components, adapted from Jones and Sheppard (2000a) 47

Figure 2.35 – Projected width of piles, adapted from Richardson and Davis (2001) 50

Figure 2.36 – Conceptual hypothesis of summing equivalent diameters, adapted from Sheppard and Renna (2010) 51

Figure 3.1 – Dimensions of complex pier models analysed at (units in millimetres): (a) LNEC's flume and (b) FEUP's flume 59

Figure 3.2 – Complex pier configurations 60

Figure 3.3 – Grading curve of the sand used in the experiments 61

Figure 3.4 – Scheme of the pile-cap positions associated with the study of the three typical situations for: (a) Models 1 and 4, (b) Models 2, 3 and 5, (c) Model 6 and (d) Model 7 63

Figure 3.5 – Scheme and photographs of LNEC's flume, based on the scheme by Cardoso (1982) 65

Figure 3.6 – Surge tank operation 66

Figure 3.7 – Scheme and photographs of the tilting flume 67

Figure 3.8 – Scheme of FEUP's flume 68

Figure 3.9 – Step 1 of the experimental procedure: (a) LNEC's flume and (b) FEUP's flume 70

Figure 3.10 – Step 2 of the experimental procedure: (a) LNEC's flume and (b) FEUP's flume 71

Figure 3.11 – Step 3 of the experimental procedure: (a) LNEC's flume and (b) FEUP's flume 72

Figure 3.12 – Step 4 of the experimental procedure: (a) LNEC's flume and (b) FEUP's flume 73

Figure 3.13 – Typical scour patterns at the end of the test: (a) LNEC's flume and (b) FEUP's flume 74

Figure 4.1 – Situation 1: (a) scheme of the temporal evolution of the scour depth (time on linear and logarithmic scales) and (b) photographs of scour hole evolution 76

Figure 4.2 – Situation 2: (a) scheme of the temporal evolution of the scour depth (time on linear and logarithmic scales) and (b) photographs of scour hole evolution 77

Figure 4.3 – Situation 3: (a) scheme of the temporal evolution of the scour depth (time on linear and logarithmic scales) and (b) photographs of scour hole evolution 77

Figure 4.4 – Influence of D_c/D_{pc} on the temporal evolution of the scour depth for Situation 1: (a) Positions A to D and (b) Position E 78

Figure 4.5 – Influence of D_c/D_{pc} on the temporal evolution of the scour depth for Situation 2 (pile cap slightly buried): (a) Position F and (b) Position G 79

Figure 4.6 – Influence of D_c/D_{pc} on the temporal evolution of the scour depth for Situation 2 (pile cap almost buried): (a) Position H and (b) Position I 80

Figure 4.7 – Photos of the scour hole evolution in test M5I1 80

Figure 4.8 – Influence of D_c/D_{pc} on the temporal evolution of the scour depth for Situation 3: (a) Position J and (b) Position K 81

Figure 4.9 – Influence of D_c/D_{pc} on the temporal evolution of the scour depth for Situation 3 (Position L) 81

Figure 4.10 – Influence of T/h on the temporal evolution of the scour depth for Situation 1: (a) Position D and (b) Position E 82

Figure 4.11 – Influence of T/h on the temporal evolution of the scour depth for Position F: (a) test in Situation 1 and (b) tests in Situation 2 83

Figure 4.12 – Influence of T/h on the temporal evolution of the scour depth for Situation 2: (a) Position G, (b) Position H and (c) Position I 83

Figure 4.13 – Influence of T/h on the temporal evolution of the scour depth for Situation 3 84

Figure 4.14 – Influence of the pile-cap elevation on the temporal evolution of the scour depth for: (a) Situation 1 (Positions M to O), (b) Situation 2 (Positions P to R) and (c) Situation 3 (Positions S and T) 86

Figure 4.15 – Experiment M2H1: (a) scour rate evolution and (b) temporal evolution of the scour depth 88

Figure 5.1 – Effect of the relative column width on the equilibrium scour depth as a function of the relative column position 94

Figure 5.2 – Interpretation of the flow structure in the cases in which the maximum equilibrium scour depth occurred (Situation 2) for: (a) Model 2, (b) Model 3 and (c) Model 5 95

Figure 5.3 – (a) Scheme with dimensions of Model Mu (Moreno *et al*., 2015a) (units in millimetres) and (b) equilibrium scour depth as a function of the relative column position observed with Models 5 and Mu 96

Figure 5.4 – Scour hole in test 4 with Model Mu (a) downstream scour hole and (b) lateral scour hole 97

Figure 5.5 – Effect of the relative pile-cap thickness on the equilibrium scour depth as a function of the relative column position for: (a) Models 4, 5 and 6 and (b) Models 1 and 2 97

Figure 5.6 –Equilibrium scour depth as a function of the relative column position for models with: (a) two alignments of piles (Model 3) and (b) one alignment of piles (Model 7) 99

Figure 5.7 – Scheme of (a) complex pier obstruction area (Model Fe1) and (b) equivalent obstruction width of the complex pier 101

Figure 5.8 – Effect of the relative pile-cap thickness on the relative maximum scour depth 102

Figure 5.9 – d_{sm}/D_{pc} as function of H_c/T for Situation 2: (a) rectangular pile-cap shape and (b) circular and rectangular round-nose pile-cap shapes 103

Figure 5.10 – Effect of the relative column width and column/pile-cap shapes on d_{sm}/d_{secu} as function of H_c/d_{secu} for Situation 3 105

Figure 6.1 – Scheme of the subtraction approach (contribution of the complex pier components on scour depth) 109

Figure 6.2 – Scour depth time evolution in tests with Model 3 for: (a) Configuration C2 and (b) Configuration C3 112

Figure 6.3 – Scour depth time evolution and final scour hole in Configurations C1, C2 and C3 for: (a) Model 4 (Position E) and (b) Model 7 (Position Q) 113

Figure 6.4 – Variation of factor K_{hc} with the relative position of the base of the column 115

Figure 6.5 – Variation of factor K_{hpg} with the relative position of the top of the pile group 116

Figure 6.6 – Variation of factor K_{hpc} with the relative position of the base of the pile cap: (a) Models 1 to 6 and (b) Model 7 117

Figure 6.7 – Scheme of the geometry of complex pier components 118

Figure 6.8 – Comparison of K_{hc} obtained through subtraction with K_{hc} obtained from tests with isolated columns 121

Figure 6.9 – Comparison of K_{hpc} obtained through subtraction with K_{hpc} obtained from tests with isolated pile caps: (a) $T/h \approx 0.30$, (b) $T/h \approx 0.45$ and (c) $T/h \approx 0.60$ 122

Figure 6.10 – Comparison of K_{hpg} obtained through subtraction with K_{hpg} obtained from tests with pile groups 122

Figure 6.11 – Comparison of factors K_{hc} , K_{hpc} and K_{hpg} obtained by the subtraction concept with the corresponding values predicted by FDOT and HEC-18 methods: (a) variation of factor K_{hc}; (b) variation of factor K_{hpc}; and (c) variation of factor K_{hpg} 124

Figure 7.1 – Comparison of observed and predicted equilibrium scour depths, for the methods of: (a) Auckland, (b) HEC-18 and (c) FDOT 128

Figure 7.2 – Conceptual variation of: (a) d_{se} with H_c and (b) D_e with H_c 131

Figure 7.3 – Longitudinal extension length of the pile cap out from the upstream piles front..... 133

Figure 7.4 – Predicted versus observed scour depths at complex piers by: (a) suggested formulation, (b) FDOT predictor, (c) Auckland predictor and (d) HEC-18 predictor 137

Figure 7.5 – Equilibrium scour depths as a function of column position with: (a) model by Grimaldi and Cardoso (2010) and (b) models by Ferraro *et al*. (2013)..... 138

LIST OF TABLES

Table 2.1 – Bed condition factors 30

Table 2.2 – Experimental models: flow parameters, bed granulometry parameters and duration of the tests 38

Table 3.1 – Geometric characteristics of the complex pier models of the experimental campaign 61

Table 3.2 – Designation of the tests performed with Configuration C1 (Models 1 to 6) 63

Table 3.3 – Designation of the tests performed with Configuration C2 (Models 1 to 6) 64

Table 3.4 – Designation of the tests performed with Configuration C3 (Models 1 to 6) 64

Table 3.5 – Designation of the tests performed with Model 7 64

Table 4.1 – Relative column position, test duration and maximum scour depth for Models 1 to 3 85

Table 4.2 – Relative column position, test duration and maximum scour depth for Models 4 to 6 85

Table 4.3 – Relative column position, test duration and maximum scour depth for Model 7 87

Table 4.4 – Relative column position, equivalent diameter of the complex pier, test duration and scour depth with 5% criterion for Models 1, 2 and 3 88

Table 4.5 – Relative column position, equivalent diameter of the complex pier, test duration and scour depth with 5% criterion for Models 4, 5 and 6 89

Table 4.6 – Relative column position, equivalent diameter of the complex pier, test duration and scour depth with 5% criterion for Model 7 89

Table 5.1 – Equilibrium scour depths (extrapolated values) with Models 1 to 6 93

Table 5.2 – Equilibrium scour depths (extrapolated values) with Model 7 93

Table 5.3 – Experimental models: flow parameters, model geometry parameters and test durations 100

Table 5.4 – Values of $(H_c/T)_{max}$ as function of relative column width 103

Table 6.1 – Relative column position, test duration, maximum and equilibrium scour depth values for tests with Configurations C2 and C3 110

Table 6.2 – Equilibrium scour depths of the reference tests 111

Table 6.3 – Equilibrium scour depths associated to each complex pier component 114

Table 6.4 – Characteristic control variables and non-dimensional parameters of studies on suspended columns 119

Table 6.5 – Characteristic control variables and non-dimensional parameters of studies on suspended pile caps 119

Table 6.6 – Characteristic control variables and non-dimensional parameters of studies on submerged pile groups 120

Table 7.1 – Control variables and non-dimensional parameters for specific pier foundations' studies 132

Table 7.2 – Control variables and non-dimensional parameters for single piers' studies with long-duration tests 136

Table 7.3 – Control variables and non-dimensional parameters for pile groups' studies with long-duration tests 136

LIST OF SYMBOLS

a_1, a_2 = parameters obtained by regression analysis;

B = channel width;

B' = constant of integration;

c_1, c_2, c_3 = parameters obtained by regression analysis;

D = pier width;

D_c = column width;

D_e = equivalent pier diameter;

D_{ec} = equivalent diameter of the column;

$D_{ec(\min)}$ = equivalent diameter of a single pier that lead to a scour depth equal to $|H_c|$;

D_{epc} = equivalent diameter of the pile cap;

D_{epg} = equivalent diameter of the pile group;

D_{e*} = maximum equivalent diameter of the complex pier;

D_p = pile width;

D_{pc} = pile-cap width;

D_{pc} = diameter of cylindrical foundation;

d_s = scour depth;

$d_{sc(\max)}$ = maximum column scour depth;

d_{scpc} = scour depth produced by the combination of the column and pile cap;

d_{se} = equilibrium scour depth;

d_{sec} = column contribution to the local scour depth;

d_{secu} = equilibrium scour depth for an uniform single pier with the same geometrical definition of the complex pier column;

d_{seC1} = equilibrium scour depth due to Configuration C1 of the complex pier;

d_{seC2} = equilibrium scour depth due to Configuration C2 of the complex pier;

d_{seC3} = equilibrium scour depth due to Configuration C3 of the complex pier;

d_{sepc} = pile cap contribution to the local scour depth;

d_{sepcu} = equilibrium scour depth for an uniform single pier with the same geometrical definition of the complex pier pile-cap;

d_{sepg} = pile group contribution to the local scour depth;

d_{sepgu} = equilibrium scour depth developed for a an unsubmerged pile group;

d_{sm} = maximum scour depth;

d_{sm} = scour depth measured at the end of the tests;

d_{smMS} = scour depth measured at time defined according to equation (4.1);

d_{sp} = scour depth at an individual pile in the same bed and approach flow conditions of the pile group;

$d_{spc(\max)}$ = maximum pile cap scour depth;

d_{spg} = maximum scour depth observed at pile group;

$d_{s5\%}$ = scour depth obtained by criterion of 5%;

d_1, d_2, d_3 = parameters obtained by regression analysis;

d_{16} = sediment size which 16% of sediment is finer;

d_{50} = median size of sediment particle size distribution;

d_{84} = sediment size which 84% of sediment is finer;

f = weighted average of the pile-cap front and side extensions beyond the column;

f_l = extension length of pile cap face out from column face;

f_p = longitudinal extension length of pile cap face out from the nearest pile front face;

f_t = extension width of pile cap face out from column face;

Fr = Froude number;

Fr_d = densimetric Froude number;

g = gravitational acceleration;

h = approach flow depth;

H_b = pile-cap position below the initial bed level at which occurs the minimum scour depth when the pile cap is completely buried in the bed;

H_c = column position (distance from the initial bed level to the bottom surface of the column);

$h_{c(\max)}$ = limiting water depth at which the flow influences the scouring process around the column;

$(H_c/T)_{\max}$ = pile-cap position at which the maximum equilibrium scour depth can be obtained;

H_d = dune height;

H_{pc} = pile-cap position (distance from the initial bed level to the bottom of the pile-cap);

$h_{pc(\max)}$ = limiting water depth at which the flow influences the scouring process around the pile cap;

H_{pg} = pile-group position (distance from the initial bed level to the top of the pile group);

$h_{pg(\max)}$ = limiting water depth at which the flow influences the scouring process around the pile group;

H_c^* = distance from the bed to the top of the footing after column scour component has been computed;

H_{pc}^* = distance between the bed and the bottom of the pile cap after column scour component has been computed;

H_{pg}^* = distance between the bed and the top of the pile group after pile cap scour component has

been computed;

H_x = pile-cap position at which occurs the maximum scour depth;

h_1 = adjusted flow depth for pile cap computations;

h_2 = adjusted flow depth for pile group computations;

K_A = pile group factor;

K_{bc} = correction factor for bed forms;

K_{bpc} = factor that accounts for the dependence of the pile-cap position on the scour hole;

K_{bpg} = buried pile group attenuation factor;

K_d = sediment coarseness factor;

K_f = pile cap extension factor;

K_g = factor describing the geometry of the channel cross-section;

K_{hc} = factor to account for the position of the bottom of the column relative to the initial bed level;

K_{hD} = flow depth-pier size factor;

K_{hD_e} = flow shallowness factor;

K_{hpc} = factor to account for the position of the bottom of the pile cap relative to the initial bed level;

K_{hpg} = factor to account for the position of the top of the pile group relative to the initial bed level;

K_I = flow intensity factor;

K_m = factor to account for the aligned rows;

k_s = height of grain roughness of the bed;

K_S = factor describing the shape of the pier;

K_{Sc} = column shape factor;

K_{sp} = pile spacing factor;

K_{Sp} = pile shape factor;

K_{Spc} = pile-cap shape factor;

K_{Spg} = factor to account for the shape of the pile group;

$K_{S(\mathrm{pg})}$ = pile-group configuration factor;

K_{spm} = factor to account for the pile spacing length (S_m) and the number of piles in line with flow (m);

K_{spn} = factor to account for the pile spacing width (S_n) and the number of piles normal to the flow (n);

K_w = correction factor for wide piers;

K_θ = factor describing the alignment of the pier;

L = pier length;

L_c = column length;

L_p = pile length;

L_{pc} = pile cap length;

m = number of piles in line with flow;

n = number of piles normal to the flow;

N = parameter that depends on the pier shape (circular or rectangular);

R = hydraulic radius of the flow cross-section;

S_e = slope of the energy line;

S_o = channel bottom slope;

S_p = smaller distance of S_m and S_n;

S_m = distance between centrelines of adjacent piles in line with the flow in a pile group;

S_n = distance between centrelines of adjacent piles perpendicular to the flow in a pile group;

t = time;

T = pile-cap thickness;

t_d = test duration;

t_{dMS} = test duration obtained by equation (4.1);

$t_{d5\%}$ = test duration obtained by criterion of 5%;

t_e = time to achieve equilibrium (scour) conditions;

T_* = distance of the pile-cap thickness that remains in the flow when it is partially immersed in the flow;

U = average approach flow velocity;

U_c = critical velocity for sediment entrainment;

U_f = average velocity of flow at the exposed footing;

U_1 = adjusted velocity for pile cap computations;

U_2 = adjusted velocity for pile group computations;

u_* = friction velocity;

u_{*c} = critical shear velocity for sediment entrainment;

W_o = equivalent obstruction width of the pier;

W_p = projected width of the pier;

W_{pg} = sum of the non-overlapping individual pile widths projected on a plane normal to the approach flow;

w_{pi} = projected width of one pile;

γ = specific weight of the water;

Δ = convergence iteration process;

Δ = sediment submerged density;

θ = pier alignment angle;

μ = fluid dynamic viscosity;

ν = fluid kinematic viscosity;

ρ = fluid density;

ρ_s = sediment density;

σ_g = geometric standard deviation of the sediment particle size distribution;

τ_o = average total bed shear stress;

τ_c = average critical bed shear stress of beginning of sediment motion;

τ_c^* = dimensionless shear stress;

φ = functional relation;

1. INTRODUCTION

1.1. BACKGROUND

From the beginning of history, the means of transportation seem to have been considered the most important factor in the progress of civilization. Since then humanity has needed to build bridges to span water bodies, mountains and roads, for the purpose of providing its passage. According to Modjeski (1922), the first bridge corresponds to a structure constructed over a branch of the Nile River as early as 4000 B.C. Among the oldest bridges are found the so-called lintel and slab bridges. The former consisted of oblong stones placed vertically in the stream and spanned by long flat, narrow stones or lintels. Sometimes lintels have been placed on piers built of smaller stones. There are some examples of these ancient bridges in England (Figure 1.1(a)), dating back to the Bronze Age, about 1400 B.C. But it is China, probably, who has built more slab bridges. Such is the type of the bridge at Chapoo which is very ancient, as shown in Figure 1.1(b). To the Romans is due the greatest progress in bridge-building. They used stone and concrete to build their bridges and used the arch as the basic architectural feature to make them strong. The first Roman Bridge was built approximately in 620 B.C. over the Tiber River. The long success of the Roman Empire depended in large measure on the vast network of roads that was constructed. At its fullest extent this included more than 900 major stone-arch bridges, many of which have been partly or wholly preserved, and some of which are even still in use, as shown in Figure 1.1(c). Ancient bridges with multiple stone-arches were also built in China, as the case of the bridge in the province of FoCheu, as shown in Figure 1.1(b).

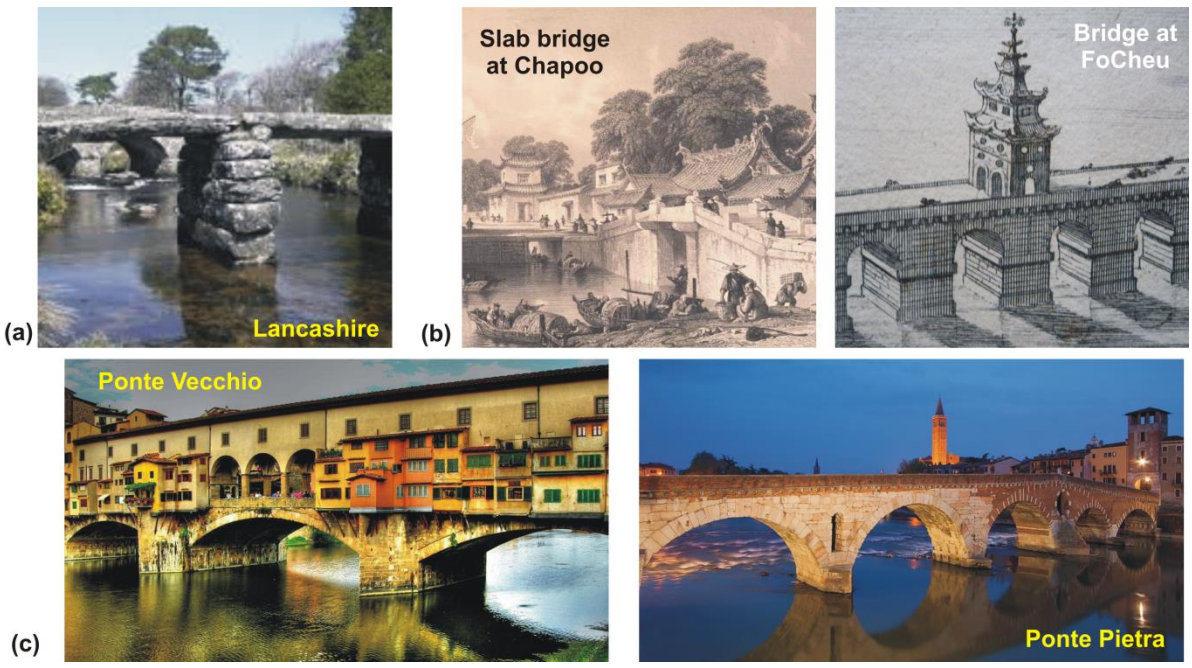

Figure 1.1 – Ancient bridges in: (a) England, (b) China and (c) Italy

In most of the river bridges built by the Romans, with multiple arches as shown in Figure 1.1(c), its central piers had the same shape in all vertical length. Later, in medieval Europe, bridge builders improved on the Roman structures by using narrower piers, thinner arch barrels and lower span-rise ratios on bridges. In recent centuries, with the advance of civilization and the development of new materials and construction methods, river bridges of greater length made their appearance, allowing to support large loads (*e.g.*, traffic or railroads). Due to physical, geotechnical and economic considerations, large river bridges are frequently built with foundations of complex geometries. Those structures are used to support bridge decks, as shown in Figure 1.2(a). Currently, two types of pier-foundations are used in new large-span bridges: (1) common complex piers (also named as pile-supported piers), which consist of a column founded on a pile cap supported by an array of piles, as outlined in Figure 1.2(b); and (2) special complex piers, which are characterized by non-conventional column and pile-cap geometries (*e.g.*, pile-supported piers with multi-columns). According to Ettema *et al*. (2011), the scour depth at special complex piers should be estimated by hydraulic-models and/or numerical models. In this study, the term "complex piers" applies to pier geometries such as the configuration represented in Figure 1.2(b), *i.e.*, a column founded on a pile cap supported by piles.

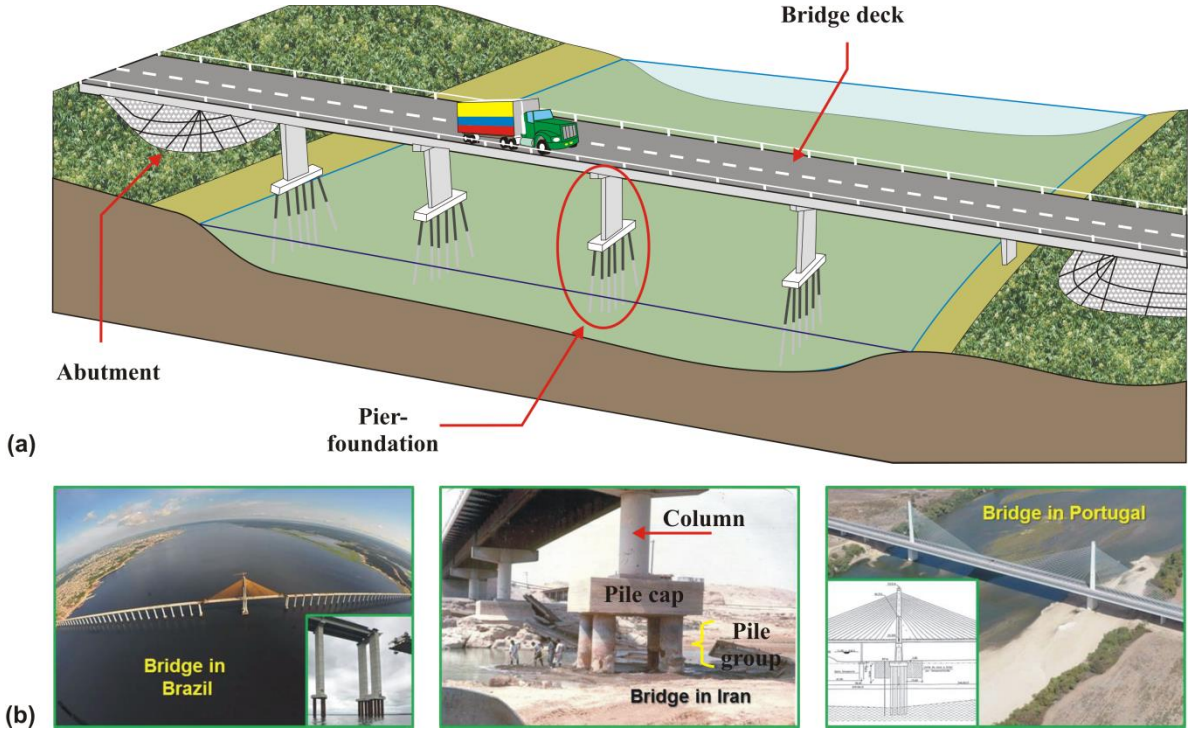

Figure 1.2 – (a) scheme of basic bridge structure and (b) photographs of common complex piers

The cost of new large bridges with complex pier foundations (as scheme in Figure 1.2(a)), amounting to billions of Euro, justifies a rigorous prediction of the scour depth, both for economic and safety reasons. Over-prediction of scour depth may lead to excessive costs of the bridge while under-prediction may leads to bridge failure. The major damage to bridges at river crossings occurs during floods. River bed local scour around bridge foundations has been recognized as one of the main causes of bridge failures or of the collapse of bridge piers and decks. After 2000 years scour is still a major problem. The United States Federal Highways Administration has estimated that on average about 50 to 60 bridges fail each year in the USA, while in New Zealand there is, on average, at least one serious bridge failure each year, as mentioned by Melville and Coleman (2000). According to Richardson *et*

al. (1993), on average 25% of bridge failures in the USA involved pier damage while 72% involved abutment damage. In Portugal recently five cases of bridge failures have been observed: Penacova bridge in 1983, Gafanha bridge in 1994, EN122 bridge in 2000, Sorraia river bridge in 2001 and Hintze Ribeiro (Entre-os-Rios bridge), in 2001, as shown in Figure 1.3. The latter bridge failure has been the most unfortunate case, causing 59 casualties. Muñoz *et al*. (2009) studied 63 real cases of reported bridge collapse in Colombia since 1986, having concluded that 24% of the cases corresponded to concrete bridges that collapsed by scour process in the abutments and/or piers. The investment of governments to mitigate the failures and damages of river bridges is enormous.

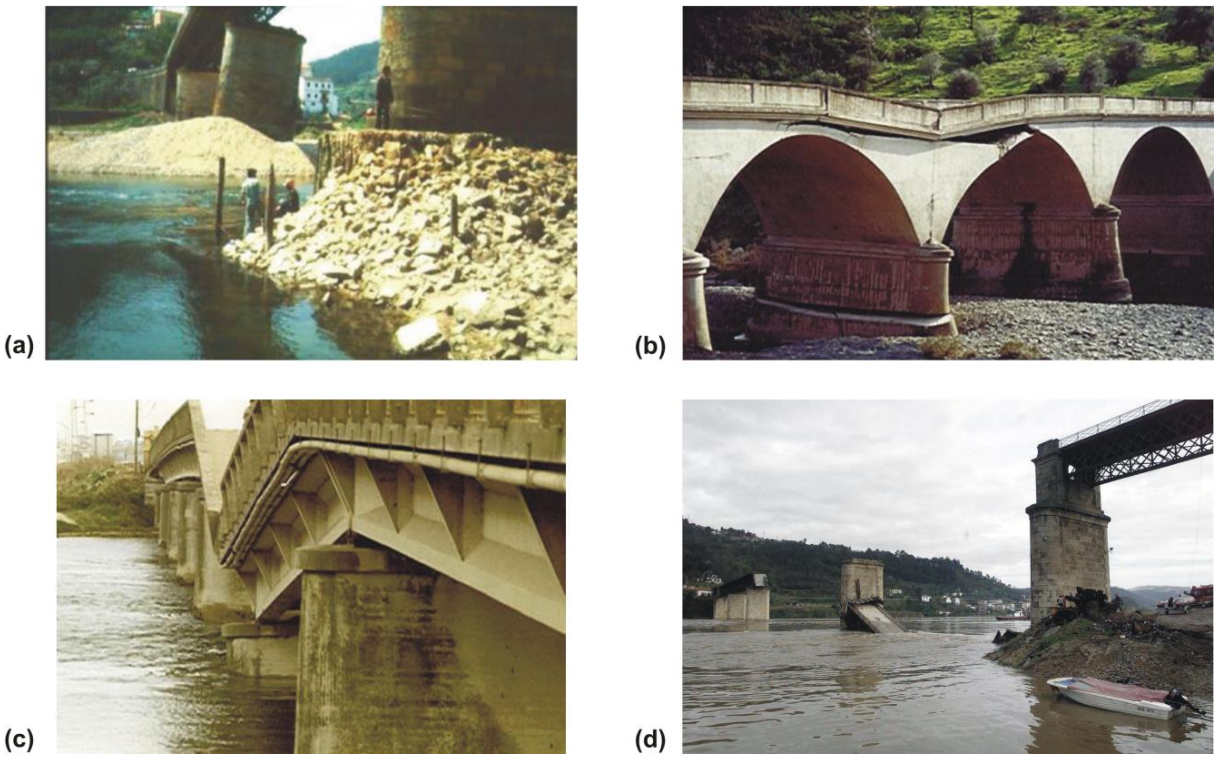

Figure 1.3 – Examples of bridge failures in Portugal: (a) Penacova bridge, (b) EN122 bridge, (c) Gafanha bridge and (d) Hintze Ribeiro bridge (photos a to c by J. Rocha)

Numerous studies have been conducted since the late 1950s on scour around bridge piers (Figure 1.4); unfortunately challenging problems remain because of the difficulties in understanding the complex flow and scouring mechanisms combined with complex geometries of bridges and various erodible bed materials. Although predictions of scour on single piers had a tremendous progress, during about seven decades, researches on complex piers are rather recent, dating back mostly to 1978. Single piers are characterized by having the same shape in all vertical length. The studies of local scour at single piers has been focused on understanding and characterizing: (1) the flow structure around single piers and the mechanisms involved in the scour process (*e.g*. Dargahi, 1989; Ahmed and Rajaratnam, 1998; Graf and Isiarto, 2002; Dey and Raikar, 2007); (2) the temporal evolution of maximum scour depth (*e.g*. Franzetti *et al*., 1982; Unger and Hager, 2007; Kothyari *et al*., 2007; Simarro *et al*., 2011; Lança *et al*., 2013b); and (3) the influence of specific parameters on the equilibrium scour depth, *i.e*., pier shape, pier alignment, flow shallowness, flow intensity, sediment coarseness and sediment gradation, (*e.g*., Laursen and Toch, 1956; Shen *et al*., 1969; Dietz, 1972; Ettema, 1976; Ettema, 1980; Chiew, 1984; Ettema *et al*., 1998b; Melville and Coleman, 2000; Sheppard *et al*., 2004; Lança *et al*., 2013b;

Fael *et al*., 2014). During the recent years, three methods have been consolidated and have been used to predict the equilibrium scour depth at single piers as well as complex piers: Auckland method (Melville and Coleman, 2000), FDOT method (Sheppard and Renna, 2010) and HEC-18 method (Arneson *et al*., 2012). Those three scour predictors were established on the basis of data obtained in hundreds of experiments run all over the world; still, both Auckland and HEC-18 methods are frequently claimed to over-predict the scour depth in natural conditions. According to Sheppard *et al*. (2004), over-prediction is due to the incorrect consideration of the effect of the sediment size factor.

Figure 1.4 – Photographs of local scour experiments at (a) single piers (Sheppard, 2003), (b) pile groups (Lança, 2013) and (c) complex piers (Sousa, 2007)

Local scouring at complex piers requires and deserves additional research work since few experimental studies are reported in the literature by comparison with local scour studies at single piers. Those few that exist, authored by Martin-Vide *et al*. (1998), Jones and Sheppard (2000a), Sheppard and Glasser (2004), Coleman (2005), Ataie-Ashtiani *et al*. (2010), Grimaldi and Cardoso (2010), Ferraro *et al*. (2013) and Amini *et al*. (2014), some of which report on short-duration scour tests. Some studies concerning local scour at pile groups, corresponding to the case of complex piers caped above the water surface, are reported in the literature. They include those of Hannah (1978), Elliott and Baker (1985), Salim and Jones (1996), Smith (1999), Zhao and Sheppard (1999), Sumer and Fredsøe (2002), Ataie-Ashtiani and Beheshti (2006), Amini *et al*. (2012) and Lança *et al*. (2013a) some of which report on short-duration scour tests.

The rigorous prediction of local scour depth around complex piers may not be guaranteed by the three consolidated predictors, *i.e*., Auckland, FDOT and HEC-18 methods. In spite of the complexity of the scour phenomena at complex piers, the three predictors were derived from limited experimental evidence. FDOT method, being the most comprehensive and using the most robust data basis, relies on the results of only 49 tests, while the possible combinations of column, pile cap and pile group geometries are infinite. It is, thus, with no surprise that the predictions of existing methods lead to erroneous results (*e.g*., Ferraro *et al*., 2013), justifying a strong research commitment and effort.

1.2. OBJECTIVES

The general objective of this study is to contribute to the understanding and characterization of local scour around complex bridge piers aligned with the approach flow under clear-water conditions. This objective is detailed as follows:

1. Production of extensive data on clear-water local scour at complex piers;

2. Description of the different stages of the time evolution in scour depth at complex piers depending on the pile-cap position relative to initial bed level;
3. Evaluation of the common criterion to stop experimental tests on complex piers (onset of the equilibrium phase of scour process);
4. Characterization and description of the effects of the pile-cap position, the relative column width, the relative pile-cap thickness and the pile-group configuration on the maximum scour depth at complex piers;
5. Estimation of the complex pier components' contribution on the total local scour depth through a new experimental approach;
6. Revision and evaluation of the three consolidated predictors of the scour depth at complex piers;
7. Proposal of a new set of equations to predict the equilibrium scour depth at complex piers.

1.3. LIST OF PUBLICATIONS WITH RESULTS FROM THE PRESENT STUDY

A number of contributions emerged during these five years of research, either by papers published (or submitted) in peer-reviewed journals or by papers published in conference proceedings. These are listed below together with the indication of the chapter that presents the published results and conclusions of each paper.

1. Moreno, M., Maia, R., Couto, L. and Cardoso, A. H. (2016). Subtraction approach to experimentally assess the contribution of the complex pier components to the local scour depth. Manuscript submitted to the Journal of Hydraulic Engineering. (Chapter 6);
2. Moreno, M., Maia, R. and Couto, L. (2016). Prediction of equilibrium local scour depth at complex bridge piers. Journal of Hydraulic Engineering. 10.1061/(ASCE)HY.1943-7900.0001153, 04016045. (Chapters 5 and 7);
3. Moreno, M., Maia, R. and Couto, L. (2015). Effects of relative column width and pile-cap elevation on local scour depth around complex piers. Journal of Hydraulic Engineering. 10.1061/(ASCE)HY.1943-7900.000108, 04015051. (Chapters 4 and 5);
4. Moreno, M., Muralha, A., Couto, L., Maia, R. and Cardoso, A. H. (2015). Influence of column width on the equilibrium scour depth at a complex pier. Proceeding of 36th IAHR World Congress, Delft – The Hague, the Netherlands, 28 June – 3 July. (Chapter 5);
5. Moreno, M., Maia, R., Pêgo, J. P., Couto, L. and Cardoso, A. H. (2014). Contribuição das componentes de um pilar complexo na profundidade de erosão localizada (in Portuguese). Proceedings 9as Jornadas de Hidráulica, Recursos Hídricos e Ambiente do Departamento de Engenharia Civil da FEUP, Porto, Portugal, 31 October. (Chapter 6);
6. Moreno, M., Couto, L., Maia, R. and Cardoso, A. (2014). Erosões localizadas em pilares complexos de pontes: desempenho de modelos de previsão existentes (in Portuguese). Revista Recursos Hídricos, 35(1), 5-22. (Chapters 2, 3 and 7);
7. Moreno, M., Maia, R., Couto, L. and Cardoso, A. (2014). Contribution of complex pier components on local scour depth. Proceeding of 3rd IAHR Europe Congress, Porto, Portugal, 14-16 April. (Chapter 6);
8. Moreno, M., Couto, L. and Maia, R. (2012). Evolución temporal de la profundidad de erosión local junto de pilas de puentes de geometría compleja (in Spanish). Proceeding of XXV Congreso Latinoamericano de Hidráulica, San José, Costa Rica, 9-12 September. (Chapters 3 and 4);

9. Moreno, M., Maia, R., Couto, L. and Cardoso, A. (2012). Evaluation of local scour depth around complex bridge piers. Proceeding of River Flow 2012, San José, Costa Rica, 5-7 April. (Chapters 3, 4 and 7);
10. Moreno, M., Couto, L. and Maia, R. (2012). Evolução temporal da profundidade de erosão localizada junto de pilares complexos (in Portuguese). Proceeding of 11º Congresso da Água, Porto, Portugal, 6-8 February. (Chapters 3 and 4).

1.4. THESIS STRUCTURE

The thesis is organized in eight chapters and one appendix. In this first chapter, a brief overview of the history of bridges development, definition of the geometry of foundation aimed at this study, and some examples of bridge failures that highlight the relevance of the research are provided. The main motivation and objectives of the work are presented. A list of the publications that emerged from this research is also included.

Chapter 2 (Literature review) is a state of the art on local scour around single and complex piers, with special emphasis on the flow structure and the mechanisms involved in the scour process, the temporal evolution of maximum scour depth, the non-dimensional parameters affecting local scouring and the equilibrium scour depth prediction at single and complex piers. In the last topic, only Auckland method (Melville and Coleman, 2000; Coleman, 2005), FDOT method (Sheppard and Renna, 2010) and HEC-18 method (Arneson *et al*., 2012) are taken into account since these three predictors are considered as consolidated. These three methods present both equations for single and complex piers.

Chapter 3 (Experimental setup) describes the two experimental facilities used in the present study to assess and characterize local scour at complex piers. It also includes the description of the experimental campaigns and of the procedures adopted in both facilities. Seven different complex pier models were tested, six of them in the flume at the National Laboratory for Civil Engineering (LNEC) and the other one in the flume at the Faculty of Engineering of the University of Porto (FEUP). The geometric variables of the complex pier models, the flow control variables and the sediment characteristics are summarized for all the experimental tests.

Chapter 4 (Temporal evolution of the scour depth at complex piers) presents the results of the scour depth time evolution observed in the tests performed with the seven complex piers, identifying the different stages that occur in the scour process. The influences of the pile-cap position, of the relative column width, of the relative pile-cap thickness and of the pile-group configuration are analysed. The common criterion to stop experimental tests on complex piers is analysed, and a new stop criterion is introduced. The chapter is based on the paper Moreno *et al*. (2015b) (*i.e*., item (3) from the list of publications in section 1.3) and on the preliminary results presented in Moreno *et al*. (2012a, 2012b, 2012c) (*i.e*., items (10), (9) and (8) in section 1.3, respectively).

Chapter 5 (Effect of complex pier geometry on equilibrium scour depth) presents the results that enhance the quantification of the influence of complex pier geometry on the equilibrium scour depth. The effects of the pile-cap position, the relative column width, the relative pile-cap thickness and the pile-group configuration are analysed. The equilibrium scour depths are obtained by extrapolation of the scour depth records. Comparison of those effects with the corresponding results obtained through other complex pier models published in literature is also performed. The chapter is based on the papers Moreno *et al*. (2015b, 2016a) (*i.e*., items (3) and (2) from the list of publications in section 1.3) and on

the preliminary results presented in Moreno *et al*. (2012b, 2015a) (*i.e*., items (9) and (4) in section 1.3, respectively).

In Chapter 6 (Complex pier components' contribution on the equilibrium scour depth) a new, physically sounder approach to experimentally assess the contribution of complex piers' components on scouring is presented and discussed. According to the new approach, the scour depth at a given component is calculated by subtracting the scour depth at two contiguous piers' components from the scour depth at the corresponding complete complex pier, this way keeping the prevailing interactions. A comparison of the results of this approach with the corresponding contributions based on tests with isolated components is also presented. The chapter is based on the paper Moreno *et al*. (2016b) (*i.e*., item (1) from the list of publications in section 1.3) and on the preliminary results presented in Moreno *et al*. (2014a, 2014c) (*i.e*., items (7) and (5) in section 1.3, respectively).

In Chapter 7 (Prediction of equilibrium scour depth around complex piers) the performance of the three most consolidated methods to predict the equilibrium scour depth at complex piers is analysed and discussed. Based on the experimental results of the present study (*i.e*., Chapters 5 and 6) and on the conceptual approaches of Auckland and FDOT methods, an alternative formulation for a predictor of equilibrium scour depth is suggested and validated. This chapter is based on the papers Moreno *et al*. (2014b, 2016a) (*i.e*., items (6) and (2) from the list of publications in section 1.3, respectively) and on the preliminary results presented in Moreno *et al*. (2012b) (*i.e*., item (9) in section 1.3).

In Chapter 8 (Conclusions and future research) the main conclusions of the present research are drawn and suggestions and recommendations for future works are given.

An appendix is included at the end of the thesis, presenting the scour data obtained for the full set of tests performed in this study. For each test, the geometric variables of the complex pier models, the flow control variables, the equilibrium scour depth, the scour depth time evolution records, a chart of the scour depth evolution and photos of the scour hole development are reported.

2. LITERATURE REVIEW

2.1. INTRODUCTION

The process of scouring in rivers and streams can result from natural phenomena or from man-made alterations (building of structures in the riverbed); both can produce effects over long reaches of the river or only locally. According to Breusers and Raudkivi (1991), the river scour can be divided into general, constriction and local scour. General scour occurs in a river or stream as the result of natural processes irrespective of whether a structure is located there. Constriction scour occurs if a structure causes narrowing the water course or flood plain rechannelling. Local scour results directly from the impact of a structure on the flow. This scour, which is a function of the type of structure, is superimposed on the general scour and on the constriction scour. For river bridges, these structures refer to abutments and pier-foundations (that include the case of the single piers, compound piers, complex piers among others). Scour may occur for two distinct sediment transport conditions: (1) under clear-water, *i.e*., in the absence of sediment movement in the bed of the approach channel; and (2) under live-bed, *i.e*., when generalized movement of the bed sediment occurs in the approach flow. The first condition corresponds to the bed shear stress being smaller or, at most, equal to the critical bed shear stress to beginning of sediment motion whereas for the second condition the bed shear stress is higher than the critical bed shear stress.

Many researchers have attempted to understand and evaluate the process of local scour around bridge piers. Typically, the investigations have been made through either laboratory model studies or field investigations, with some disparities between them, the values obtained through laboratory tests tending to over-estimate the field values. One possible reason is that most of the design relationship for local scour depths were based on limited range of experiments and/or did not consider the various factors affecting scour process. As a result of these investigations, a large number of equations has been proposed for estimating equilibrium scour depth at bridge piers (see Sheppard *et al*., 2011). In this chapter, only the Auckland method (Melville and Coleman, 2000; Coleman, 2005), the FDOT method (Sheppard and Renna, 2010) and the HEC-18 method (Arneson *et al*., 2012) are taken into account since these three predictors are considered consolidated and applicable to complex bridge piers. These three methods present both equations for single and complex piers.

This chapter is a review of the available and most relevant literature on the subject of local scour around bridge piers with non-cohesive material, where the clear-water condition is emphasized. The local scour around bridge piers depends strongly on the geometry of the pier. This reason is one that justifies the chapter being divided in local scour around single piers (section 2.2) and local scour around complex piers (section 2.3). The characteristic flow structure around those structures and the different mechanisms involved in the local scour phenomena caused are described in sections 2.2.1 and 2.3.1. Dimensional analyses are formulated in sections 2.2.2 and 2.3.2. Some aspects of the time dependent development phase of the scour process are treated in sections 2.2.3 and 2.3.3. The criteria used to stop the experimental tests are described in sections 2.2.4 and 2.3.4. According to dimensional

analysis, the various dimensionless parameters that influence the scour process are discussed in sections 2.2.5 and 2.3.5. Those parameters are associated with the flow, the bed material and the pier geometry. And finally, the methods that engineers actually use for estimating the maximum scour depth at bridge piers are presented in sections 2.2.6 and 2.3.6. When presenting the methods, the symbols of some variables are changed and harmonized with the purpose of their comparison.

2.2. LOCAL SCOUR AROUND SINGLE PIERS

2.2.1 FLOW STRUCTURE

Local scour at a single pier is attributable to the forces exerted on the bed by the complex, highly three-dimensional and unsteady flow field generated by the pier. The flow field is marked by turbulence structures with a wide range of scales, and by a pronounced downflow at the pier's leading edge (Kirkil *et al*., 2009). The flow field in the scour hole around single piers has been studied in the last four decades, with a higher incidence in the last two. Research has been made mostly through experimentation with different techniques, *e.g*., flow visualization techniques (hydrogen-bubble, dyes, bentonite solution), Acoustic Doppler Velocimetry (ADV), Acoustic Doppler Velocity Profilers (ADVP) and Particle Image Velocimetry (PIV) in both plane and scoured beds under clear-water and live-bed conditions at cylindrical piers (reference obstacle). Numerical techniques like Large-Eddy Simulation (LES), Reynolds-Averaged Navier–Stokes (RANS), Detached-Eddy Simulation (DES) or hybrid RANS-LES can be used to reveal the flow field, its structures and interactions.

The most relevant studies on flow field around cylindrical piers include the ones of Melville (1975), Melville and Raudkivi (1977), Morton and Evans-Lopez (1986), Dargahi (1989, 1990), Ahmed and Rajaratnam (1997, 1998), Graf and Istiarto (2002), Muzzammil and Gangadhariah (2003), Rao *et al*. (2004), Ettema *et al*. (2006), Zhao and Huhe (2006), Dey and Raikar (2007), Unger and Hager (2007), Link *et al*. (2008), Nogueira *et al*. (2008), Sadeque *et al*. (2008), Kirkil *et al*. (2008, 2009), Diab (2011), Khosronejad *et al*. (2012) and Radice and Tran (2012). The flow field at a single pier is a complex three-dimensional turbulent phenomenon resulting from strong flow-pier-sediment interaction, which increases with the development of the scour hole. According to the results of these studies, the basic mechanisms that cause local scour at cylindrical piers may be summarized as:

1. In the proximity of the pier, the flow velocity goes to zero on the upstream face of the pier. Due to the stagnation pressure in front of the pier, the water surface is raised, forming a surface roller, called bow wave, as shown in Figure 2.1. The particular pressure gradient produces descending trajectories (downflow) on the pier face. From those, the ones more close to the front face pier edges are deviated laterally. The resulting downflow acts like a vertical jet eroding a groove in front of the pier base and undermining the scour hole slope formed above, as shown in Figure 2.1.
2. The downflow rolls up again as it continues to create a hole and by interaction with the incoming flow forms a complex vortex system, called horseshoe vortex, as shown in Figure 2.2. This develops as a result of flow separation at the upstream face of the scour hole. The horseshoe vortex carries out the transport of eroded particles away past the pier. As the scour depth increases, the strength of the horseshoe vortex weakens, leading to a reduction of the scouring rate. The horseshoe vortex is part of a system of structures of turbulence that, together with the downflow and the flow acceleration close to the sides of the pier, are the prime erosive flow mechanisms. The turbulence structures (*e.g*., coherent structures in the

form of necklace vortices, eddies shed in the separated shear layers, large-scale wake rollers) are not isolated from each other. They are intrinsically connected within the flow field. According to Zhao and Huhe (2006), the horseshoe vortex system contains a primary horseshoe vortex (1), a horseshoe vortex close to the pier base (2), and the secondary horseshoe vortices (3 to 6), as outlined in Figure 2.2(c). The scale of the horseshoe vortices increase with increasing scouring depth.

3. At the downstream face of the pier wake vortices appear by the separation of the flow at the sides of the pier and that are moved downstream by the approach flow. Both the horseshoe and the wake vortices erode sediment from the base region around the pier. The wake vortices work as miniature tornados lifting sediment from the bed and transporting it downstream by the flow. Figure 2.3 displays the wake vortex system at the downstream face of the pier observed in different pier studies.

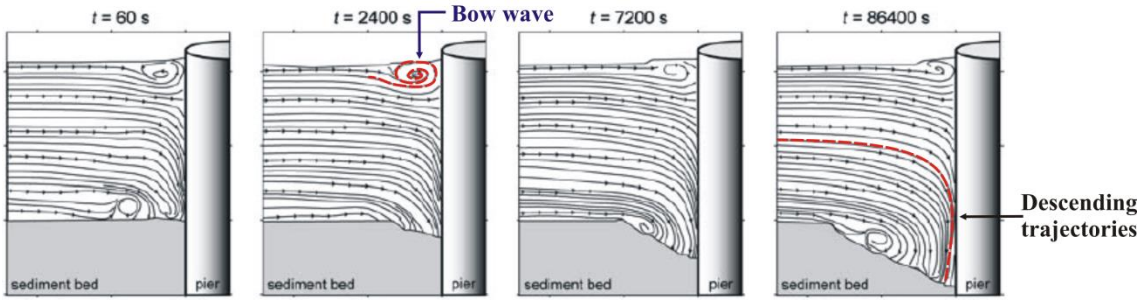

Figure 2.1 – Streamline plots of the flow at various times, adapted from Unger and Hager (2007)

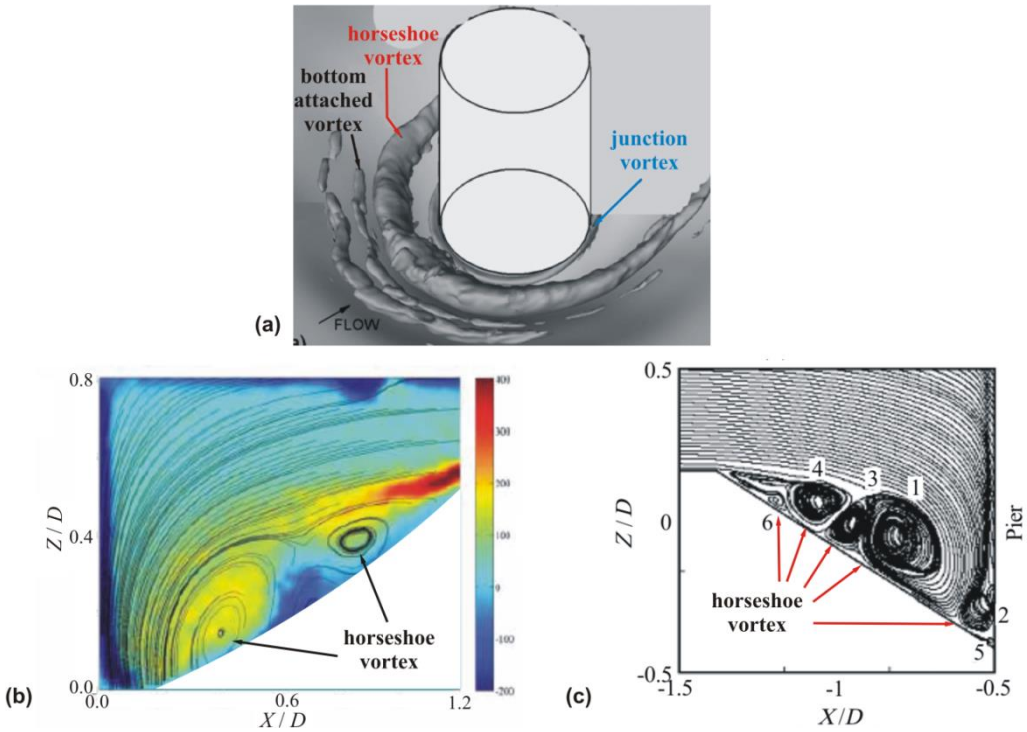

Figure 2.2 – (a) visualization of the vortex system inside the scour hole, adapted from Kirkil *et al*. (2008), (b) visualization of transverse section of the vorticity map, adapted from Nogueira *et al*. (2008) and (c) visualization of the horseshoe vortex system in a transversal section, adapted from Zhao and Huhe (2006)

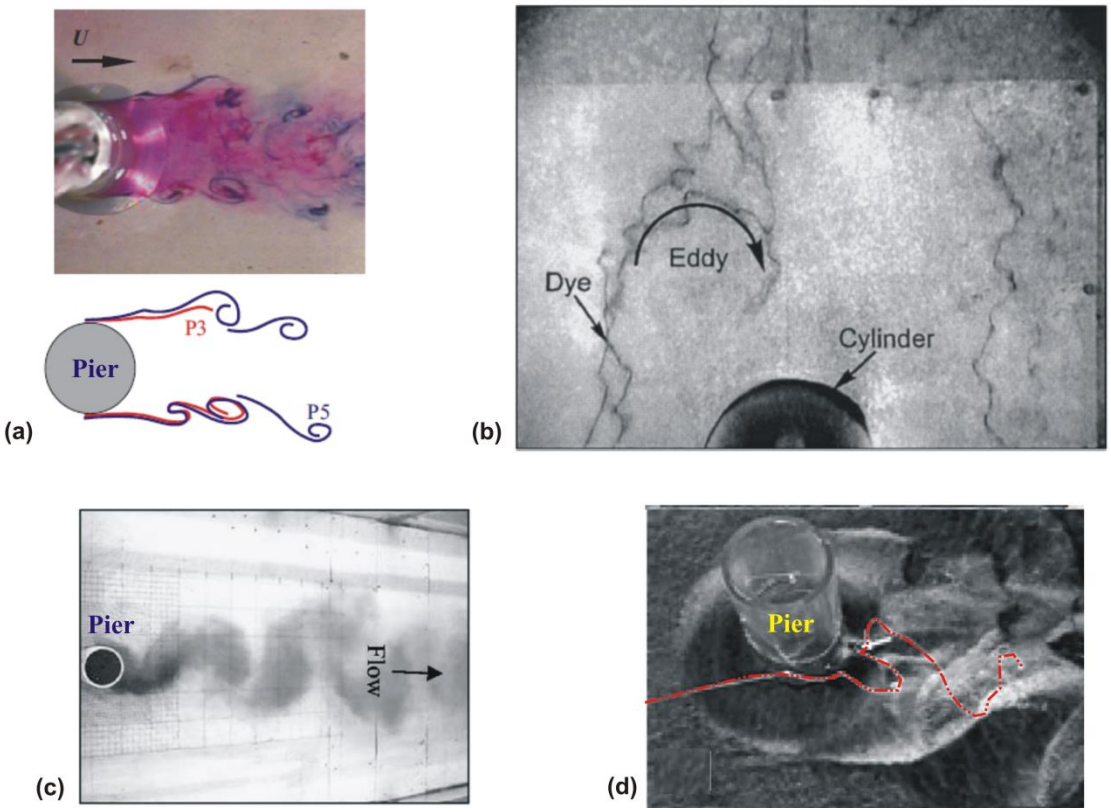

Figure 2.3 – Visualization of wake vortices at downstream of the pier made by: (a) Rao *et al*. (2004), (b) Ettema *et al*. (2006), (c) Sadeque *et al*. (2008) and (d) Kirkil *et al*. (2008)

Figure 2.4 shows a present author interpretation of the flow structure around a single cylindrical pier, taking into account the previous description of the different components.

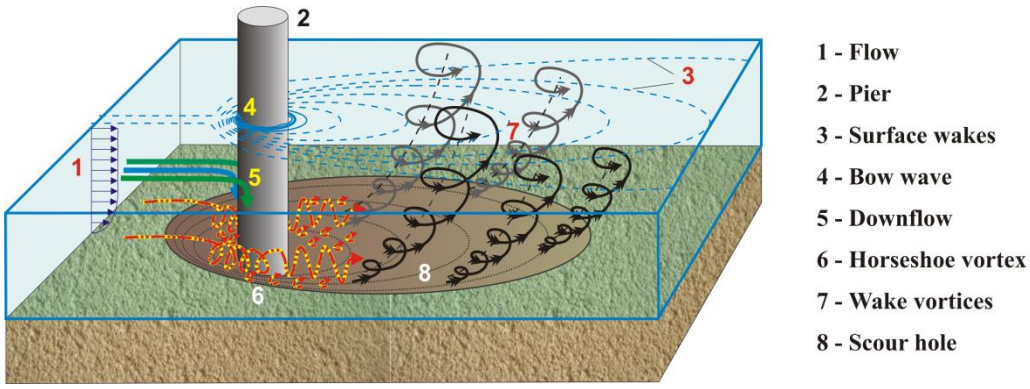

Figure 2.4 – Flow structure around cylindrical bridge piers

Few studies have been performed in recent years to evaluate the flow structure around non-circular piers. Those include the ones of Raikar and Dey (2008) and Diab *et al*. (2009, 2010). They carried out tests with square piers in order to characterize the development of the turbulent horseshoe vortex

system flow in different stages of the scour process (including the equilibrium). The measurements were performed through an ADV. They analysed the size of the horseshoe vortex, the turbulence intensities and Reynolds stresses at different azimuthal planes. Additionally, Chang *et al*. (2010) described the main features of the flow field and turbulence structure in the vicinity of a rectangular pier at a small angle of attack.

2.2.2 DIMENSIONAL ANALYSIS

As defined in many studies, as for example in Lança (2013), the maximum scour depth around single piers, d_s, at a given instant, t, can be described by the following set of independent variables and parameters:

$$d_s = f\begin{bmatrix}\text{flow } (h, S_e, g),\ \text{fluid } (\rho, \mu),\ \text{bed material } (d_{50}, \sigma_g, \rho_s) \\ \text{pier } (D, L, K_S, \theta),\ \text{channel } (B, S_o, K_g),\ \text{time } (t)\end{bmatrix} \tag{2.1}$$

where, h = approach flow depth; S_e = slope of energy line; g = gravitational acceleration; ρ = fluid density; μ = fluid dynamic viscosity; d_{50} = median size of sediment particle size distribution (such that 50% by weight are smaller); σ_g = geometric standard deviation of the sediment particle size distribution; ρ_s = sediment density; D = pier width; L = pier length; K_S = factor describing the shape of the pier; θ = pier alignment angle; B = channel width; S_o = channel bottom slope; K_g = factor describing the geometry of the channel cross-section; t = time.

Figure 2.5 shows the scheme of a single pier with the respective variables described above.

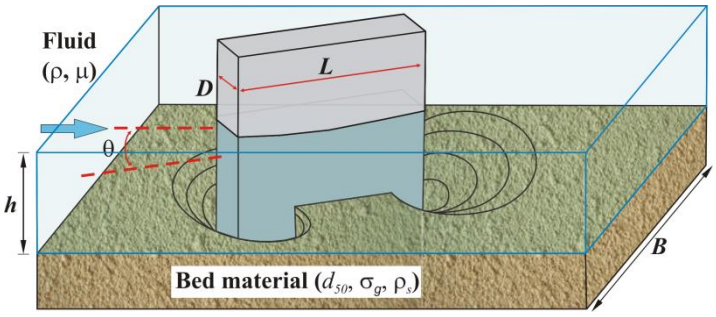

Figure 2.5 – Set of variables describing the scour process with influence in the scour depth at a single pier

It should be noted that the critical velocity for sediment entrainment, U_c, is not considered since it is fully defined by h, S_e, g, ρ, μ, d_{50} and ρ_s. For uniform flows, $S_e = S_o$, the friction velocity, u_*, is given by $u_* = \sqrt{gRS_e} = \sqrt{gRS_o}$, where $R = \varphi(B, h, K_g)$ is the hydraulic radius of the flow cross-section and φ stands for functional relationship. Since the sediment submerged density of the flow is given by $\Delta = (\rho_s - \rho)/\rho$, equation (2.1) can be written as

$$d_s = \varphi(\sigma_g, \Delta, K_S, \theta, K_g, h, d_{50}, D, L, B, u_*, g, \rho, \mu, t) \tag{2.2}$$

Choosing D, u_* and μ for basic variables and applying the Vaschy-Buckingham theorem, equation (2.2) becomes

$$\frac{d_s}{D} = \varphi\left(\sigma_g, \Delta, K_S, \theta, K_g, \frac{h}{D}, \frac{d_{50}}{D}, \frac{L}{D}, \frac{B}{D}, \frac{gD}{u_*^2}, \frac{u_* D\rho}{\mu}, \frac{u_* t}{D}\right) \quad (2.3)$$

Any non-dimensional parameter of equation (2.3) can be replaced by any combination of that parameter with others as soon as the resulting set remains independent, thus

$$\frac{d_s}{D} = \varphi\left(\sigma_g, \Delta, K_S, K_\theta, K_g, \frac{h}{D}, \frac{D}{d_{50}}, \frac{B}{D}, \frac{\tau_o}{\rho g \Delta d_{50}}, \frac{u_* d_{50}}{\nu}, \frac{u_* t}{D}\right) \quad (2.4)$$

where, $K_\theta = \varphi(\theta, L/D)$ is the factor describing the alignment of the pier and φ stands for functional relationship; $\nu = \mu/\rho$ is the fluid kinematic viscosity and $\tau_o = \rho u_*^2$ is the average total bed shear stress. The equation (2.4) can also be written as

$$\frac{d_s}{D} = \varphi\left(\sigma_g, \Delta, K_S, K_\theta, K_g, \frac{h}{D}, \frac{D}{d_{50}}, \frac{B}{D}, \frac{\tau_o}{\tau_c}\frac{\tau_c}{\Delta\gamma d_{50}}, \frac{u_* d_{50}}{\nu}, \frac{u_* t}{D}\right) \quad (2.5)$$

where, τ_c = average critical bed shear stress of beginning of sediment motion and $\gamma = \rho g$ is the specific weight of the water. The Shields' diagram curve, first presented by Shields in 1936, is expressed by a dimensionless variables relationship, equation (2.6),

$$\tau_c^* = \frac{\tau_c}{\Delta\gamma d_{50}} = \varphi'\left(\frac{u_* d_{50}}{\nu}\right) \quad (2.6)$$

The Shields values of τ_c^* are commonly used to denote conditions under which bed sediments are stable but on the verge of being entrained. Therefore, the parameters of equation (2.6) can be replaced by

$$\left[\frac{\tau_o}{\tau_c}\frac{\tau_c}{\Delta\gamma d_{50}}, \frac{u_* d_{50}}{\nu}\right] \rightarrow \frac{u_*}{u_{*_c}} \quad (2.7)$$

where u_{*c} = critical shear velocity for sediment entrainment. Equation (2.5) can be rewritten as

$$\frac{d_s}{D} = \varphi\left(\sigma_g, \Delta, K_S, K_\theta, K_g, \frac{h}{D}, \frac{D}{d_{50}}, \frac{B}{D}, \frac{u_*}{u_{*_c}}, \frac{u_* d_{50}}{\nu}, \frac{u_* t}{D}\right) \quad (2.8)$$

The non-dimensional parameter u_*/u_{*_c} is frequently replaced by U/U_c for practical reasons. Here, U = average approach flow velocity, *i.e.*, average flow velocity in the channel reach upstream the obstacle, and U_c = critical average approach flow velocity (of beginning of sediment motion). That replacement is virtually exact in the particular case of fully developed flow on a rough flatbed, where the logarithm law of the wall, equation (2.9)

$$\frac{U}{u_*} = 5.75 log\left(\frac{R}{k_s}\right) + B' \quad (2.9)$$

does apply. In the equation, k_s = height of grain roughness and B' is a constant of integration. For the condition of beginning of sediment motion, $U = U_c$ and equation (2.9) remains valid, *i.e.*,

$$\frac{U_c}{u_{*_c}} = 5.75log\left(\frac{R}{k_s}\right) + B' \tag{2.10}$$

This implies that, for a rough flatbed, the identity $u_*/u_{*_c} = U/U_c$ is unconditionally valid. The same result can be derived for a hydraulically smooth or transition flatbed. Consequently, equation (2.8) becomes

$$\frac{d_s}{D} = \varphi\left(\sigma_g, \Delta, K_S, K_\theta, K_g, \frac{h}{D}, \frac{D}{d_{50}}, \frac{B}{D}, \frac{U}{U_c}, \frac{u_* d_{50}}{\nu}, \frac{u_* t}{D}\right) \tag{2.11}$$

Equation (2.11) is a general equation to describe the local scour at single piers in natural channels. However, as most tests are carried out in rectangular channels, it is important that the relation B/D is greater than 10 so that wall effects are negligible (Laursen and Toch, 1956) and K_g does not influence scour depth. If the bed material is composed of sand with constant density, the variable Δ can be eliminated from the derivation thus obtaining

$$\frac{d_s}{D} = \varphi\left(\sigma_g, K_S, K_\theta, \frac{h}{D}, \frac{D}{d_{50}}, \frac{B}{D}, \frac{U}{U_c}, \frac{u_* d_{50}}{\nu}, \frac{u_* t}{D}\right) \tag{2.12}$$

Equation (2.12) can be rearranged as

$$\frac{d_s}{D} = \varphi\left(\frac{U}{U_c}, \sigma_g, \frac{D}{d_{50}}, \frac{h}{D}, \frac{u_* d_{50}}{\nu}, K_S, K_\theta, \frac{u_* t}{D}\right) \tag{2.13}$$

In equation (2.13), U/U_c = flow intensity (imprint of the approach flow velocity); σ_g = geometric standard deviation of the sediment particle size distribution; D/d_{50} = relative particle size; h/D = relative pier length; $u_* d_{50}/\nu$ = shear Reynolds number; K_S = pier shape factor; K_θ = pier alignment factor; $u_* t/D$ = non-dimensional time.

Equation (2.13) constitutes the framework for subsequent analysis. The effects of each non-dimensional parameter on the relative scour depth are discussed next. The last non-dimensional parameter on the right side of equation (2.13), correspondent to the temporal evolution of scour depth at single piers, is discussed in section 2.2.3. The other non-dimensional parameters of equation (2.13) are discussed in section 2.2.5.

2.2.3 TIME EVOLUTION OF SCOUR DEPTH

In accordance with Couto and Cardoso (2001), for clear-water conditions, when the bed material in the natural flow upstream of the scour area is at rest, the maximum depth of the scour hole increases quickly with time in the beginning of the scour process. In the areas where the side slope angle of the excavated hole exceeds the angle of repose of the submerged bed material, large quantities of sediment slide into the scour hole and become available to be transported downstream. Through this sliding mechanism, the contour limits of the scour hole extend in all directions, namely upstream, involving bed zones where the shear stress is below the critical value. Sediment grains are transported both along the bed and in suspension in the water column and may be deposited near the downstream limits of the scour hole. This mass of deposited sediment is prone to be shifted downstream as scour progresses. The increase on scour depth and scour hole volume induces the reduction of bed shear stress within

the scour hole until it becomes insufficient to erode and transport sediment particles downstream. This usually occurs after a rather large time interval. As scour progresses, the scour rate decreases and the equilibrium scour depth, d_{se}, is reached asymptotically, as shown in Figure 2.6(a).

For live-bed conditions, when the flow induces a general movement of the bed material, in the scour hole area there is a simultaneous removal of grains originated from the scoured bed around the obstacle and of those from the general bed scouring trapped by the scour hole when moving downstream. In the initial phase of scouring, the quantity of material that leaves the scour hole exceeds the quantity of material coming in and the scour depth increases. After some time, both quantities become equal. Equilibrium is reached much faster under live-bed conditions than for clear-water; live-bed equilibrium is known as dynamic equilibrium since the scour depth may oscillate between certain limits as show in Figure 2.6(b). Under this condition, the local scour depth fluctuates periodically about a mean value, the fluctuations corresponding to the passage of bed forms through the scour hole. In this context, it is pertinent to define the maximum scour depth, d_{sm}, as the sum of the average equilibrium scour depth, d_{se}, with a value that depends on the semi-amplitude of bedforms. For clear-water flow conditions, $d_{sm} = d_{se}$, since the semi-amplitude of bedforms is zero.

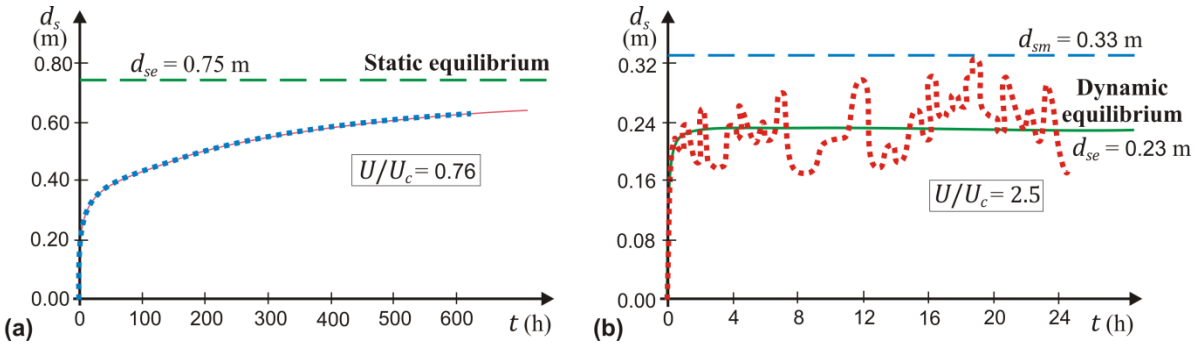

Figure 2.6 – Evolution of scour depth with time under: (a) clear-water condition (adapted from Sheppard *et al*., 2004) and (b) live-bed condition (adapted from Sheppard and Miller, 2006)

According to some researchers (Chabert and Engeldinger, 1956; Ettema, 1980; Couto and Cardoso, 2001), irrespective of the scour condition (clear-water or live-bed), the curves relating the scour depth evolution with time may be subdivided into three reaches corresponding to an equal number of phases of the scouring process:

- the initial phase, where scour depth increases very quickly (a couple of hours in laboratory conditions);
- the principal phase, where the scour hole systematically increases in depth and areal extent, though at a progressively decreasing rate (until three or four weeks in laboratory for clear-water conditions);
- the equilibrium phase, where the scour depth (or average scour depth, for live-bed condition) may only show a slight increase.

In principle, the three phases can be graphically identified, as shown in Figure 2.7 for a long-duration test (35 days) performed by Lança *et al*. (2010), on the basis of slope changes displayed on logarithmic plots of the scour depth against time. In fact, in most practical situations, the slope associated with the initial phase is not easily distinguishable from the slope of the principal phase. It is clear that the non-dimensional times (Ut/D) at which each phase occurs depend on pier dimensions, sediment characteristics and flow conditions of the experiment.

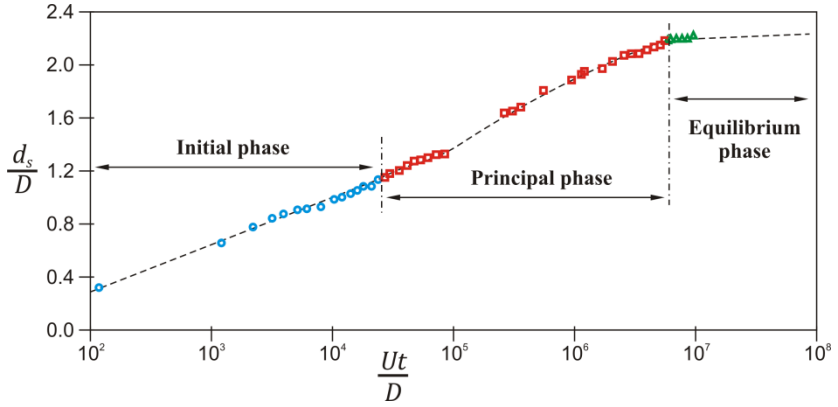

Figure 2.7 – Phases of the scouring process under clear-water condition, adapted from Lança *et al*. (2010)

Since the mid of last century, a number of attempts to describe the temporal development of clear-water scour have been made by various authors. Mention can be made, among others, to the contributions by Shen *et al*. (1966), Breusers *et al*. (1977), Franzetti *et al*. (1982), Sumer *et al*. (1992), Bertoldi and Jones (1998), Melville and Chiew (1999), Oliveto and Hager (2002, 2005), Kothyari *et al*. (2007), Sheppard *et al*. (2011) or Lança *et al*. (2013b). Some of the mentioned contributions consider only cylindrical piers. The relevant contributions are described next.

Oliveto and Hager (2002, 2005) and Kothyari *et al*. (2007) used the results from their experiments and suggested the following expression for the temporal evolution of the scour depth:

$$\frac{d_s}{D^{2/3}h^{1/3}} = 0.068N\frac{\mathrm{Fr}_d^{1.5}}{\sqrt{\sigma_g}}\log\left(\frac{\sqrt{\Delta g d_{50}}}{D^{2/3}h^{1/3}}t\right) \tag{2.14}$$

where N = parameter that depends on the pier shape (1 for circular and 1.25 for rectangular piers) and Fr_d = densimetric Froude number = $U/\sqrt{\Delta g d_{50}}$.

Sheppard *et al*. (2011) analysed scour depth information from 569 experimental tests and 928 field data. They presented a modified form of the equation proposed by Melville and Chiew (1999) to describe the scour depth time evolution as

$$\frac{d_s}{d_{se}} = 1 - exp\left\{-0.04\left|\frac{U_c}{U}ln\left(\frac{t}{t_e}\right)\right|^{1.6}\right\} \tag{2.15}$$

where the time needed to attain equilibrium, t_e, can be calculated by the following expressions:

$$t_e(\text{days}) = \begin{cases} 200\dfrac{D}{U}\left(\dfrac{U}{U_c}-0.4\right) & \text{for } \dfrac{h}{D} > 6 \\ 127.8\dfrac{D}{U}\left(\dfrac{U}{U_c}-0.4\right)\left(\dfrac{h}{D}\right)^{0.25} & \text{for } \dfrac{h}{D} \le 6 \end{cases} \tag{2.16}$$

Lança *et al*. (2013b) carried out 38 rather long local scour tests at single cylindrical piers to improve the scour depth time evolution equation by making use of the exponential function suggested by Franzetti *et al*. (1982). The resulting expression is,

$$\frac{d_s}{d_{se}} = 1 - exp\left[-1.22\left(\frac{D}{d_{50}}\right)^{-0.764}\left(\frac{Ut}{D}\right)^{0.09\left(\frac{D}{d_{50}}\right)^{0.244}}\right] \tag{2.17}$$

It is worth stressing that this contribution only applies to cylindrical piers inserted in uniform, fully developed turbulent flows, in wide rectangular channels with a flatbed composed of uniform, non-ripple forming sand, close to the condition of beginning of sediment motion ($U/U_c \approx 1$).

2.2.4 EQUILIBRIUM SCOUR DEPTH IN LABORATORY TESTS

The equilibrium concept is rather subjective and different authors present different approaches to cope with it. Franzetti *et al*. (1982) described equilibrium as the state of scour development where no further change occurs with time and stressed that this condition may take an infinite time to occur. Olivetto and Hager (2002, 2005) argued that equilibrium cannot be achieved in finite time and that the scour hole never stops to develop; they have stated that end scour as the equilibrium state between vortical agents and the resistance of sediment to be scoured does not normally exist. In opposition, other authors defend the equilibrium scour concept, the question being the time needed to reach equilibrium. Many research works (*e.g*., Melville and Chiew, 1999; Barkdoll, 2000; Kothyari *et al*., 2007; Sheppard *et al*., 2011), postulated a finite time to reach equilibrium scour. Others state that equilibrium scour cannot be achieved in a finite time (*e.g*., Franzetti *et al*., 1982; Bertoldi and Jones, 1998; Simarro *et al*., 2011; Lança *et al*., 2013b) or implicitly discard that scour depth values are upper bounded.

Assuming that equilibrium scour exists and this is achieved in infinite time, it is important to establish the minimum duration of the experimental tests required to achieve equilibrium conditions, *i.e*., until the scouring rate becomes insignificant or practically null and scour depth is close enough to its ultimate value. In this direction, Melville and Chiew (1999) assumed the time to achieve equilibrium scour to be the time at which the rate of scouring reduces to 5% of the pier diameter in the succeeding 24-hour period. Coleman *et al*. (2003) defined the equilibrium time as the time at which the rate of scour reduces to 5% of the smaller of the pier diameter or the flow depth in the succeeding 24-hour period. More recently, Sheppard *et al*. (2011) recommend the use of equation (2.16) to estimate the time duration of the tests. This equation provides longer test durations than it may be obtained with the discussed 5% criterion. Furthermore, Lança *et al*. (2010), Simarro *et al*. (2011) and Lança *et al*. (2013b) have suggested that the tests must be performed at least during 7 days.

According to Lança *et al*. (2010) and Simarro *et al*. (2011), the extrapolation to infinite time of at least seven-day-long scour depth records, adjusted by a six-parameter polynomial function (equation (2.18)) or a three-parameter exponential function (equation (2.19)), renders robust values of the equilibrium scour depth, d_{se}, at single cylindrical piers. The six-parameter polynomial function corresponds to an extension of Bertoldi and Jones (1998) equation as suggested by Lança *et al*. (2010), thus

$$d_s(t) = d_1\left(1 - \frac{1}{1 + d_1 c_1 t}\right) + d_2\left(1 - \frac{1}{1 + d_2 c_2 t}\right) + d_3\left(1 - \frac{1}{1 + d_3 c_3 t}\right) \tag{2.18}$$

where d_s is the scour depth at instant t and d_1, c_1, d_2, c_2, d_3 and c_3 are parameters obtained by regression analysis. The equilibrium scour depth is obtained for $t = \infty$ when $d_{se} = d_1 + d_2 + d_3$.

The three-parameter exponential function corresponds to the equation proposed by Franzetti *et al.* (1982)

$$d_s(t) = d_{se}\left[1 - exp\left(-a_1\left[\frac{Ut}{D}\right]^{a_2}\right)\right] \quad (2.19)$$

where d_s is the scour depth at instant t, the parameters d_{se}, a_1 and a_2 are obtained by regression analysis.

2.2.5 EFFECTS OF SPECIFIC PARAMETERS ON MAXIMUM LOCAL SCOUR DEPTH

2.2.5.1 Framework

This section is dedicated to discuss the different effects that influence the equilibrium scour depth, *i.e.*, the first seven parameters of equation (2.13). Those parameters are: (1) flow intensity effect, represented by U/U_c ratio; (2) sediment grading effect, represented by σ_g; (3) sediment coarseness effect, represented by D/d_{50} ratio; (4) flow shallowness effect, represented by h/D ratio; (5) viscosity effect, represented by $u_* d_{50}/\nu$; (6) pier shape effect, represented by K_S; and (7) pier alignment effect, represented by K_θ.

Large quantities of laboratory tests were performed in order to analyse these seven effects. From the published data and compiled by the present author, more than 1200 tests correspond to clear-water conditions and more than 650 tests correspond to live-bed conditions. Some of the tests performed under clear-water conditions were carried out for short durations as compared to the time needed to sufficiently approach the equilibrium phase. In fact, only 84 tests (approximately 7% of the compiled data) have durations higher than 7 days (time predefined in section 2.2.4). Most of those were performed in Portugal (Simarro *et al.*, 2011; Lança *et al.*, 2013b; Fael *et al.*, 2014). In the following sections, not only those 84 tests but also tests under clear-water conditions with durations between three and seven days will be taken into account in the analysis of the mentioned six effects. In this analysis some tests performed under live-bed conditions are also considered.

All figures presented in the following sections (2.2.5.2 to 2.2.5.8), characterizing the influence of the seven effects on the equilibrium scour depth, were elaborated by the present author taking into account the selected data from literature.

2.2.5.2 Flow intensity effect

As mentioned in section 2.1, local scour at bridge piers can occur under clear-water or live-bed conditions. According to the early work of Chabert and Engeldinger (1956) and latter works such as Melville and Coleman (2000), clear-water scour occurs for $U < U_c$, for which there is no supply of sediment to the scour hole from upstream. Live-bed scour occurs when sediment is continuously supplied to the scour hole and d_{se} is attained when there is a balance between the sediment supply and that transported out of the hole. The effect of those sediment transport stages (represented by the ratio U/U_c) on the equilibrium scour depth is also reported as "flow intensity effect". Figure 2.8 plots d_{se}/D as a function of U/U_c for laboratory data with cylindrical piers, coarse sands ($d_{50} \geq 0.6$ mm),

uniform material ($\sigma_g \leq 1.50$), $30 \leq D/d_{50} \leq 100$ and $h/D \geq 2$. The data with these experimental conditions were selected in order to minimize the influence of other effects. The figure includes data by Ettema (1976, 1980), Jain and Fischer (1979), Chee (1982), Chiew (1984), Melville (1984), Ettema *et al*. (1998a), Melville and Chiew (1999), Lee and Sturm (2009), Simarro *et al*. (2011), Lança *et al*. (2013b), Lopez *et al*. (2014) and unpublished data by Jones (reported by Sheppard *et al*., 2011).

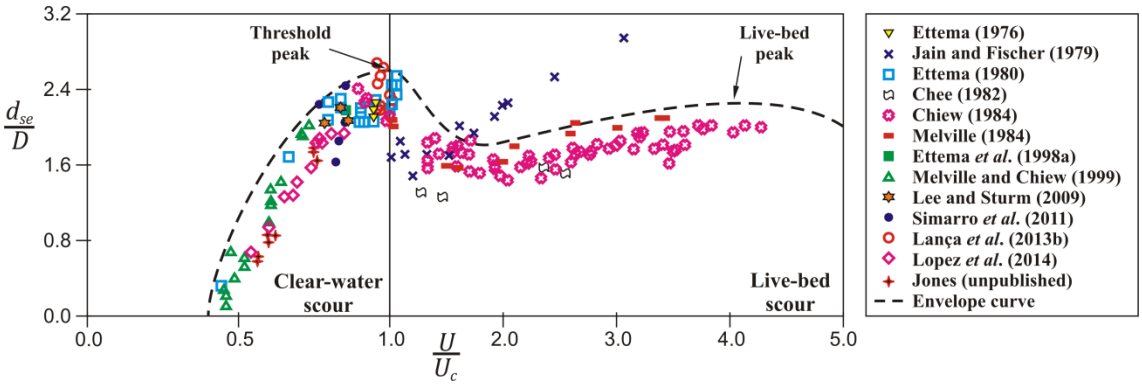

Figure 2.8 – Equilibrium scour depth as a function of velocity, for comparatively coarse uniform bed sediment

For very low velocities, scour does not develop around obstacles and the bed behaves as if it was fixed. According to Melville and Chiew (1999), the scouring process begins long before the approach velocity is strong enough to initiate sediment transport, at about 40% of the threshold velocity of the bed sediment, as shown in Figure 2.8. In clear-water conditions, the relative scour depth, d_{se}/D, increases as the relative approach velocity, U/U_c, is increased until the former reaches a maximum of about 2.6 times the pier diameter at critical velocity, *i.e.*, $U/U_c = 1$. The maximum scour depth is called the threshold peak. According to Melville (2008), in live-bed conditions, after $U/U_c > 1$, d_{se}/D first decreases with the relative approach velocity and then increases again to a second peak, these changes being relatively small, but the threshold peak is not exceeded providing the sediment is uniform. The second peak occurs at about the transition flatbed stage of sediment transport on the channel bed and is termed the live-bed peak, as shown in Figure 2.8 (represented by the envelope curve in the range $1 < U/U_c < 5$). The scour depth variations under live-bed conditions are a consequence of the size and steepness of the bed features occurring at particular flow velocities (Chee, 1982; Chiew, 1984; Melville, 1984). The steeper and higher the bed forms, the lesser the observed scour depth because the sediment supplied with the passage of a given bed form is not fully removed from the scour hole prior to the arrival of the next bed form. The live-bed peak occurs at about the transition flatbed condition when the bed forms are very long and of negligible height. Antidunes dissipate some energy at higher velocities and the local scour depth appears to decrease again. The magnitude of the scour depth fluctuations due to bed-form migration is approximately equal to the half-amplitude of the bed forms, indicating that the scour depth due to bed forms is about one-half the bed-form height (Chee, 1982; Chiew, 1984).

The higher values of d_{se}/D obtained by Jain and Fischer (1979) for the range $2.0 < U/U_c < 3.5$ in comparison to the corresponding values for the other three live-bed studies considered (Chee, 1982; Chiew, 1984; Melville, 1984) (Figure 2.8) may be associated to differences in the scour measuring technique used in the studies.

2.2.5.3 Sediment grading effect

Variations of the particle size distribution of the bed sediment (*i.e.*, $\sigma_g = \sqrt{d_{84}/d_{16}}$) can have a significant influence on equilibrium scour depths around bridge piers. Ettema (1976) and Chiew (1984) carried out tests under clear-water conditions for different values of σ_g in order to evaluate the effect of nonuniform sediments on d_{se}/D. Both researchers observed a decrease in d_{se}/D values with increasing values of σ_g. The reduction in scour depths is attributed to armouring of the scour hole by coarser particles in the original bed mixture. Figure 2.9(a) plots d_{se}/D as a function of σ_g for laboratory data obtained from some researchers with cylindrical piers, $d_{50} \geq 0.6$ mm, $h/D \geq 2$, $0.8 \leq U/U_c \leq 1.0$ and $30 \leq D/d_{50} \leq 100$. The data with these experimental conditions were selected in order to minimize the influence of other effects. The figure includes data by Ettema (1976, 1980), Chiew (1984), Melville and Chiew (1999), Lee and Sturm (2009), Simarro *et al*. (2011) and Lança *et al*. (2013b). According to Figure 2.9(a), d_{se}/D decreases with σ_g for $\sigma_g > 1.50$ until a minimum value of approximately 0.48 for $\sigma_g = 5.5$. The relative equilibrium scour depth, d_{se}/D, may be considered constant for $\sigma_g \leq 1.50$. For nonuniform bed mixtures ($\sigma_g > 1.50$), selective sediment transport of the finer particles typically occurs for flow velocities smaller than the critical velocity of beginning of motion associated with d_{50}. The selective sediment transport leads to the formation of a superficial armour layer composed of the courser grains that finally inhibits sediment transport as well as the formation of scour holes (at least partly). Consequently, the maximum scour depth is not observed for $U \approx U_c$, where U_c is the critical velocity associated with the median size grains, d_{50}, of the mixture. In those cases, the maximum scour depth is observed for the live-bed peak (Figure 2.8), where the velocity triggers the rupture of the armour layer guaranteeing the displacement of the coarse grains.

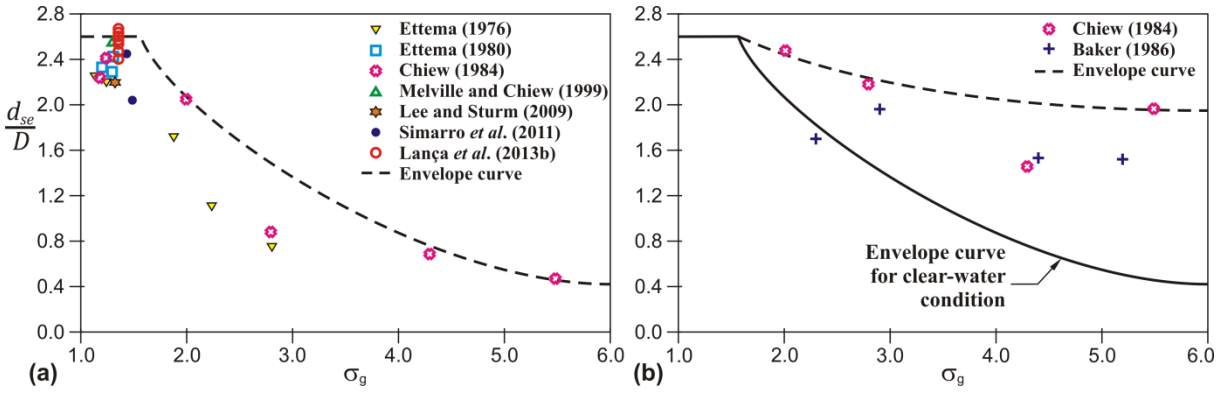

Figure 2.9 – Equilibrium scour depth as a function of the geometric standard deviation of sediment sizes for tests under: (a) clear-water conditions and (b) live-bed conditions

Figure 2.9(b) shows the results of the studies conducted by Chiew (1984) and Baker (1986) under live-bed conditions. The values of d_{se}/D plotted in the figure correspond to values observed at the live-bed peak. In the figure a decrease in d_{se}/D values with increasing values of σ_g is again observed; however, this effect is not as marked as in the case of clear-water conditions, represented by the envelope curve of Figure 2.9(a).

2.2.5.4 Sediment coarseness effect

The effect of relative sediment size (defined by the ratio D/d_{50}) on the equilibrium scour depth is also reported as "sediment coarseness effect". For several decades, most researchers (*e.g.*, Raudkivi and Ettema, 1983; Melville and Sutherland, 1988; Melville and Coleman, 2000) have successively assumed that d_{se}/D would be unaffected by D/d_{50} for values of $D/d_{50} > 100$. This may be justified by the fact that the tests in these studies were performed for a narrow range of D/d_{50}. In the last decade, studies by Sheppard *et al*. (2004, 2014), Lee and Sturm (2009), Sheppard and Renna (2010) and Lança *et al*. (2011, 2013b) have shown that the relative sediment size can significantly affect the scour depth even for $D/d_{50} > 100$. The tests of these studies were performed for large values of D/d_{50} (up to 4168). According to these studies, d_{se}/D decreases with increasing D/d_{50}, for $D/d_{50} > 100$, as shown in Figure 2.10. This figure plots d_{se}/D as a function of D/d_{50} for laboratory data with cylindrical piers, $\sigma_g \leq 1.50$, $0.8 \leq U/U_c \leq 1.0$ and $h/D \geq 2$. The data with these experimental conditions were selected in order to minimize the influence of other effects. The figure includes data by Ettema (1976, 1980), Chiew (1984), Ettema *et al*. (1998a), Sheppard *et al*. (2004), Lee and Sturm (2009), Simarro *et al*. (2011) and Lança *et al*. (2013b). Due to experimental limitations, *i.e.*, dimensions of laboratory facilities, a small number of tests that comply with the mentioned experimental conditions for $D/d_{50} > 300$ can be observed. For this reason, in this range, experimental data with fine sands ($d_{50} < 0.6\,mm$) and coarse sands with $1.0 \leq h/D \leq 1.5$ are also included in the figure for completeness (pointed out by two ellipses, respectively).

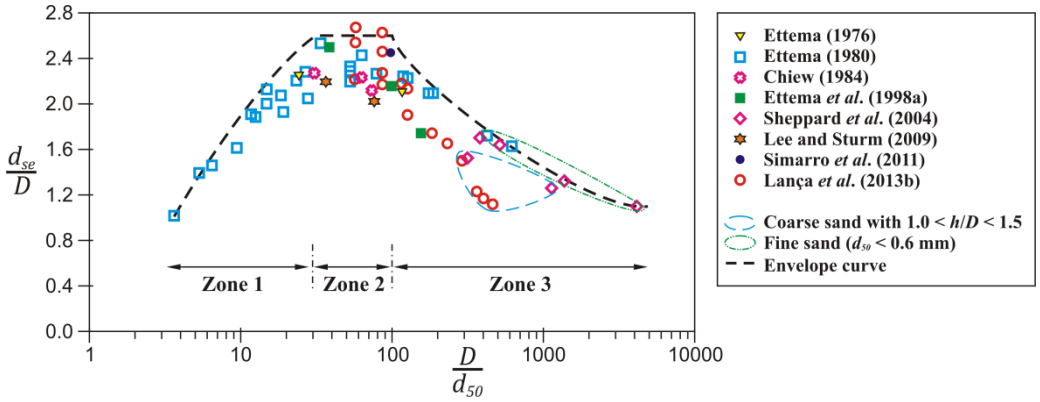

Figure 2.10 – Equilibrium scour depth as a function of bed material size

Figure 2.10 shows that the maximum scour depth occurs in the range of $30 < D/d_{50} < 100$ in which the material size does not influence the scour depth. According to the envelope curve of the scour data plotted in Figure 2.10, the effect of D/d_{50} on local scour depth can be identified and separated in three zones. In Zone 1 ($D/d_{50} < 30$) the sediment is coarse relative to pier diameter. A significant proportion of the energy of the downflow is dissipated in the coarse bed material at the base of the scour hole. In Zone 2 ($100 > D/d_{50} > 30$) the sediment is of an intermediate size. The sediment is entrained mainly from the groove with only a limited entrainment under the horseshoe vortex. The supply of sediment to the groove is accomplished by sliding down the lateral slope in the hole. In Zone 3 ($D/d_{50} > 100$) the sediment is fine relative to pier diameter. The sediment is entrained from the groove by the downflow and from the hole slope by the horseshoe vortex until equilibrium is reached. These definitions were based on zone descriptions by Raudkivi and Ettema (1983).

2.2.5.5 Flow shallowness effect

The effect of the approach flow depth in relation to the pier size (defined by the ratio h/D) on the equilibrium scour depth is also reported as "flow shallowness effect". Melville and Coleman (2000) compiled the experimental data of several researchers (some of these data for short durations) to study the effect of h/D on d_{se}/D. According to results of those studies, Melville and Coleman (2000) suggest that for shallow flows compared to the pier size (wide piers), the scour depth increases proportionately with the flow depth and is independent of the pier size. Conversely, for deep flows compared to the pier size (narrow piers), the scour depth increases proportionately with pier size and is independent of the flow depth; while for intermediate depth flows, the scour depth depends on both flow depth and pier size. These three trends are clearly defined by the envelope curve of the experimental data in Figure 2.11, where wide piers are characterized by $h/D < 0.2$ while narrow piers are associated to $h/D > 2.0$. The figure plots d_{se}/D as a function of h/D for laboratory data with cylindrical piers, $d_{50} \geq 0.6$ mm, $\sigma_g \leq 1.50$, $0.8 \leq U/U_c \leq 1.0$ and $30 \leq D/d_{50} \leq 100$. The data with those experimental conditions were selected in order to minimize the influence of other effects. The figure includes data by Ettema (1980), Chiew (1984), Graff (1995), Ettema *et al*. (1998a), Melville and Chiew (1999), Sheppard *et al*. (2004), Lee and Sturm (2009), Simarro *et al*. (2011), Lança *et al*. (2013b) and unpublished data by Coleman (reported by Sheppard *et al*., 2011). Due to the limited number of tests that comply with the mentioned conditions for $h/D < 0.5$, tests with coarse sands and $D/d_{50} > 300$ are also included in the figure for completeness (pointed out by an ellipse).

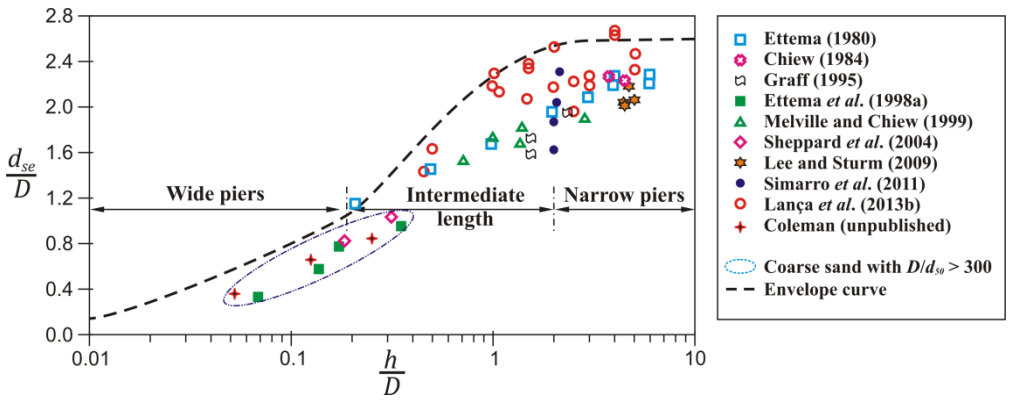

Figure 2.11 – The influence of flow shallowness on equilibrium scour depth

According to Melville (2008), the scour process at wide piers features a zone of slow moving fluid existing ahead of the pier on the line of symmetry. In this zone, scour activity is reduced and the central portion of the width of the pier is ineffective in generating scour. In deeper flows, the strength of the horseshoe vortex and associated downflow is related to the transverse size of the pier. For intermediate size piers (or intermediate flow depths), flow depth influences local scour depth when the horseshoe vortex is affected by the formation of the surface roller. The two vortices have opposite directions of rotation. In principle, so long as they do not interfere with each other, the local scour depth is independent of flow depth, which is the case of narrow piers. With decreasing flow depth, the surface roller becomes more dominant and renders the horseshoe vortices less capable of entraining sediment. Thus, the local scour depth is reduced for shallower flows.

2.2.5.6 Viscosity effect

Most of the important works on local scouring at single piers (*e.g.*, Ettema, 1980; Chiew, 1984; Melville and Chiew, 1999; Oliveto and Hager, 2002; Sheppard *et al.*, 2004; Lança *et al.*, 2013b) do not consider the influence of viscosity on their experiments. The assumption seems to be that the flow is fully rough turbulent inside the scour hole, *i.e.*, free of viscous effects, due to the presence of highly turbulent flow structures irrespective of the approach flow regime. In contrast, few studies (Shen *et al.*, 1969; Nicollet and Ramette, 1971; Lança *et al.*, 2015) indicate that the equilibrium scour depth depends on the pier Reynolds number, UD/υ, or on the sediment Reynolds number, Ud_{50}/υ, parameters that consider the effect of viscosity.

Figure 2.12 plots d_{se}/D as a function of Ud_{50}/υ for laboratory data obtained by Nicollet and Ramette (1971) and Lança *et al.* (2013b, 2015) with cylindrical piers, $d_{50} \geq 0.6$ mm, $h/D \geq 1.5$ and $30 \leq D/d_{50} \leq 100$. The data with these experimental conditions were selected in order to minimize the influence of other effects. The data obtained by Shen *et al.* (1969) were not considered by the fact that these have a strong influence of sediment coarseness parameter, since $D/d_{50} = 633$. The figure shows (1) that scouring is independent of the sediment Reynolds number for $200 < Ud_{50}/\upsilon < 300$ and (2) a slight decrease of the dimensionless scour depth as the sediment Reynolds number increases for $Ud_{50}/\upsilon > 300$. In turn, a slight increase of d_{se}/D with increase h/D is observed.

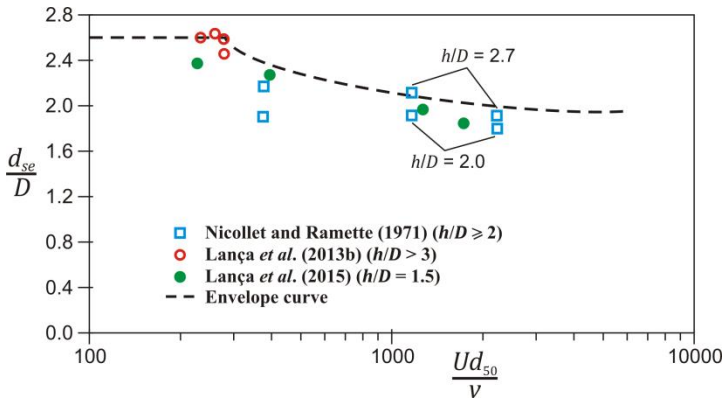

Figure 2.12 – Equilibrium scour depth as a function of the sediment Reynolds number

2.2.5.7 Pier shape effect

The shape effect is usually accounted for through the coefficient K_S that is the ratio between the maximum scour depth at a pier of a given shape and the maximum scour depth at the cylindrical pier (standard obstacle) for otherwise equal conditions of the approach flow and bed material. Figure 2.13 shows the comparison of the scour holes around two piers, each with different shape, measured in tests with the same bed granulometry and flow conditions. Figure 2.13(a) corresponds to the case of a cylindrical pier and Figure 2.13(b) corresponds to the case of a square pier. According to those results, both the area of the scour hole and the maximum scour depth have higher values for the square pier compared to the cylindrical pier. This is due to the fact that the square pier shape: (1) alters significantly more the surrounding streamlines of the flow around the obstacle; and (2) slightly increases the magnitude of the downflow, the size of the horseshoe vortex and the vorticity, as compared with the cylindrical pier shape. The maximum scour depth observed at the square pier (Figure 2.13(a)) is approximately 1.23 times the corresponding depth at the cylindrical pier (Figure 2.13(b)).

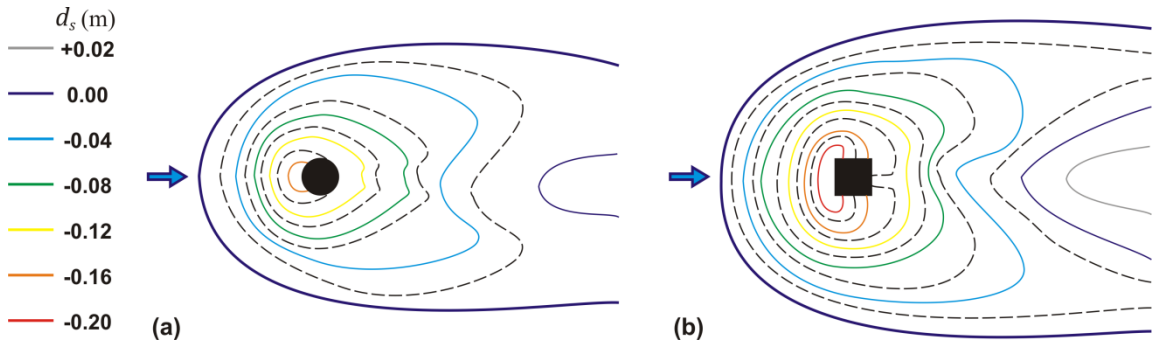

Figure 2.13 – Scour holes around different pier shapes: (a) cylindrical pier (adapted from Rey and Raikar, 2007) and (b) square pier (adapted from Raikar and Dey, 2008)

Factors to account for pier shapes other than cylindrical have been published by many researchers (*e.g.*, Tison, 1940; Chabert and Engeldinger, 1956; Laursen and Toch, 1956; Dietz, 1972; Diab, 2011; Fael *et al.*, 2014). Figure 2.14 shows the variation of shape factors K_S with the relation L/D (L = pier length) for four common pier shapes: (1) rectangular (Figure 2.14(a)); (2) rectangular round-nose or oblong (Figure 2.14(b)); (3) lenticular (Figure 2.14(c)); and (4) elliptic (Figure 2.14(d)).

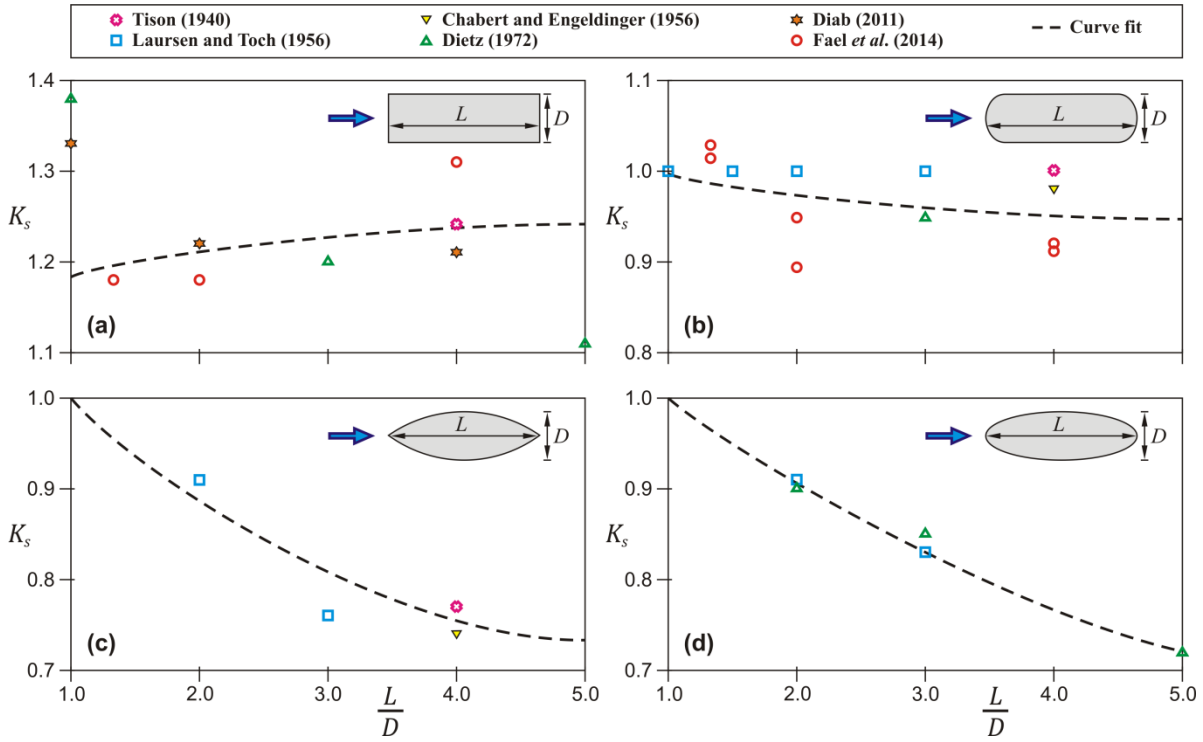

Figure 2.14 – Shape factor (K_S) as a function of L/D for: (a) rectangular piers, (b) rectangular round-nose or oblong piers, (c) lenticular piers and (b) elliptic piers

The values apply to piers aligned with the flow and are referenced to a value of $K_S = 1.0$ for cylindrical piers. The curve fit of the experimental data is also included in each figure. It is clear that the influence of L/D on the estimation of factor K_S is minor for rectangular (square-nose) and

rectangular round-nose pier shapes and is higher for lenticular and elliptic pier shapes. Values of the factor K_S for other shape piers (not so common) were compiled by Melville and Coleman (2000).

2.2.5.8 Pier alignment effect

The effect of pier alignment is important when the shape of the pier is different from cylindrical. The alignment angle, θ, corresponds to the angle defined between the pier axis and the flow direction at a plane parallel to the channel bottom, as shown in Figure 2.5. The two schemes in Figure 2.15 represent the scour hole formed around one rectangular pier aligned to the same direction of the flow and another scour hole formed around the same pier but oriented in an angle θ with the flow direction.

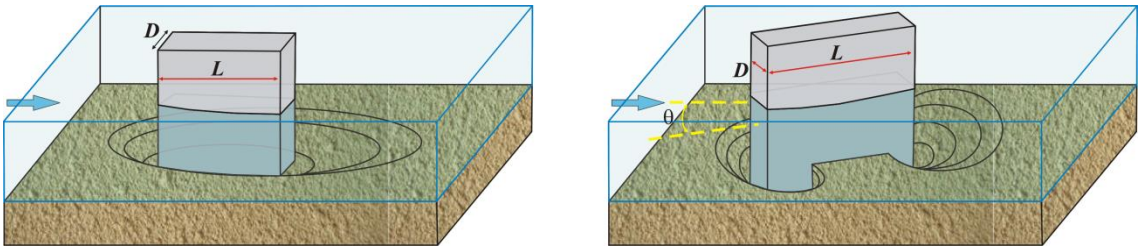

Figure 2.15 – Schemes of the scour hole in relation with the pier alignment angle

Figure 2.16 shows diagrams of scour hole around rectangular piers oriented in different angles to flow direction. The shape of the hole is a function of pier orientation angle and L/D ratio. The point of maximum depth changes with the variation of the pier orientation angle. According to Ettema *et al.* (1998b) the scour process starts at locations of greatest velocity and vorticity at the pier corners, and then envelops the entire pier.

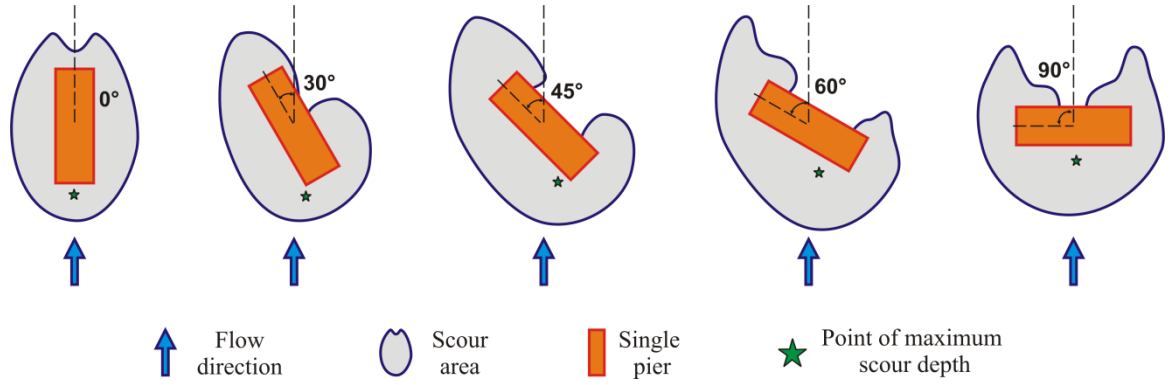

Figure 2.16 – Diagrams of scour hole around rectangular piers oriented in different angles to flow direction

The effect of the alignment angle of bridge piers in the scour depth developed around those piers has been initially evaluated by Laursen and Toch (1956). This effect is considered through the alignment factor, K_θ. This factor relates the scour depth associated to a given θ with the scour depth at the same pier for θ = 0º. The pier alignment factors (K_θ) obtained by Ettema *et al.* (1998b) and Fael *et al.* (2014), for rectangular piers with different angles and L/D ratios, are presented in Figure 2.17.

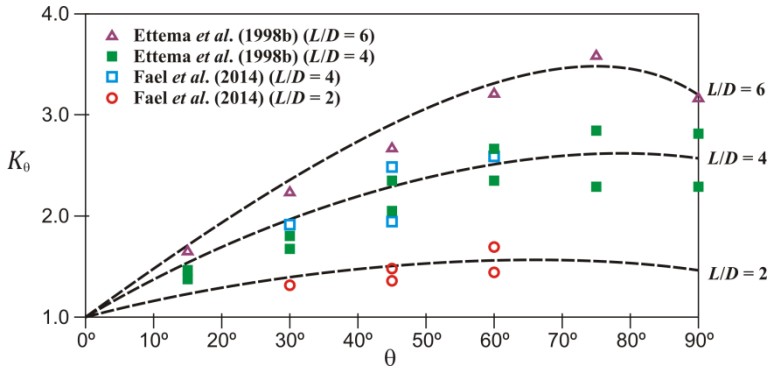

Figure 2.17 – Local scour depth variation with pier alignment (rectangular piers)

From Figure 2.17, it is evident that K_θ increases when L/D increases. This may be justified by the fact that the area of the pier exposed to the flow, for a particular angle, increases for larger L/D ratios. In turn, for each L/D ratio, the factor K_θ increases with increasing θ until K_θ attains a maximum value. According to Ettema *et al.* (1998b), a maximum occurs when the projected width of the pier is largest, which occurs when $\theta = tan^{-1}(L/D)$ for a skewed rectangular pier.

2.2.6 METHODS FOR ESTIMATION OF LOCAL SCOUR DEPTHS

2.2.6.1 Auckland Method

Melville and Coleman (2000) compiled the information of some researchers, most of those from the Auckland University (*e.g.*, Ettema, 1976; Raudkivi and Ettema, 1977; Breusers *et al.*, 1977; Ettema, 1980; Raudkivi and Sutherland, 1981; Chee, 1982; Chiew, 1984; Raudkivi, 1986), and formulated a method to predict the maximum scour depth at pier foundations (*i.e.* abutments, single piers, nonuniform piers). The method is based in the design method proposed by Melville and Sutherland (1988), established on the basis of a large set of experimental data that included wide variations in flow velocity and depth, sediment size and gradation, and pier size, shape, and alignment. According to Melville and Coleman (2000) the design method is supported on the following relation for the equilibrium depth of local scour:

$$d_{se} = K_{hD} K_I K_d K_S K_\theta \tag{2.20}$$

where d_{se} = equilibrium scour depth; K_{hD}, K_I, K_d, K_S and K_θ are the factors that account for the depth-pier size, flow intensity, sediment coarseness, pier shape, and pier alignment, respectively. Variables d_{se} and K_{hD} correspond dimensionally to a length, while the other K's are dimensionless.

The depth-pier size factor can be expressed by the following expression:

$$K_{hD} = \begin{cases} 2.4D & \text{for } \dfrac{h}{D} > 1.43 \\ 2\sqrt{D \times h} & \text{for } 0.2 < \dfrac{h}{D} < 1.43 \\ 4.5h & \text{for } \dfrac{h}{D} < 0.2 \end{cases} \tag{2.21}$$

where D = single pier width; h = flow depth directly upstream of the pier.

The flow intensity factor can be expressed by the following equation:

$$K_I = \begin{cases} \frac{U}{U_c} & \text{for } \frac{U}{U_c} < 1 \\ 1.0 & \text{for } \frac{U}{U_c} \geq 1 \end{cases} \quad (2.22)$$

where U = mean velocity of flow directly upstream of the pier; U_c = critical flow velocity.

The sediment coarseness factor can be expressed by the following equation:

$$K_d = \begin{cases} 0.57log\left(2.24\frac{D}{d_{50}}\right) & \text{for } \frac{D}{d_{50}} \leq 25 \\ 1.0 & \text{for } \frac{D}{d_{50}} > 25 \end{cases} \quad (2.23)$$

where d_{50} = median size of sediment particle size distribution.

The pier shape factor should be estimated according to Figure 2.14 for rectangular, oblong, rectangular round-nose, lenticular and elliptic shapes. For cylindrical shape, K_S should be considered as 1.0. The pier alignment factor can be calculated by:

$$K_\theta = \left(\frac{L}{D}sin\theta + cos\theta\right)^{0.65} \quad (2.24)$$

where θ = pier alignment angle; L and D are the dimensions of the pier. For circular piers, $K_\theta = 1.0$. If L/D is larger than 12, the value of L/D = 12 should be used in equation (2.24).

According to experimental data reported in section 2.2.5, the Auckland method provides higher values of factor K_I for clear-water conditions and it does not consider the reduction effect on factor K_d for $D/d_{50} > 100$.

2.2.6.2 FDOT Method

Sheppard and Renna (2010) presented a method to predict the maximum scour depth at single piers for the Florida Department of Transportation (FDOT). This method is based on different studies developed by Sheppard at Florida University since 1995 (*e.g.*, Sheppard, 1999; Pritsivelis, 1999; Jones and Sheppard, 2000b; Sheppard *et al*., 2000, 2004). These studies were performed with experimental tests in four different Laboratories (three in US: University of Florida in Gainesville, Florida, Colorado State University in Fort Collins, Colorado, and the Conte USGS-BRD Laboratory in Turners Falls, Massachusetts; the fourth, University of Auckland in Auckland, New Zealand). According to Sheppard *et al*., (2014), the scour depth predictor in clear-water conditions is:

$$\frac{d_{se}}{D_e} = 2.5K_{hD_e}K_IK_d \quad (2.25)$$

where d_{se} = equilibrium scour depth; D_e = equivalent diameter of the pier; K_{hD_e} = flow shallowness factor; K_I = flow intensity factor; K_d = sediment size factor.

The scour at single structures with shapes different from the circular can be analysed using their "equivalent diameter", D_e. The equivalent diameter is the diameter of a circular pier that will experience the same equilibrium scour depth of the single pier in study under the same sediment and flow conditions. This is defined as:

$$D_e = K_S W_p \tag{2.26}$$

where K_S = pier shape factor; W_p = projected width of the pier. The variable K_S can be calculated by

$$K_S = \begin{cases} 1 & \text{for circular piers} \\ 0.86 + 0.97\left(\left|\theta - \frac{\pi}{4}\right|\right)^4 & \text{for rectangular piers} \end{cases} \tag{2.27}$$

where θ = flow skew angle in radians.

The flow shallowness factor can be expressed by the following expression

$$K_{hD_e} = \tanh\left[\left(\frac{h}{D_e}\right)^{0.4}\right] \tag{2.28}$$

where h = flow depth directly upstream of the pier.

The flow intensity factor can be expressed by the following expression

$$K_I = 1 - 1.2\left[\ln\left(\frac{U}{U_c}\right)\right]^2 \qquad \text{for } 0.4 < \frac{U}{U_c} \leq 1 \tag{2.29}$$

where U = mean velocity of the flow directly upstream of the pier; U_c = critical flow velocity.

The sediment coarseness factor can be expressed by the following equation

$$K_d = \frac{\left(\frac{D_e}{d_{50}}\right)}{0.4\left(\frac{D_e}{d_{50}}\right)^{1.2} + 10.6\left(\frac{D_e}{d_{50}}\right)^{-0.13}} \tag{2.30}$$

where d_{50} = median size of sediment particle size distribution.

2.2.6.3 HEC-18 Method

The HEC-18 method was developed by the Hydrologic Engineering Center of the Federal Highway Administration (FHWA) in the United States of America. This method is based on the laboratory data of circular piers by Chabert and Engeldinger (1956) and Shen *et al*. (1969). HEC-18 method has been modified by Richardson and Davis (1995, 2001) and Arneson *et al*. (2012). The equation for

maximum local pier scour under clear-water recommended by the FHWA, Circular HEC-18 (Arneson *et al*., 2012), is stated as:

$$\frac{d_{se}}{D} = 2.0 K_S K_\theta K_{bc} K_w \left(\frac{h}{D}\right)^{0.35} \mathrm{Fr}^{0.43} \tag{2.31}$$

where d_{se} = equilibrium scour depth; D = pier width; K_S = pier shape factor; K_θ = pier alignment factor; K_{bc} = correction factor for bed forms; K_w = correction factor for wide piers; h = flow depth directly upstream of the pier; $\mathrm{Fr} = U/\sqrt{gh}$ is the Froude number directly upstream of the pier; U = mean velocity of flow directly upstream of the pier; g = gravitational acceleration. In this method the influence of bedforms on the equilibrium scour depth is considered, effect not taken into account in the other two methods (Auckland and FDOT).

The correction factor K_S for pier shape should be determined as: $K_S = 1.0$ for circular and round-nosed shapes; $K_S = 1.1$ for square-nosed shapes; and $K_S = 0.9$ for sharp-nosed shapes. The pier alignment factor can be estimated according to equation (2.24) for non-cylindrical piers. For circular piers, K_θ assumes the value 1.0. For higher values of the angles ($\theta > 5°$), K_θ dominates and K_S should be considered as 1.0

The bed condition factor should be estimated using Table 2.1. This factor results from the fact that for plane-bed conditions, which is typical of most bridge sites for the flood frequencies employed in scour design, the maximum scour may be 10 percent greater than computed with Equation (2.31). In the unusual situation where a dune bed configuration with large dunes exists at a site during flood flow, the maximum pier scour may be 30 percent greater than the predicted equation value. This may occur on very large rivers, such as the Mississippi. For smaller streams that have a dune bed configuration at flood flow, the dunes will be smaller and the maximum scour may be only 10 to 20 percent larger than equilibrium scour. For antidune bed configuration the maximum scour depth may be 10 percent greater than the computed equilibrium pier scour depth (Arneson *et al*., 2012).

Table 2.1 – Bed condition factors

Bed condition	Dune height (m)	K_{bc}
Clear-Water Scour	-	1.1
Plane bed and Antidune flow	-	1.1
Small Dunes	$\mathbf{0.6 \leq H_d < 3.0}$	1.1
Medium Dunes	$3.0 \leq H_d < 9.0$	1.1 to 1.2
Large Dunes	$H_d \geq 9.0$	1.3

In general, the wide piers factor is equal to 1.0; nevertheless, this factor should be changed when: $h/D < 0.8$, $D/d_{50} > 50$ and the Froude Number of the flow is subcritical. This factor can be estimated by the following equation:

$$K_w = 2.58 \left(\frac{h}{D}\right)^{0.34} \mathrm{Fr}^{0.65} \tag{2.32}$$

In accordance with Ettema *et al*. (2011) the HEC-18 method has the following limitations:

- The Froude number dependence expressed in Equation (2.31) may be valid when comparing results for the same bed materials, but not when comparing different bed materials;
- The parameter D/d_{50} is missing from Equation (2.31). Consequently, this equation does not expressly reflect several significant effects of bed particle size, including the parameter's influence on flow-field vorticity, an important aspect driving scour;
- The veracity of factor K_w in Equation (2.31) is uncertain.

2.3. LOCAL SCOUR AROUND COMPLEX PIERS

2.3.1 FLOW STRUCTURE

At complex piers, the flow structure and its interaction with the mobile bed are rather more complex than at single piers. As mentioned in section 2.2.1, numerous studies have been performed to examine the flow structure around single piers (cylindrical shape mostly), while few studies are known for the case of complex piers. Some researchers studied the flow structure around pile groups, corresponding to complex piers caped above the water surface. The studies included those of Hannah (1978), Usera *et al*. (2010), Ataie-Ashtiani and Aslani-Kordkandi (2012), Movahedi *et al*. (2013) and Chang *et al*. (2013). According to those studies, scour around pile groups is caused by two types of flow structures: (1) those causing local scour at individual piles, *i.e*., downflow, horseshoe vortex, wake vortices and the bow wave; and (2) those due to the interaction of the different piles. According to Hannah (1978), four mechanisms that are not present in scouring at single piers were identified in pile groups:

1. Scour reinforcement: The flatter bed topography induced by the rear piles may facilitate the mobility of upcoming bed grains, thus reinforcing the scour depth at the upstream piles, as compared with the scour depth at an isolated equal diameter pier. This effect tends to attenuate as the pile spacing increases.
2. Sheltering: The presence of an upstream pile can cause a reduction of the effective approach velocity for downstream piles, weakening the strength of the associated horse-shoe vortices and reducing the scour depth at downstream piles. As pile spacing increases the sheltering effect tends to become negligible.
3. Wake vortices interaction: The vortices from the upstream piles are convected downstream and may interact with the rear piles. In this case, the interaction of wake vortices may lead to a downstream increase in sediment entrainment capacity. The scour increase caused by this phenomenon depends on the convection speed of the vortices and the distance between their path and the piles. At specific skew-angles, the rear piles are closer to the most energetic paths traced by the wake vortices from the front piles and scour increases.
4. Compressed horse-shoe vortices: In pile group alignments with at least two columns of piles transverse to the approach flow, except at very close spacing, each pile has its own horse-shoe vortex. As pile spacing decreases, the inner arms of the horse-shoe vortices are compressed, velocities within the arms increase and scour depths tend to increase.

Figure 2.18 shows a present author interpretation of the flow structure and local scour around a pile group in a scoured-bed according to previous descriptions.

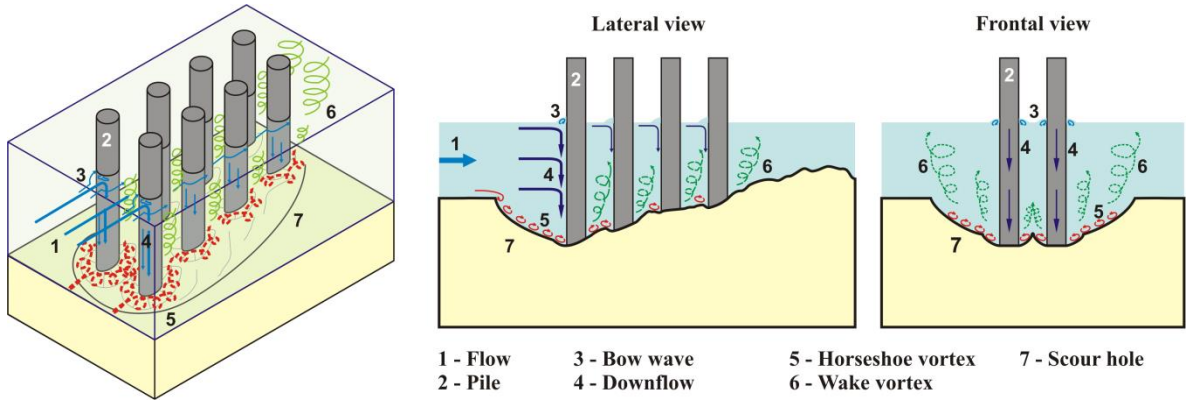

Figure 2.18 – Scheme of flow structure and local scour around pile groups

Lagasse *et al*. (2010) and Pagliara and Carnacina (2011) studied the flow structure around a single pier with a rectangular debris cluster, which may be very similar to the flow pattern around complex piers with the pile cap partially immersed in the flow. They concluded that the flow is significantly obstructed and forced to plunge beneath the upstream face of the debris. As the flow beneath the debris approaches the pier, the diving and spiral horseshoe patterns are still observed. Figure 2.19(a) shows the flow image for one of the tests performed by Pagliara and Carnacina (2011), in which the horseshoe, the downflow and the stream lines above the downstream mound formed are represented.

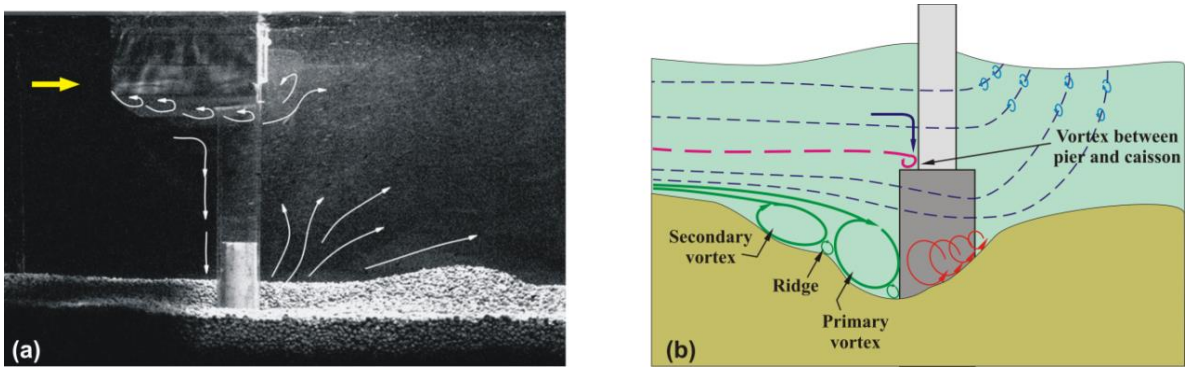

Figure 2.19 – Flow structure around: (a) a rectangular debris cluster (adapted from Pagliara and Carnacina 2011) and (b) pier with caisson (adapted from Veerappadevaru *et al*. 2011)

Veerappadevaru *et al*. (2011, 2012), Kumar and Kothyari (2012) and Kumar *et al*. (2012) studied the flow structure around cylindrical columns founded on cylindrical caissons. The results of these studies show that the scour depth depends on the temporal vortex strength. In the cases where the caisson is partially buried in the initial bed level, the scour hole is formed in front and around the caisson pier by vortices wrapping around it. Two main vortices exist upstream from the caisson pier (primary and secondary vortex), as illustrated in Figure 2.19(b). The primary vortex causes scour near the caisson pier and the scoured sediment is transported either as suspended or as bed load towards the tail water. The secondary vortex supports the steep slope of the scour hole and transports most dislodged sediment sideways but few are entrained by the primary vortex (Veerappadevaru *et al*. 2011).

Figure 2.20 shows a present author interpretation of the flow structure around a complex pier based on previous descriptions of flow structure around pile groups, single piers with debris and pier-caissons.

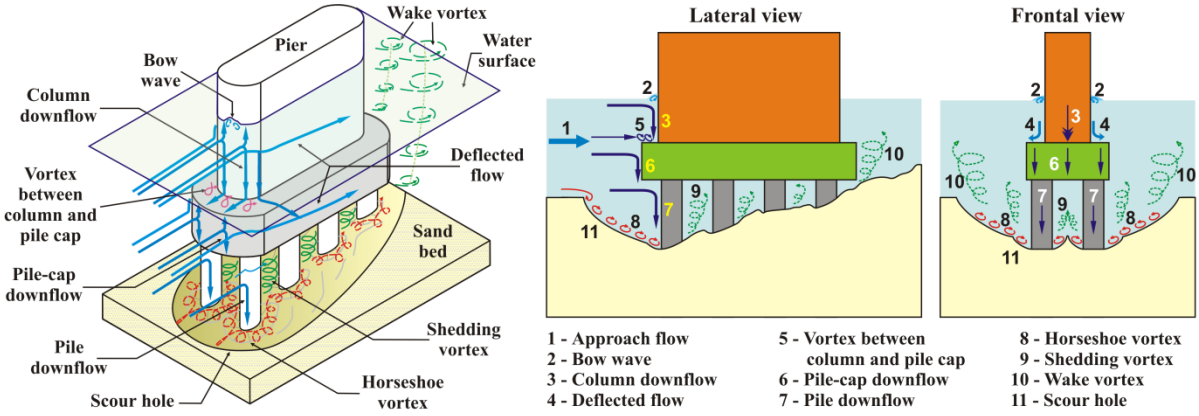

Figure 2.20 – Scheme of the flow structure around complex piers

Recently, Beheshti and Ataie-Ashtiani (2010) studied the flow field around a complex pier positioned on a rough fixed bed with all components exposed to the approaching flow. They found that: (1) the approaching boundary layer upstream the pile cap is separated into two vertical opposite directions, inducing an upward flow towards the column and a contracted downward flow below the pile cap and toward the piles; (2) the upward flow on the pile cap interacts with the downflow in front of the column and deflects it towards the side of the pier; and (3) the flow at the rear of the pile cap is very complex, as the flow is simultaneously expanded to different directions. Some of those flow interactions are also represented in Figure 2.20.

2.3.2 DIMENSIONAL ANALYSIS

The maximum scour depth around a complex pier, d_s, at a given instant, t, can be described by the following set of independent variables and parameters, similar to the equivalent set of variables used in equation (2.1) to describe the local scour depth around a single pier:

$$d_s = f\left[\begin{array}{c}\text{flow } (h, S_e, g),\ \text{fluid } (\rho, \mu),\ \text{bed material } \left(d_{50}, \sigma_g, \rho_s\right), \\ \text{complex pier } \begin{pmatrix}\theta, D_c, L_c, K_{Sc}, D_{pc}, L_{pc}, K_{Spc}, T, H_c, \\ f_l, f_t, D_p, L_p, f_p, K_{Sp}, m, n, S_m, S_n\end{pmatrix}, \\ \text{channel } \left(B, S_o, K_g\right),\ \text{time } (t)\end{array}\right] \tag{2.33}$$

where, θ = complex pier alignment angle; D_c = column width; L_c = column length; K_{Sc} = column shape factor; D_{pc} = pile-cap width; L_{pc} = pile-cap length; K_{Spc} = pile-cap shape factor; T = pile-cap thickness; H_c = column position (distance from the initial bed level to the bottom surface of the column); f_l = extension length of pile cap face out from column face; f_t = extension width of pile cap face out from column face; D_p = pile width; L_p = pile length; f_p = longitudinal extension length of pile cap face out from the nearest pile front face; K_{Sp} = pile shape factor; m = number of piles in line with flow; n = number of piles normal to the flow; S_m = pile spacing in the direction m (centreline-to-centreline); S_n = pile spacing in the direction n (centreline-to-centreline).

Figure 2.21 shows the scheme of a complex pier with the respective variables described above.

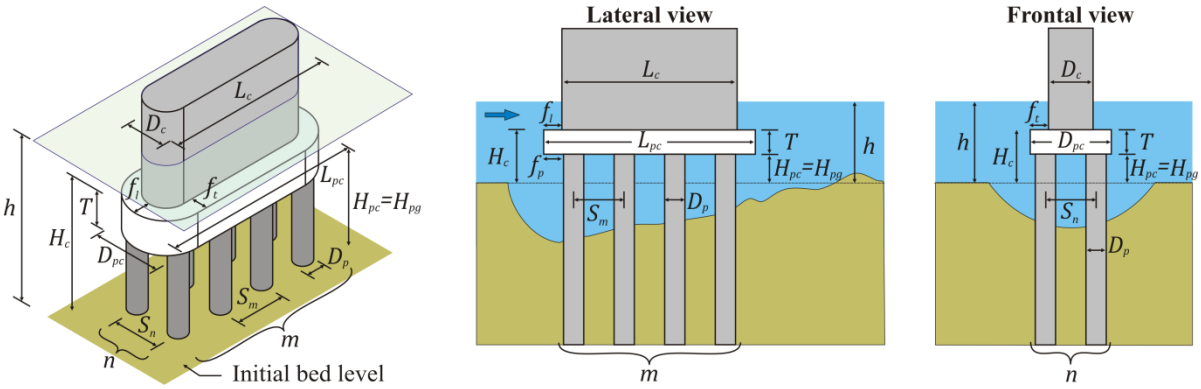

Figure 2.21 – Scheme of complex pier geometry

It should be noted, as discussed in section 2.2.2, that the critical velocity for sediment entrainment, U_c, is not considered since it is fully defined by h, S_e, g, ρ, μ, d_{50} and ρ_s. For uniform flows: $S_e = S_o$; the friction velocity, u_*, is given by $u_* = \sqrt{gRS_e} = \sqrt{gRS_o}$, where $R = \varphi(B, h, K_g)$ is the hydraulic radius of the flow cross-section, and; φ stands for functional relationship. Since the sediment submerged density of the flow is given by $\Delta = (\rho_s - \rho)/\rho$, equation (2.33) can be written as

$$d_s = \varphi\begin{pmatrix} h, g, \rho, \mu, d_{50}, \sigma_g, \Delta, \theta, D_c, L_c, K_{Sc}, D_{pc}, L_{pc}, K_{Spc}, T, \\ H_c, f_l, f_t, D_p, L_p, f_p, K_{Sp}, m, n, S_m, S_n, B, u_*, K_g, t \end{pmatrix} \tag{2.34}$$

Choosing D_c, u_* and μ for basic variables and applying the theorem of Vaschy-Buckingham, equation (2.34) becomes

$$\frac{d_s}{D_c} = \varphi\left(\begin{matrix} \sigma_g, \Delta, K_{Sc}, \theta, K_g, \frac{h}{D_c}, \frac{d_{50}}{D_c}, \frac{L_c}{D_c}, \frac{B}{D_c}, \frac{gD_c}{u_*^2}, \frac{u_* D_c \rho}{\mu}, \frac{u_* t}{D_c}, \\ K_{Spc}, \frac{D_{pc}}{D_c}, \frac{L_{pc}}{D_c}, \frac{T}{D_c}, \frac{H_c}{D_c}, \frac{f_l}{D_c}, \frac{f_t}{D_c}, \frac{D_p}{D_c}, \frac{L_p}{D_c}, \frac{f_p}{D_c}, K_{Sp}, m, n, \frac{S_m}{D_c}, \frac{S_n}{D_c} \end{matrix}\right) \tag{2.35}$$

In this last equation, the first line of non-dimensional parameters corresponds to equivalent parameters of the equation for single piers (see equation (2.3)) and the second line corresponds to new parameters referent to complex pier geometry (pile cap and pile group). Taking into account the analysis performed in section 2.2.2 for single piers, summarized in equation (2.13), the equation (2.35) can also be written as

$$\frac{d_s}{D_c} = \varphi\left(\begin{matrix} \sigma_g, K_{Sc}, K_\theta, \frac{h}{D_c}, \frac{D_c}{d_{50}}, \frac{U}{U_c}, \frac{u_* d_{50}}{\upsilon}, \frac{u_* t}{D_c}, \\ K_{Spc}, \frac{D_{pc}}{D_c}, \frac{L_{pc}}{D_c}, \frac{T}{D_c}, \frac{H_c}{D_c}, \frac{f_l}{D_c}, \frac{f_t}{D_c}, \frac{D_p}{D_c}, \frac{L_p}{D_c}, \frac{f_p}{D_c}, K_{Sp}, m, n, \frac{S_m}{D_c}, \frac{S_n}{D_c} \end{matrix}\right) \tag{2.36}$$

Any non-dimensional parameter of equation (2.36) can be replaced by any combination of that parameter with others as soon as the resulting set remains independent, thus

$$\frac{d_s}{D_c} = \varphi\left(\begin{array}{c}\sigma_g, K_{Sc}, K_\theta, \frac{h}{D_c}, \frac{D_c}{d_{50}}, \frac{U}{U_c}, \frac{u_* d_{50}}{\upsilon}, \frac{u_* t}{D_c}, \\ K_{Spc}, \frac{D_c}{D_{pc}}, \frac{T}{h}, \frac{H_c}{h}, \frac{f_l}{f_t}, \frac{f_p}{D_p}, K_{Sp}, m, \frac{S_m}{D_p}, n, \frac{S_n}{D_p}\end{array}\right) \tag{2.37}$$

where, $K_{Sc} = \varphi(L_c/D_c)$; $K_{Spc} = \varphi(L_{pc}/D_{pc})$; $K_{Sp} = \varphi(L_p/D_p)$.

Equation (2.37) constitutes the framework for subsequent analysis, where the effects of some characteristic variables and non-dimensional parameters that affect scouring at complex piers are discussed and characterized. It should be recalled that the first eight non-dimensional parameters (upper-line) were discussed in section 2.2 for single piers.

2.3.3 TIME EVOLUTION OF SCOUR DEPTH

Melville and Raudkivi (1996) studied nonuniform piers comprising a cylindrical column of diameter D_c founded on a larger cylinder of diameter D_{pc} and concluded that the temporal development of the scour hole is dependent on the ratio D_c/D_{pc} and on the depth from the initial bed level to the top of the foundation. Recent studies (*e.g.*, Sousa, 20007; Ataie-Ashtiani *et al.*, 2010; Ferraro *et al.*, 2013) show that the scour depth evolution in complex piers follows different stages in comparison with single piers. That is associated with the progressive physical presence in the scour hole evolution of one, two or the three structural components of the complex pier. The duration and trend of the different stages depend on the geometry of the complex piers and on the pile-cap position relative to the initial bed level. Sheppard and Glasser (2004) suggested addressing the evaluation of local scour at complex piers considering three typical situations, which depend on the positioning of the pile cap. These situations are defined as:

- Situation 1 - characterized by the bottom of the pile cap being above the initial bed level. In this situation the following cases may occur: (1) pile cap above and out of the water; (2) pile cap partially immersed in the water; and (3) pile cap under the water and its bottom surface above the bed, as shown in Figure 2.22.
- Situation 2 - characterized by the pile cap being partially buried in the initial bed corresponding to cases where the top of the pile cap is: (4) above the bed level; and (5) levelled with the bed surface, as shown in Figure 2.22.
- Situation 3 - characterized by the pile cap being completely buried in the bed corresponding to cases where the top of the pile cap: (6) becomes apparent along the scouring process; or (7) remains buried below the bottom of the scour hole, as shown in Figure 2.22.

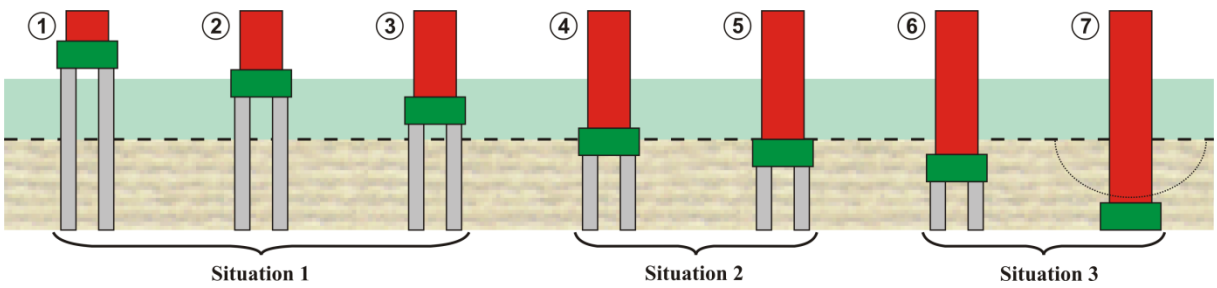

Figure 2.22 – Complex pier situations as a function of the relative pile-cap position

In position (1), characterized by the bottom of the pile cap being out of the water, the scour depth time evolution at complex piers corresponds to the temporal evolution observed around pile groups, as shown in Figure 2.23.

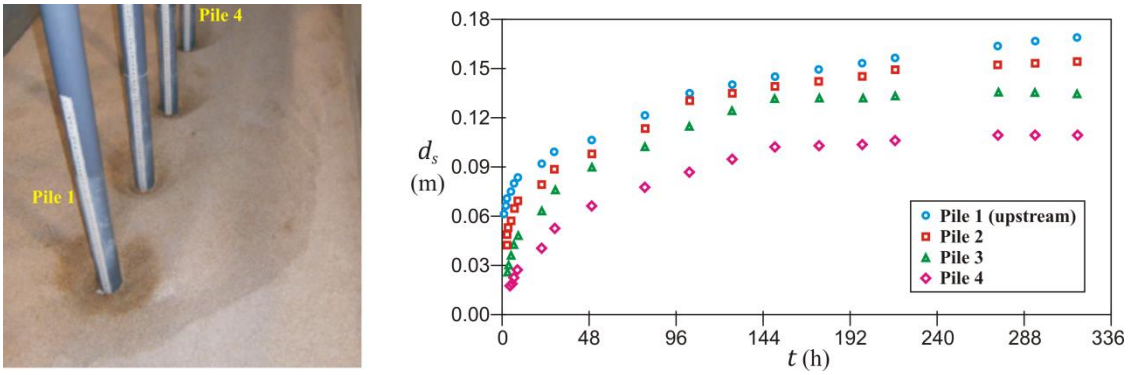

Figure 2.23 – Temporal evolution of scour depth at pile groups, adapted from Lança *et al*. (2013a)

According to Lança *et al*. (2013a), when the pile group is aligned to the flow, the scour process begins in front of each pile, with individual holes, until they merge into one single global scour hole due to interaction of the flow structure around the piles (with the presence of the four mechanisms before mentioned – scour reinforcement, sheltering, wake vortices interaction and compressed horse-shoe vortices). The maximum scour depth is located in front of the upstream pile of the group. On the contrary, the maximum scour depth can be located in the middle or the downstream piles, when the pile group is not aligned with the flow.

In position (2), characterized by the pile cap being partially immersed in the water, the scour depth evolution is similar to that observed in the position (1), in which the scour process occurs in front of the piles. In position (3), characterized by the pile cap under the water and above the bed, the trend of the temporal evolution of the sour depth is similar to that observed in the first two positions, as shown in Figure 2.24. According to Sousa (2007), the presence of the three components of the complex pier in the flow leads to an increase of the scour rate and of the respective scour depth. The maximum scour depth is identified in front of the upstream piles.

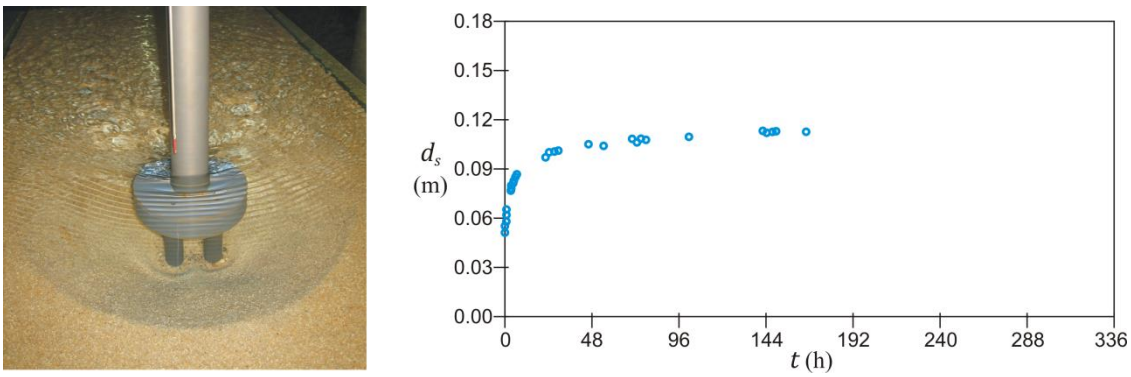

Figure 2.24 – Temporal variation of scour depth at complex piers in position (3), adapted from Sousa (2007)

In position (4), characterized by the pile cap being partially buried in the bed, the scour process starts at the front of the pile cap, and depending of the pile cap thickness and the partially buried depth, the scour may migrate below the pile cap towards the frontal piles (Ferraro *et al*. 2013), as shown in Figure 2.25. According to Ataie-Ashtiani *et al*. (2010) and Ferraro *et al*. (2013), for complex pier where the top of the pile cap is close to the initial bed level, *i.e*., position (5), the scour process is similar to the above described for position (4).

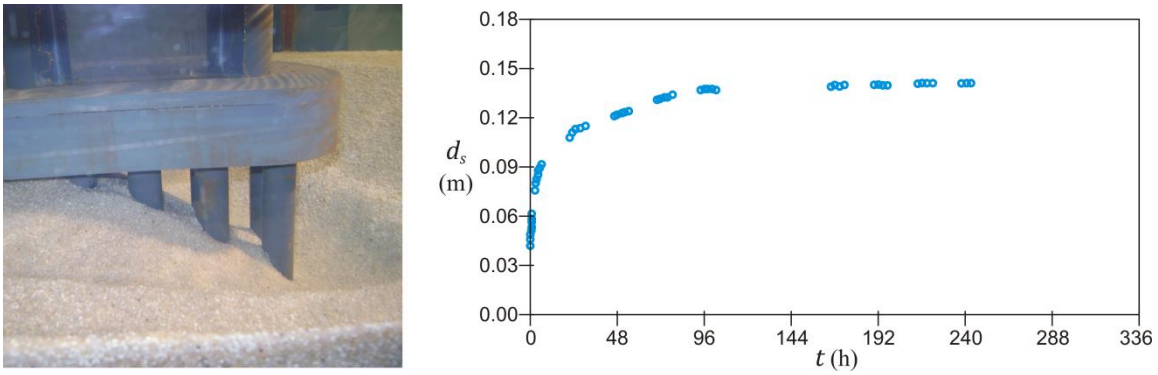

Figure 2.25 – Scour depth time evolution at complex piers in position (4), adapted from Ferraro *et al*. (2013)

According to Ferraro *et al*. (2013), once the pile cap is entirely buried, *i.e*., position (6) of Figure 2.22, the scour starts at the column side or in front of the column until the scour hole partly uncovers the top of the pile cap. Next, the scour depth remains unchanged for a while, with a value equal to the depth of the top of the pile cap below the initial bed level. That stage ends with the scour process continuing in front of the pile cap, as shown in Figure 2.26. This description of the scour depth evolution is in accordance with the results obtained by various researchers in studies of cylindrical columns founded on cylindrical caissons (*e.g*., Melville and Raudkivi, 1996; Umeda *et al*., 2010; Lu *et al*., 2011; Kothyari and Kumar, 2012).

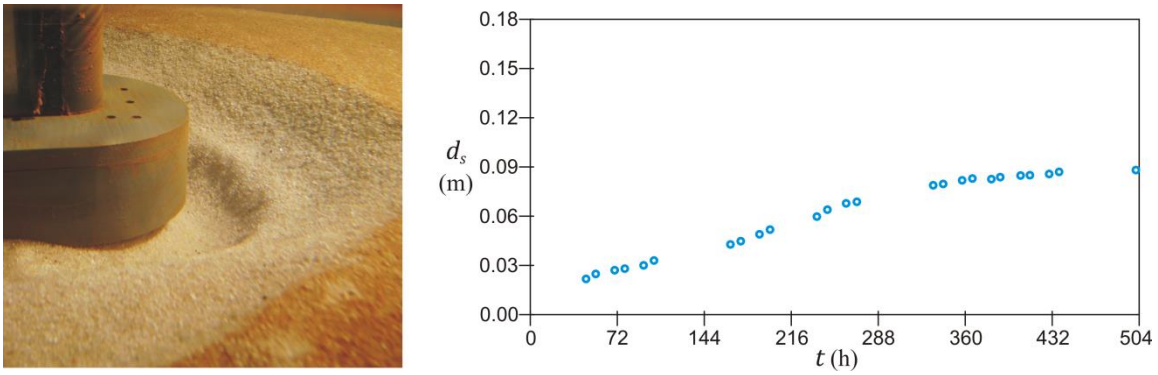

Figure 2.26 – Scour depth time evolution at complex piers in position (6), adapted from Ferraro *et al*. (2013)

In position (7), characterized by the pile cap remaining buried below the bottom of the scour hole, the scour depth time evolution is similar to the one observed for single piers, as shown in Figure 2.7.

2.3.4 EQUILIBRIUM SCOUR DEPTH IN LABORATORY TESTS

As mentioned in section 2.2.4 for single piers, it can be assumed that the equilibrium scour exists and it is achieved in infinite time. Again the question is which should be the minimum duration of the experimental tests, with complex piers, to achieve equilibrium conditions. In this regard, some authors (*e.g.*, Coleman, 2005; Melville *et al*., 2006; Ataie-Ashtiani *et al*., 2010) suggest the same criterion proposed by Melville and Chiew (1999) for experimental tests with single piers, as was described in section 2.2.4. The mentioned authors use, as reference, the smaller value of 5% of the complex pier characteristic length (*e.g.*, its equivalent pier diameter) and of the flow depth. In the case of pile groups, Lança *et al*. (2013a) suggest that the duration of scour tests should be more than 7 days, which is the duration considered adequate for single cylindrical piers (according to Simarro *et al*., 2011), since the scouring process can be expected to be more complex and slower.

2.3.5 EFFECTS OF SPECIFIC PARAMETERS ON MAXIMUM LOCAL SCOUR DEPTH

2.3.5.1 Framework

As mentioned in section 1.1, few studies on scouring at complex piers under clear-water conditions were performed in recent years. The next five were identified: (1) Coleman (2005); (2) Ataie-Ashtiani *et al*. (2010); (3) Grimaldi and Cardoso (2010); (4) Ferraro *et al*. (2013); and (5) Amini *et al*. (2014). A total of thirteen complex pier models were analysed in these five studies, as shown in Table 2.2. The values of the most important control variables characterizing the set of tests performed with those models are summarized in Table 2.2. For each model the number of tests (each corresponding to a pile-cap position in relation to the initial bed level) and the test durations, t_d, are also included. In all the thirteen experimental models coarse sand ($d_{50} \geq 0.6$ mm) was used, accounted for being insusceptible to the formation of ripples in the approach flow reach.

Table 2.2 – Experimental models: flow parameters, bed granulometry parameters and duration of the tests

Study	Model	Nº tests	B (m)	U (m/s)	U_c (m/s)	h (m)	d_{50} (mm)	t_d (days)
Coleman (2005)	Co1	11	1.50	0.33	0.44	0.60	0.84	NS
	Co2	11	1.50	0.37	0.44	0.60	0.84	NS
	Co3	8	1.50	0.34	0.41	0.33	0.84	NS
Ataie-Ashtiani *et al*. (2010)	AA1	39	0.60	0.22-0.26	0.30-0.31	0.13-0.16	0.60	0.4-3.1
	AA2	22	0.60	0.23-0.26	0.30-0.34	0.14-0.16	0.60	0.4-2.1
Grimaldi and Cardoso (2010)	GC	12	0.70	0.28	0.30	0.10	0.83	4.8-18.1
Ferraro *et al*. (2013)	Fe1	10	0.70	0.27	0.30	0.10	0.83	8.3-37.0
	Fe2	11	0.70	0.27	0.30	0.10	0.83	3.2-41.2
Amini *et al*. (2014)	A1	7	1.52	0.36	0.38	0.24	0.80	1.0
	A2	7	1.52	0.36	0.38	0.24	0.80	1.0
	A3	13	1.52	0.36	0.38	0.24	0.80	1.0
	A4	13	1.52	0.36	0.38	0.24	0.80	1.0
	A5	16	1.52	0.36	0.38	0.24	0.80	1.0

Note: NS = not specified.

Figure 2.27 shows the dimensions of the thirteen complex pier models identified in the literature.

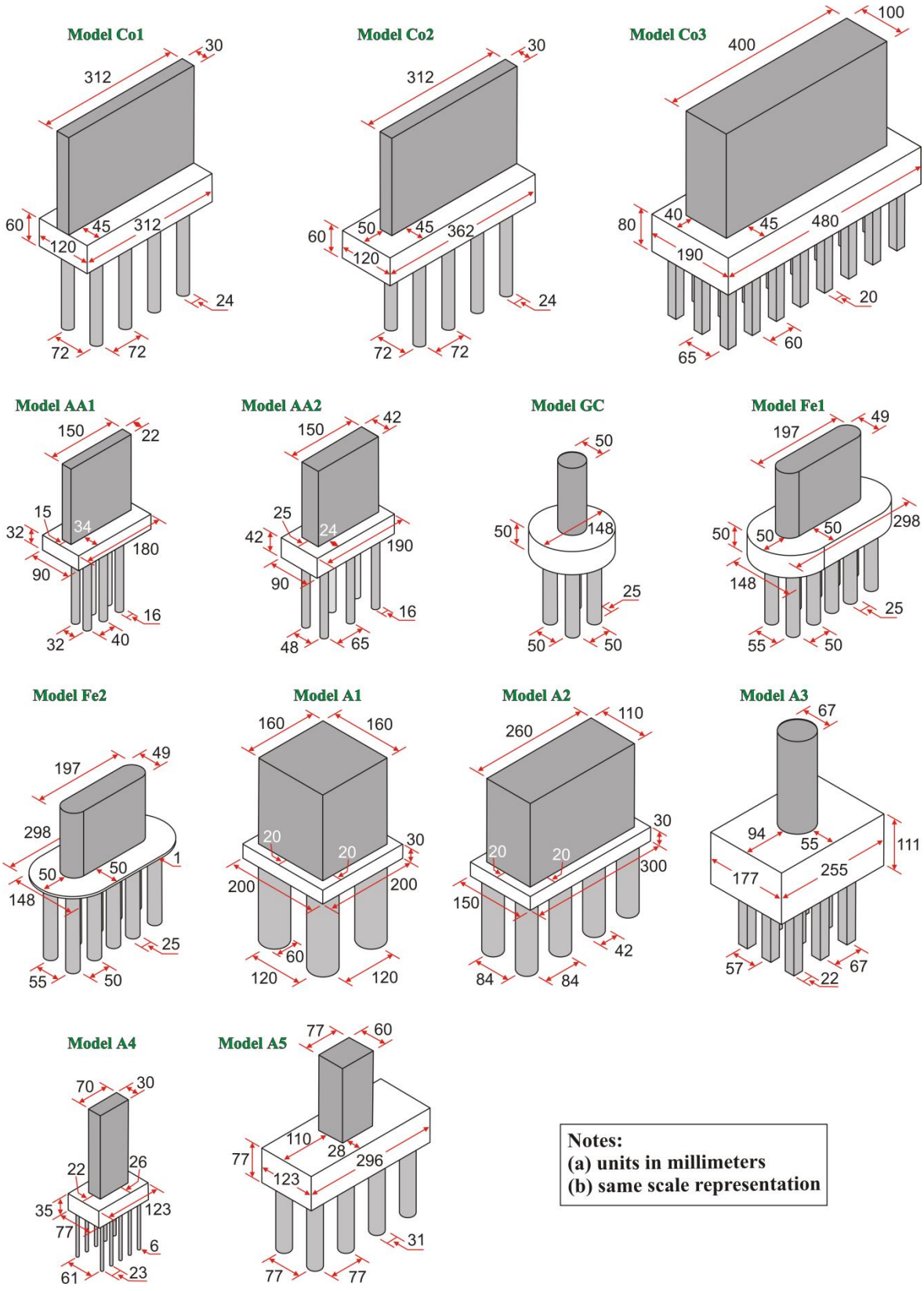

Figure 2.27 – Dimensions of complex pier models used in the five studies from literature

2.3.5.2 Relative column position

The experimental range of all thirteen models reported in the literature (Table 2.2) covered the three pile-cap situations (see Figure 2.22) by considering different values of H_c/h. The measured scour depth values, d_s, are plotted against H_c/h (considered negative when the top of the pile cap is below the initial bed level) in Figure 2.28 for the test series in the mentioned thirteen models. Each chart of the figure includes: (1) two vertical lines at $H_c/h = 0$ and $H_c/h = T/h$, which are used to delimit the regions associated to the three mentioned situations; and (2) the envelope curve of the experimental scour data. Although some of the tests performed with the thirteen models analysed were of short duration, those allowed to characterize qualitatively the variation of the scour depth with the relative column position.

Figure 2.28(a) shows a schematic conceptual variation of d_s with H_c/h, distinguishing five different defining zones and stages: (1) the scour depth is only influenced by the pile group; (2) the increment of the scour depth is associated with the presence of the column and pile cap in the flow (increasing the area exposed to the flow); (3) the reduction in the scour depth, from the maximum value, is due to the pile cap overhang dimension tendency to weaken the flow structure (*e.g.*, downflow, horseshoe vortices); (4) the increment in the scour depth values is due to this depth being controlled by the position of the top of the pile cap (on decreasing H_c/h ratio); and (5) the scour depth is only influenced by the column.

Analysing the Figure 2.28, it could be concluded that the d_s variation in ten of the thirteen models is analogous of that Figure 2.28(a), *i.e.*, being possible to identify the five stages with exception of Model Fe2 (Figure 2.28(i)), Model A1 (Figure 2.28(j)) and Model A2 (Figure 2.28(k)). This may be justified by the fact that: (1) the Model Fe2 has a thin pile-cap thickness, implying no contribution of the pile cap on the scour depth; (2) the Model A1 has a column width close to the pile cap width ($D_c/D_{pc} = 0.80$), in which the d_s variation is similar to that observed by Martin-Vide *et al.* (1998) in a pier founded on an alignment of piles; and (3) the Model A2 has also a large D_c/D_{pc} ratio (0.73). From the results of Figure 2.28 it can be concluded that the d_s variation with H_c/h depends also on the parameters D_c/D_{pc} and T/h as well as the shape of the three complex pier components.

The comparison of the envelope curves in Models GC (Figure 2.28(g)) and Fe1 (Figure 2.28(h)) suggests that similar column and pile-cap configuration sets with circular or round-nose rectangular shape are leading to similar scour depth values since the widths of these two components are equal, as shown in Figure 2.27. These findings are in agreement with those obtained in Figure 2.14 for single piers.

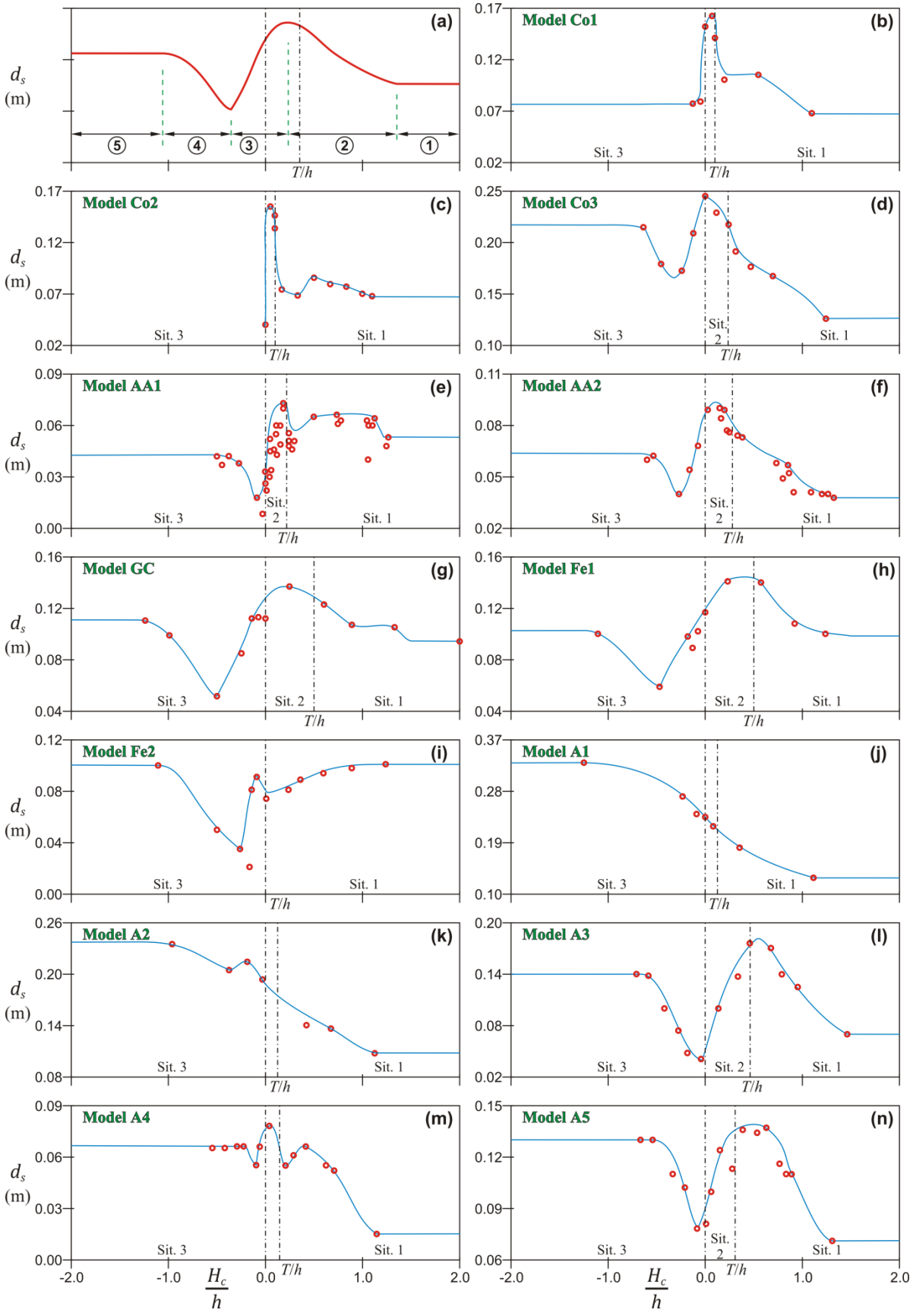

Figure 2.28 – Scour depth as function of the relative column position

2.3.5.3 Relative column width

Few studies have been performed to evaluate the effect of the relative column width, D_c/D_{pc} (relation between the column and the pile cap widths), on the maximum scour depth. This effect has been studied in compound foundations: (1) rectangular columns founded on rectangular caissons (*e.g.* Jones *et al.*, 1992; Parola *et al.*, 1996); and (2) cylindrical columns founded on cylindrical caissons (*e.g.*, Melville and Raudkivi, 1996; Umeda *et al.*, 2010; Lu *et al.*, 2011). These authors concluded that the scour depth depends on the caisson extension lengths beyond the external face of the column (represented in the correspondent studies geometries by D_c/D_{pc}) and the relative column position, H_c/h. Data obtained by Melville and Raudkivi (1996) were selected and the representation of their results was rearranged with the purpose of highlighting the effect of D_c/D_{pc}, as shown in Figure 2.29. It is clear that the scour depth increases with the increment of the ratio D_c/D_{pc}.

Regarding studies on complex piers, the effect of D_c/D_{pc} on d_s has been analysed in the work of Coleman (2005), Sheppard and Renna (2010), Ataie-Ashtiani *et al.* (2010) and Arneson *et al.* (2012). Coleman (2005) used the results of Melville and Raudkivi (1996), in relation to the effect of D_c/D_{pc} and H_c on d_s, to suggest a predictor to calculate the local scour at complex piers when the pile cap is partially buried in the bed. Comparing the scouring results obtained by Coleman (2005) for two of the models used, Co1 and Co2 (see Figure 2.27) – presented in Figure 2.28(b) for Model Co1 and in Figure 2.28(c) for Model Co2 –, it can be concluded that the higher scour depth values of Model Co1 over the full H_c/h range is due to the fact that, in this model (where $f_l/f_t = 0$), the downflow in front of the column is not affected by the upstream pile-cap extension.

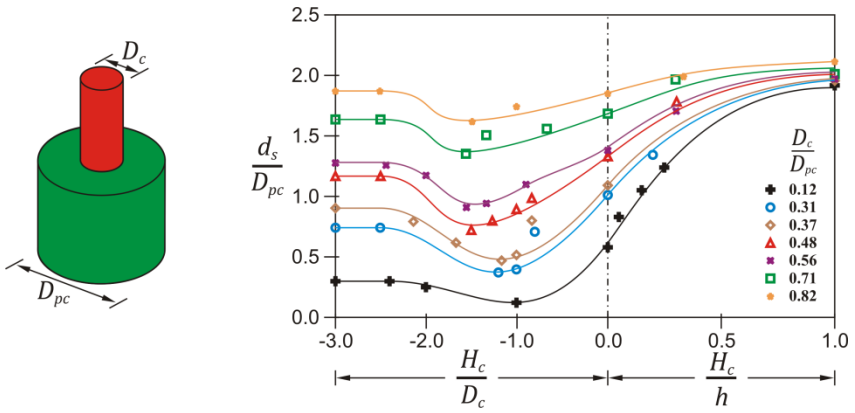

Figure 2.29 – Effect of the relative column width on scour depth as function of the relative column position, based on Melville and Raudkivi (1996) data

Results of experimental tests carried out by Jones (1989), Salim and Jones (1996) and Jones and Sheppard (2000a) were considered in the development of the FDOT predictor (Sheppard and Renna, 2010) and of the HEC-18 predictor (Arneson *et al.*, 2012). These tests were performed to evaluate the effect of the pile-cap front and side extension lengths beyond the column external face on the maximum scour depth. Jones (1989) observed that when the top of the pile cap was placed at or below the initial bed level, maximum local scour was 20% less than for the different tested conditions with the pile cap above the bed. Jones and Sheppard (2000a) carried out experiments on suspended columns with a thin plate attached to the bottom, positioned above the stream bed, to create and study the overhang length effect. Ataie-Ashtiani *et al.* (2010) considered that, in complex piers with rectangular

shapes, the upstream and lateral overhang distances from the corresponding column faces has an important effect on scour depth in the cases where the pile cap is partially or completely buried. Ataie-Ashtiani *et al*. (2010) established a new expression to calculate the equivalent diameter suggested by Coleman (2005) by taking into account the results of their rectangular complex piers studies.

2.3.5.4 Pile-cap thickness

Ferraro *et al*. (2013) carried out experiments with two complex pier models (Fe1 and Fe2, Table 2.2) to study the effect of the relative pile-cap thickness, T/h, on the maximum scour depth as a function of the relative column position, H_c/h. In these two models only the pile-cap thickness was changed, as shown in Figure 2.27. Model Fe1 corresponds to a thick pile cap case whereas Model Fe2 represents a case with a thin pile cap, as shown in Figure 2.30(a). The variation of maximum scour depth with H_c/h for the two mentioned models is presented in Figure 2.30(b). The results of d_{se} variation with H_c/h (Figure 2.30(b)) show that, in general, the complex pier with the thicker pile cap generates deeper scour holes. The increase in scour depth values from the test with Model Fe2 ($T/h = 0.01$) to the test with Model Fe1 ($T/h = 0.50$) is justified by the larger area exposed frontal to the flow due to the pile cap front in Model Fe1 compared to Model Fe2. For the thicker pile cap case (Model Fe1) the maximum scour depth occurred when the pile cap was partially buried in the initial bed level. In this condition, the thicker pile cap intercepted a greater flow portion and diverted it towards the bed, that increasing the strength of the erosive agents (downflow and horseshoe vortex).

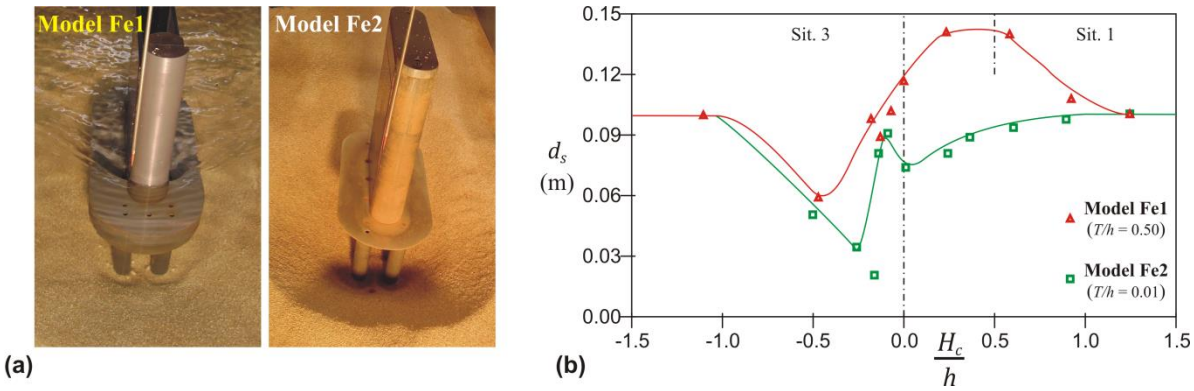

Figure 2.30 – Effect of the pile-cap thickness on scour depth: (a) complex pier models and (b) scour depth variation as function of the relative column position, adapted from Ferraro *et al*. (2013)

2.3.5.5 Pile-group configuration

Knowledge of local scouring at pile groups is not extensive, with small number of studies reported in the literature. They include those of Hannah (1978), Elliott and Baker (1985), Salim and Jones (1996), Zhao and Sheppard (1999), Smith (1999), Sumer and Fredsøe (2002), Ataie-Ashtiani and Beheshti (2006), Amini *et al*. (2012) and Lança *et al*. (2013a). Excepting the studies of Smith (1999) and Lança *et al*. (2013a), the tests were performed for short durations. These studies focus on the effect of pile spacing, S_n/D_p and S_m/D_p, skew-angle, θ, as well as number of columns and number of rows of the pile group, n and m respectively.

Figure 2.31 shows the effect of the relative pile spacing (S_n/D_p or S_m/D_p) on the relative pile group scour depth, d_{spg}/d_{sp} (d_{spg} = maximum scour depth observed at pile group and d_{sp} = scour depth observed at an individual pile in the same bed and approach flow conditions), for different

configurations of the pile group, all aligned with the approach flow. The figure includes the experimental data obtained by Hannah (1978), Ataie-Ashtiani and Beheshti (2006) and Lança *et al.* (2013a). Even though the corresponding tests of the first two studies were carried out with short durations, it can be assumed that the corresponding ratio d_{spg}/d_{sp} approaches to that which would be obtained with tests of longer durations.

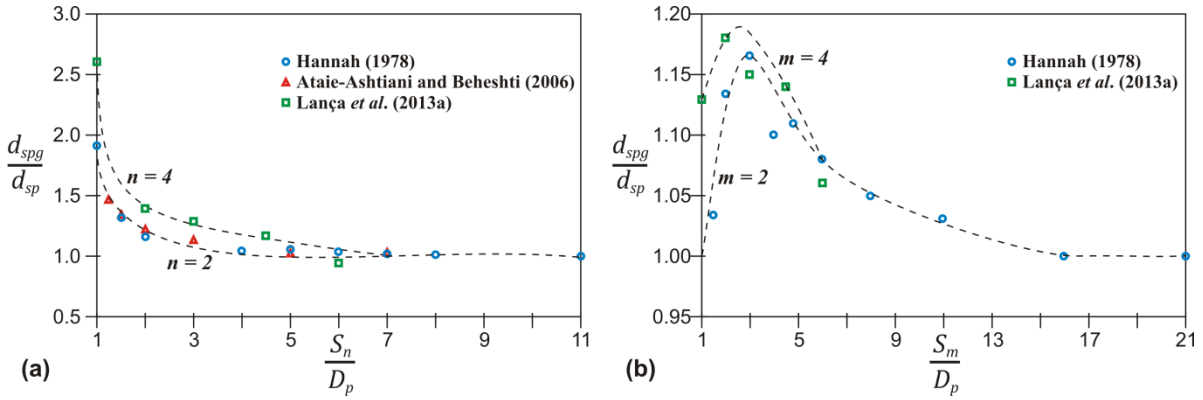

Figure 2.31 – Effect of the relative pile spacing on the relative scour depth for pile groups with: (a) a single row (m = 1) and (b) a single column (n = 1)

Figure 2.31(a) displays d_{spg}/d_{sp} as a function of the relative spacing perpendicular to the flow, S_n/D_p. This figure includes tests with pile groups of a single row (one transverse alignment), *i.e.*, m = 1 (see Figure 2.21). The results shows that the maximum scour depth occurs for S_n/D_p = 1 and gradually diminishes with the increase of the relative pile spacing. This may explained by the fact that the interference between adjacent piles diminishes leading to incipient individual scour holes. Further increase on S_n/D_p shows that the individual scour holes tend to separate and, for $S_n/D_p \geq 7$, a clear and individual scour hole corresponds to each pile. Figure 2.31(b) shows d_{spg}/d_{sp} as function of the relative spacing in the direction of the flow, S_m/D_p. This figure includes tests with pile groups of a single column (one longitudinal alignment), *i.e.*, n = 1 (see Figure 2.21). For S_m/D_p = 1, the piles touch each other and the scour depth at the front of the pile group for m = 2 would be practically equal to the one obtained at a single pile ($d_{spg}/d_{sp} = 1$); whereas, for that same case (S_m/D_p = 1) increasing the number of pile rows (m higher than 2) it will only lead to a slight increase of d_{spg}/d_{sp}. The maximum scour depth at a pile group (irrespective of m) is obtained for S_m/D_p between 2 to 3. This may be associated to the scour reinforcement mechanism described in section 2.3.1. Then, the interaction between piles reduces gradually until S_m/D_p = 12. For S_m/D_p > 12, the scour depth in the upstream pile would be again the same as the one corresponding to an isolated pile.

In Figure 2.32(a), the values of relative scour depths of the pile group, d_{spg}/d_{sp}, are plotted against the pile spacing, S_p/D_p (S_p representing longitudinal and transverse pile spacing, since it is considered that S_m = S_n), and θ. This figure is a representation of the results obtained by Lança *et al.* (2013a) for a pile group with m = 4 and n = 2 and cylindrical piles. According to Salim and Jones (1996), collapsed pile groups (*i.e.*, S_p/D_p = 1) tend to behave as single piers whose dimensions are the sum of the dimensions of the individual piles, wherein the variation with skew-angle is similar to the observed in Figure 2.17.

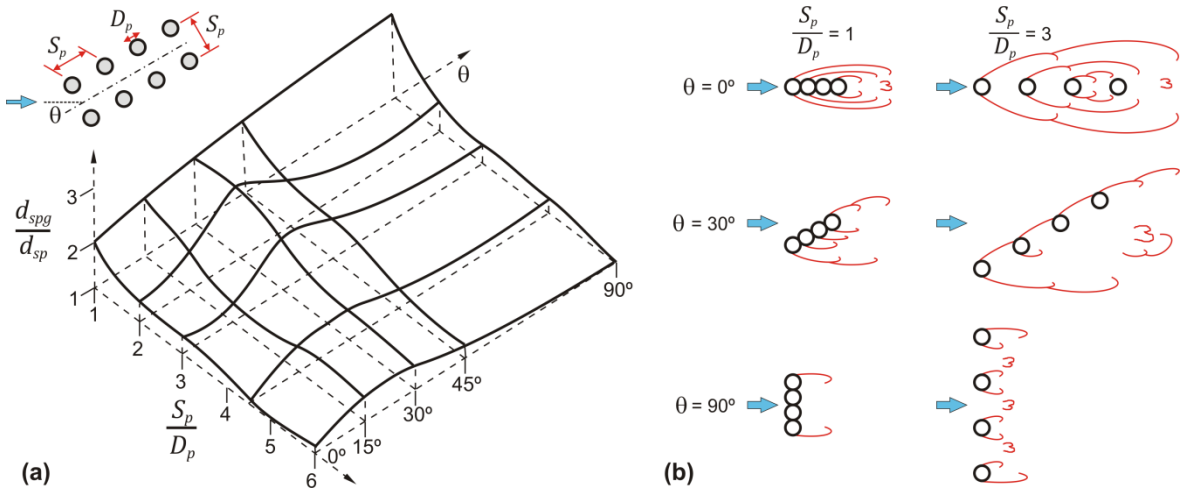

Figure 2.32 – (a) variation of d_{spg}/d_s with S_p/D_p and θ, adapted from Lança *et al*. (2013a) and (b) system of wake vortices at an alignment of piles, adapted from Lança *et al*. (2012)

In Figure 2.32(a), with the exception of S_p/D_p = 1, the maximum scour depth occurs for $\theta = 30°$. For this configuration ($\theta = 30°$), the maxima scour depths tend to occur at the rear piles of the first column, which may be interpreted as an indication that such piles are located in the path of the most energetic wake vortices generated upstream, as illustrated in Figure 2.32(b). In pile groups with cylindrical piles, other studies (*e.g.*, Hannah, 1978; Zhao and Sheppard, 1999) concluded that the maximum scour depth is observed for 25º and 40º respectively. The difference of results between the study by Lança *et al*. (2013a) and the studies by Hannah (1978) and Zhao and Sheppard (1999) may be associated to the short test durations in the last studies.

2.3.6 METHODS FOR ESTIMATION OF LOCAL SCOUR DEPTHS

2.3.6.1 Auckland Method

The Auckland design method for complex piers was initially proposed by Melville and Coleman (2000) based on the concept of the equivalent pier diameter, D_e, introduced by Melville and Raudkivi (1996) (on a study of cylindrical columns founded on cylindrical caissons). These authors defined D_e as the diameter of a single pier that would induce the same scour depth as the actual nonuniform pier, for the same flow and sediment. Melville and Coleman (2000) suggest that the equilibrium scour depth at complex piers may be calculated using the equation developed by the same authors for single piers (section 2.2.6.1), which reads,

$$d_{se} = K_{hD} K_I K_d K_S K_\theta \tag{2.38}$$

where K_S = foundation shape factor. In the expressions for the factors K_{hD}, K_d and K_θ (*i.e.*, equations (2.21), (2.23) and (2.24), respectively) D_e is used instead of D.

Coleman (2005) reformulated the initial procedure by considering that D_e depends on the column position relative to the initial bed level, H_c. This author uses expressions previously published in the literature for piers with different types of foundations (*e.g.*, pile groups, pile groups with a floating debris raft, piers founded on caissons or pile caps) to calculate the corresponding value of D_e.

Coleman (2005) identified five cases depending on the pile-cap position relative to the initial bed level (H_c), as shown in Figure 2.33. For both Case I and Case II, the top of the pile cap is completely buried below the initial bed level, in Case I (but not in Case II) remaining always buried and below the base of the scour hole formed. For Case III, the pile cap is partially buried in the bed or above the bed under flow. For Case IV, the pile cap is only partially immersed in the flow. For Case V, the pile cap is out of the flow.

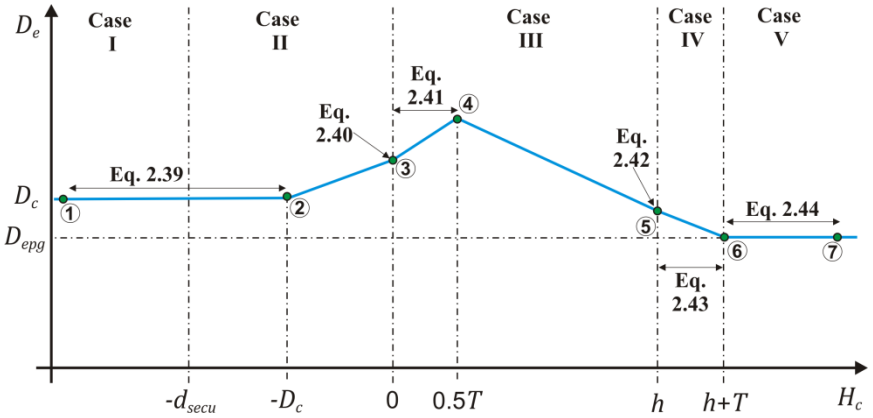

Figure 2.33 – Conceptual variation of equivalent diameter with column position, adapted from Coleman (2005)

Equations adopted by Coleman (2005) to estimate D_e are

$$D_e = D_c \qquad \text{for} \quad H_c \leq D_c \tag{2.39}$$

$$D_e = D_c \left[\left(\frac{D_c}{D_{pc}} \right)^{\left(\frac{D_c}{D_{pc}}\right)^3 - 0.307} \right] \qquad \text{for} \quad H_c = 0 \tag{2.40}$$

$$D_e = D_c \left[\left(\frac{D_c}{D_{pc}} \right)^{\left(\frac{D_c}{D_{pc}}\right)^3 + 0.10 - 0.47\sqrt{0.75 + \frac{H_c}{D_c}}} \right] \qquad \text{for} \quad 0.5T \geq H_c > 0 \tag{2.41}$$

$$D_e = \left[\frac{0.52T D_{pc} + (h - 0.52T) D_{epg}}{h} \right] \qquad \text{for} \quad H_c = h \tag{2.42}$$

$$D_e = \left[\frac{0.52T_* D_{pc} + (h - 0.52T_*) D_{epg}}{h} \right] \qquad \text{for} \quad h + T \geq H_c > h \tag{2.43}$$

$$D_e = D_{epg} \qquad \text{for} \quad H_c \geq h + T \tag{2.44}$$

where, D_{epg} = equivalent diameter of the pile group, $T_* = h - (H_c - T)$ = distance of the pile-cap thickness that remains in the flow when it is partially immersed in the flow.

Figure 2.33 shows the conceptual variation of D_e as a function of H_c, in which the five cases defined above are included. For Case I, that is $H_c < -d_{secu}$, (d_{secu} = equilibrium scour depth for an uniform single pier with the same geometrical definition of the complex pier column), equation (2.39) is appropriated because only the column is exposed to the flow. However this equation can be used until $H_c = -D_c$ ignoring potential pile-cap limitation of scour depths. For pile cap completely buried, the combination of equations (2.39) and (2.40) with a linear transition from (2) to (3) of Figure 2.33 is proposed. For pile cap partially buried, left zone of Case III, the equation (2.41) is applicable, having been verified for $0.10 < D_c/D_{pc} \leq 0.85$ and $T \leq 3D_c$ (Melville and Raudkivi, 1996). For the other zone of Case III, the combination of equations (2.41) and (2.42) with a linear variation from (4) to (5) of Figure 2.33 is assumed. For pile cap completely immersed in the flow and its top at the level of the water surface, equation (2.42) is proposed. This equation was suggested by Melville and Dongol (1992) according to a study of local scour at piers with idealized debris rafts at the water surface. For Case IV, equation (2.43) that is a variation of (2.42) is adopted. For Case V, where the pile cap is out of the flow, equation (2.44) is appropriated because only the pile group is exposed to the flow. In the last case, D_{epg} is calculated using the procedures of Richardson and Davis (2001), which are specified in the following section.

2.3.6.2 HEC-18 Method

The HEC-18 design method for complex piers was suggested by Richardson and Davis (2001) and revised by Arneson *et al*. (2012). According to this predictor, a superposition approach, comprising the conceptual separation of the pier components (*i.e.*, column, pile cap and pile group) represented in Figure 2.34 and the determination of the scour depths for individual components is adopted. This approach was suggested by Jones and Sheppard (2000a).

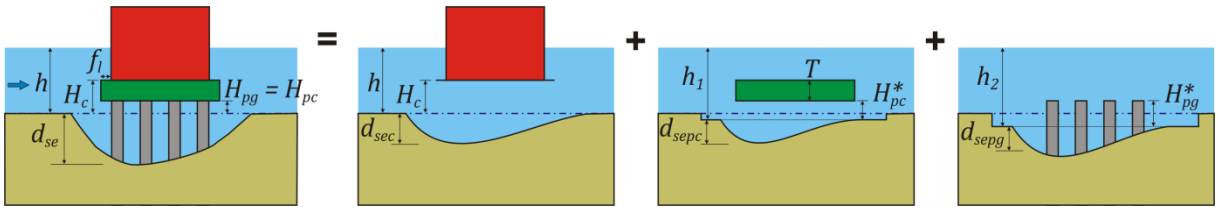

Figure 2.34 – Conceptual hypothesis for superimposing scour components, adapted from Jones and Sheppard (2000a)

The total scour depth from superposition of components is given by:

$$d_{se} = d_{sec} + d_{sepc} + d_{sepg} \tag{2.45}$$

where d_{se} = total equilibrium scour depth, d_{sec} = column contribution to the local scour depth, d_{sepc} = pile-cap contribution to the local scour depth and d_{sepg} = pile-group contribution to the local scour depth.

The contribution of the column on the local scour depth can be expressed by the following equation:

$$\frac{d_{sec}}{D_c} = \begin{cases} 0 & \text{for} \quad H_c \geq h \\ K_{hc}\left[2.0K_S K_\theta K_{bc} K_w \left(\frac{h}{D_c}\right)^{0.35}\left(\frac{U}{\sqrt{gh}}\right)^{0.43}\right] & \text{for} \quad H_c < h \end{cases} \tag{2.46}$$

where K_{hc} = factor to account for the height of the column relative to the initial bed level. Other factors are the same as described in section 2.2.6.3, in which the geometry of the column is used. The K_{hc} factor is estimated by the following expression:

$$K_{hc} = \begin{cases} \left(0.4075 - 0.0669\frac{f_l}{D_c}\right) - \left(0.4271 - 0.0778\frac{f_l}{D_c}\right)\left(\frac{H_c}{D_c}\right) + \\ \left(0.1615 - 0.0455\frac{f_l}{D_c}\right)\left(\frac{H_c}{D_c}\right)^2 - \left(0.0269 - 0.012\frac{f_l}{D_c}\right)\left(\frac{H_c}{D_c}\right)^3 \end{cases} \tag{2.47}$$

The adjusted flow depth for pile cap scour contribution computations, h_1, the distance between the bed and the bottom of the pile cap after the column scour component has been computed, H_{pc}^*, and the adjusted velocity for pile cap scour contribution computations, U_1, are estimated by the following expressions:

$$h_1 = h + 0.5d_{sec} \tag{2.48}$$

$$H_{pc}^* = H_{pc} + 0.5d_{sec} \tag{2.49}$$

$$U_1 = U\left(\frac{h}{h_1}\right) \tag{2.50}$$

The estimation of the scour depth caused by the pile cap is divided into two situations. In Situation 1, the bottom of the pile cap is above the bed (at the beginning of the scour process or after the bed has been lowered by scour caused by the column component), in which the scour depth can be expressed by

$$\frac{d_{sepc}}{D_{epc}} = 2.0K_S K_\theta K_{bc} K_w \left(\frac{h_1}{D_{epc}}\right)^{0.35}\left(\frac{U_1}{\sqrt{gh_1}}\right)^{0.43} \tag{2.51}$$

where D_{epc} = the width of the equivalent pier that produces the same scour depth of the pile cap. The other factors are the same as described in section 2.2.6.3, in which the geometry of the pile cap is used. However, for skewed flow, the factor K_θ is calculated with the relation L_{pc}/D_{pc}. The equivalent pier width can be calculated by the following expression:

$$\frac{D_{epc}}{D_{pc}} = exp\left(-2.705 + 0.51\ln\left[\frac{T}{h_1}\right] - 2.783\left[\frac{H_{pc}^*}{h_1}\right]^3 + \frac{1.751}{exp\left(\frac{H_{pc}^*}{h_1}\right)}\right) \quad (2.52)$$

where the maximum value of h_1 is $3.5D_{pc}$.

In Situation 2, characterized by the bottom of the pile cap being on or below the bed level (at the beginning of the scour process or after the bed has been lowered by scour caused by the column component), the scour process does not reach the pile group, implying that $d_{sepg} = 0$. The pile-cap contribution on scour depth for Situation 2 can be estimated by:

$$\frac{d_{sepc}}{D_{pc}} = 2.0K_S K_\theta K_{bc} K_w \left(\frac{H_c^*}{D_{pc}}\right)^{0.35} \left(\frac{U_f}{\sqrt{gH_c^*}}\right)^{0.43} \quad (2.53)$$

where H_c^* = distance from the bed to the top of the pile cap after the scour associated to the column has been computed and U_f = average velocity of flow at the exposed footing. This velocity is calculated using the following equation:

$$U_f = U_1 \frac{\ln\left(10.93\frac{H_c^*}{k_s} + 1\right)}{\ln\left(10.93\frac{h_1}{k_s} + 1\right)} \quad (2.54)$$

where k_s = height of grain roughness of the bed, normally taken as d_{84} for sand size bed material and $3.5d_{84}$ for gravel and coarser bed material (d_{84} = sediment size which 84% of sediment is finer).

The adjusted flow depth for pile group scour contribution computations, h_2, the distance between the bed and the top of the pile group after pile cap scour component has been computed, H_{pg}^*, and the adjusted velocity for pile group scour contribution computations, U_2, are estimated by the following expressions:

$$h_2 = h + 0.5d_{sec} + 0.5d_{sepc} \quad (2.55)$$

$$H_{pg}^* = H_{pg} + 0.5d_{sec} + 0.5d_{sepc} \quad (2.56)$$

$$U_2 = U\left(\frac{h}{h_2}\right) \quad (2.57)$$

When the pile group is exposed to flow, the scour depth component for the pile group can be expressed by the following equation:

$$\frac{d_{sepg}}{D_{epg}} = \begin{cases} 0 & \text{for } H_{pg}^{*} \leq 0 \\ K_{hpg}\left[2.0K_S K_{bc} K_w \left(\frac{h_2}{D_{epg}}\right)^{0.35} \left(\frac{U_2}{\sqrt{gh_2}}\right)^{0.43}\right] & \text{for } H_{pg}^{*} > 0 \end{cases} \quad (2.58)$$

where K_{hpg} = factor to account for the position of the top of the pile group relative to the initial bed level. The other factors are the same described in section 2.2.6.3, in which the equivalent width of the pile group is used. The K_{hpg} factor is estimated by the following expression:

$$K_{hpg} = \left[3.08\left(\frac{H_{pg}^{*}}{h_2}\right) - 5.23\left(\frac{H_{pg}^{*}}{h_2}\right)^2 + 5.25\left(\frac{H_{pg}^{*}}{h_2}\right)^3 - 2.10\left(\frac{H_{pg}^{*}}{h_2}\right)^4\right]^{\frac{1}{0.65}} \quad (2.59)$$

The equivalent width of the pile group, D_{epg}, is the product of the sum of the non-overlapping individual pile widths projected on a plane normal to the approach flow, W_{pg}, by the pile spacing factor, K_{sp}, and the factor for the number of aligned rows, K_m, *i.e.*,

$$D_{epg} = W_{pg} K_{sp} K_m \quad (2.60)$$

For the calculation of W_{pg}, Richardson and Davis (2001) suggested to exclude piles other than those of the two rows and one column closest to the plane of projection, as shown in Figure 2.35.

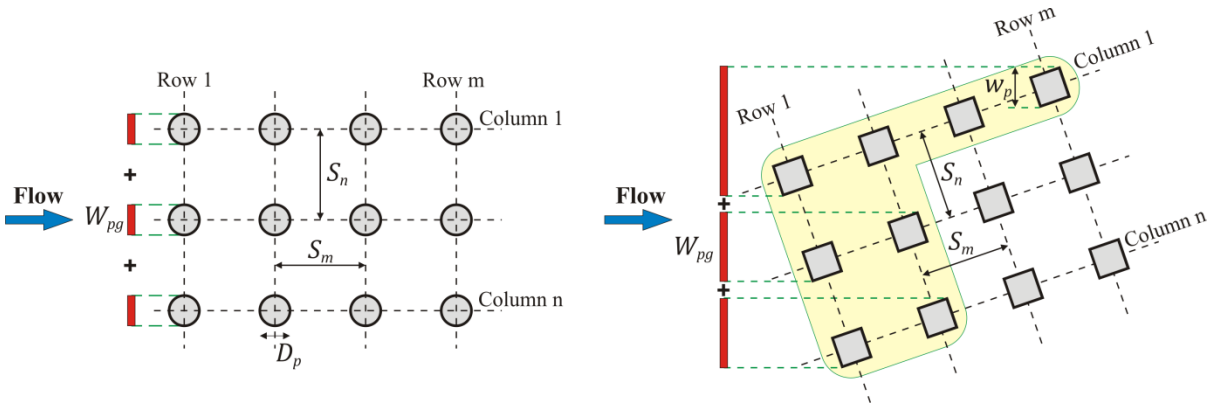

Figure 2.35 – Projected width of piles, adapted from Richardson and Davis (2001)

The pile group spacing factor is defined as

$$K_{sp} = 1 - \frac{4}{3}\left[1 - \frac{w_{pi}}{W_{pg}}\right]\left[1 - \frac{1}{\left(S_p/w_{pi}\right)^{0.6}}\right] \quad (2.61)$$

where w_{pi} = projected width of one pile and S_p = smaller distance of S_m and S_n of Figure 2.35. The variable w_{pi} can be calculated as

$$w_{pi} = \begin{cases} D_p Cos\theta + L_p Sin\theta & \text{for square piles} \\ D_p & \text{for circular piles} \end{cases} \quad (2.62)$$

The factor for the number of aligned rows is

$$K_m = \begin{cases} 0.9 + 0.1m - \dfrac{(m-1)}{14}\left[2.4 - \dfrac{1.1S_p}{D_p} + \dfrac{0.1S_p^2}{(D_p)^2}\right] & \text{for } \theta = 0 \\ 1 & \text{for } \theta > 0 \end{cases} \quad (2.63)$$

If $m > 6$, the value of $m = 6$ should be used in equation (2.63).

2.3.6.3 FDOT Method

In accordance with Sheppard *et al*. (2004) and Sheppard and Renna (2010), the equilibrium scour depth at complex piers can be calculated by equation (2.23). They suggest that the scour depth associated with each pier component can be evaluated as the scour depth at one equivalent single cylindrical pier that would induce the same scour depth as that pier component, for the same sediment and flow conditions, as illustrated in Figure 2.36. This, in turn, depends on pier shape, size, location and alignment relative to the flow direction as well as on flow characteristics and sediment properties. The equivalent diameter of the complex pier, D_e, can be approximated by the sum of the equivalent diameters of the complex pier components, thus

$$D_e = D_{ec} + D_{epc} + D_{epg} \quad (2.64)$$

where D_{ec} = equivalent diameter of the column; D_{epc} = equivalent diameter of the pile cap; D_{epg} = equivalent diameter of the pile group.

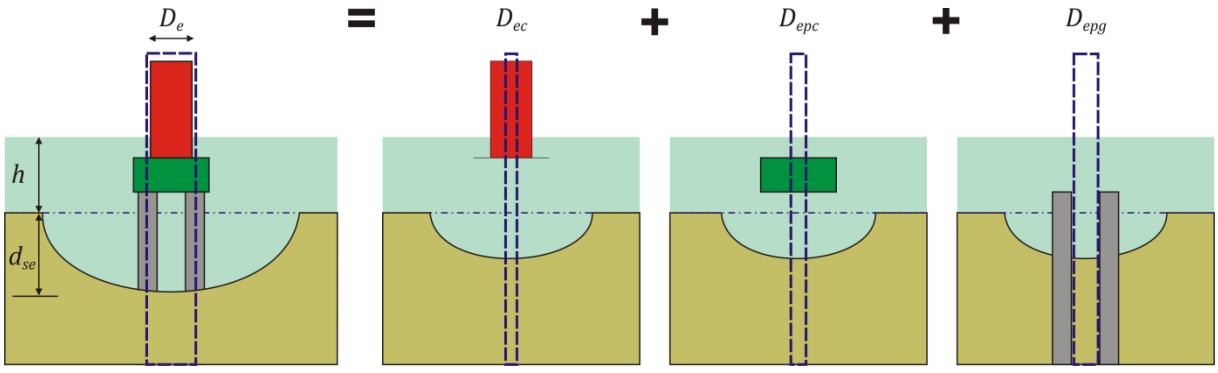

Figure 2.36 – Conceptual hypothesis of summing equivalent diameters, adapted from Sheppard and Renna (2010)

Sheppard and Renna (2010) analysed three configurations of complex piers, according to the pile-cap position. The first configuration is characterized by the fact that the bottom of the pile cap is above the

initial bed level (Case 1), the second configuration corresponds to the pile cap being partially buried in the bed (Case 2) and the third configuration is represented by the pile cap completely buried in the bed (Case 3).

Scour depth prediction for Case 1:

The equivalent diameter of the column, D_{ec}, can be computed by

$$D_{ec} = \begin{cases} K_s K_\theta K_f K_{hc} D_c & \text{for } H_c < h_{c(\max)} \\ 0 & \text{for } H_c \geq h_{c(\max)} \end{cases} \tag{2.65}$$

where K_s = column shape factor; K_θ = column skew factor; K_f = pile cap extension factor; K_{hc} = factor to account for the position of the bottom of the column relative to the initial bed level and $h_{c(\max)}$ = limiting water depth at which the flow influences the scouring process around the column. The limiting variable $h_{c(\max)}$ and those factors are estimated by the following expressions:

$$h_{c(\max)} = \begin{cases} 3K_s K_\theta D_c & \text{for } h \geq 3K_s K_\theta D_c \\ h & \text{for } h < 3K_s K_\theta D_c \end{cases} \tag{2.66}$$

$$K_s = \begin{cases} 0.86 + 0.97 \left| \theta \frac{\pi}{180°} - \frac{\pi}{4} \right|^4 & \text{for rectangular columns} \\ 1 & \text{for circular columns} \end{cases} \tag{2.67}$$

$$K_\theta = \frac{D_c \cdot cos\theta + L_c \cdot sin\theta}{D_c} \tag{2.68}$$

$$K_f = \begin{cases} 1 & \text{for } \frac{f}{D_c} < 1 \\ 0.75 + 0.5\left(\frac{f}{D_c}\right) - 0.25\left(\frac{f}{D_c}\right)^2 & \text{for } 1 \leq \frac{f}{D_c} \leq 3 \\ 0 & \text{for } \frac{f}{D_c} > 3 \end{cases} \tag{2.69}$$

where f is the weighted average of the pile cap front and side extensions beyond the corresponding column faces. This is computed by the following equation

$$f = \begin{cases} \frac{3f_l + f_t}{4} & \text{for } \theta \leq 45° \\ \frac{f_l + 3f_t}{4} & \text{for } \theta > 45° \end{cases} \tag{2.70}$$

$$K_{hc} = \left\{ \begin{array}{l} 0.41 - 1.34\left[\dfrac{H_c}{h_{c(\max)} + d_{sc(\max)}}\right] + 0.86\left[\dfrac{H_c}{h_{c(\max)} + d_{sc(\max)}}\right]^2 \\ +1.40\left[\dfrac{H_c}{h_{c(\max)} + d_{sc(\max)}}\right]^3 - 1.65\left[\dfrac{H_c}{h_{c(\max)} + d_{sc(\max)}}\right]^4 \end{array} \right\} \tag{2.71}$$

where $d_{sc(\max)}$ = maximum column scour depth, which is calculated using $D = K_s K_\theta D_c$ in the single pier equations (section 2.2.6.2).

The equivalent diameter of the pile cap, D_{epc}, can be computed by

$$D_{epc} = \begin{cases} K_s K_\theta K_{hpc} D_{pc} & \text{for } H_{pc} < h_{pc(\max)} \\ 0 & \text{for } H_{pc} \geq h_{pc(\max)} \end{cases} \tag{2.72}$$

where K_s = pile cap shape factor; K_θ = pile cap skew factor; K_{hpc} = factor to account for the position of the bottom of the pile cap relative to the initial bed level and $h_{pc(\max)}$ = limiting water depth at which the flow influences the scouring process around the pile cap. The limiting variable $h_{pc(\max)}$ and those factors are estimated by the following equation

$$h_{pc(\max)} = \begin{cases} D_{ec} + 1.5 K_s K_\theta D_{pc} & \text{for } h \geq \left(D_{ec} + 1.5 K_s K_\theta D_{pc}\right) \\ h & \text{for } h < \left(D_{ec} + 1.5 K_s K_\theta D_{pc}\right) \end{cases} \tag{2.73}$$

$$K_s = \begin{cases} 0.86 + 0.97\left|\theta \dfrac{\pi}{180^\circ} - \dfrac{\pi}{4}\right|^4 & \text{for rectangular pile caps} \\ 1 & \text{for circular pile caps} \end{cases} \tag{2.74}$$

$$K_\theta = \frac{D_{pc} \cdot cos\theta + L_{pc} \cdot sin\theta}{D_{pc}} \tag{2.75}$$

$$K_{hpc} = \left(\begin{array}{l} -1.34\left\{\left[\dfrac{H_{pc}}{h_{pc(\max)} + d_{spc(\max)}}\right] - \left[\dfrac{H_c}{h_{pc(\max)} + d_{spc(\max)}}\right]\right\} \\ +0.86\left\{\left[\dfrac{H_{pc}}{h_{pc(\max)} + d_{spc(\max)}}\right]^2 - \left[\dfrac{H_c}{h_{pc(\max)} + d_{spc(\max)}}\right]^2\right\} \\ +1.40\left\{\left[\dfrac{H_{pc}}{h_{pc(\max)} + d_{spc(\max)}}\right]^3 - \left[\dfrac{H_c}{h_{pc(\max)} + d_{spc(\max)}}\right]^3\right\} \\ -1.65\left\{\left[\dfrac{H_{pc}}{h_{pc(\max)} + d_{spc(\max)}}\right]^4 - \left[\dfrac{H_c}{h_{pc(\max)} + d_{spc(\max)}}\right]^4\right\} \end{array} \right) \tag{2.76}$$

where $d_{spc(\max)}$ = maximum pile cap scour depth, which is calculated using $D = K_s K_\theta D_{pc}$ in the single pier equations (section 2.2.6.2). In the equation (2.76), if $H_c > h_{pc(\max)}$, then $H_c = h_{pc(\max)}$.

The equivalent diameter of the pile group, D_{epg}, can be computed by

$$D_{epg} = K_{Spg} K_{sp} K_m K_{hpg} W_{pg} \tag{2.77}$$

where K_{Spg} = pile group shape factor; K_{sp} = pile spacing factor; K_m = factor for number of aligned rows; K_{hpg} = factor to account for the height of the pile group relative to the initial bed level and W_{pg} = sum of the non-overlapping individual pile widths projected on a plane normal to the approach flow, calculated according to Figure 2.35. The shape factor for the pile group can be estimated by the following equation

$$K_{Spg} = \frac{K_{Sp} - K_{S(pg)}}{9}\left(\frac{S_p}{w_{pi}}\right) + K_{Sp} - \frac{10}{9}\left(K_{Sp} - K_{S(pg)}\right) \tag{2.78}$$

where K_{Sp} = pile shape factor and $K_{S(pg)}$ = pile group configuration factor. The variable w_{pi} can be calculated by equation (2.62) while these two factors can be determined by

$$K_{Sp} = \begin{cases} 0.86 + 0.97\left|\theta\dfrac{\pi}{180°} - \dfrac{\pi}{4}\right|^4 & \text{for rectangular piles} \\ 1 & \text{for circular piles} \end{cases} \tag{2.79}$$

$$K_{S(pg)} = \begin{cases} 0.86 + 0.97\left|\theta\dfrac{\pi}{180°} - \dfrac{\pi}{4}\right|^4 & \text{for pile groups with } \dfrac{S_p}{D_p} \leq 3 \text{ and } n > 1 \\ 1 & \text{for pile groups with } \dfrac{S_p}{D_p} > 3 \text{ or } n = 1 \end{cases} \tag{2.80}$$

where S_p = smaller distance of S_m and S_n of Figure 2.35.

The factor for pile spacing can be calculated by equation (2.61). The factor for number of aligned rows can be estimated by the following expression

$$K_m = \begin{cases} 1 & \text{for } |\theta| \geq 5° \text{ or } \dfrac{S_p}{D_p} > 7, \text{ or } m = 1 \\ 0.98 + 0.017m & \text{for } |\theta| < 5°, \dfrac{S_p}{D_p} \leq 6 \text{ and } m < 8 \end{cases} \tag{2.81}$$

Equation (2.81) was provided by Sheppard (personal communication) to correct the original equation (Sheppard and Renna 2010). The factor that accounts for the location of the top of the group can be calculated by the following equation

$$K_{hpg} = \begin{cases} \left(\dfrac{H_{pg} + d_{scpc}}{h_{pg(\max)}}\right)^{0.1} & \text{for} \quad \left(\dfrac{H_{pg} + d_{scpc}}{h_{pg(\max)}}\right) \leq 1 \\ 1 & \text{for} \quad \left(\dfrac{H_{pg} + d_{scpc}}{h_{pg(\max)}}\right) > 1 \end{cases} \tag{2.82}$$

where d_{scpc} = scour depth produced by the combination of the column and pile cap using $D = D_{ec} + D_{epc}$ in the single pier equations (section 2.2.6.2) and $h_{pg(\max)}$ = limiting water depth at which the flow influences the scouring process around the pile group, which it is estimated by

$$h_{pg(\max)} = \begin{cases} K_{Spg}K_{sp}K_mW_{pg} & \text{for} \quad h + d_{scpc} > K_{Spg}K_{sp}K_mW_{pg} \\ h + d_{scpc} & \text{for} \quad h + d_{scpc} \leq K_{Spg}K_{sp}K_mW_{pg} \end{cases} \tag{2.83}$$

Scour depth prediction for Case 2:

Since the bottom of the column is above the bed for Case 2, the procedure for computing D_{ec} is the same as for Case 1, thus

$$D_{ec} = K_sK_\theta K_fK_{hc}D_c \qquad \text{for} \quad H_c < h_{c(\max)} \tag{2.84}$$

The respective factors can be calculated using the set of equations (2.66) to (2.71).

In this case, the procedure for computing D_{epc} requires iterative calculations since the shape and size of the structure exposed to the flow can change with the progress of the local scour. The procedure is, according to Sheppard and Renna (2010): (1) set $i = 0$; (2) estimate $d_{s[c+pc(0)]} = d_{sc}$ using the D_{ec} calculated by equation (2.84) in the single pier equations (section 2.2.6.2); (3) calculate the distance from the pre-locally scoured bed to the bottom of the scour hole until an equilibrium scour is reached or the pile cap is uncovered, H^*_{pc}, by equation (2.85); (4) compute the equivalent diameter of the pile cap $D_{epc(i)}$ by equation (2.86), in this equation if $H_c > h_{pc(\max)}$ set $H_c = h_{pc(\max)}$; (5) compute the scour depth due to the column and the portion of the pile cap that is exposed, $d_{s[c+pc(i)]}$, using the single piers equations (section 2.2.6.2) with a $D = D_{ec} + D_{epc(i)}$; and (6) check for convergence using equation (2.88), if $\Delta \leq 0.05$ the procedure ends, otherwise set $i = i + 1$ and return to step (3) of the procedure.

$$H^*_{pc} = \begin{cases} H_{pc} & \text{for} \quad d_{s[c+pc(i)]} \geq |H_{pc}| \\ -d_{s[c+pc(i)]} & \text{for} \quad d_{s[c+pc(i)]} < |H_{pc}| \end{cases} \tag{2.85}$$

$$D_{epc(i)} = K_sK_\theta K_{hpc}D_{pc} \qquad \text{for} \quad H_{pc} < h_{pc(\max)} \tag{2.86}$$

where $h_{pc(\max)}$, K_s and K_θ can be estimated by equations (2.73), (2.74) and (2.75) respectively, while K_{hpc} is estimated by

$$K_{hpc} = \begin{pmatrix} -1.34\left\{\left[\frac{H_{pc}^{*}}{h_{pc(\max)} + d_{spc(\max)}}\right] - \left[\frac{H_c}{h_{pc(\max)} + d_{spc(\max)}}\right]\right\} \\ +0.86\left\{\left[\frac{H_{pc}^{*}}{h_{pc(\max)} + d_{spc(\max)}}\right]^2 - \left[\frac{H_c}{h_{pc(\max)} + d_{spc(\max)}}\right]^2\right\} \\ +1.40\left\{\left[\frac{H_{pc}^{*}}{h_{pc(\max)} + d_{spc(\max)}}\right]^3 - \left[\frac{H_c}{h_{pc(\max)} + d_{spc(\max)}}\right]^3\right\} \\ -1.65\left\{\left[\frac{H_{pc}^{*}}{h_{pc(\max)} + d_{spc(\max)}}\right]^4 - \left[\frac{H_c}{h_{pc(\max)} + d_{spc(\max)}}\right]^4\right\} \end{pmatrix} \quad (2.87)$$

where $d_{spc(\max)}$ = maximum pile cap scour depth, which is calculated using $D = K_s K_\theta D_{pc}$ in the single pier equations (section 2.2.6.2).

$$\Delta = \left|\frac{d_{s[c+pc(i)]} - d_{s[c+pc(i-1)]}}{d_{s[c+pc(i-1)]}}\right| \quad (2.88)$$

In this case, D_{epg} is calculated depending if the pile group is exposed in the scour hole, thus

$$\begin{aligned} D_{epg} &= K_{Spg} K_{sp} K_m K_{hpg} W_{pg} && \text{for } d_{scpc} > |H_{pg}| \\ D_{epg} &= 0 && \text{for } d_{scpc} \le |H_{pg}| \end{aligned} \quad (2.89)$$

where d_{scpc} = scour depth produced by the combination of the column and pile cap using a diameter $D = D_{ec} + D_{epc}$ in the single pier equations (section 2.2.6.2). K_{Spg}, K_{sp} and K_m can be estimated by equations (2.78), (2.61) and (2.81) respectively. The variable W_{pg} can be calculated according to Figure 2.35 while K_{hpg} is estimated by the following equation

$$K_{hpg} = \begin{cases} \left(\frac{H_{pg} + d_{scpc}}{h_{pg(\max)}}\right)^{0.1} & \text{for } \left(\frac{H_{pg} + d_{scpc}}{h_{pg(\max)}}\right) \le 1 \\ 1 & \text{for } \left(\frac{H_{pg} + d_{scpc}}{h_{pg(\max)}}\right) > 1 \end{cases} \quad (2.90)$$

where $h_{pg(\max)}$ = limiting water depth at which the flow influences the scouring process around the pile group, which is estimated by

$$h_{pg(\max)} = \begin{cases} K_{Spg} K_{sp} K_m W_{pg} & \text{for } h + d_{scpc} > K_{Spg} K_{sp} K_m W_{pg} \\ h + d_{scpc} & \text{for } h + d_{scpc} \le K_{Spg} K_{sp} K_m W_{pg} \end{cases} \quad (2.91)$$

Scour depth prediction for Case 3:

The equivalent diameter of the column, D_{ec}, can be computed by

$$D_{ec} = \begin{cases} K_s K_\theta K_f K_{hc} D_c & \text{for } d_{sc(\max)} > |H_c| \\ K_s K_\theta D_c & \text{for } d_{sc(\max)} \leq |H_c| \end{cases} \quad (2.92)$$

where $d_{sc(\max)}$ = maximum column scour depth, which is calculated using $D = K_s K_\theta D_c$ in the single pier equations (section 2.2.6.2). The factors can be calculated through equations (2.66) to (2.71).

If the scour depth due to the column enables the top of the pile cap to be reached, *i.e.*, $d_{sc(\max)} > |H_c|$, and D_{ec} calculated by equation (2.92) is smaller than $D_{ec(\min)}$ (equivalent diameter of a single pier that leads to a scour depth equal to $|H_c|$), $D_{ec} = D_{ec(\min)}$.

In this case, in the procedure for computing D_{epc} iterative calculations is necessary as mentioned for Case 2. According to Sheppard and Renna (2010), the procedure is: (1) set $i = 0$; (2) estimate $d_{s[c+pc(0)]} = d_{sc}$ using the D_{ec} calculated by equation (2.84) in the single pier equations (section 2.2.6.2); (3) calculate H_{pc}^* by equation (2.85); (4) compute $D_{epc(i)}$ by equation (2.93), in this equation if $H_c > h_{pc(\max)}$ set $H_c = h_{pc(\max)}$; (5) compute the scour depth due to the column and the portion of the pile cap that is exposed, $d_{s[c+pc(i)]}$, using the single piers equations (section 2.2.6.2) with a $D = D_{ec} + D_{epc(i)}$; and (6) check for convergence using equation (2.88), if $\Delta \leq 0.05$ the procedure ends, otherwise set $i = i + 1$ and return to step (3) of the procedure.

$$D_{epc(i)} = K_s K_\theta K_{hpc} K_{bpc} D_{pc} \qquad \text{for } H_{pc} < h_{pc(\max)} \quad (2.93)$$

where K_{bpc} = factor that accounts for the dependence of the pile-cap position on the scour hole. $h_{pc(\max)}$, K_s, K_θ and K_{hpc} can be estimated by equations (2.73), (2.74), (2.75) and (2.87) respectively, while K_{bpc} is estimated by

$$K_{bpc} = \begin{cases} 0.93\left(\frac{H_c}{d_{sc(\max)}}\right)^2 + 1.93\left(\frac{H_c}{d_{sc(\max)}}\right) + 1 & \text{for } -d_{scpc} \leq H_c \\ 0 & \text{for } -d_{scpc} > H_c \end{cases} \quad (2.94)$$

where $d_{sc(\max)}$ = maximum column scour depth, which is calculated using $D = K_s K_\theta D_c$ in the single pier equations (section 2.2.6.2).

In this case, D_{epg} is calculated depending if the pile group is exposed in the scour hole, thus

$$D_{epg} = \begin{cases} K_{Spg} K_{sp} K_m K_{hpg} K_{bpg} W_{pg} & \text{for } d_{scpc} > |H_{pg}| \\ 0 & \text{for } d_{scpc} \leq |H_{pg}| \end{cases} \quad (2.95)$$

where $K_{bpg} =$ buried pile group attenuation factor and d_{scpc} = scour depth produced by the combination of the column and pile cap using $D = D_{ec} + D_{epc}$ in the single pier equations (section 2.2.6.2). K_{Spg}, K_{sp} and K_m can be estimated by equations (2.78), (2.61) and (2.81) respectively. W_{pg} can be calculated according to Figure 2.35 while K_{hpg} is estimated by the following equation

$$K_{hpg} = \begin{cases} \left(\frac{H_{pg} + d_{scpc}}{h_{pg(\max)}}\right)^{0.1} & \text{for } \left(\frac{H_{pg} + d_{scpc}}{h_{pg(\max)}}\right) \leq 1 \\ 1 & \text{for } \left(\frac{H_{pg} + d_{scpc}}{h_{pg(\max)}}\right) > 1 \end{cases} \tag{2.96}$$

where $h_{pg(\max)}$ = limiting water depth at which the flow influences the scouring process around the pile group, which is estimated by

$$\begin{aligned} h_{pg(\max)} &= K_{Spg} K_{sp} K_m W_{pg} && \text{for } h + d_{scpc} > K_{Spg} K_{sp} K_m W_{pg} \\ h_{pg(\max)} &= h + d_{scpc} && \text{for } h + d_{scpc} \leq K_{Spg} K_{sp} K_m W_{pg} \end{aligned} \tag{2.97}$$

K_{bpg} can be calculated as

$$K_{bpg} = \frac{H_{pg} + d_{scpc}}{d_{scpc}} \tag{2.98}$$

3. EXPERIMENTAL SETUP

3.1. INTRODUCTION

Details for the experimental campaign performed in the present study are provided in this chapter. The experimental work planned in this study to understand and characterize pier's local scour was carried out in two flumes located, respectively, at the Hydraulics and Environment Department, National Laboratory for Civil Engineering (LNEC) and at the Faculty of Engineering of the University of Porto (FEUP). A total of 92 tests were performed using seven different complex pier models. Six of them were analysed at LNEC's flume, *i.e.*, Model 1 to Model 6 in Figure 3.1(a), while the remaining one was evaluated at FEUP's flume, *i.e.*, Model 7 in Figure 3.1(b). The dimensions of the seven pier models analysed in the present study are considerably higher than the pier models used in the five studies from literature (see Figure 2.27). The experimental setup includes: (1) the description of the experimental campaign; (2) the description of the laboratory facilities (two flumes); and finally (3) the experimental procedures in both flumes.

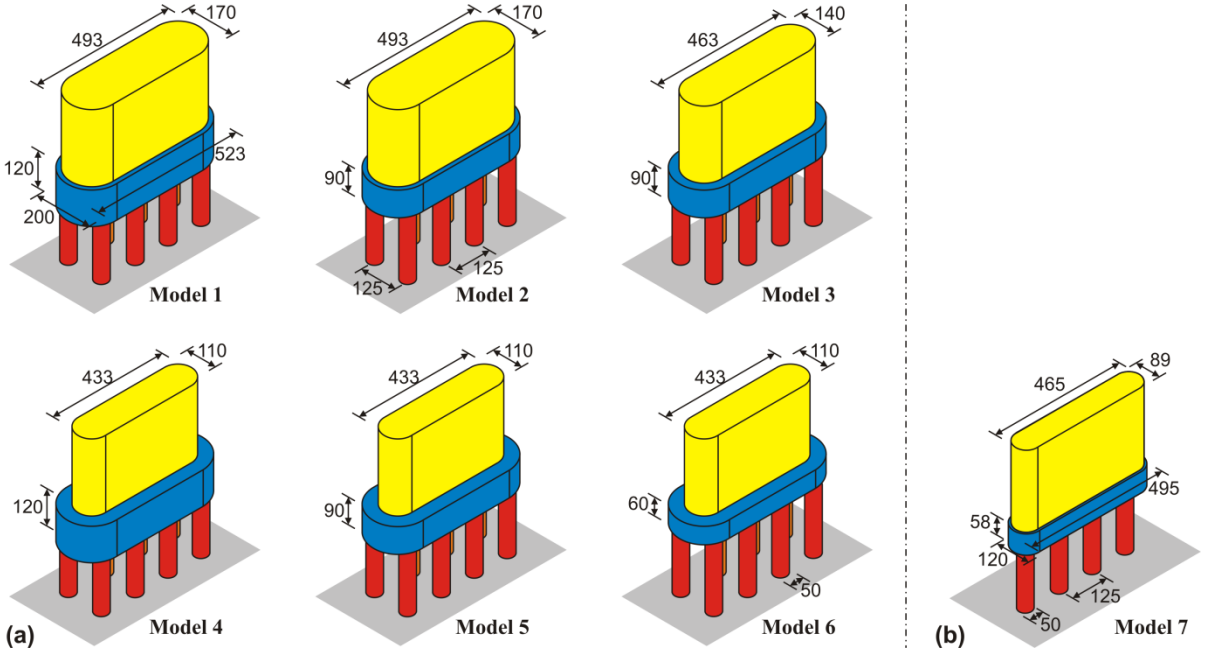

Figure 3.1 – Dimensions of complex pier models analysed at (units in millimetres): (a) LNEC's flume and (b) FEUP's flume

In the experimental campaign three configurations of the complex pier models were considered, as shown in Figure 3.2. The Configuration C1 corresponds to the complete complex pier structure (*i.e.*, complex pier with the three components) while the Configuration C2 corresponds to the mentioned

complete structure without the column and the Configuration C3 corresponds to the complete structure without the pile group.

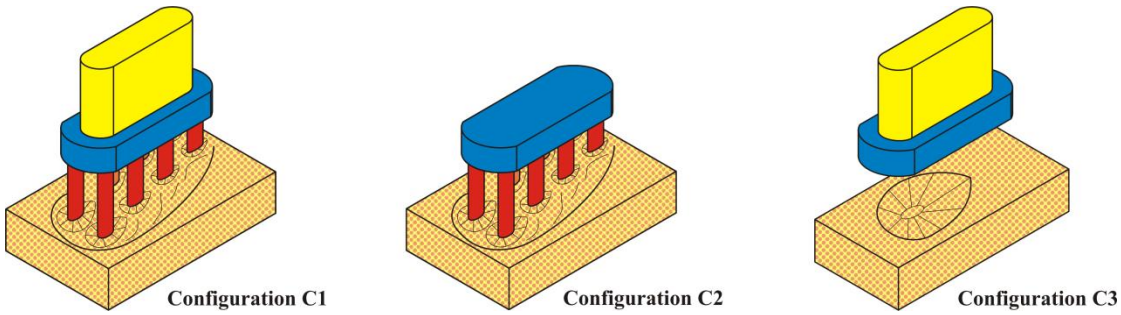

Figure 3.2 – Complex pier configurations

A total of 48 tests were performed for Configuration C1 in order to quantify the influence of the complex pier position (relative to the initial bed level) and complex pier geometry on the temporal evolution of the scour depth (results and discussion presented in Chapter 4) and on the equilibrium scour depth (results and discussion presented in Chapter 5). The results of these 48 tests were also used to evaluate the three mentioned methods to predict equilibrium scour depths (results and discussion presented in Chapter 7). The following effects on the equilibrium scour depth were analysed:

1. The combined effects of the relative column width, D_c/D_{pc}, and the relative column position, H_c/h, were evaluated on the basis of the results obtained with Model 2 ($D_c/D_{pc} = 0.85$), Model 3 ($D_c/D_{pc} = 0.70$) and Model 5 ($D_c/D_{pc} = 0.55$). In the tests with these three different models only the column dimensions (width and length) were changed, as shown in Figure 3.1(a).
2. The combined effects of the relative pile-cap thickness, T/h, and the relative column position, H_c/h, were analysed on the basis of the results obtained with Model 4 ($T/h = 0.60$), Model 5 ($T/h = 0.45$) and Model 6 ($T/h = 0.30$). For these three models (4, 5 and 6, all of them with $D_c/D_{pc} = 0.55$), only the pile cap thickness was changed, as shown in Figure 3.1(a).
3. The effect of the pile-group configuration (characterized by the number of pile columns, n) was evaluated on the basis of the results obtained with Model 3 ($n = 2$, Figure 3.1(a)) and Model 7 ($n = 1$, Figure 3.1(b)).

A total of 44 tests were performed for Configurations C2 and C3. The results of these tests as well as the results of some tests with Configuration C1 were used to quantify the contribution of the complex pier components on the total equilibrium scour depth (results and discussion presented in Chapter 6).

3.2. EXPERIMENTAL CAMPAIGN

3.2.1 COMPLEX PIER MODELS

As mentioned above, seven complex pier models were built in order to assess the influence of its geometry on the development of the scour hole. These models were designed with a rectangular round-nose column founded on a rectangular round-nose pile cap, supported by a pile group. The arrangement of this last component consists of: two alignments of four cylindrical piles in the case of

Models 1 to 6 (Figure 3.1(a)) and one alignment of four cylindrical piles for Model 7 (Figure 3.1(b)). The longitudinal axis of the complex pier models was aligned with the approach flow, *i.e.*, $\theta = 0°$. The geometric characteristics of the seven models are summarized in Table 3.1.

Table 3.1 – Geometric characteristics of the complex pier models of the experimental campaign

Variable	Model 1	Model 2	Model 3	Model 4	Model 5	Model 6	Model 7
D_c (m)	0.170	0.170	0.140	0.110	0.110	0.110	0.089
L_c (m)	0.493	0.493	0.463	0.433	0.433	0.433	0.465
f_l (m)	0.015	0.015	0.030	0.045	0.045	0.045	0.015
f_t (m)	0.015	0.015	0.030	0.045	0.045	0.045	0.015
D_{pc} (m)	0.200	0.200	0.200	0.200	0.200	0.200	0.120
L_{pc} (m)	0.523	0.523	0.523	0.523	0.523	0.523	0.495
T (m)	0.120	0.090	0.090	0.120	0.090	0.060	0.058
D_p (m)	0.050	0.050	0.050	0.050	0.050	0.050	0.050
f_p (m)	0.030	0.030	0.030	0.030	0.030	0.030	0.035
m	4	4	4	4	4	4	4
n	2	2	2	2	2	2	1
S_m (m)	0.125	0.125	0.125	0.125	0.125	0.125	0.125
S_n (m)	0.125	0.125	0.125	0.125	0.125	0.125	-

3.2.2 EXPERIMENTAL CONDITIONS

In both flumes, the recess boxes – where the test models were installed – were filled with quartz sand so that a corresponding scour hole would develop. A uniform sediment and coarse material was used in the bed with the purpose of preventing ripples formation. Figure 3.3 shows the grading curve of the sand obtained by mechanical sieving. According to the grading curve, the median particle size (d_{50}) was 0.86 mm corresponding to coarse sand (defined by $d_{50} \geq 0.6$ mm). The geometric standard deviation of the grain-size distribution ($\sigma_g = \sqrt{d_{84}/d_{16}}$) was 1.28. This confirms that the sediment is uniform and therefore the bed material gradation effect on d_{se} is avoided, according to section 2.2.5.4.

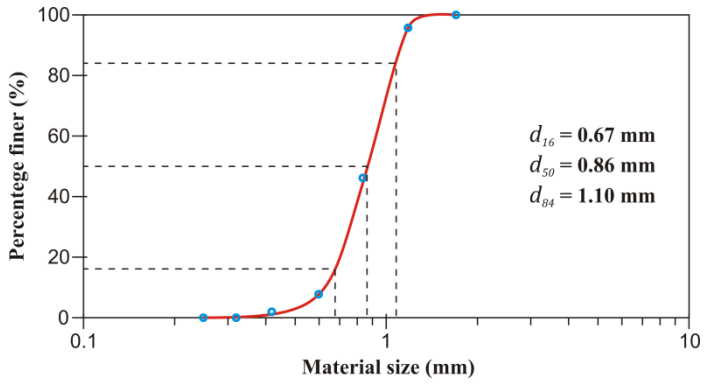

Figure 3.3 – Grading curve of the sand used in the experiments

The maximum scour depth can be achieved under clear-water condition when the approach velocity, U, is close to critical velocity, U_c, as shown in Figure 2.8. The tests on LNEC's flume (Models 1 to 6) were carried out with constant approach flow depth, $h = 0.20$ m, and average velocity, $U = 0.26$ m/s. The tests on FEUP's flume (Model 7) were carried out with $h = 0.18$ m and $U = 0.31$ m/s. The critical velocity was considered around the value $U_c \approx 0.32$ m/s and was obtained from Neill (1967) equation:

$$U_c = \sqrt{2.5\left(\frac{h}{d_{50}}\right)^{0.2} g\Delta d_{50}} \tag{3.1}$$

This equation was validated by Grimaldi *et al*. (2009) through tests of the incipient motion of the bed material carried out also in the flume used in this study (LNEC's flume), with similar sediment and flow conditions. The resulting flow intensity ratios were $U/U_c \approx 0.80$ and $U/U_c \approx 0.97$ at LNEC's and FEUP's flumes, respectively.

According to Chiew and Melville (1987), the flow contraction effect is negligible when $D_{pc}/B < 0.10$ (B is the flume width). According to Yalin (1971), the wall effect is also negligible when $B/h > 5$. The chosen relations $D_{pc}/B = 0.10$ and $B/h = 10$ (in Models 1 to 6) and $D_{pc}/B = 0.12$ and $B/h = 5.6$ (in Model 7), could then guarantee the absence of contraction and wall effects.

3.2.3 TESTS

In order to evaluate scouring effects around complex piers, twelve different positions of the complex pier in relation to the initial bed level (each position corresponding to a value of H_c/h) were analysed for the Models 1 to 6 (henceforth referred to as Positions A to L) and eight different pile-cap positions in Model 7 (henceforth referred to as Positions M to T), as shown in Figure 3.4. These pile-cap positions (represented by H_c/h) were selected in order to cover extensively the three typical situations described in section 2.3.3, *i.e.*, Situation 1 - characterized by the bottom of the pile cap being above the initial bed level, Situation 2 - characterized by the pile cap being partially buried in the bed and Situation 3 - characterized by the pile cap being completely buried in the bed, as also shown in Figure 3.4.

Each test is named by associating the complex pier model (see Figure 3.1), the pile-cap position (see Figure 3.4) and the complex pier configuration (see Figure 3.2). For example, the designation M4E2 applies to the test with Model 4 in the Position E, where $H_c/h = 0.67$, for Configuration C2 (complex pier without the column). The designations of the tests performed with the seven complex pier models are summarized in Table 3.2, Table 3.3, Table 3.4 and Table 3.5. The tests on these tables which name is marked with an asterisk (*) at the end correspond, in fact, to non-performed tests because the scour depth results corresponding to other performed for that pile-cap position do also apply to the tests. For example, in the Position A, where both column and pile cap emerge out of the flow ($H_c/h = 1.70$), the measurements of tests M1A1, M2A1, M3A1, M4A1, M5A1 and M6A1 correspond to a single test (M1A1). The same applies to tests: (1) M1B1, M2C1, M3C1, M4B1, M5C1 and M6D1; (2) M1C1, M2D1, M3D1, M4C1 and M5D1; (3) M1D1 and M4D1; (4) M1K1 and M2K1; (5) M1L1 and M2L1; (6) M4J1, M5J1 and M6J1; (7) M4K1, M5K1 and M6K1; (8) M4L1, M5L1 and M6L1; (9) M2D1 and M4D2; (10) M2D2, M3D2 and M5D2; (11) M1D3 and M4D3; and (12) M2D3, M3D3 and M5D3.

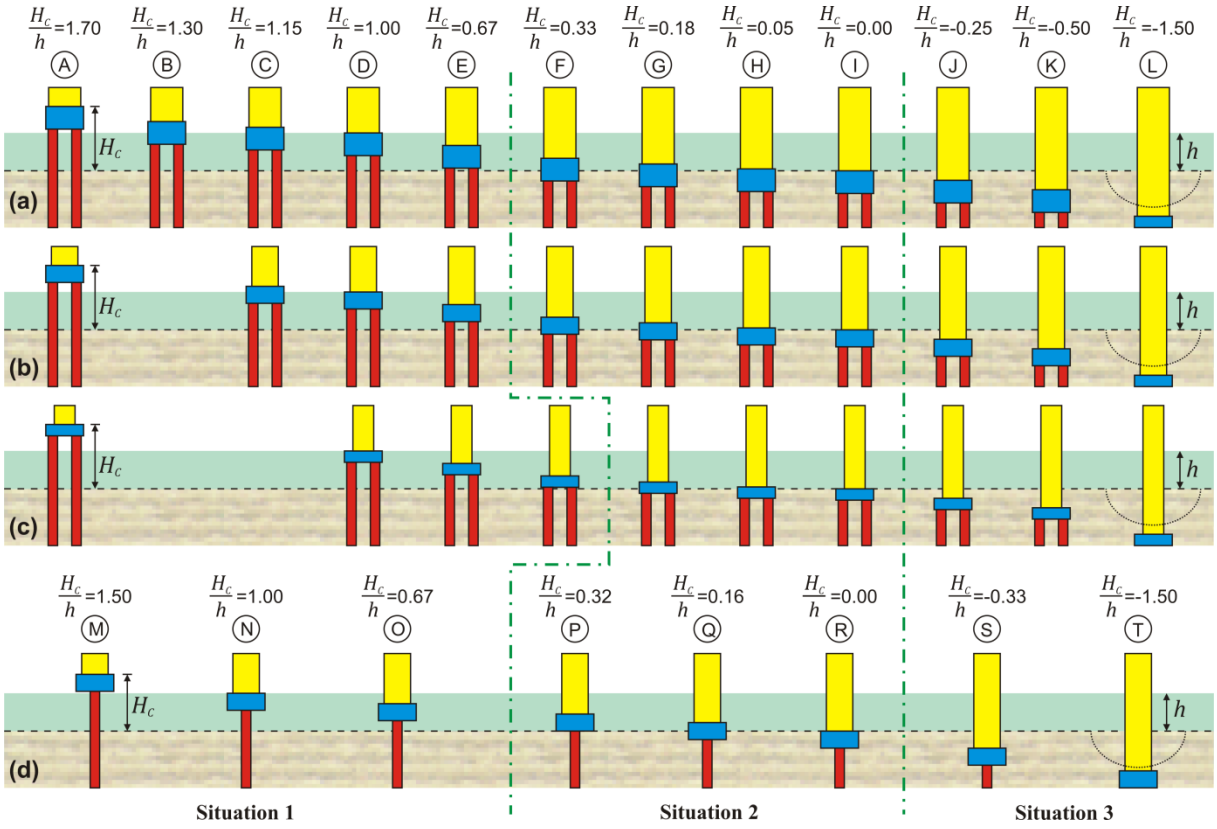

Figure 3.4 – Scheme of the pile-cap positions associated with the study of the three typical situations for: (a) Models 1 and 4, (b) Models 2, 3 and 5, (c) Model 6 and (d) Model 7

Table 3.2 – Designation of the tests performed with Configuration C1 (Models 1 to 6)

Position	H_c/h	Model 1	Model 2	Model 3	Model 4	Model 5	Model 6
A	1.700	M1A1	M2A1*	M3A1*	M4A1*	M5A1*	M6A1*
B	1.300	M1B1*			M4B1*		
C	1.150	M1C1*	M2C1*	M3C1*	M4C1*	M5C1*	
D	1.000	M1D1	M2D1*	M3D1*	M4D1*	M5D1	M6D1
E	0.667	M1E1	M2E1	M3E1	M4E1	M5E1	M6E1
F	0.333	M1F1	M2F1	M3F1	M4F1	M5F1	M6F1
G	0.185				M4G1	M5G1	M6G1
H	0.050	M1H1	M2H1	M3H1	M4H1	M5H1	M6H1
I	0.000	M1I1	M2I1	M3I1	M4I1	M5I1	M6I1
J	−0.235		M2J1	M3J1			
	−0.250				M4J1*	M5J1*	M6J1
K	−0.500	M1K1*	M2K1	M3K1	M4K1*	M5K1*	M6K1
L	−1.500	M1L1*	M2L1	M3L1	M4L1*	M5L1*	M6L1

Table 3.3 – Designation of the tests performed with Configuration C2 (Models 1 to 6)

Position	H_c/h	Model 1	Model 2	Model 3	Model 4	Model 5	Model 6
D	1.000	M1D2*	M2D2*	M3D2*	M4D2*	M5D2*	M6D2*
E	0.667	M1E2*	M2E2*	M3E2*	M4E2	M5E2	M6E2
F	0.333	M1F2*	M2F2*	M3F2*	M4F2	M5F2	M6F2
G	0.185				M4G2	M5G2	M6G2
H	0.050	M1H2*	M2H2*	M3H2*	M4H2	M5H2*	M6H2*

Table 3.4 – Designation of the tests performed with Configuration C3 (Models 1 to 6)

Position	H_c/h	Model 1	Model 2	Model 3	Model 4	Model 5	Model 6
D	1.000		M2D3*	M3D3*	M4D3	M5D3	
E	0.667		M2E3	M3E3	M4E3	M5E3	M6E3
F	0.333		M2F3	M3F3	M4F3	M5F3	M6F3
G	0.185					M5G3	M6G3
H	0.050		M2H3	M3H3			

Table 3.5 – Designation of the tests performed with Model 7

Position	H_c/h	Configuration C1	Configuration C2	Configuration C3
M	1.500	M7M1		
N	1.000	M7N1	M7N2*	M7N3
O	0.667	M7O1	M7O2	M7O3
P	0.322	M7P1	M7P2	M7P3
Q	0.161	M7Q1	M7Q2	M7Q3
R	0.000	M7R1	M7R2	M7R3
S	−0.330	M7S1		M7S3
T	−1.500	M7T1		

3.3. LNEC'S FLUME

3.3.1 HYDRAULIC CIRCUIT

The laboratory facility – tilting flume (CIV) – is located in LNEC's Maritime Hydraulics Pavilion. The CIV was designed for hydraulic studies concerning sediment transport. It integrates a specific hydraulic circuit, as illustrated in the schema of the Figure 3.5, complemented by photographs of the main elements that are referenced by numbers in correspondence to the schema's legend. The pumping system [5] supplies the upstream tank [9] through the impulsion pipes [7]; afterwards, the flow runs in the flume [17] until it is discharged in the downstream tank [2], the tank is the supply source of the closed circuit. According to Cardoso (1982), the CIV is equipped with three centrifugal pumps [5] that allow water discharges to be pumped with a total capacity of 1.0 m^3/s. The impulsion system, linked between the downstream reservoir and supply tank of the flume, consists of three pipes in parallel [7] associated with each pump.

Figure 3.5 – Scheme and photographs of LNEC's flume, based on the scheme by Cardoso (1982)

The discharge is measured with an electromagnetic flow-meter positioned on the feeder pipe [8]. The supply tank [9] is a rectangular tank 3.0-m-long, 2.5-m-wide and 1.4-m in height. The water supply is provided close to the bottom of the tank through three diffusers [10] reducing the entry inflow rate in the tank. At the exit of the diffusers section there are devices suited to improve the flow uniformity at the channel entrance, including a horizontal metallic grid [11] and a vertical perforated plate [12]. The flume [17] is 40.7-m-long, 1.0-m-deep and 2.0-m-wide. The channel is supported by a metal structure with a fixed support [15] located on the upstream channel. Four hydraulic jacks [16], separated 9.5 meters each, permit to vary the channel slope from 0% to 2.5%. At the exit of the supply tank a rubber gasket [13] that permits the movement (slope variation) of the flume was installed. In the present experimental campaign the flume slope was fixed at 0.02%. The downstream discharge tank [2] has 18.1-m-long, 6.9-m maximum depth and 2.5-m average width, with a useful volume of 150 m^3. The deepest zone of the tank works as a suction chamber of the pumps that carry the flow through impulsion pipes to the supply tank. The surge tank [1] is part of the discharge system. At the beginning of the tests, water is pumped from the surge tank, using a submersible pump, to the discharge tank to supply the volume of water that will be on the flume while at the end of the tests the water returns to the surge tank, as shown in Figure 3.6. A weir, between the discharge tank and the surge tank, permits that the hydraulic head of the pump remains constant (discharge tank).

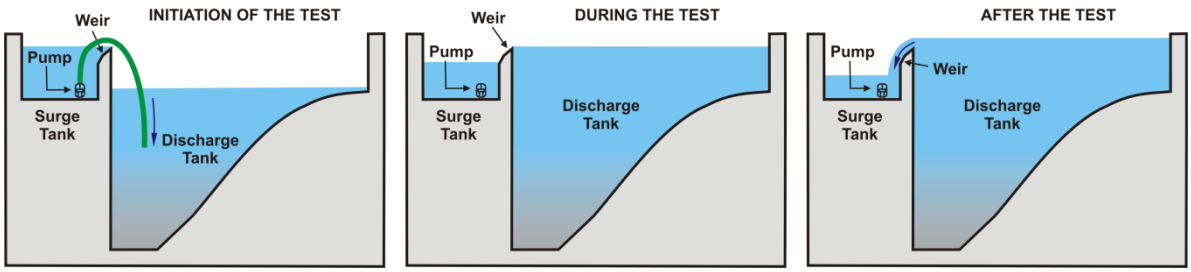

Figure 3.6 – Surge tank operation

3.3.2 TILTING FLUME

A concrete false bottom was installed in the flume in order to perform simultaneously two tests per run. Two 5-m-long and 0.40-m-deep recess boxes filled with sand were left in the false bottom, as illustrated in the schema of the Figure 3.7. Each of the sand boxes was preceded by a 2.0-m-long accelerating ramp [1] and a 7.0-m-long fixed-bed reach [2] and was followed by a 3.0-m-long fixed-bed reach. A stilling recess area [6] (with a downstream accelerating ramp) was designed at the end of the first 3.0-m-long fixed-bed reach, so as to store the sand removed by the flow from the upstream sand recess box and to stop the spread of any organized flow structures originated in the upstream sand recess box. The accelerating ramp [1], in the stilling recess area, tends to regenerate a uniform flow distribution. A 0.3-m-thick and 0.2-m-long fine gravel mattress [4] placed inside a metallic mesh was embedded at the upstream end of the sand recess boxes, being levelled with the adjacent concrete, to avoid scouring at the transition with the sand bed. The complex pier models [5] were built in two different materials: aluminium for the pile group and concrete for the column and the pile cap. The piles were designed with pieces of different lengths to allow obtaining the different positions of the pile (Figure 3.4 (a to c)). The downstream sluice gate [7] allows the water level regulation inside the channel. The flume is equipped with one manual carriage at the upstream recess box [9] and one other in the downstream recess box [10]. Both move along the longitudinal axis of the channel on two precisely levelled rails. They are used to access the experiment area for measuring purposes the scour

depth. Two point gauges to measure the flow depth were used, one located at upstream part of the flume [8] and one located at downstream part of the flume [11]. The point gauges were mounted on aluminium bars.

Figure 3.7 – Scheme and photographs of the tilting flume

3.4. FEUP'S FLUME

Figure 3.8 presents schematically the hydraulic circuit of the FEUP's flume in which the main components are detailed by means of photographs numbered in correspondence to the schema's legend. The water is pumped from the lower reservoir [1] through four pumps [2] to supply the constant head reservoir [4]. The dimensions of the reservoirs are: [1] 12.0-m-width, 8.0-m-length and 2.5-m-height; and [4] 12.3-m-length, 3.3-m-width and 1.3-m-height. The constant head reservoir is provided with a "trop-plein" structure that allows keeping a constant water level in the reservoir.

Figure 3.8 – Scheme of FEUP's flume

The flow discharge is measured by two electromagnetic flow-meters [5] installed at pipes situated between the constant head reservoir and the settling chamber [7]. The maximum flow discharge is 90 l/s. The transition from the constant head reservoir to the channel fixed bed [10] is made by a free fall and ascending ramps [8]. These ramps promote the uniform flow distribution at the entrance of the

channel. At that entrance, immediately after the downstream ramp, a 3.0 m long bed reach was covered with small gravel [9] to provide proper roughness and guarantee fully developed flow. The flume is 33.15-m-long, 1.00-m-wide and 1.00-m-deep. The central bed recess box starts at 16.00 m from the entrance; the length of the recess box [13] is 3.20 m and its depth is 0.35 m. The hopper [14] collects the entrained sediments and the downstream gate [16] allows the water level regulation inside the channel. The complex pier model [12] was built in two different materials: PVC pipes for the pile group and perspex for the column and the pile cap. The piles were designed with pieces of different lengths to permit obtaining the different positions of the piles (Figure 3.4(d)). The flume is equipped with a moving platform supported in its lateral walls. The platform, located over the recess box was used to fix a point gauge [11] to measure scour depths. The flow depth was measured by using a point gauge [15] located at the downstream part of the flume.

3.5. EXPERIMENTAL PROCEDURES

The procedures of the tests carried out at the LNEC's and the FEUP's flumes were based on the procedure followed by Grimaldi (2005), on a study which included tests on local scour around cylindrical single piers with countermeasures at LNEC's facility. The procedures include the following five steps: (1) complex piers preparation and fixation, (2) preparation of the sand bed, (3) flow-discharge and flow-depth stabilization, (4) scour depth measurement, and (5) end of the experiment.

3.5.1 COMPLEX PIERS PREPARATION AND FIXATION

The components of the complex piers models were built separately in order to perform tests in the three mentioned configurations (Figure 3.2). The complex pier models analysed at LNEC's flume were built in two different materials: aluminium for the pile group and concrete for the column and pile cap, as shown in Figure 3.9(a), whereas, the complex pier model analysed at FEUP's flume was also built in two different materials: PVC pipes for the pile group and Perspex for the column and the pile cap, as shown in Figure 3.9(b). The procedures of complex pier fixation on the bed were different in both flumes.

The procedure at the LNEC's flume for tests with Configuration C1 (full complex pier) was: (a) 8 piles of 0.18-m-height were placed and fixed to the two recess boxes floor; (b) other pieces of piles, with the same diameter and different heights, were screwed to the fixed piles to obtain the required pile height; (c) the pile cap was joined to the piles through eight screws (one for each pile); and finally (d) the column was placed above the pile cap and assembled through two long screws, as shown in Figure 3.9(a). For tests with Configuration C2 (complex pier without the column) steps (a) to (c) were followed whereas for tests with Configuration C3 (complex pier with no pile group), the column and the pile cap were suspended by a metallic structure that includes one vertical screw passing through the two elements welded to a thin plate, as shown in Figure 3.9(a).

The procedure at the FEUP's flume for tests with Configuration C1 was: (e) an acrylic board with four stoppers was placed and fixed to the recess box floor; (f) the four PVC piles were fixed to the board placing them in the respective stoppers (50-mm-height perspex cylinders with diameters equal to the inside pile diameter); (g) the pile cap was assembled in the PVC piles through four orifices on the bottom of the pile cap with dimensions equal to the outside pile diameter; and finally (h) the column

was placed above the pile cap and assembled through six pins. For tests with Configuration C2, steps (e) to (g) were followed whereas for tests with Configuration C3, the column and the pile cap were assembled through six pins and the two elements were suspended by a metallic structure that includes two vertical screws passing through the pile cap and column, as shown in Figure 3.9(b).

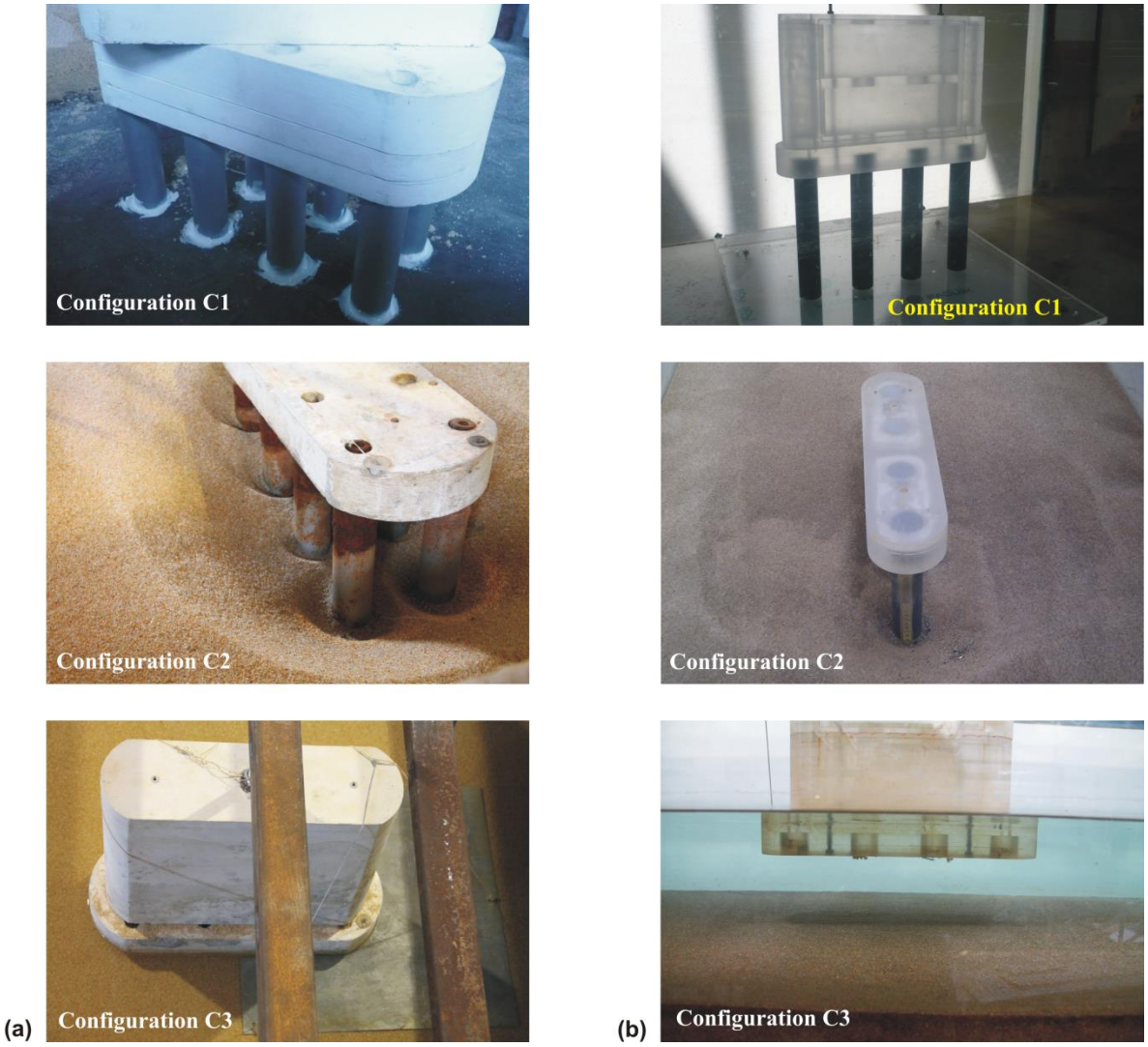

Figure 3.9 – Step 1 of the experimental procedure: (a) LNEC's flume and (b) FEUP's flume

3.5.2 PREPARATION OF THE SAND BED

First, the sand bed was accommodated in the flume recess box(es) (two for LNEC's flume). Then, the sand bed was completely saturated with water and drained at least once to guarantee the adequate sand compaction. An aluminium bar was used to level the sand bed surface with the adjacent concrete bed. Adjustments of the lateral edges and of the zone around the complex pier were done manually. The sand zone around the model configuration was covered with thin metallic plates (filter fabric combined with a thin metallic grid in the case of FEUP's tests) to avoid uncontrolled scour at the beginning of each test, as shown in Figure 3.10.

Figure 3.10 – Step 2 of the experimental procedure: (a) LNEC's flume and (b) FEUP's flume

3.5.3 FLOW-DISCHARGE AND FLOW-DEPTH STABILIZATION

The flumes were slowly filled with water to allow air entrapped in the sediment to escape. For this purpose a discharge of approximately 3 l/s was used in both flumes. When the flow depth in the flumes was about 5 cm, the flow-rate was increased gradually, imposing a high water depth and low flow velocity, as shown in Figure 3.11. The flow depths were regulated by adjusting the downstream sluice gates, as shown in [7] of Figure 3.7 (LNEC's flume) and in [16] of Figure 3.8 (FEUP's flume). Discharges were measured by electromagnetic flow meters, as shown in [8] of Figure 3.5 (LNEC's flume) and in [5] of Figure 3.8 (FEUP's flume). In each test carried out at LNEC's flume, the flow discharge values were recorded approximately every 5 minutes through a computer and those were verified, at least, twice a day in the monitor, as shown in Figure 3.11(a). Whereas, the approach flow depth was verified, at least, twice a day by hydrometers located at upstream and downstream sections of the channel, as shown in [8] and [11] of Figure 3.7. In each test performed at FEUP's flume, the flow discharge and the approach flow depth were verified twice a day in the flow-meter display (Figure 3.11(b)) and by a hydrometer located downstream part of the channel, respectively.

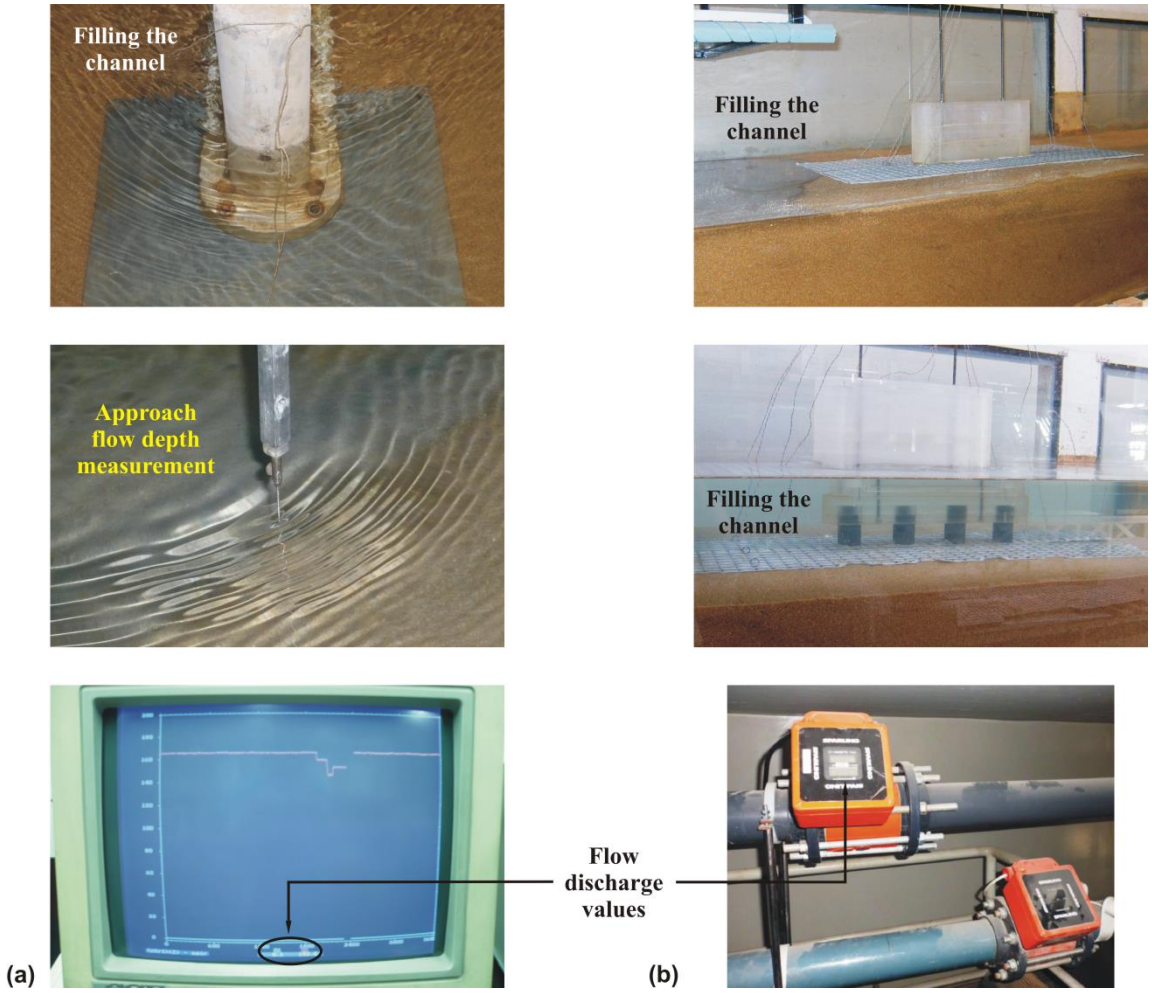

Figure 3.11 – Step 3 of the experimental procedure: (a) LNEC's flume and (b) FEUP's flume

3.5.4 SCOUR DEPTH MEASUREMENT

Once the flow depth and the discharge were established, the thin plates were carefully removed ant the tests started. Scour process was immediately initiated and the scour depth was measured every ≈ 10 minutes during the first hour to the accuracy of ± 0.1 mm with an adapted point gauge. Afterwards, the intervals between measurements increased and, after the first day, two or three measurements were carried out per day. Depending on the test and scour time evolution, one, two or the three complex pier elements were in contact with the bed surface. For this reason, the point gauges were adapted to measure the scour depth in front of: (1) the column; (2) the pile cap; and (3) one of the upstream piles, as shown in Figure 3.12(a) for Models 1 to 6 and in Figure 3.12(b) for Model 7. In the case of measurements in front of the piles, the point gauge was inserted in a small hole drilled through the pile cap for Models 1 to 6 while in the case of Model 7 a metric tape glued in front of the upstream pile was used.

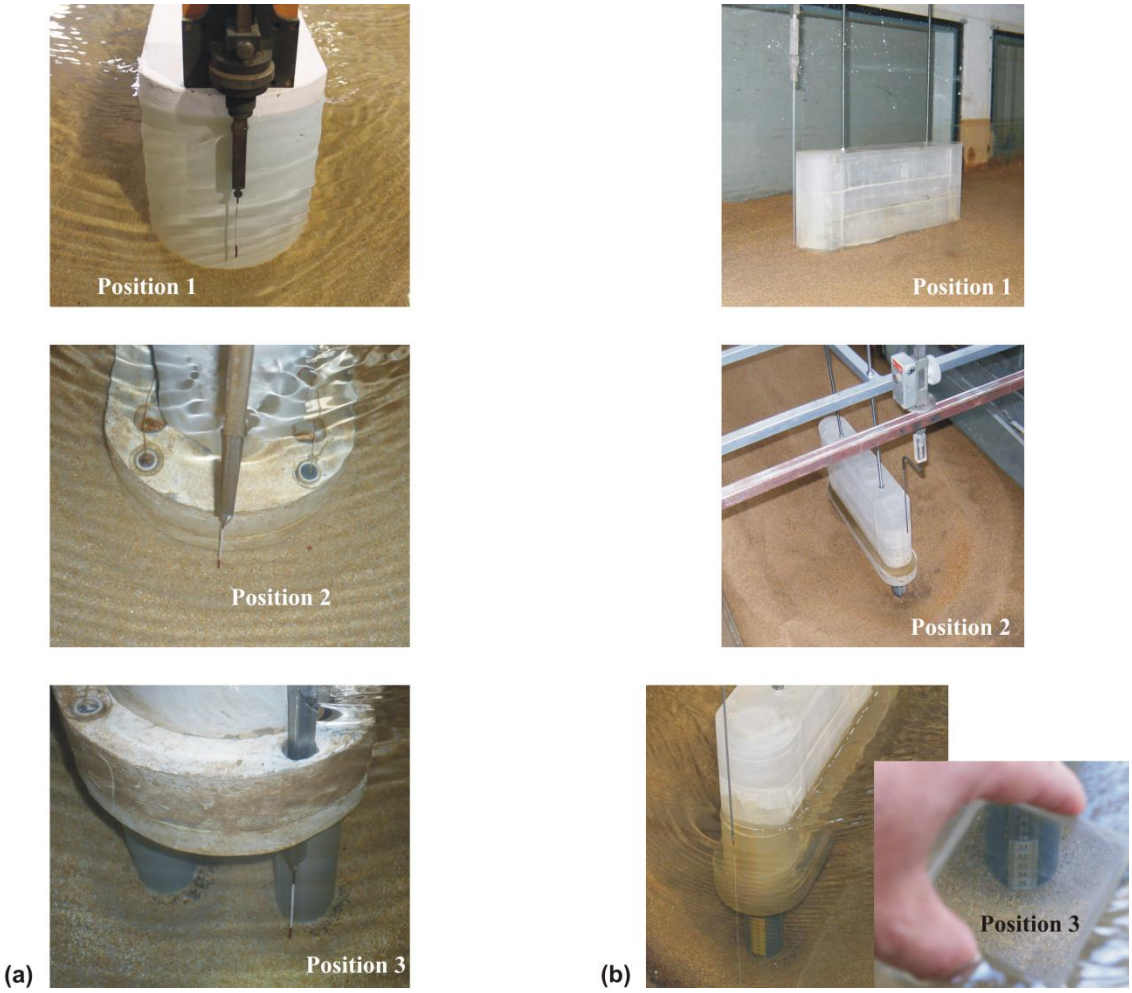

Figure 3.12 – Step 4 of the experimental procedure: (a) LNEC's flume and (b) FEUP's flume

3.5.5 END OF THE EXPERIMENT

In the particular case of scour around complex piers equilibrium criterion has not yet been established as mentioned in section 2.3.4. As explained in that section, some authors suggest the use of the same criterion proposed by Melville and Chiew (1999) for tests with single piers. The analysis performed with the results of preliminary tests showed that the application of the criterion of Melville and Chiew (1999) to complex piers would imply test durations much smaller than those required to obtain the different scouring phases detected. For this reason, in the present study minimal durations depending of the pile-cap positon (and larger than the ones obtained by the Melville and Chiew (1999) criterion) were established. In the case of tests with Models 1 to 6 (analysed at LNEC's flume) and for Configuration C1, the minimum durations were 14, 17 and 20 days, respectively when (1) the pile cap is above the bed, (2) is partially buried or (3) completely buried in the bed. In the other two configurations a minimum duration of 14 days was considered. In the case of Model 7 (analysed at FEUP's flume) a minimum duration of 7 days was established for the three configurations. The difference of the minimum durations between the tests at FEUP's and at LNEC's flumes is due to fact that the geometry of Model 7 resembles a single pier and in tests with such piers at least 7 days duration is required, as suggested by Lança *et al.* (2013b). Once a given experiment was stopped, the flume was slowly drained. After that, the scour hole pattern was photographed. Figure 3.13 shows the

recess box, the complex piers and the scour hole at the end of the tests, after flume's depletion, for the three mentioned pile-cap positions, *i.e.*, pile cap above the initial bed level, pile cap partially buried in the bed and pile cap completely buried in the bed.

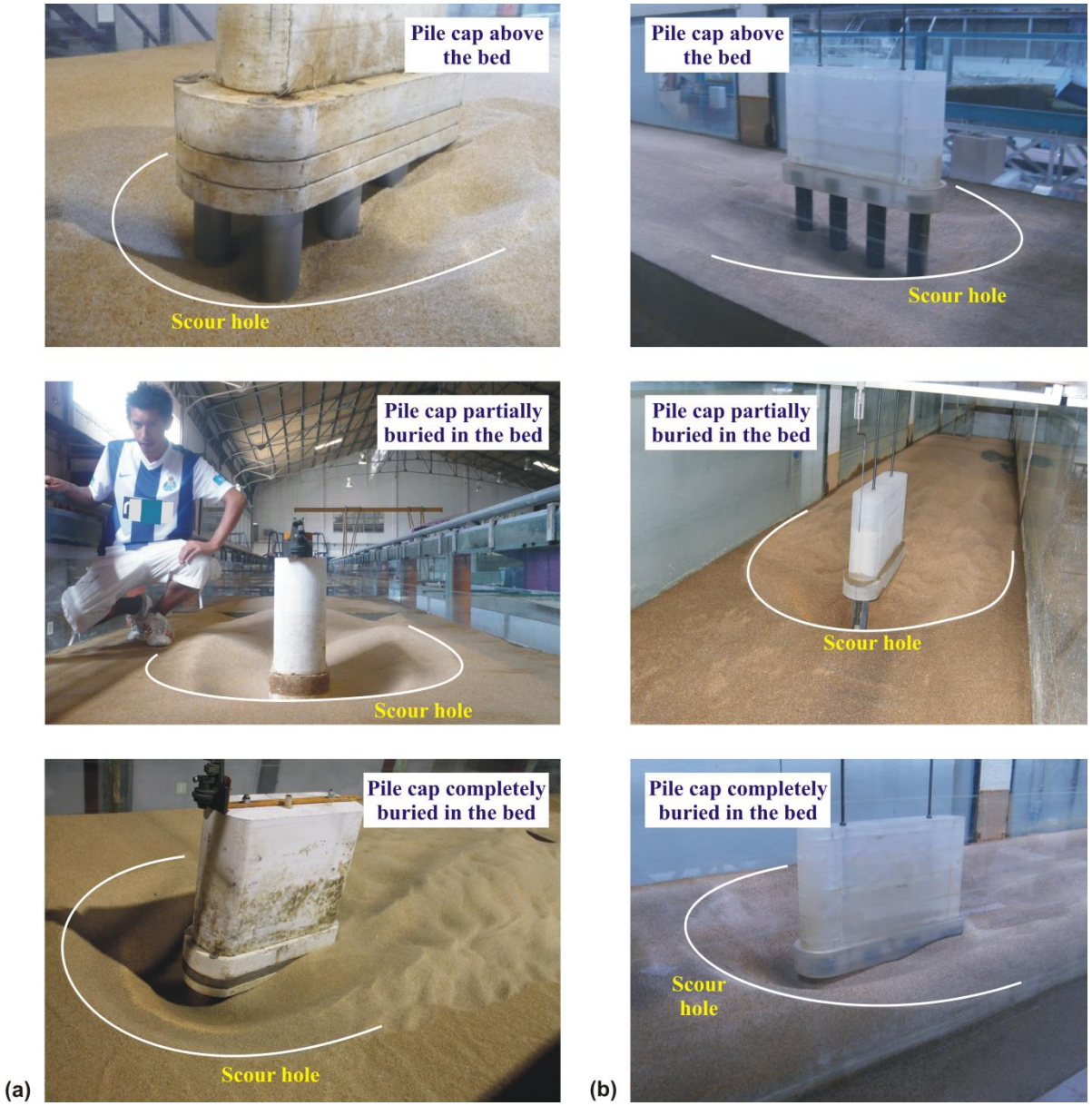

Figure 3.13 – Typical scour patterns at the end of the test: (a) LNEC's flume and (b) FEUP's flume

It should be stressed that the approach reach located upstream of the piers remained undisturbed along the entire duration of the experiments, for all test model configurations; this long term stability could ensure that local scour hole development and depths were not affected by upstream bed degradation that could potentially occur otherwise.

4. TEMPORAL EVOLUTION OF THE SCOUR DEPTH AT COMPLEX PIERS

4.1. INTRODUCTION

The temporal evolution of the scour depth at single piers under clear-water flow conditions follows a logarithmic trend and three phases of the scour process may be identified: initial phase, principal phase and equilibrium phase (*e.g.*, Ettema, 1980; Couto and Cardoso, 2001) as discussed in section 2.2.3. The principal phase of the scouring process at complex bridge piers can display different stages, depending on the pile-cap position relative to the initial bed level as described in section 2.3.3. In accordance with experimental results of Ataie-Ashtiani *et al.* (2010) and Ferraro *et al.* (2013), these stages are associated with the progressive physical presence in the scour hole developed of one, two, or the three structural components of the complex pier. As mentioned in section 2.3.3, the temporal evolution of the scour depth observed at pile groups (*e.g.*, Hannah, 1978; Lança *et al.*, 2013a) can be adopted to the case of complex piers when the pile cap is out of the water as well as the scour depth time evolution observed at pier-caissons (*e.g.*, Melville and Raudkivi, 1996; Lu *et al.*, 2011; Kothyari and Kumar, 2012) can be adopted to the case of complex piers when the pile cap is completely buried in the bed. From the five studies identified on scouring at complex piers (Table 2.2) only the studies of Ataie-Ashtiani *et al.* (2010) and Ferraro *et al*. (2013) included the analysis of the effect of the pile-cap position on the temporal evolution of the scour depth. Ferraro *et al*. (2013) investigated also the effect of the pile-cap thickness on the temporal evolution of the scour depth by means of results obtained with two models (Fe1 and Fe2 in Figure 2.27).

Due to the limited number of studies in this topic, as only two studies could be reported, 48 long-duration tests were performed in the present work in order to quantify the influence of the complex pier position (relative to the initial bed level) and complex pier geometry on the temporal evolution of the scour depth. Those 48 tests correspond to tests carried out with the seven complex pier models studied (Figure 3.1) for Configuration C1 (complete complex pier). The results of the tests performed at LNEC's flume (*i.e.*, with Models 1 to 6) were used to analyse: (1) the combined effects of the relative column width, D_c/D_{pc}, and the relative column position, H_c/h, on the scour depth time evolution (presented in section 4.2.2); and (2) the combined effects of the relative pile-cap thickness, T/h, and the relative column position, H_c/h, on the temporal evolution of the scour depth (presented in section 4.2.3). The results of the tests performed at FEUP's flume (*i.e.*, with Model 7) were used to analyse: (1) the effect of the relative column position, H_c/h, on the temporal evolution of the scour depth (presented in section 4.3.1); and (2) the influence of the pile-group configuration. As mentioned in section 2.3.4, some authors (*e.g.*, Coleman, 2005; Ataie-Ashtiani *et al.*, 2010) use as a criterion to stop laboratory tests on complex piers (equilibrium scour stage) the same criterion proposed by Melville and Chiew (1999) for tests with single piers. The results of the 48 tests were also used to evaluate the referred criterion applicability, as presented in section 4.4.

4.2. SCOUR DEPTH TIME EVOLUTION IN TESTS WITH MODELS 1 TO 6 (LNEC'S MODELS)

4.2.1 GENERAL APPROACH

According to results of tests carried out for Models 1 to 6 (at LNEC's flume), the scour process in the three clear and distinguished situations considered (Figure 2.22) may be typically described as follows:

1. In Situation 1, characterized by the fact that the bottom of the pile cap is above the initial bed level, the temporal evolution of the maximum scour depth is similar to that of the single pier case, following a unique stage, as illustrated in Figure 4.1(a) (curve S1-A). In this situation, the scour process initiates in front of each of the upstream piles, with individual holes, until they merge into one single scour hole; the maximum scour depth is located in front of the upstream piles of the group. Figure 4.1(b) shows photos of the referred scour hole development.

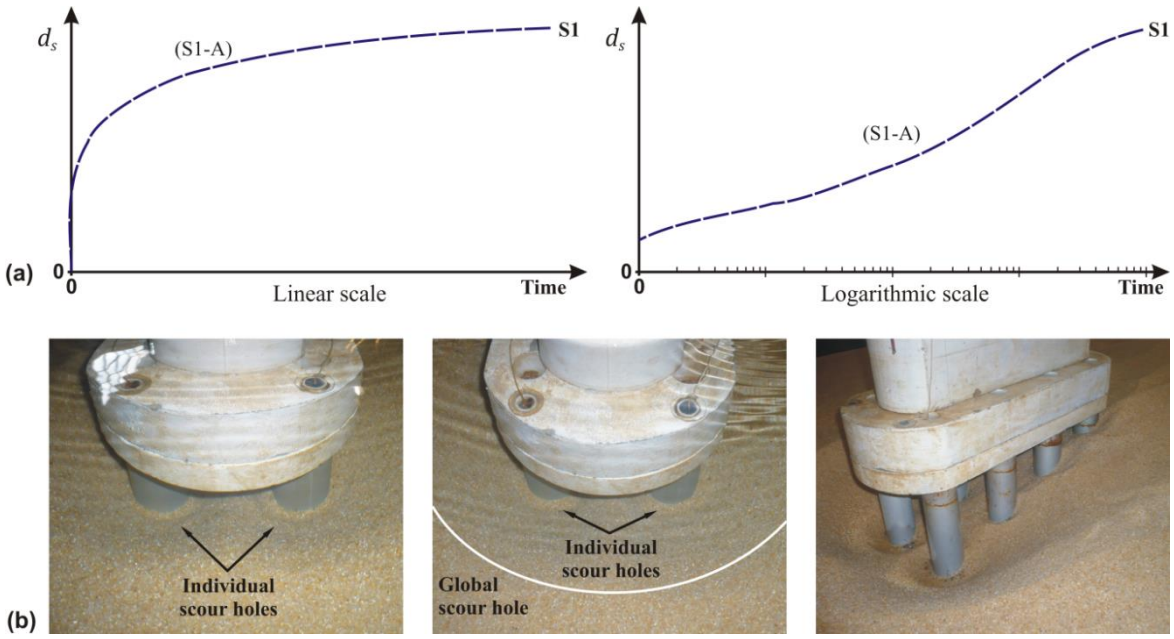

Figure 4.1 – Situation 1: (a) scheme of the temporal evolution of the scour depth (time on linear and logarithmic scales) and (b) photographs of scour hole evolution

2. In Situation 2, corresponding to the case where the pile cap is partially buried in the bed, the scour depth evolution does not follow a unique trend, as identified in Situation 1, but has rather different stages. Three stages are typically identified (Figure 4.2(a)): (i) initially, the scour process develops in front of the pile cap (curve S2-A); (ii) after a lapse of time, which depends on the pile-cap position and thickness, the scour process progresses below the pile cap (curve S2-B); and (iii) finally the scour process continues underneath the pile cap, in front of the upstream piles (curve S2-C). Figure 4.2(b) shows the scour hole development associated with those three stages.
3. In Situation 3, when the pile cap is completely buried in the bed, the scour depth record also displays different stages depending on the top of the pile-cap position below the initial bed level. Three stages are also typically identified (Figure 4.3(a)): (j) initially, the scour process develops in front of the column until the scour hole partly uncovers the top of the pile cap

(curve S3-A); (jj) that period is followed by a stage (curve S3-B) when the scour depth does not evolve during a (more or less significant, depending of D_c/D_{pc} ratio) lapse of time and the maximum scour depth is equal to the distance from the initial bed level to the top of the pile cap; and (jjj) on the following stage, the scour process continues in front of the pile cap (curve S3-C). Figure 4.3(b) shows the scour hole development associated with those three stages.

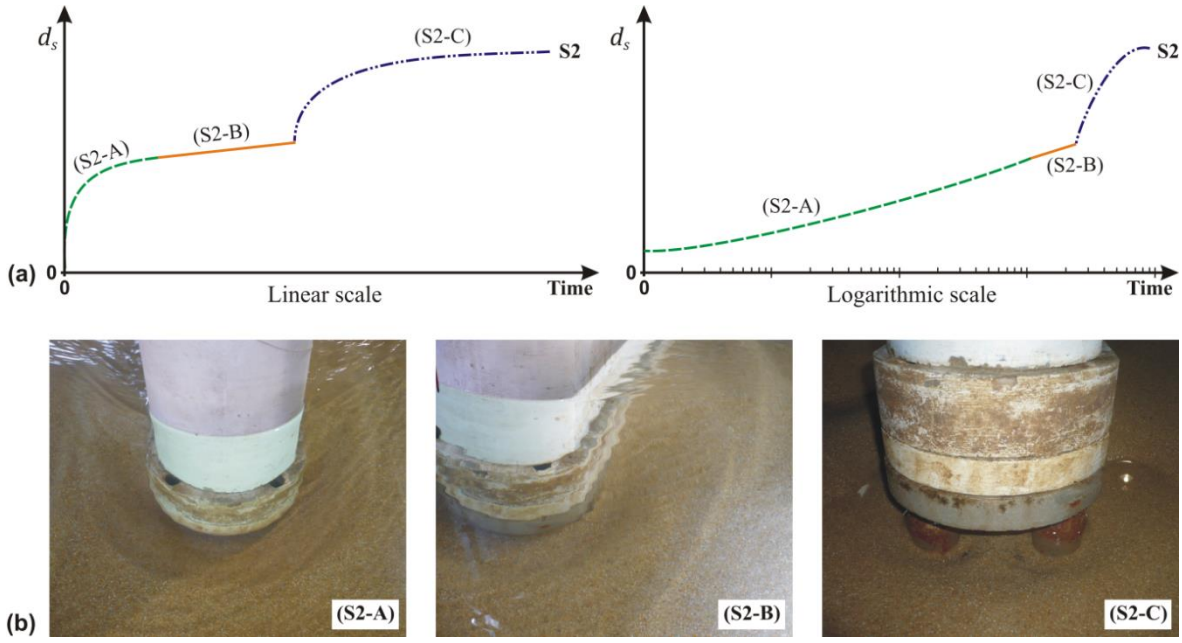

Figure 4.2 – Situation 2: (a) scheme of the temporal evolution of the scour depth (time on linear and logarithmic scales) and (b) photographs of scour hole evolution

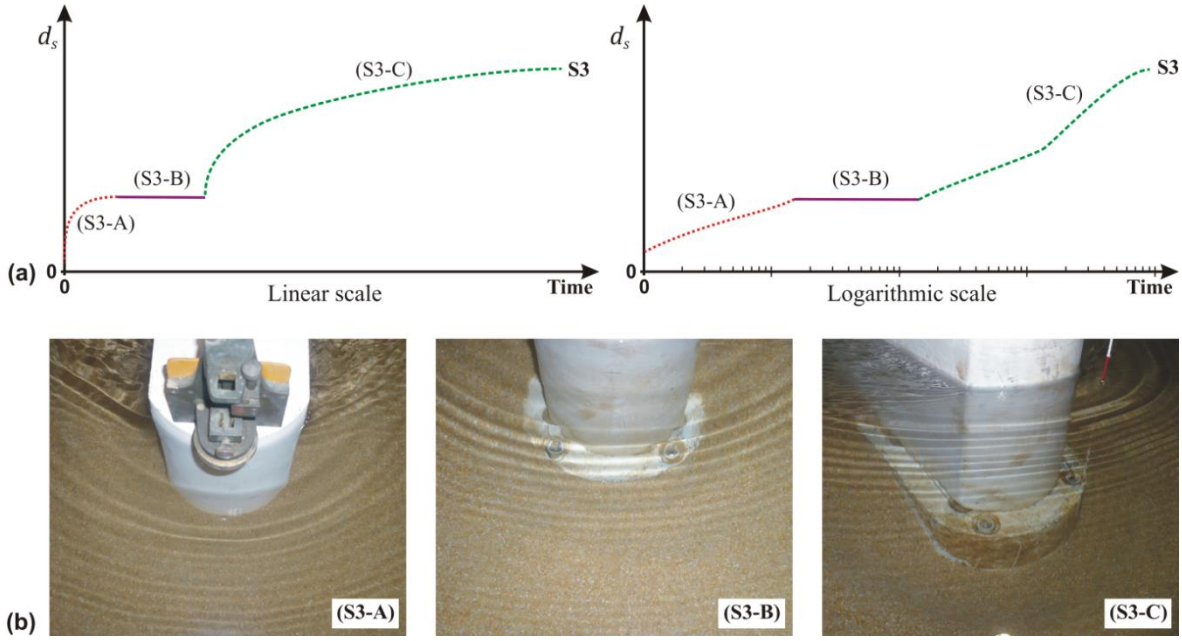

Figure 4.3 – Situation 3: (a) scheme of the temporal evolution of the scour depth (time on linear and logarithmic scales) and (b) photographs of scour hole evolution

The scour depth time evolution illustrated in Figure 4.1, Figure 4.2 and Figure 4.3, respectively for Situations 1, 2 and 3, corresponds to the general case of each of the situations. In Situations 2 and 3, the presence of the two last corresponding stages depends on the complex pier geometry, particularly on the relative column width, D_c/D_{pc}, and on the relative pile-cap thickness, T/h. These effects are discussed below.

4.2.2 INFLUENCE OF RELATIVE COLUMN WIDTH AND POSITION

The combined effects of the relative column width, D_c/D_{pc}, and the relative column position, H_c/h, on the temporal evolution of the scour depth were evaluated through the results obtained with Model 2 ($D_c/D_{pc} = 0.85$), Model 3 ($D_c/D_{pc} = 0.70$) and Model 5 ($D_c/D_{pc} = 0.55$). In the tests with these three different models only the column dimensions (width and length) were changed (see Table 3.1). Eleven relative pile-cap positions were evaluated for the three models, as shown in Figure 3.4(b). The eleven positions are associated with three typical situations: (1) Positions A to E correspond to Situation 1; (2) Positions F to I correspond to Situation 2; and (3) Positions J to L correspond to Situation 3.

Figure 4.4 shows the time records of the scour depth evolution for tests of Situation 1 (Positions A to E), in which the same trend of curve S1 is followed (Figure 4.1), *i.e.*, being the evolution characterized by a unique curve. The temporal evolution of the scour depth in this situation is similar to that observed in pile groups (*e.g.*, Lança *et al.*, 2013a). Figure 4.4(a) displays the influence on the scour depth evolution of pile cap submergence in water, by considering the pile cap: fully emerged out of the flow (Position A); partially submerged in the flow (Position C); and completely immersed in the flow, with the column out of the flow (Position D). The increment in the scour depth values is associated with the presence of the pile cap in the flow (Positions C and D) being the area exposed to the flow (*i.e.*, front of the pile cap) greater than that corresponding to the upstream piles. As the column is out of the flow in Positions A, C and D, the results of scour depth evolution with Model 2 (Figure 4.4(a)) apply to the other two models.

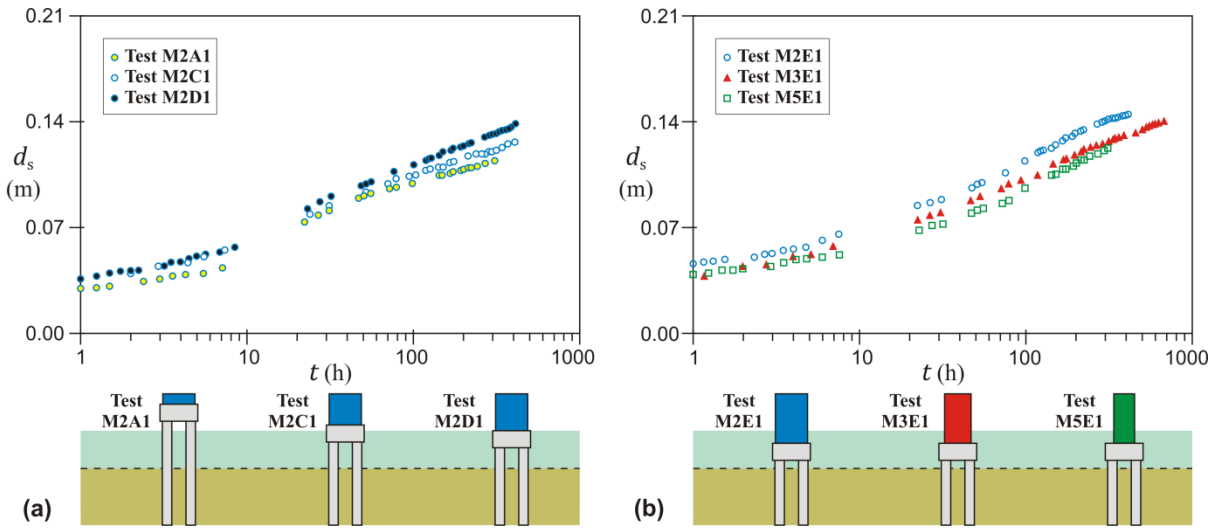

Figure 4.4 – Influence of D_c/D_{pc} on the temporal evolution of the scour depth for Situation 1: (a) Positions A to D and (b) Position E

In Position E, with the three components of the complex pier exposed to the flow, the obstruction of the complex pier induces higher scour depth values over time than for the other three positions (A, C and D), as can be observed by comparing the values of Figure 4.4(b) with the values in Figure 4.4(a). In this Position E, the increment in the scour depth values with the column width is clear: the higher values are obtained with Model 2 ($D_c/D_{pc} = 0.85$) while the smaller values are obtained with Model 5 ($D_c/D_{pc} = 0.55$).

In Situation 2, when the pile cap is only slightly buried in the bed (*e.g.*, tests in Position F, which is an illustrative case of this situation), the scour depth temporal evolution curves (Figure 4.5(a)) display a similar trend, with three stages, as described for the general case of tests in this situation (Figure 4.2). These findings are in agreement with those of Ferraro *et al.* (2013). One test was performed for Position G exclusively in the case of Model 5 (where, for $t = 0$, approximately 60% of the pile-cap thickness is buried in the bed), in which only the first two stages of the illustrative general scour depth temporal evolution for Situation 2 (Figure 4.2) have been identified, as depicted in Figure 4.5(b).

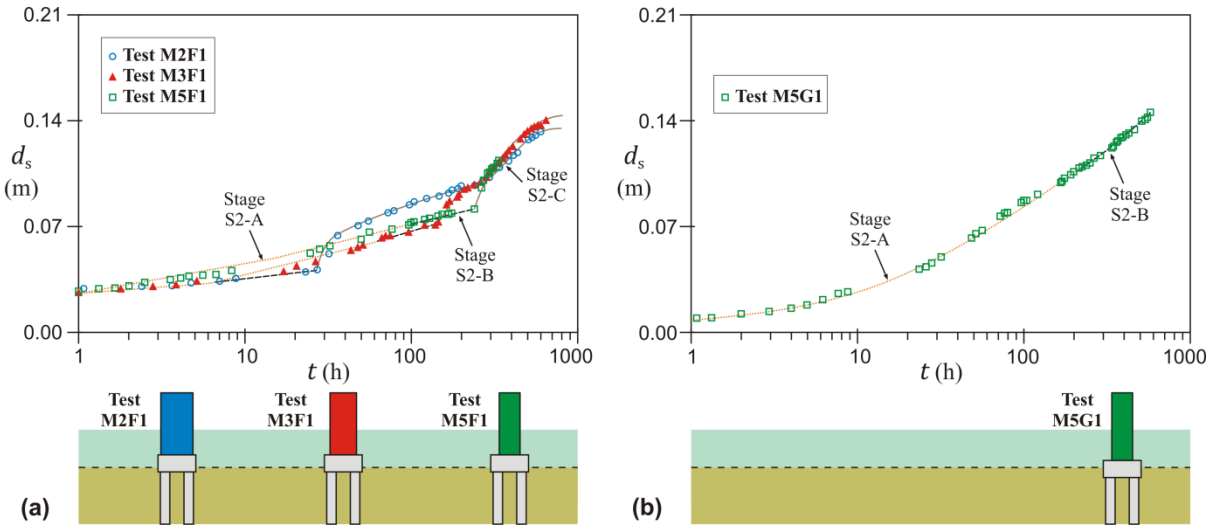

Figure 4.5 – Influence of D_c/D_{pc} on the temporal evolution of the scour depth for Situation 2 (pile cap slightly buried): (a) Position F and (b) Position G

When the pile cap is almost buried at the initiation of the scour process, *i.e.*, the top surface of the pile cap is near or flushes the initial bed level (Positions H and I), the last two stages may even not occur, as shown in Figure 4.6. In fact, for these two positions (H and I), the number of stages may be different, depending on the D_c/D_{pc} ratio, as can be identified in Figure 4.6: (1) the three stages for the highest relative column-to-pile-cap width ratio (Model 2, $D_c/D_{pc} = 0.85$); (2) only the first stage, *i.e.*, scour process in front of the pile cap, for the smaller relative column-to-pile-cap width ratio (Model 5, $D_c/D_{pc} = 0.55$); and (3) the first two stages for intermediate cases (Model 3, $D_c/D_{pc} = 0.70$). In fact, in line with Melville and Raudkivi (1996) and Ataie-Ashtiani *et al.* (2010), when $H_c \approx 0$, the front and side pile-cap extension lengths do cause not only a delay in the beginning of the scour process but also a slow initial scour rate. For these cases, when D_c/D_{pc} ratio is small (*e.g.*, Model 5, $D_c/D_{pc} = 0.55$), the scour depth evolution (tests M5H1 and M5I1) follows a similar trend to the one observed in experiments of single piers with collar countermeasure (*e.g.*, Mashahir *et al.*, 2004; Alabi, 2006), in which a reduction of the downflow in front of the column and a reduction of the horseshoe vortices were detected. Figure 4.7 pictures the main stages of the scour hole evolution in test M5I1, that can be

resumed as: (1) stage A, two grooves developed first at the lateral part of the pile cap; (2) stage B, the grooves extended to the upstream part of the pile cap, around its rim, and joined at pile cap centreline; and (3) stage C, the scour process continued in front of the pile cap.

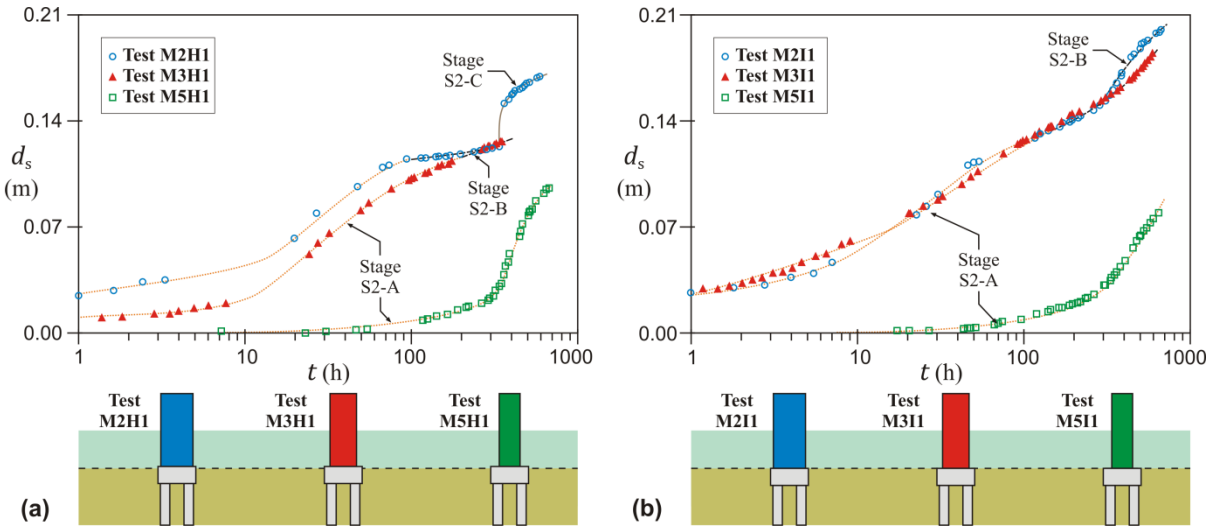

Figure 4.6 – Influence of D_c/D_{pc} on the temporal evolution of the scour depth for Situation 2 (pile cap almost buried): (a) Position H and (b) Position I

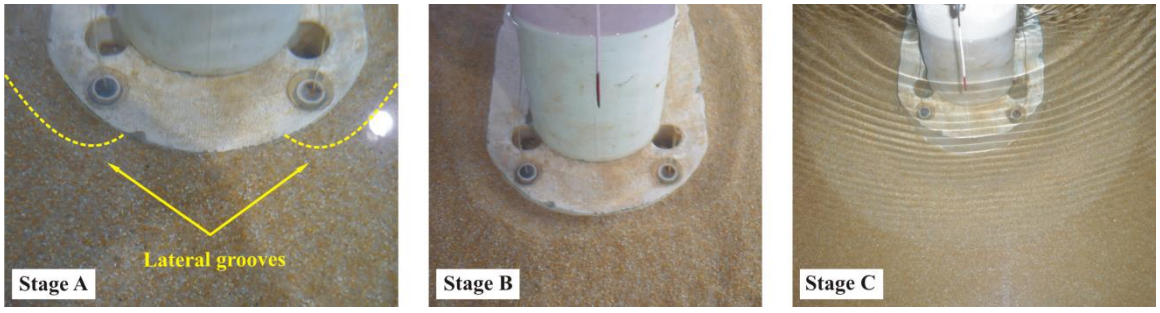

Figure 4.7 – Photos of the scour hole evolution in test M5I1

In Situation 3, characterized by the pile cap being completely buried in the bed, when the pile cap is exposed in the scour hole (*e.g.*, tests in Positions J and K), the scour depth temporal evolution curves (Figure 4.8) display a similar trend, with three stages, as described for the general case of tests in this situation (Figure 4.3). This observation is in line with the findings of Melville and Raudkivi (1996), Ataie-Ashtiani *et al*. (2010), Lu *et al*. (2011) and Ferraro *et al*. (2013). In accordance with Melville and Raudkivi (1996), when D_c/D_{pc} is close to 1 (*e.g.*, Model 2) the duration of the intermediate stage (S3-B) is short and the scour depth evolution resembles to the one corresponding to single piers, as shown in Figure 4.8(a) for test M2J1 and in Figure 4.8(b) for test M2K1. It also comes clear that the duration of the two last stages (B and C) is highly sensitive to H_c/h and D_c/D_{pc}. The increment in scour depth values (temporal evolution) is directly associated with the increment in the column width (as that component is present throughout the scour hole development), as shown in Figure 4.8. The presence and duration of the last two stages (see Figure 4.3) depend on the pile-cap front extension length and on the pile-cap position below the initial bed level.

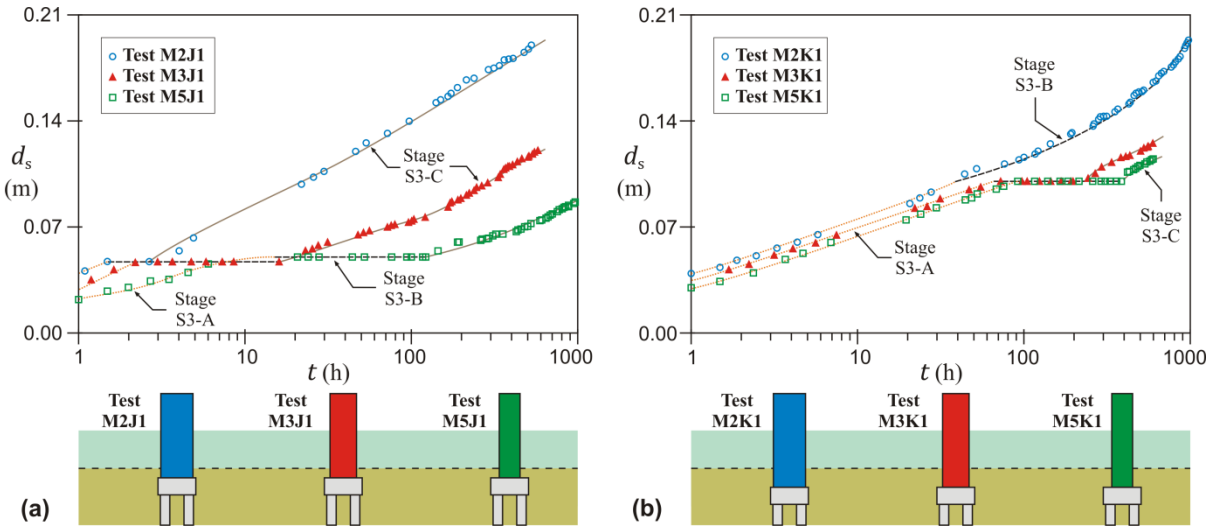

Figure 4.8 – Influence of D_c/D_{pc} on the temporal evolution of the scour depth for Situation 3: (a) Position J and (b) Position K

Finally, in Position L, characterized by the top of the pile cap remaining below the base of the scour hole, only the first stage, corresponding to scour process development in front of the column, was observed as shown in Figure 4.9. The results show that the increment in the scour depth is associated with the increment in the column width.

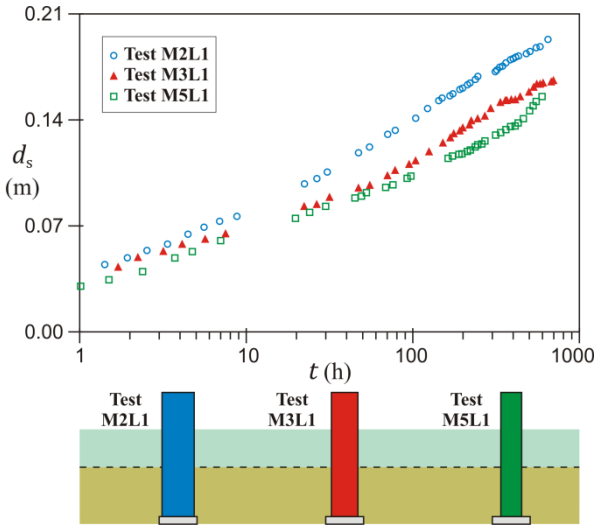

Figure 4.9 – Influence of D_c/D_{pc} on the temporal evolution of the scour depth for Situation 3 (Position L)

4.2.3 INFLUENCE OF PILE-CAP THICKNESS AND POSITION

The combined effects of T/h and H_c/h on the scour depth time evolution were evaluated through the results obtained with Model 4 ($T/h = 0.60$), Model 5 ($T/h = 0.45$) and Model 6 ($T/h = 0.30$). For these three models, all with $D_c/D_{pc} = 0.55$, only the pile-cap thickness was changed (see Table 3.1). According to results presented by Ferraro *et al*. (2013) and discussed in section 2.3.5.4, it is expected

that maximum scour depths (in the time evolution) occur for models with thicker pile caps, as those correspond to a larger area exposed to the flow. In Situation 1, characterized by the pile cap above the initial bed level, the increment in scour depth values with the increment of the pile-cap thickness is clear for Positions D and E, as shown in Figure 4.10. The temporal evolution of the scour depth for the six tests in this situation does show a trend similar to curve S1-A, presented in Figure 4.1.

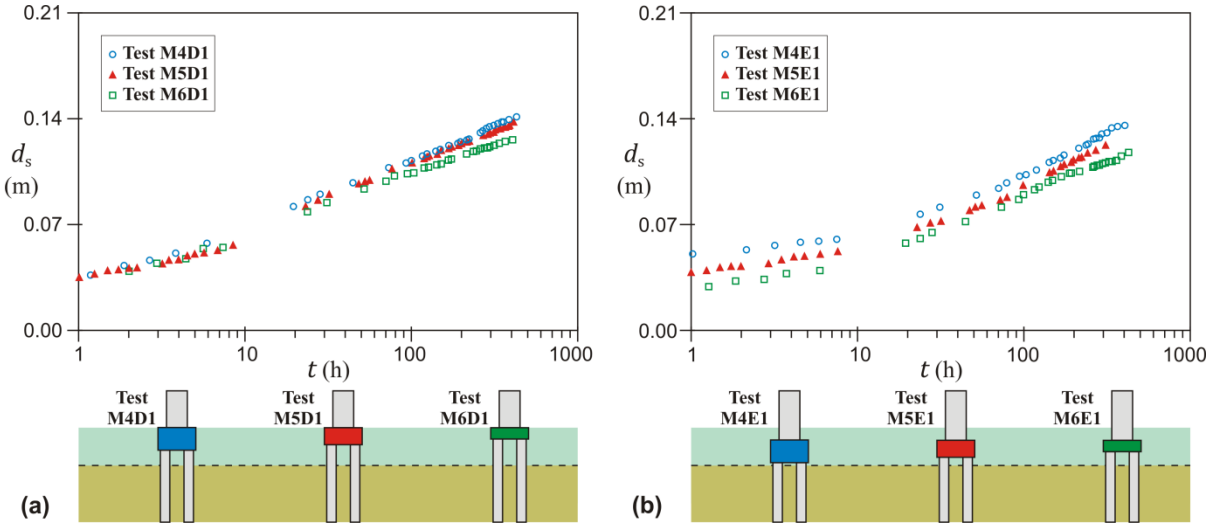

Figure 4.10 – Influence of *T*/*h* on the temporal evolution of the scour depth for Situation 1: (a) Position D and (b) Position E

In Position F ($H_c/h = 0.33$), depending on the pile-cap thickness, the bottom of the pile cap can be (1) above the initial bed level (Situation 1), *i.e.*, test M6F1 ($T/h = 0.30$) or (2) below the initial bed level, (Situation 2), *i.e.*, tests M4F1 and M5F1 ($T/h = [0.60, 0.45]$, respectively), as shown in Figure 3.4. Figure 4.11 displays the scour depth evolution recorded in those three tests. The maximum scour depth was observed in the test with the larger pile-cap thickness (M4F1), as shown in Figure 4.11(b). Additionally, it should be noticed that the large increase on scour depth occurred in test M5F1 after approximately 240 hours (10 days), due to influence of the upstream piles where higher scouring rate occurs, compared to the one in front of the pile cap, as shown in Figure 4.11(b). The trend of the scour depth time evolution at test M6F1 is similar to the one observed in Situation 1 for Positions D and E.

Figure 4.12 shows the temporal evolution of the scour depth for the three models in Positions G, H and I, in which all tests are associated to Situation 2. In Models 4 and 5, with thicker pile caps, *i.e.*, $T/h = [0.60, 0.45]$ respectively, the temporal evolution of the scour depth is similar for all three positions. However, in accordance with Figure 4.12(b), a delayed (of about 100 hours) in the beginning of the scour depth evolution of test M5H1 in relation to test M4H1, *i.e.*, for Position H, was observed. Initial scour rate should be relatively similar in both tests; a possible justification can be the bed compaction. For those three positions (G, H and I), the scour rate in the Model 6 is higher than in the other two models, as shown in Figure 4.12. This may be justified by the fact that in Model 6, characterized by the thinner pile-cap thickness, the pile group contributes on the scour process once this component is reached on scouring process.

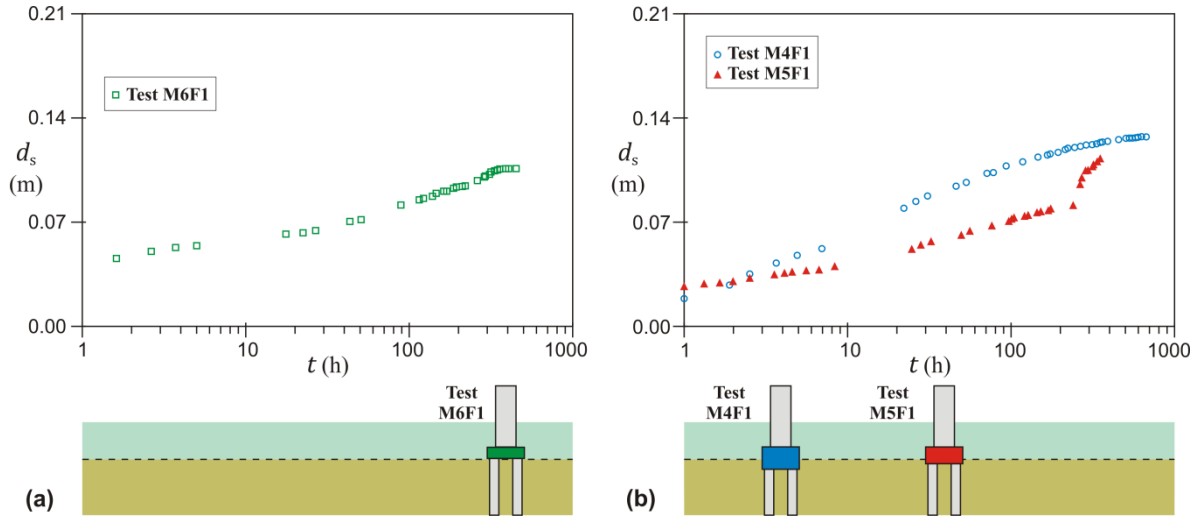

Figure 4.11 – Influence of *T*/*h* on the temporal evolution of the scour depth for Position F: (a) test in Situation 1 and (b) tests in Situation 2

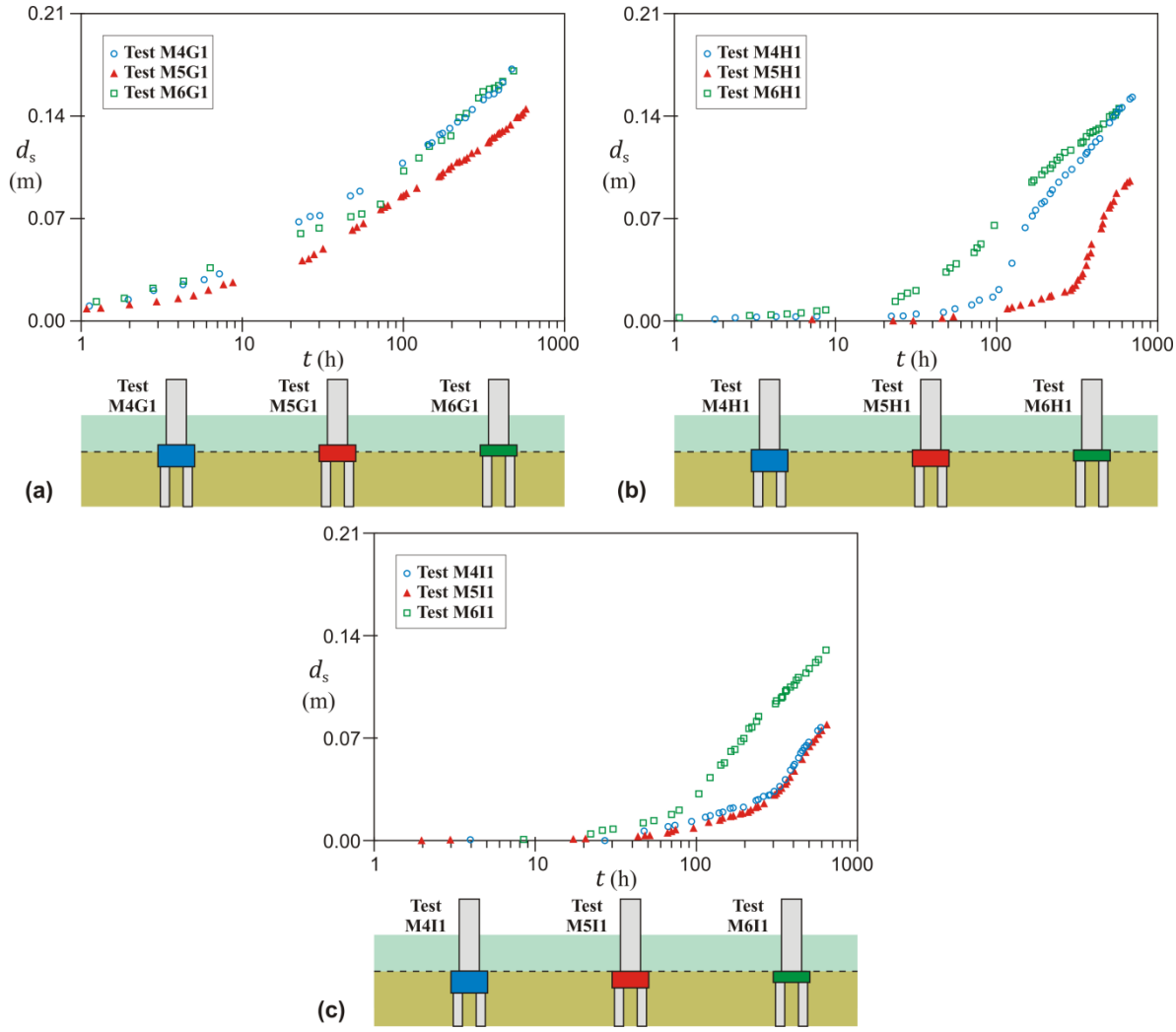

Figure 4.12 – Influence of *T*/*h* on the temporal evolution of the scour depth for Situation 2: (a) Position G, (b) Position H and (c) Position I

In the three positions of Situation 3 (J, K and L), characterized by the pile cap being initially completely buried in the bed, the temporal evolution of the scour depth does not depend on the pile-cap thickness, due to the fact that the scour hole does not reach the bottom of the pile cap in any of the models analysed (4 to 6). Figure 4.13 shows the scour depth time evolution obtained in tests with Model 4, in which those temporal evolutions apply to the other two models.

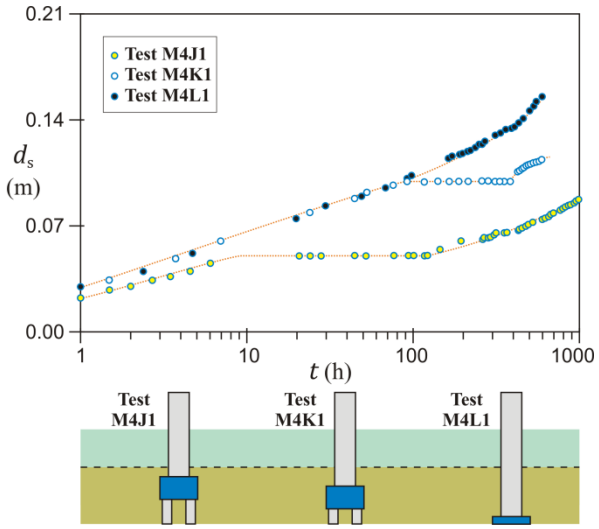

Figure 4.13 – Influence of *T*/*h* on the temporal evolution of the scour depth for Situation 3

In Positions J and K, the scour depth temporal evolution curves (Figure 4.13) display a similar trend, with three stages, as described for the general case of tests in this situation (Figure 4.3), while in Position L, characterized by the top of the pile cap remaining below the base of the scour hole, only the first stage was observed.

4.2.4 MAXIMUM SCOUR DEPTHS

Table 4.1 (Models 1 to 3) and Table 4.2 (Models 4 to 6) summarize the values of the relative column position, H_c/h, test duration, t_d, and deepest scour depth measured at the end of the tests, d_{sm}, of the 40 tests reported in sections 4.2.2 and 4.2.3 (all tests with Configuration C1).

Table 4.1 – Relative column position, test duration and maximum scour depth for Models 1 to 3

	Model 1		Model 2		Model 3	
H_c/h	t_d (h)	d_{sm} (m)	t_d (h)	d_{sm} (m)	t_d (h)	d_{sm} (m)
1.700	310.0	0.114	310.0	0.114	310.0	0.114
1.300	405.8	0.126	-	-	-	-
1.150	412.7	0.139	405.8	0.126	405.8	0.126
1.000	428.1	0.142	412.7	0.139	412.7	0.139
0.667	452.9	0.154	411.7	0.145	675.0	0.141
0.333	551.8	0.148	599.4	0.133	646.3	0.141
0.050	596.7	0.195	593.0	0.169	350.8	0.127
0.000	525.5	0.183	670.9	0.200	594.3	0.185
−0.235	-	-	526.6	0.190	576.3	0.121
−0.500	1125.8	0.199	1125.8	0.199	599.6	0.126
−1.500	647.5	0.193	647.5	0.193	696.1	0.166

Table 4.2 – Relative column position, test duration and maximum scour depth for Models 4 to 6

	Model 4		Model 5		Model 6	
H_c/h	t_d (h)	d_{sm} (m)	t_d (h)	d_{sm} (m)	t_d (h)	d_{sm} (m)
1.700	310.0	0.114	310.0	0.114	310.0	0.114
1.300	405.8	0.126	-	-	-	-
1.150	412.7	0.139	405.8	0.126	-	-
1.000	428.1	0.142	412.7	0.139	405.8	0.126
0.667	405.8	0.136	310.6	0.123	428.2	0.118
0.333	674.9	0.127	430.8	0.116	453.0	0.106
0.185	478.5	0.172	576.6	0.145	481.1	0.171
0.050	696.2	0.153	671.1	0.095	576.6	0.145
0.000	593.0	0.077	646.5	0.079	647.4	0.130
−0.250	1126.0	0.089	1126.0	0.089	1126.0	0.089
−0.500	594.6	0.115	594.6	0.115	594.6	0.115
−1.500	596.8	0.155	596.8	0.155	596.8	0.155

4.3. SCOUR DEPTH TIME EVOLUTION IN TESTS WITH MODEL 7 (FEUP'S MODEL)

4.3.1 INFLUENCE OF THE PILE-CAP POSITION

Eight tests with different pile-cap position were performed with Model 7. Those tests include: three to Situation 1, three to Situation 2 and two to Situation 3, as shown in Figure 3.4(d). Figure 4.14(a) shows the temporal evolution of the scour depth for the three tests of Situation 1 (Positions M, N and O), all the corresponding curves showing similar trends to curve S1-A (Figure 4.1). The slight increment in the scour depth values from Position M to Position O may be justified by the corresponding small increment of the area exposed to the flow. For the three tests of Situation 2

(Positions P, Q and R), the three characteristic stages described for Models 1 to 6 (curve S2 of Figure 4.2) were also observed. However, the scour depth evolution trend in these tests is more similar to the typical one obtained for tests of Situation 1, as shown in Figure 4.14(b). This may be justified by the fact that the longitudinal axis of the pile cap overlaps that of the alignment of piles (Figure 3.1), this enabling the upstream pile to contribute to the scour process immediately after the entire front of the pile cap is exposed in the scour hole. Figure 4.14(c) shows the scour depth time evolution for the two tests of Situation 3 (Positions S and T), where once again, due to the particular complex pier geometry, the trend of the curves obtained is similar to that observed for Models 1 and 2. In test M7S1 the three characteristic stages of curve S3 (Figure 4.3) were observed, where the duration of the intermediate stage (S3-B) was short as observed in tests M2J1 and M2K1 of Model 2. In test M7T1, characterized by the top of the pile cap remaining below the base of the scour hole, only the first stage was observed, as expected.

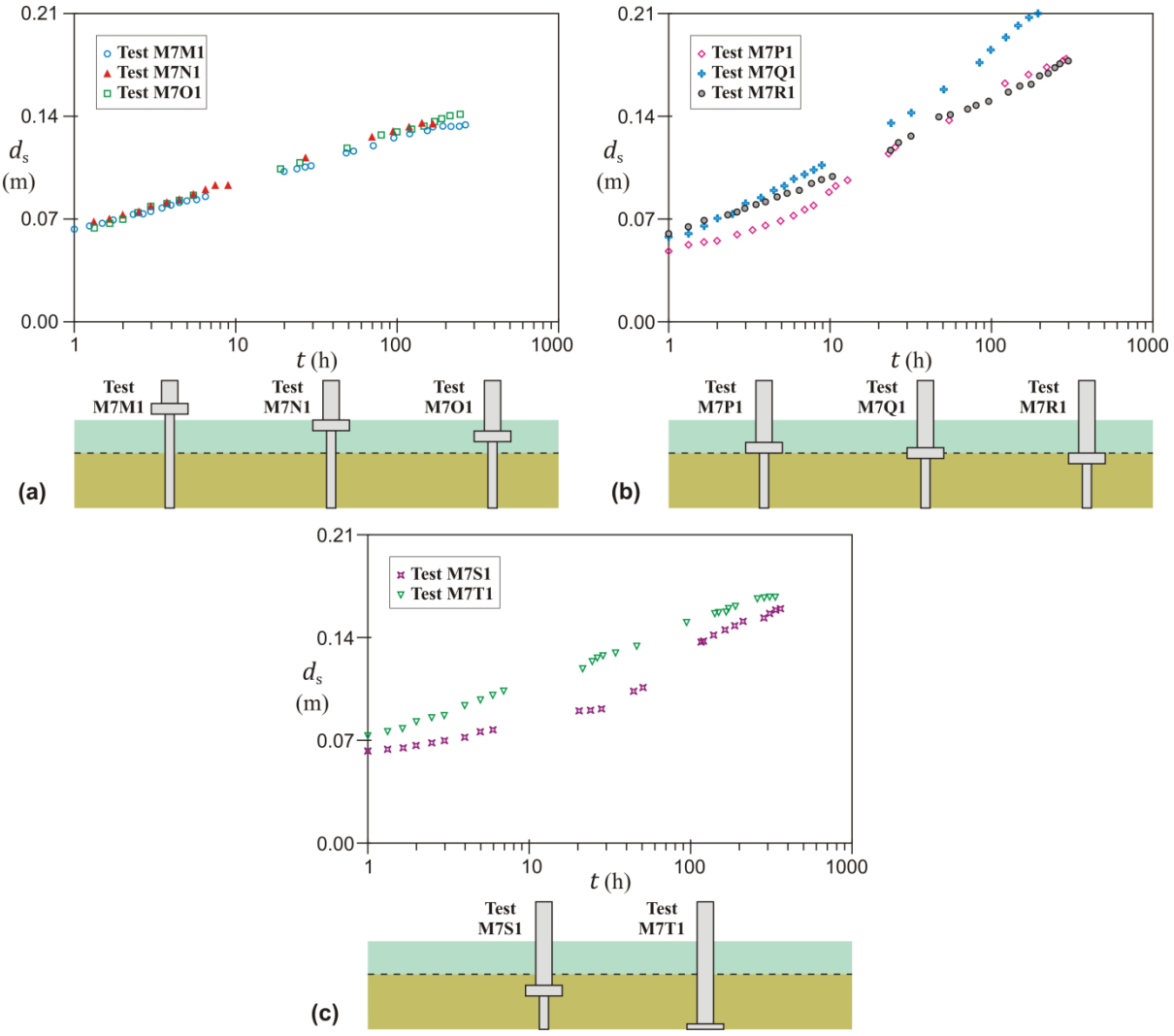

Figure 4.14 – Influence of the pile-cap elevation on the temporal evolution of the scour depth for: (a) Situation 1 (Positions M to O), (b) Situation 2 (Positions P to R) and (c) Situation 3 (Positions S and T)

4.3.2 MAXIMUM SCOUR DEPTHS

Table 4.3 summarizes the values of the relative column position, H_c/h, test duration, t_d, and deepest scour depth measured at the end of the tests, d_{sm}, of the 8 tests reported in the previous section (all tests with Configuration C1).

Table 4.3 – Relative column position, test duration and maximum scour depth for Model 7

H_c/h	t_d (h)	d_{sm} (m)
1.500	264.5	0.134
1.000	166.5	0.135
0.667	245.2	0.141
0.322	291.0	0.178
0.161	273.0	0.213
0.000	299.2	0.178
−0.333	360.0	0.151
−1.500	334.7	0.167

4.4. CRITERION TO STOP LABORATORY EXPERIMENTS

As mentioned in section 2.3.4, some authors (*e.g.*, Coleman, 2005; Melville *et al.*, 2006; Ataie-Ashtiani *et al.*, 2010) use as a criterion to stop laboratory tests with complex piers (equilibrium scour stage) the same criterion proposed by Melville and Chiew (1999) for tests with single piers. Thus, the time needed to develop equilibrium scour depth, t_e, is defined as the time at which the scour hole develops to a depth at which the rate of increase in scour does not exceed 5% of the pier diameter in the subsequent 24 h period. In complex piers, the mentioned authors use, as reference, the smaller value of 5% of the complex pier characteristic length (*e.g.*, its equivalent pier diameter, D_e) and of the flow depth (h). In all 48 tests performed in this study for Configuration C1 (*i.e.*, complete complex pier), the equivalent pier diameter (according to equations suggested by Coleman 2005, presented in detail in section 2.3.6.1) was used as the smaller dimension length of the complex pier for the evaluation of Melville and Chiew (1999) criterion.

The scour depth evolution recorded in test M2H1 was selected here to exemplify this criterion. Figure 4.15(a) shows the temporal variation of the relative scouring rate ($\Delta d_s/D_e$) in 24 hours associated to the scour depth evolution for that test. According to this figure, the time to obtain a scouring rate of 5% (mentioned criterion) is approximately 3.9 days. For this duration, the experimental scour depth was 0.115 m as shown in Figure 4.15(b). Hence, if hypothetically, test M2H1 had been finished immediately after 3.9 days (regarding the mentioned 5% criterion) the bottom of the scour hole developed would not have reached the pile group. In fact, in this experiment, the scour process began in front of the upstream piles after approximately 14 days (Figure 4.15(b)), when the rate of scour depth evolution increased very rapidly, higher than 5%, as shown in Figure 4.15(a). After the test duration of 24.7 days, a scour depth of 0.169 m was achieved, which is 47% higher than the scour depth obtained by the 5% criterion.

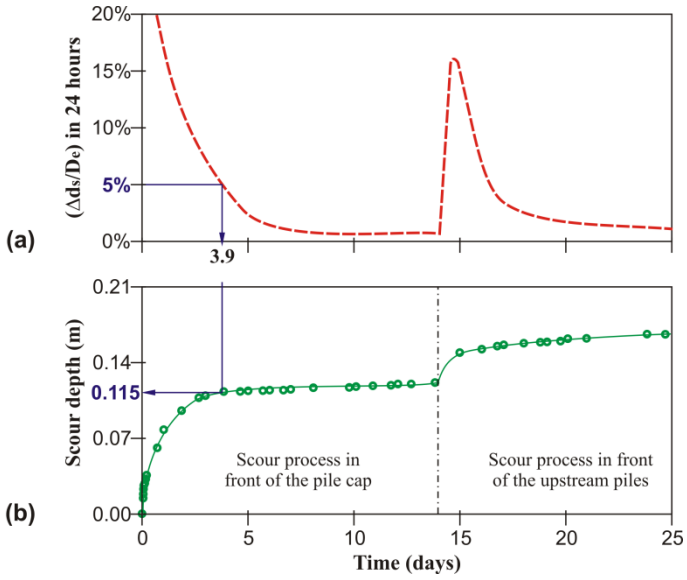

Figure 4.15 – Experiment M2H1: (a) scour rate evolution and (b) temporal evolution of the scour depth

Table 4.4 (Models 1 to 3), Table 4.5 (Models 4 to 6) and Table 4.6 (Model 7) summarize the minimum test duration, $t_{d5\%}$, in which the scour rate fulfils the criterion of 5% suggested by Melville and Chiew (1999) and the corresponding scour depths, $d_{s5\%}$, for all experiments of Configuration C1 with the seven models. The equivalent diameter of the complex pier, D_e, used in the analyses is also included. As mentioned in section 3.2.3, some tests were used to cover the same pile-cap position in different models; therefore, the results of one test in those pile-cap positions were only included in the tables.

Table 4.4 – Relative column position, equivalent diameter of the complex pier, test duration and scour depth with 5% criterion for Models 1, 2 and 3

H_c/h	Model 1			Model 2			Model 3		
	D_e (m)	$t_{d5\%}$ (h)	$d_{s5\%}$ (m)	D_e (m)	$t_{d5\%}$ (h)	$d_{s5\%}$ (m)	D_e (m)	$t_{d5\%}$ (h)	$d_{s5\%}$ (m)
1.700	0.089	71.9	0.096						
1.000	0.124	93.4	0.109						
0.667	0.143	115.0	0.111	0.136	123.3	0.119	0.127	94.2	0.102
0.333	0.162	46.6	0.087	0.157	78.6	0.080	0.138	74.3	0.064
0.050	0.162	188.5	0.158	0.162	93.7	0.115	0.139	99.7	0.102
0.000	0.162	172.6	0.154	0.162	117.3	0.129	0.138	103.7	0.128
−0.235				0.164	97.6	0.140	0.139	72.2	0.070
−0.500				0.167	93.9	0.114	0.139	97.5	0.100
−1.500				0.170	104.0	0.141	0.140	103.7	0.113

Table 4.5 – Relative column position, equivalent diameter of the complex pier, test duration and scour depth with 5% criterion for Models 4, 5 and 6

H_c/h	Model 4			Model 5			Model 6		
	D_e (m)	$t_{d5\%}$ (h)	$d_{s5\%}$ (m)	D_e (m)	$t_{d5\%}$ (h)	$d_{s5\%}$ (m)	D_e (m)	$t_{d5\%}$ (h)	$d_{s5\%}$ (m)
1.000				0.115	127.8	0.120	0.106	94.7	0.103
0.667	0.126	52.3	0.090	0.120	72.4	0.086	0.114	100.2	0.094
0.333	0.129	78.8	0.088	0.125	76.6	0.068	0.121	89.0	0.082
0.185	0.126	175.0	0.128	0.126	104.0	0.087	0.124	173.1	0.123
0.050	0.121	55.3	0.008	0.121	54.1	0.002	0.121	121.0	0.091
0.000	0.120	47.6	0.006	0.120	51.5	0.003	0.120	54.5	0.019
−0.250				0.115	52.4	0.050			
−0.500				0.111	76.0	0.100			
−1.500				0.110	163.2	0.114			

Table 4.6 – Relative column position, equivalent diameter of the complex pier, test duration and scour depth with 5% criterion for Model 7

H_c/h	D_e (m)	$t_{d5\%}$ (h)	$d_{s5\%}$ (m)
1.500	0.050	154.5	0.130
1.000	0.061	118.5	0.133
0.667	0.072	123.5	0.131
0.322	0.083	171.0	0.169
0.161	0.088	196.1	0.209
0.000	0.086	176.0	0.162
−0.333	0.088	164.0	0.145
−1.500	0.089	150.3	0.156

According to the results of Table 4.4, Table 4.5 and Table 4.6, it can be concluded that the relation between the scour depth obtained with the 5% criterion, $d_{s5\%}$, and the ending scour depth measured in the tests, d_{sm}, was on average 81.2%, 72.3% and 74.1% for Situations 1 to 3, respectively. In fact, these values exclude tests with Models 4, 5 and 6 for positions $H_c/h = [0.05, 0.0]$ in which the correspondent relations ($d_{s5\%}/d_{sm}$) obtained were abnormally lower than 15%; the considerable discrepancy in these cases may be explained by the fact that scour rate values less than the 5% criterion limit have been achieved quite early in the development of the scouring process. On the other hand, the time duration to reach the equilibrium condition should be on average 102, 109 and 107 hours for Situations 1, 2 and 3 respectively ($t_{d5\%}$ in Table 4.4, Table 4.5 and Table 4.6). Nevertheless, those time durations were smaller than those required to obtain the different scouring phases detected (namely, stages B and C in Situations 2 and 3).

It is assumed herein that the expressions developed by Sheppard *et al*. (2011), taking into account the findings of Melville and Chiew (1999), for estimating the time to reach 90% of d_{se} are adequate to estimate test durations at complex piers. In accordance, the test duration, t_{dMS}, is evaluated by

$$t_{dMS}(\text{days}) = \begin{cases} 200\dfrac{D_e}{U}\left(\dfrac{U}{U_c}-0.4\right)e^{-1.83\frac{U}{U_c}} & \text{for } \dfrac{h}{D_e} > 6 \\ 127.8\dfrac{D_e}{U}\left(\dfrac{U}{U_c}-0.4\right)\left(\dfrac{h}{D_e}\right)^{0.25} e^{-1.83\frac{U}{U_c}} & \text{for } \dfrac{h}{D_e} \leq 6 \end{cases} \quad (4.1)$$

Equation (4.1) is valid for $0.4 < U/U_c < 1.0$. In this equation, the pier width of the original expression (Sheppard *et al*., 2011) was replaced by an equivalent diameter D_e of the complex pier. The application to the tests of this study (Configuration C1) enabled to obtain the scour depth (d_{smMS}) measured at the time duration defined (240 hours $< t_{dMS} <$ 390 hours) according to equation (4.1) and the corresponding ratio $d_{smMS}/d_{sm} \approx [0.95, 0.81, 0.87]$ for Situations 1 to 3, respectively. These results confirm that equation (4.1) is a good approximation to estimate *a priori* the time duration of the scour tests to be performed. In these calculations, the equivalent diameters, D_e, were calculated with the expressions suggested by Coleman (2005) (presented in detail in section 2.3.6.1). As one of the objectives of this study is to present a method to predict the equilibrium scour at complex piers (Chapter 7), the present author recommends using equations (7.7) to (7.17) to estimate D_e in future application of equation (4.1).

4.5. CONCLUSIONS

From the previous discussion, the most important conclusions of this chapter can be drawn:

1. Seven complex pier models, characterized in Table 3.1, were used to quantify the influence of the complex pier position and geometry on the scour depth time evolution. The experimental results were classified according to three pile cap situations: (i) Situation 1, characterized by the bottom of the pile cap being above the initial bed level; (ii) Situation 2, characterized by the pile cap being partially buried in the initial bed configuration; and (iii) Situation 3, characterized by the pile cap being initially completely buried in the bed. In Situation 1, the pile group is the main component of the complex pier to contribute to the scour process while in Situation 2, most of the scour process is associated to the column and the pile cap. In Situation 3, the column is the main component to contribute to the scour process;
2. The temporal evolution of scour depth at complex piers is generally influenced by the relative column position (H_c/h), by the relative column width (D_c/D_{pc}), by the relative pile-cap thickness (T/h) and by the pile-group configuration. The different stages in the scour depth time evolution are associated with the number of structural elements of the complex pier that are exposed to the flow inside the scour hole developed along the scouring process; and
3. The criterion established to stop the tests by Melville and Chiew (1999) for single piers, also commonly used in complex piers, was evaluated. This criterion seems to no longer have such a good performance when more than one component of the complex pier is exposed to the flow in the scour hole. In general, the application of this criterion would imply much smaller experiment running times than those required for the different scouring phases (*e.g.*, the different stages presented in sections 4.2 and 4.3 for the complex pier models of this study). Equation (4.1), based on Sheppard *et al*. (2011), can be used to estimate the time recommended to stop the tests with complex piers.

5. EFFECT OF COMPLEX PIER GEOMETRY ON EQUILIBRIUM SCOUR DEPTH

5.1. INTRODUCTION

According to the dimensional analysis performed in section 2.3.2, the equilibrium scour depth at complex piers, d_{se}, may depend of the following non-dimensional parameters

$$\frac{d_{se}}{D_c} = \varphi\left(\begin{array}{c} \sigma_g, K_{Sc}, K_\theta, \frac{h}{D_c}, \frac{D_c}{d_{50}}, \frac{U}{U_c}, \frac{u_* d_{50}}{\upsilon}, \frac{u_* t}{D_c}, \\ K_{Spc}, \frac{D_c}{D_{pc}}, \frac{T}{h}, \frac{H_c}{h}, \frac{f_l}{f_t}, \frac{f_p}{D_p}, K_{Sp}, m, \frac{S_m}{D_p}, n, \frac{S_n}{D_p} \end{array}\right) \quad (2.37)$$

It should be recalled that: (1) the first seven non-dimensional parameters of the upper-line in equation (2.37) have been extensively studied for single piers (see section 2.2.5); (2) the last non-dimensional parameter of the upper-line in equation (2.37) – that corresponds to the temporal evolution of the scour depth at complex piers – (or similar form of this relationship depending on pier width adopted) was described and discussed in Chapter 4; and (3) the last five non-dimensional parameters of the lower-line in equation (2.37) have been extensively studied for pile groups (see section 2.3.5.5).

As mentioned in section 2.3.5, the five studies identified as relevant on scouring at complex piers are focused on characterizing and quantifying the influence of the relative column position, H_c/h ($H_c =$ distance from the initial bed level to the top of the pile cap; $h =$ approach flow depth), on d_{se}. The results of those studies indicate that d_{se} depends directly on H_c/h and that the maximum scour depth occurs when the pile cap is partially buried in the bed. Additionally, Ferraro *et al*. (2013) studied the effect of the relative pile-cap thickness, T/h ($T =$ pile-cap thickness), on d_{se}. They concluded that, in general, the maximum scour depth values measured on complex piers increase with increasing pile-cap thickness. Furthermore, the effect of the relative column width, D_c/D_{pc} ($D_c =$ column width; $D_{pc} =$ pile-cap width), on d_{se} has been extensively studied for different geometries of the complex piers (*i.e*., at columns founded on caissons, section 2.3.5.3). Sheppard and Renna (2010) and Arneson *et al*. (2012) presented a design chart to account for the shielding effect due to the pile-cap extension (from column faces) lengths as function of H_c/h. The chart was obtained based on tests with column/pile-cap sets suspended on the approach flow.

In the present study, the availability of two comparatively large flumes (sections 3.3 and 3.4) rendered possible to generate additional scour data at complex piers, *i.e*., 48 long-duration (7 to 47 days) tests obtained from seven different complex pier geometries (Figure 3.1). All 48 tests were performed with Configuration C1 (*i.e*., complex pier with the three elements, Figure 3.2). The aim of this chapter is to: (1) investigate the influence of the relative column position, the relative column width, the relative

pile-cap thickness and the pile-group configuration on the maximum local scour depth with the results of the 48 tests performed; and (2) compare the results of the present experimental study with the results of studies performed up to the present date on complex pier models (*i.e.*, the thirteen models in Table 2.2). Within the first objective the combined effects of the different parameters mentioned before were analysed, namely: (a) D_c/D_{pc} and H_c/h on d_{se} on the basis of the results obtained with Model 2 ($D_c/D_{pc} = 0.85$), Model 3 ($D_c/D_{pc} = 0.70$) and Model 5 ($D_c/D_{pc} = 0.55$), in which only the column dimensions (width and length) were changed (Table 3.1); (b) T/h and H_c/h on d_{se} by means of the results obtained with Model 4 ($T/h = 0.60$), Model 5 ($T/h = 0.45$) and Model 6 ($T/h = 0.30$), in which only the pile-cap thickness was changed (Table 3.1); and (c) the pile-group configuration (characterized by the number of alignments, n) and H_c/h on d_{se} on the basis of the results obtained with Model 3 ($n = 2$) and Model 7 ($n = 1$).

The current chapter is organized as follows: a brief introduction was presented in the current section (5.1); equilibrium scour depths obtained for the 48 tests performed in this study are summarized in section 5.2; main results concerning the influences of H_c/h, D_c/D_{pc} and T/h on d_{se} based on the tests performed in this work are presented and discussed in sections 5.3 to 5.5; section 5.6 discusses the comparison of the main results obtained in the present experimental data with the published experimental data; and section 5.7 is dedicated to the related main conclusions.

5.2. EQUILIBRIUM SCOUR DEPTHS

According to the early work of Chabert and Engeldinger (1956) and latter works such as Ettema (1980), it can be assumed that, for clear-water conditions, the equilibrium stage in the scour evolution is attained asymptotically, as discussed in sections 2.2.4. Hence, in order to estimate the equilibrium scour depth, d_{se}, the recorded experimental scour depth values, summarized in the Appendix, were extrapolated to time infinite by means of the following equation:

$$d_s = d_{se}\left[1 - e^{-a\left(\frac{Ut}{D_e}\right)^b}\right] \tag{5.1}$$

where, d_s = the scour depth at time t; U = the mean velocity of the approach flow; D_e = the equivalent diameter of the complex pier; and a and b = parameters obtained by regression analysis.

Equation (5.1) is a modification of the Franzetti *et al.* (1982) equation, in which the single cylindrical pier diameter of the original expression was replaced by the parameter D_e. This change is due to the fact that the complex pier has three structural components, each with a different width. The equivalent diameter, D_e, was calculated with the equations suggested by Coleman (2005) (see section 2.3.6.1).

Equation (5.1) was fitted to the experimental data obtained from the 48 tests performed with Configuration C1. In tests in which the scour depth time evolution presented a unique trend (*e.g.*, all tests of Situation 1) the adjustment was applied using all experimental data. In the other experiments, which showed two or more scour depth time evolution stage trends, the adjustment was carried out taking into account only the experimental data associated to the ultimate stage of the scour depth time evolution curve. The equilibrium scour depth values obtained by extrapolation for all experiments with equation (5.1) are summarised in Table 5.1 for Models 1 to 6 and in Table 5.2 for Model 7.

Table 5.1 – Equilibrium scour depths (extrapolated values) with Models 1 to 6

Pile-cap position	$\frac{H_c}{h}$	Model 1 d_{se} (m)	Model 2 d_{se} (m)	Model 3 d_{se} (m)	Model 4 d_{se} (m)	Model 5 d_{se} (m)	Model 6 d_{se} (m)
A	1.700	0.123	0.123	0.123	0.123	0.123	0.123
B	1.300	0.144			0.144		
C	1.150	0.156	0.144	0.144	0.156	0.144	
D	1.000	0.168	0.156	0.156	0.168	0.156	0.144
E	0.667	0.193	0.185	0.175	0.173	0.161	0.141
F	0.333	0.199	0.192	0.177	0.160	0.159	0.136
G	0.185				0.201	0.168	0.195
H	0.050	0.218	0.189	0.175	0.184	0.118	0.176
I	0.000	0.223	0.245	0.225	0.113	0.112	0.157
J	−0.235		0.212	0.162			
J	−0.250				0.103	0.103	0.103
K	−0.500	0.228	0.228	0.184	0.148	0.148	0.148
L	−1.500	0.240	0.240	0.218	0.178	0.178	0.178

Table 5.2 – Equilibrium scour depths (extrapolated values) with Model 7

Pile-cap position	H_c/h	d_{se} (m)
M	1.500	0.139
N	1.000	0.141
O	0.667	0.150
P	0.322	0.188
Q	0.161	0.230
R	0.000	0.188
S	−0.333	0.168
T	−1.500	0.176

5.3. COMBINED EFFECTS OF RELATIVE COLUMN WIDTH AND POSITION

The combined effects of the relative column with, D_c/D_{pc}, and the relative column position, H_c/h, on the equilibrium scour depth, d_{se}, were evaluated on the basis of the results obtained with Models 2, 3 and 5 (Figure 3.1). By considering those three models, four recognized parameters that influence d_{se} could change: (1) the width of the column (D_c); (2) the pile-cap front and side overhang length (f_l and f_t in Figure 2.21); (3) the sediment coarseness ratio (expressed by D_e/d_{50}); and (4) the flow shallowness ratio (expressed by h/D_e). Nevertheless, it can be considered that the effects of sediment coarseness and flow shallowness are practically the same for all the three models (2, 3 and 5) and the corresponding H_c/h positions. These two effects were calculated by the equations suggested by Sheppard *et al*. (2014), *i.e*., equations (2.28) and (2.30). Taking that into account, in this study the d_{se} variations in the three models are associated only with the ratio D_c/D_{pc} and the pile-cap overhang length.

The values of d_{se} are plotted against H_c/h in Figure 5.1 for the three discussed models. The figure includes two vertical lines at $H_c/h = 0$ and $H_c/h = T/h$, which are used to delimit the regions associated to the three situations analysed: pile cap above the bed (Sit. 1, $H_c/h > T/h$), pile cap partially buried in the bed (Sit. 2, $0 \leq H_c/h \leq T/h$) and pile cap completely buried in the bed (Sit. 3, $H_c/h < 0$). In general, the d_{se} variation with H_c/h is similar for the three models. The increment in d_{se} values, associated to each model, is related to the increment of the column width and also to the corresponding reduction of the pile-cap front and side extension lengths, *i.e.*, an increase in D_c/D_{pc} ratio.

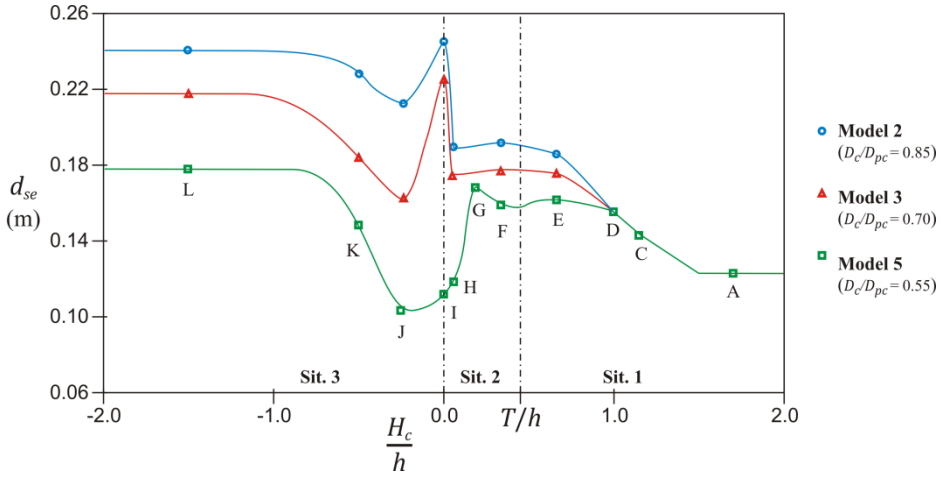

Figure 5.1 – Effect of the relative column width on the equilibrium scour depth as a function of the relative column position

For Situation 1, when compared to Position A (column and pile cap out of the water), an increase in d_{se} with increasing submergence of the pile cap occurs for Position C (partial submergence) and for Position D (fully submergence), as shown in Figure 5.1. That increase is justified by the frontal area exposed to the flow due to the pile cap being larger than the one corresponding to the upstream piles (Position A). For these two positions (C and D) d_{se} is identical for all models as the pile group and the pile cap have the same geometrical definition and the column is still out of water. The increase of d_{se} in Position E (all three elements exposed to the flow) relative to Position D is different for the three models, with d_{se} clearly increasing with the column width size (and so, with the area exposed to the flow).

In Situation 2, when the pile cap is only slightly buried in the bed (Position F), the d_{se} values and comparative differences between the three models are similar to that observed in Position E, as shown in Figure 5.1. Nevertheless, when the pile cap is almost buried in the bed (Position H), although a similar trend does occur for the two wider-column models (Models 2 and 3, $D_c/D_{pc} \geq 0.70$) when compared to the value of d_{se} at Position F for the same models, a sharp decrease in d_{se} for Model 5 ($D_c/D_{pc} = 0.55$) is observed in a similar comparison. That different behaviour is mostly associated with the pile-cap overhang dimension's influence on the flow structure around the column above the pile cap: for large column-to-pile-cap width ratios ($D_c/D_{pc} \geq 0.70$), the downflow along the upstream face of the column is only negligibly affected by the reduced pile-cap overhang dimension on its way downwards the upstream face of the pile cap when the scour hole is developed, whereas for smaller column-to-pile-cap width ratios ($D_c/D_{pc} = 0.55$) the pile-cap overhang length is enough to deflect the downflow along the column and to reduce the strength of the horseshoe vortex in order to influence

and disturb the scouring process. In addition to that, and specifically for this last case, it should be mentioned that (1) the pile group stops contributing to the scour process at Position H, as the scour hole no longer exposes completely the front face of the pile cap; and (2) the interaction of the bottom flow boundary layer with the deflected downflow of the column affects also the development of both the downflow and the horseshoe vortex system around the pile cap. Quite close to Position H, Position I corresponds to the lower limit of Situation 2, with the pile cap initially flush with the bed. The mentioned overhanging enhanced protecting effect, translated into a delay in the beginning of the scour process and on a reduction of the initial scour rate, may justify the slight decrease (and a minimum, for Situation 2) on d_{se} for Model 5 from Position H to Position I. The similar analysis for Models 2 and 3 does show again a very different behaviour comparatively to Model 5, this time by a very sharp increase in d_{se} in Position I compared to Position H. In fact, for these two cases a maximum of d_{se} is achieved for Position I. That apparently can be explained by (1) the disappearance of the pile-cap protrusion from the bed level and, so, of any obstruction from the bed flow boundary layer to the downflow at the beginning of the scour process; and (2) the contribution of a larger obstruction area (*i.e.*, corresponding to the entire pile cap thickness) exposed inside the developed scour hole, therefore leading to an increase of horseshoe vortex intensity and the corresponding scour rate. Concerning Model 5, the described specific comparative behaviour for Positions F to I enabled prediction of the occurrence of a maximum value of d_{se} on an intermediate position, corresponding (or close) to Position G, as shown in Figure 5.1.

In accordance with Ataie-Ashtiani *et al*. (2010) and Ferraro *et al*. (2013), the maximum d_{se} value always occurs in Situation 2, when the three components of the complex pier are progressively exposed to the flow during the scour process, the scouring development being dominated by the pile cap (larger-width element of the pier). The specific position at which this maximum occurs depends on D_c/D_{pc} ratio (Figure 5.1): in Models 2 and 3 the maximum d_{se} occurred at Position I ($H_c/h = 0.0$) whereas in Model 5 it occurred at Position G ($H_c/h = 0.18$). For Model 5 at Position G, the maximum d_{se} may be explained by (1) the pile-cap protrusion above mentioned effects of obstruction of the flow boundary layer at the beginning of the scour process, do contribute, in this case, to the development of both the downflow and the horseshoe vortex system around the pile cap; and (2) the contribution of the upstream piles on the scour process, condition that does not occur in Model 5 when the top surface of the pile cap is near or flushes the initial bed level (Situation 2). The first reason was also referred by Parola *et al*. (1996) in experiments on piers with rectangular foundations. Figure 5.2 shows the scour hole developed in the three tests where the corresponding maximum scour depth occurs, in which the mentioned tentative interpretations of the flow structure around the complex pier are illustrated.

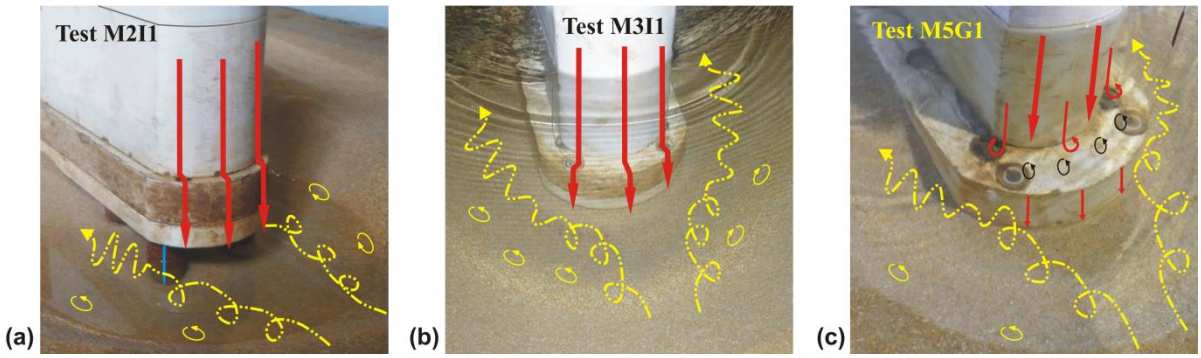

Figure 5.2 – Interpretation of the flow structure in the cases in which the maximum equilibrium scour depth occurred (Situation 2) for: (a) Model 2, (b) Model 3 and (c) Model 5

The equilibrium scour depth behaviour as a function of H_c/h in Situation 3 (Figure 5.1) was similar to the one obtained by Melville and Raudkivi (1996) and Umeda *et al*. (2010) for tests with cylindrical piers founded on cylindrical caissons. The d_{se} reduction at Position J in comparison to d_{se} values at Position I is due to the effect of the overhanging of the pile cap from the column, made active after the top of this element is reached on the scour process, by that interfering on the scour hole development process (by physical obstruction on the cavity and by weakening the flow structure induced by the column while confined by the above-adjacent sand bed). In agreement with Melville and Raudkivi (1996), the increase on d_{se} values on decreasing H_c/h ratio from Position J to Positions K and L, is due to the scour depth being controlled by the position of the top of the pile cap in the scour hole. The rate of increase depends on D_c/D_{pc} ratio, being higher for smaller values of D_c/D_{pc}.

Additionally, six long-duration tests were performed at LNEC's facility (see Moreno *et al*., 2015a) with a narrow-column complex pier model ($D_c/D_{pc} = 0.40$). In this model (referenced as Model Mu), the geometry and dimensions of the pile cap and pile group were the same used in the Models 2, 3 and 5, *i.e*., only the column dimensions were changed, as shown in Figure 5.3(a). The six tests were carried out for the same flow conditions and sediment granulometry used in the three mentioned models. The equilibrium scour depth values of those six tests were compared with the results of Model 5 (narrow-column model), as presented in Figure 5.3(b). Curves that describe the variation of d_{se} with H_c/h were traced. In general, the d_{se} variation with H_c/h is similar for both models. This result is in agreement with the physical explanations described above for the narrow-column model. The higher values of d_{se} correspond to Model 5 ($D_c/D_{pc} = 0.55$), which leads to confirm the result of Figure 5.1, and to make evidence that lowering D_c/D_{pc} ratio less scour is produced. The reduction in d_{se} values from Model 5 to Model Mu may be explained by the fact that: (1) the reduction of the column width in Model Mu implies a reduction of the downflow along that structural element; and (2) the corresponding increment of the pile-cap extension lengths better potentiates the deflection of the downflow along the column and reduces the strength of the horseshoe vortex.

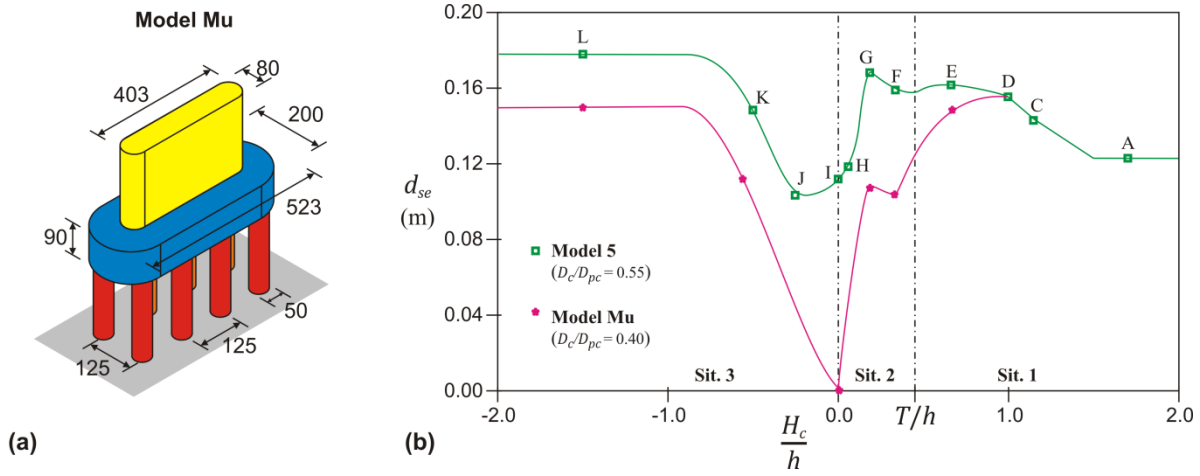

Figure 5.3 – (a) Scheme with dimensions of Model Mu (Moreno *et al*., 2015a) (units in millimetres) and (b) equilibrium scour depth as a function of the relative column position observed with Models 5 and Mu

The most significant difference in the scour depth values observed in the two models occurs in Position I ($H_c/h = 0$), as shown in Figure 5.3(b). The deviation in the two curves is stressed out in the vertical line where no scour at the reference measuring point was observed during the test with Model Mu (experiment with $D_c/D_{pc} = 0.40$). In Position I for both tests it was observed that (1) the

scour process started at the downstream end of the pile cap under the action of wake vortices; and (2) scour holes were also formed along both lateral sides of the pile cap. Those stages are pictured in Figure 4.7 for test M5I1 (with Model 5) and in Figure 5.4 for the test with Model Mu.

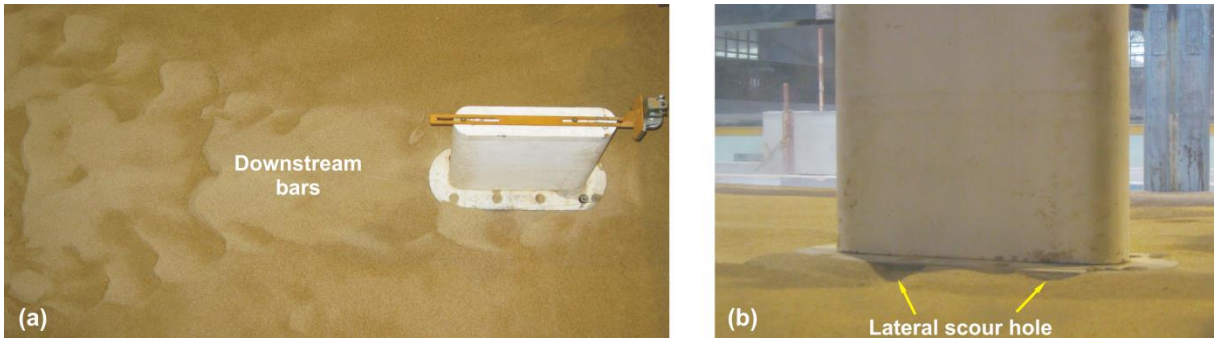

Figure 5.4 – Scour hole in test 4 with Model Mu (a) downstream scour hole and (b) lateral scour hole

In test M5I1 the lateral scour grooves extended to the upstream part of the pile cap (see Figure 4.7) while in the test with Model Mu, after 25 days (600 hours), scouring did not reach the front of the pile cap, as shown in Figure 5.4. This may be associated to the larger pile-cap overhang length in Model Mu in comparison to the respective length in Model 5.

5.4. COMBINED EFFECTS OF RELATIVE PILE-CAP THICKNESS AND RELATIVE COLUMN POSITION

The combined effects of the relative pile-cap thickness, T/h, and the relative column position, H_c/h, on the equilibrium scour depths, d_{se}, were evaluated on the basis of the results obtained with Models 4, 5 and 6 (all with $D_c/D_{pc} = 0.55$, Figure 3.1). The values of d_{se} are plotted against H_c/h in Figure 5.5(a) for the three mentioned models. The figure includes one vertical line at $H_c/h = 0$ and three vertical segments at $H_c/h = T/h$ (which represent the different T/h ratios of the studied models), these being used to delimit the regions associated to the three situations.

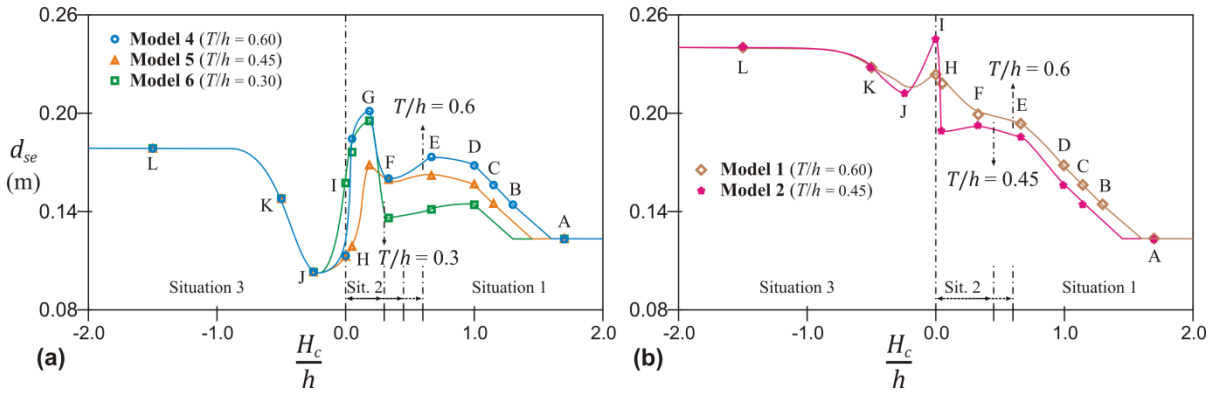

Figure 5.5 – Effect of the relative pile-cap thickness on the equilibrium scour depth as a function of the relative column position for: (a) Models 4, 5 and 6 and (b) Models 1 and 2

When the bottom of the pile cap is above the initial bed level (Situation 1), the comparative increment in d_{se} values is related to the increment in T/h, as shown in Figure 5.5(a). In turn, in all T/h ratios,

the increment in d_{se} values from Position A (column and pile cap out of the water) to Position D (only the column out of the water) is associated with the increment in the pile-cap frontal area exposed to the flow. The variation in d_{se} values from Position D to Position E (for which all the three components are exposed to the flow) depends on the D_c/D_{pc} ratio (effect explained in the previous section for Model 5) as well as on the T/h ratio. Thus: (1) the small increase in the greater T/h ratios (*i.e.*, Models 4 and 5) may be justified by the fact that the downflow along the (higher) exposed area of the pile cap balances the weakened downflow originated along the upstream face of the column (D_c/D_{pc} effect); whereas (2) the small decrease in the smaller T/h ratio (*i.e.*, Model 6) may be related to the diminution in the downflow along the upstream face of the pile cap (reduction in the frontal obstruction area). This last explanation also applies to the reduction in d_{se} values from Position E to Position F in Model 6. These results corroborate the findings of Ferraro *et al*. (2013) (see section 2.3.5.4).

When the pile cap is partially buried in the bed (Situation 2), the d_{se} variation with H_c/h does not follow a similar behaviour to the one described for Situation 1, *i.e.*, deeper scour holes for greater values of T/h, as shown in Figure 5.5(a). In this situation, the variation in d_{se} with H_c/h, from Position F to Position I, is strongly dependent on the pile-group (upstream piles) contribution to the scour process, which occurs when the front face and the bottom surface (in front of the upstream piles) of the pile cap are completely exposed in the scour hole. In the case of the thinner pile cap (Model 6, $T/h = 0.30$), the upstream piles contribute to the scour process for all the pile-cap positions in this situation. This justifies (1) the marked increase in d_{se} values from Position F to Position G for Model 6, higher than the corresponding value for Model 5 and close to the value achieved for Model 4; and (2) the fact that at Position I the d_{se} value for Model 6 is higher than the ones observed for the other two models (4 and 5), as shown in Figure 5.5(a).

When the pile cap is completely buried in the bed (Situation 3), the d_{se} variation with H_c/h is similar in the three models (4, 5 and 6), as shown in Figure 5.5(a) (Positions J to L). This implies that, in this situation, the effect of T/h on d_{se} proved to be negligible. This result can be justified by the fact that, in any of the three models, the front face of the pile cap is no longer completely exposed during the scour hole development process. The physical explanations for the variation of d_{se} with H_c/h from Position J to Position L were described in the previous section for Model 5.

In addition to the above described, the influence of T/h and H_c/h on d_{se} was also analysed by using the results obtained with Models 1 and 2 (all with $D_c/D_{pc} = 0.85$, Figure 3.1). The corresponding values of d_{se} are plotted against H_c/h in Figure 5.5(b). The figure includes one vertical line at $H_c/h = 0$ and two vertical segments at $H_c/h = T/h$, similarly to the representation in Figure 5.5(a). In Situation 1 and in all positions of Situation 2, with exception of Position I, the increment in d_{se} values are related to the increment of the relative pile-cap thickness (T/h), as expected. In Position I, the higher d_{se} value was observed for the thinner pile cap (Model 2, $T/h = 0.45$). This may be associated with the contribution of the pile group on the scour process, since the pile cap is completely exposed in the scour hole, as explained before for Models 4 to 6. In Situation 3, the effect of T/h on d_{se} was also negligible, as observed for Models 4 to 6.

5.5. EFFECT OF PILE-GROUP CONFIGURATION

The combined effects of the number of alignments in the pile group, n, and H_c/h on d_{se} were evaluated on the basis of the results obtained in the test series with Model 3 ($n = 2$) and Model 7

($n = 1$). Model 3 was selected by the fact that the relations $D_c/D_{pc} = 0.70$ and $T/h = 0.45$ are relatively similar to those of Model 7 ($D_c/D_{pc} = 0.74$; $T/h = 0.32$). The values of d_{se} are plotted against H_c/h in Figure 5.6 for the two discussed test series. The figure includes two vertical lines at $H_c/h = 0$ and $H_c/h = T/h$, which are used to delimit the regions associated to the three situations. Similarly to the results of the effects analysed in the previous sections, the influence of the number of alignments of the pile group on the scour process is most evident in Situations 1 and 2.

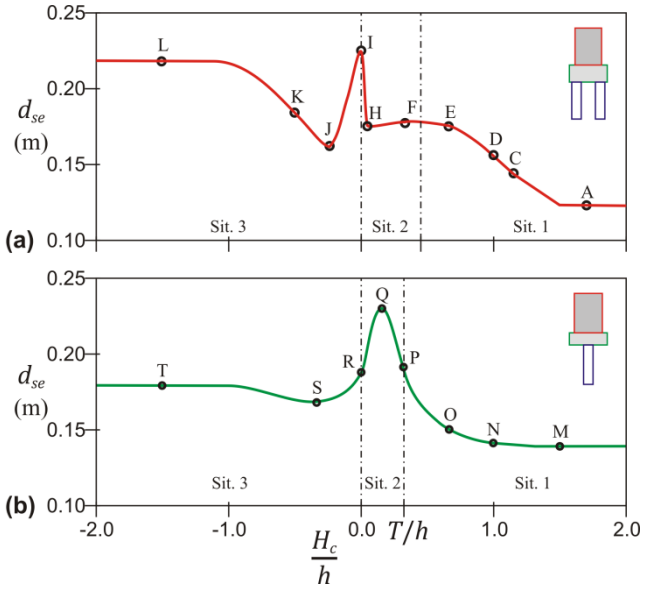

Figure 5.6 –Equilibrium scour depth as a function of the relative column position for models with: (a) two alignments of piles (Model 3) and (b) one alignment of piles (Model 7)

In Situation 1, characterized by the pile cap being above the initial bed level, the relative increase in d_{se} values when H_c/h ratio decreases from the position where the pile cap is out of the water (Positions A and M) to the positions where all three elements are exposed to the flow (Positions E and P) is higher in Model 3, as shown in Figure 5.6. This is assumedly attributable to the fact that the area exposed to the flow in this model (which has two alignments of piles) is larger than the corresponding area in Model 7, with only one alignment of piles.

In Situation 2, corresponding to the case where the pile cap is partially buried in the bed, for Model 7, a marked increase in d_{se} in Position Q, when compared to Position P (Figure 5.6(b)), may be justified by: (1) the increment in the pile cap exposed area in the scour hole; and by (2) the fact that the longitudinal axis of the pile cap and of the pile alignment is the same. This implies that the upstream pile can contribute to the scour process immediately after the entire front of the pile cap becomes exposed in the scour hole. Nevertheless, in this situation, for Model 3 (Figure 5.6(a)), the contribution of the pile group (upstream piles) to the scour process is reduced by the mismatch between the longitudinal axes of both alignments of piles and that of the pile cap. This implies a lesser exposed area of each upstream pile in comparison to the case where a pile is aligned with the longitudinal axis of the pile cap attributable to the concavity of the scour hole.

In Situation 3, characterized by the pile cap being initially completely buried in the bed, the pile-group configuration shows no influence on d_{se} in both models. This can be justified by the fact that the upstream piles were not sufficiently exposed to the flow to generate vortices around it.

5.6. COMPARISON OF THE PRESENT EXPERIMENTAL STUDY WITH RESULTS REPORTED IN LITERATURE

5.6.1 ASSESSMENT OF EXPERIMENTAL DATA

This section includes the comparison of the results obtained from the thirteen models reported in the literature (see Table 2.2) with the results obtained in the present study (from seven models) and extensively described and discussed in the previous sections of this chapter. Table 5.3 summarizes the most relevant flow characteristics and geometry parameters of those twenty complex pier models. The table includes also the duration of the reported tests. The same model designations used in Table 2.2 are used in Table 5.3 for the models from literature.

Table 5.3 – Experimental models: flow parameters, model geometry parameters and test durations

Model	U/U_c	B/h	W_o/B	D_c/D_{pc}	f_l/f_t	T/h	h/D_{e*}	D_{e*}/d_{50}	t_d (days)
Co1	0.75	2.5	0.07	0.25	0.00	0.10	9.92	72	NS
Co2	0.85	2.5	0.07	0.25	1.11	0.10	9.92	72	NS
Co3	0.83	4.5	0.10	0.53	0.89	0.24	1.97	141	NS
AA1	0.72-0.85	3.9-4.5	0.07	0.24	0.44	≈0.22	≈3.50	70	0.4-3.1
AA2	0.74-0.80	3.9-4.3	0.09	0.47	0.96	≈0.28	≈3.00	83	0.4-2.1
GC	0.92	7.0	0.14	0.34	1.00	0.50	0.91	92	4.8-18.1
Fe1	0.92	7.0	0.14	0.33	1.00	0.50	0.93	90	8.3-37.0
Fe2	0.92	7.0	0.13	0.33	1.00	0.01	0.98	87	3.2-41.2
A1	0.95	6.3	0.12	0.80	1.00	0.13	1.32	225	1.0
A2	0.95	6.3	0.10	0.73	1.00	0.13	1.84	172	1.0
A3	0.95	6.3	0.11	0.38	1.71	0.46	1.69	179	1.0
A4	0.95	6.3	0.05	0.39	0.85	0.15	4.32	65	1.0
A5	0.95	6.3	0.08	0.49	3.93	0.32	2.39	126	1.0
1 (PS)	0.80	10.0	0.09	0.85	1.00	0.60	1.22	191	12.9-46.9
2 (PS)	0.80	10.0	0.09	0.85	1.00	0.45	1.22	190	12.9-46.9
3 (PS)	0.80	10.0	0.08	0.70	1.00	0.45	1.41	165	12.9-29.0
4 (PS)	0.80	10.0	0.08	0.55	1.00	0.60	1.55	150	12.9-46.9
5 (PS)	0.80	10.0	0.08	0.55	1.00	0.45	1.58	148	12.9-46.9
6 (PS)	0.80	10.0	0.07	0.55	1.00	0.30	1.60	145	12.9-46.9
7 (PS)	0.97	5.6	0.10	0.74	1.00	0.32	2.03	103	6.9-15.0

Note: Co = Coleman (2005); AA = Ataie-Ashtiani *et al*. (2010); GC = Grimaldi and Cardoso (2010); Fe = Ferraro *et al*. (2013); A = Amini *et al*. (2014); PS = Present study; W_o = equivalent width of obstruction of the pier; D_{e*} = maximum equivalent diameter (calculated according to Coleman 2005); NS = not specified.

The wall effect is negligible when $B/h > 5$ (B = flume width) in which the velocity field is two-dimensional at the central section of the channel, in line with Yalin (1971). According to that criterion and to the values in Table 5.3, tests with Models Co1 and Co2 may be markedly reflecting wall effects while tests with Models Co3, AA1 and AA2 may have a slight influence of wall effects.

In fact, in the specific case of complex piers, there are no studies that define the equivalent obstruction width of the pier, W_o, for the calculation of the effect of horizontal contraction. The author of the present study considers that the contraction effect may be calculated taking into account the ratio W_o/B. In studies of single piers (*e.g.*, Chiew and Melville, 1987), the contraction effect is negligible when $W_o/B < 0.10$, in which W_o is equal to the single pier width. In the present study, the W_o values of the twenty models were calculated as the ratio between the maximum obstruction area of the pier (in a cross section perpendicular to the channel walls) and the flow depth. The maximum area of obstruction was obtained after analysing different positions of the complex pier relative to the initial bed level, as illustrated in Figure 5.7. According to Table 5.3, tests with Models GC, Fe1, Fe2, A1 and A3 may have a slight influence of the contraction effect since $W_o/B > 0.10$

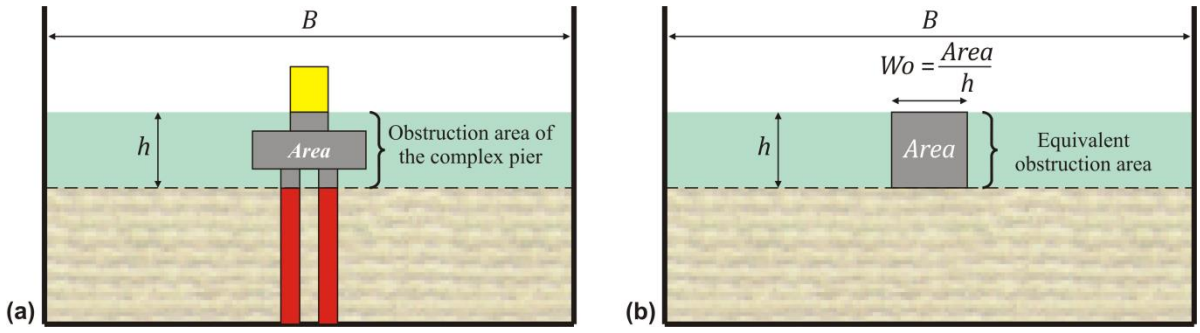

Figure 5.7 – Scheme of (a) complex pier obstruction area (Model Fe1) and (b) equivalent obstruction width of the complex pier

As presented in Table 5.3, all tests performed by Ataie-Ashtiani *et al*. (2010) and by Amini *et al*. (2014) were carried out with short durations (between 0.4 and 3.1 days) in comparison with the minimum duration suggested by several authors, *i.e.*, 7 days (see section 2.3.4). In accordance, it is possible that the equilibrium scour depth has not been reached in the tests of those five models (AA1, AA2, A1, A2, A3, A4 and A5).

Given that the scour depth data reported by each of the mentioned authors was not extrapolated – and most of the scour depth records were not available, not allowing the required extrapolation of d_{se} values – the comparative analysis of the literature and the present study results was performed and will be described by taking into account the scour depth values measured at the end of the tests, d_{sm}. Similar behaviour could be identified in the equilibrium scour depth variation as a function of H_c/h obtained by considering the extrapolated values and the measured values for the models where the time series are available (Models of Fe1, Fe2, GC and of the present study). The corresponding extrapolated values did show a shift of 10-20% (depending on the complex pier models) to the measured values.

As the experimental tests were not performed under the same conditions (see Table 5.3), the measured scour depth values were adjusted taking into account the influence of flow shallowness, h/D_e, of flow intensity, U/U_c, and of sediment coarseness, D_e/d_{50}. The adjustment process was accomplished through equations (2.28) to (2.30), using the D_e values previously calculated in section 4.4. In the following paragraphs the comparison of the scour depth results is performed for the three situations previously discussed, *i.e.*, pile cap above the initial bed level (Situation 1), pile cap partially buried (Situation 2) and pile cap completely buried in the bed (Situation 3). The results of Model Fe2 – due to the particular dimension of the pile-cap thickness – and the results of all models by Amini *et al*. (2014)

(Models A1–A5 in Table 5.3) – due to the extremely short durations of the tests – were excluded from that analysis.

5.6.2 COMPARISON IN SITUATION 1

The evaluation of the effect of T/h on d_{sm} was performed only for Situation 1 (where the pile cap is above the initial bed level) and particularly for the position where the pile cap is completely immersed in the flow, with the column out of the flow. The values of d_{sm}/d_{spg} (d_{spg} = maximum scour depth of the pile group, *i.e.*, complex pier with the bottom of the pile cap out of the water) are plotted against T/h in Figure 5.8. It is clear that the parameter T/h influences d_{sm}/d_{spg}, leading to increasing normalized scour depth as T/h increases, as observed for the envelope curve of experimental data. This result corroborates the findings of Melville and Dongol (1992) and Lagasse *et al*. (2010) on experimental tests for piers with idealized debris rafts at the water surface. Melville and Dongol (1992) tested cylindrical shapes while Lagasse *et al*. (2010) tested rectangular shapes of the idealized debris (component which can resemble the pile cap of the complex pier).

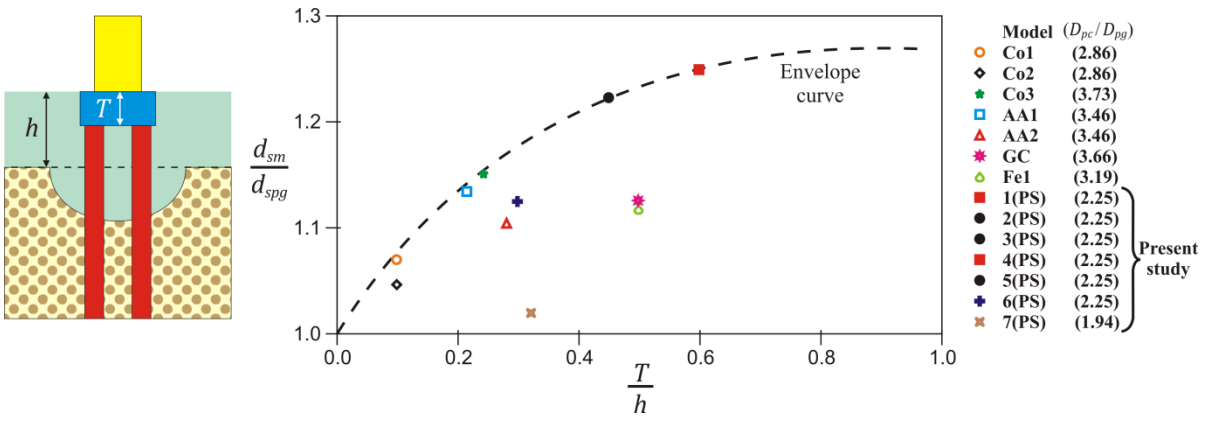

Figure 5.8 – Effect of the relative pile-cap thickness on the relative maximum scour depth

According to Figure 5.8, it may be concluded that other parameters than T/h affect d_{sm}/d_{spg}, and those can be the main factors that varied from the different studies, namely the shape of the pile cap, the number of pile alignments and the ratio f_p/D_p (f_p = longitudinal extension length of the pile cap out from the upstream pile front; D_p = pile width).

5.6.3 COMPARISON IN SITUATION 2

For a comparative analysis of complex pier models under Situation 2 (*i.e.*, $0 \leq H_c \leq T$), d_{sm} and H_c values were normalized, respectively, by D_{pc} (as the pile cap is the main component to contribute to the scour process in that situation) and by T (parameter that defines the upper limit of H_c for that situation). The adjusted values of d_{sm}/D_{pc} are plotted against H_c/T in Figure 5.9. In the left plot, Figure 5.9(a) corresponds to models with rectangular pile caps whereas Figure 5.9(b) relates to models with circular and rectangular round-nose pile caps. The analysis highlights that in general, the relative difference in d_{sm} values may be associated with the effect of the relative column width, D_c/D_{pc}; the effect of the pile-cap extensions symmetry, f_l/f_t; the pile-cap shape; the relative pile-cap thickness, T/h; and the test duration, t_d. As mentioned in section 2.3.5.2, similar column/pile-cap configuration

sets with circular or round-nose rectangular shapes (*i.e.*, with identical component's widths) lead to similar scour depth values, as shown in Figure 5.9(b) for Models GC and Fe1. The reduction in d_{sm}/D_{pc} values from Model Co1 to Model Co2, as shown in Figure 5.9(a), is mostly associated with the increment of the pile-cap front extension length (*i.e.*, increase of f_l/f_t ratio), as previously explained in section 2.3.5.3.

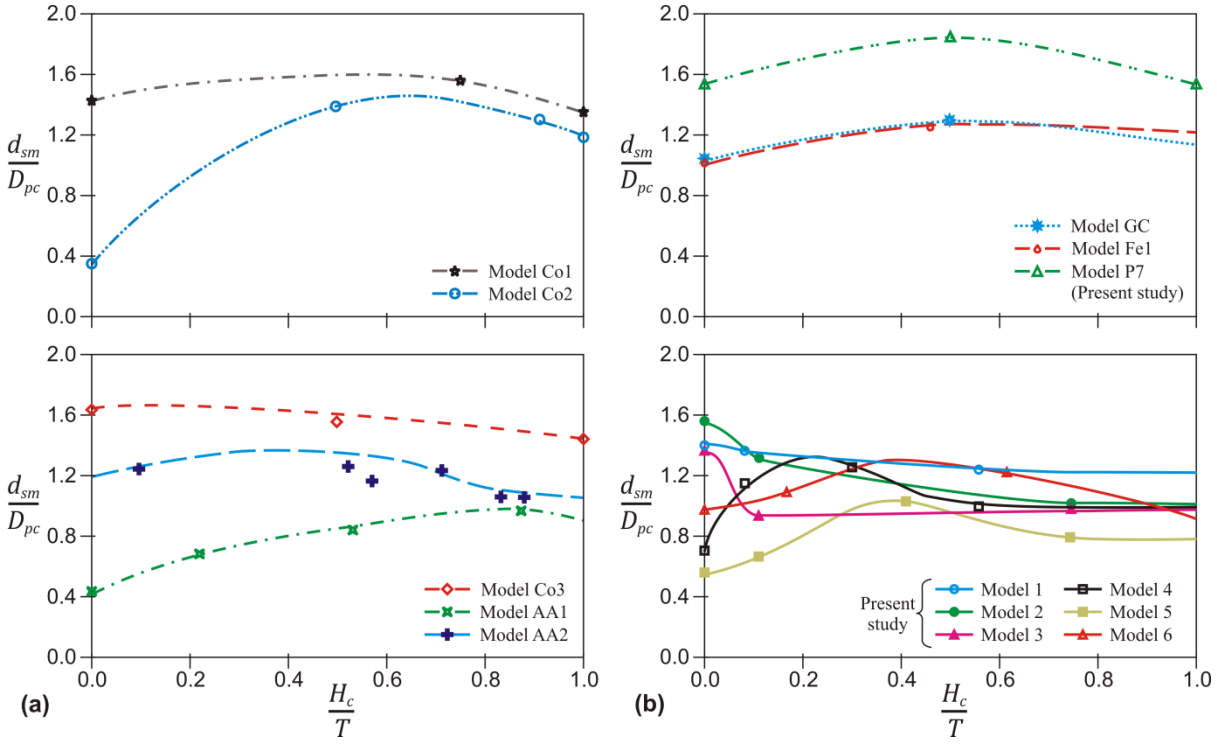

Figure 5.9 – d_{sm}/D_{pc} as function of H_c/T for Situation 2: (a) rectangular pile-cap shape and (b) circular and rectangular round-nose pile-cap shapes

The assessment of the critical relative column position at which the maximum scour depth can occur, $(H_c/T)_{\max}$, is important in terms of complex pier design. The experimental fitting curves presented for the different models on Figure 5.9 do enable to obtain the corresponding values of $(H_c/T)_{\max}$, included in Table 5.4.

Table 5.4 – Values of $(H_c/T)_{max}$ as function of relative column width

Models from Literature	$\frac{D_c}{D_{pc}}$	$\left(\frac{H_c}{T}\right)_{max}$	Models of present study	$\frac{D_c}{D_{pc}}$	$\left(\frac{H_c}{T}\right)_{max}$
Model AA1	0.24	0.83	Model 4	0.55	0.26
Model Co1	0.25	0.75	Model 5	0.55	0.39
Model Co2	0.25	0.66	Model 6	0.55	0.37
Model Fe1	0.33	0.62	Model 3	0.70	0.00
Model GC	0.34	0.58	Model 7	0.74	0.50
Model AA2	0.47	0.47	Model 1	0.85	0.00
Model Co3	0.53	0.28	Model 2	0.85	0.00

It is clear that $(H_c/T)_{\max}$ decreases with increasing D_c/D_{pc} ratio for the models from literature. In the three models of the present study with $D_c/D_{pc} = 0.55$ (Models 4, 5 and 6) the values of $(H_c/T)_{\max}$ obtained fit into a narrow range, where the corresponding value for Model Co3 does also fit. Whereas, in three models of the present study with $D_c/D_{pc} \geq 0.70$ (Models 3, 1 and 2) $(H_c/T)_{\max}$ is null (= 0). In accordance, it can be assumed (by extrapolation of the trend line associated to $(H_c/T)_{\max}$ values in the range $D_c/D_{pc} \leq 0.55$) that the ratio $D_c/D_{pc} = 0.65$ is the minimum value for which the maximum scour depth occurs at position $H_c = 0$. Taking into account that the value of $(H_c/T)_{\max}$ observed for Model 7 of the present study is atypical, what may be justified by the fact that this model is the only one with a sole alignment of piles. As explained in section 5.5, Model 7 presents different characteristics of the scour process, in particular on the contribution of the pile group when the complex pier is positioned in Situation 2 (for which the maximum scour depth occurs).

The analysis of results reveals that the column position is directly influenced by D_c/D_{pc}. Nevertheless, that position may also be influenced by the flow shallowness, h/D_{pc}, and by the symmetry of the pile-cap extensions, f_l/f_t. The following regression equation takes the full parameters' dependence in due account, excluding the value of Model 7.

$$\left(\frac{H_c}{T}\right)_{\max} = \begin{cases} 0 & \text{for } \dfrac{D_c}{D_{pc}} > 0.65 \\ \dfrac{\left[0.9 + 0.1\left(\dfrac{f_l}{f_t}\right)^{0.4}\right]\left[0.84 - 3.1\left(\dfrac{D_c}{D_{pc}}\right)^{3.1}\right]}{K_{spc}\left[\tanh\left(\dfrac{h}{D_{pc}}\dfrac{1}{\sqrt{D_c/D_{pc}}}\right)\right]^{0.2}} & \text{for } 0.15 \leq \dfrac{D_c}{D_{pc}} \leq 0.65 \end{cases} \tag{5.2}$$

where K_{spc} = pile-cap shape factor (1.04 for rectangular shape and 1.0 for circular or round-nose rectangular shapes). In the range $0.15 < D_c/D_{pc} < 0.65$, the determination coefficient is $r^2 = 0.76$ and the root mean square error is RMSE = 0.12. The lower limit of the range was fixed at 0.15, as this value corresponds to a complex pier configuration with $f_l \approx 3D_c$ (with $f_l/f_t \approx 1$), a value that may be considered as a maximum practical ratio in engineering terms.

5.6.4 Comparison in Situation 3

For a comparative analysis of the complex pier models under Situation 3 (*i.e.*, $H_c < 0$), the d_{sm} and H_c values were both normalized by d_{secu} (depth of local scour for a uniform single pier with the same geometrical definition of the complex pier column). The variable d_{secu} was selected as the normalization factor since the column is the main component to contribute to the scour process in this situation. Figure 5.10 displays the effect of D_c/D_{pc} and of the column/pile-cap shapes on d_{sm}/d_{secu} as function of H_c/d_{secu}, where each D_c/D_{pc} ratio is included in brackets on the model's legend. Similarly to what was mentioned for Situation 2, the Models CG (circular column/pile-cap shapes) and Fe1 (round-nose rectangular column/pile-cap shapes) do show an analogous scour depth variation, as shown in Figure 5.10(a), where these results are compared with the ones obtained by Melville and Raudkivi (1996) for a cylindrical column-caisson model with $D_c/D_{pc} = 0.37$ (represented by MR). The apparent reduction of d_{sm} in Models CG and Fe1 compared to Model MR is due to the smaller scour rate that occurs for $-0.3 < H_c/d_{sc} < 0$, where the scour process is developing below the pile

cap. This may be due to the discontinuity between the pile cap's front and the scour hole's bottom, that leads to a reduction of the strength of the downflow and horseshoe vortices for Models CG and Fe1.

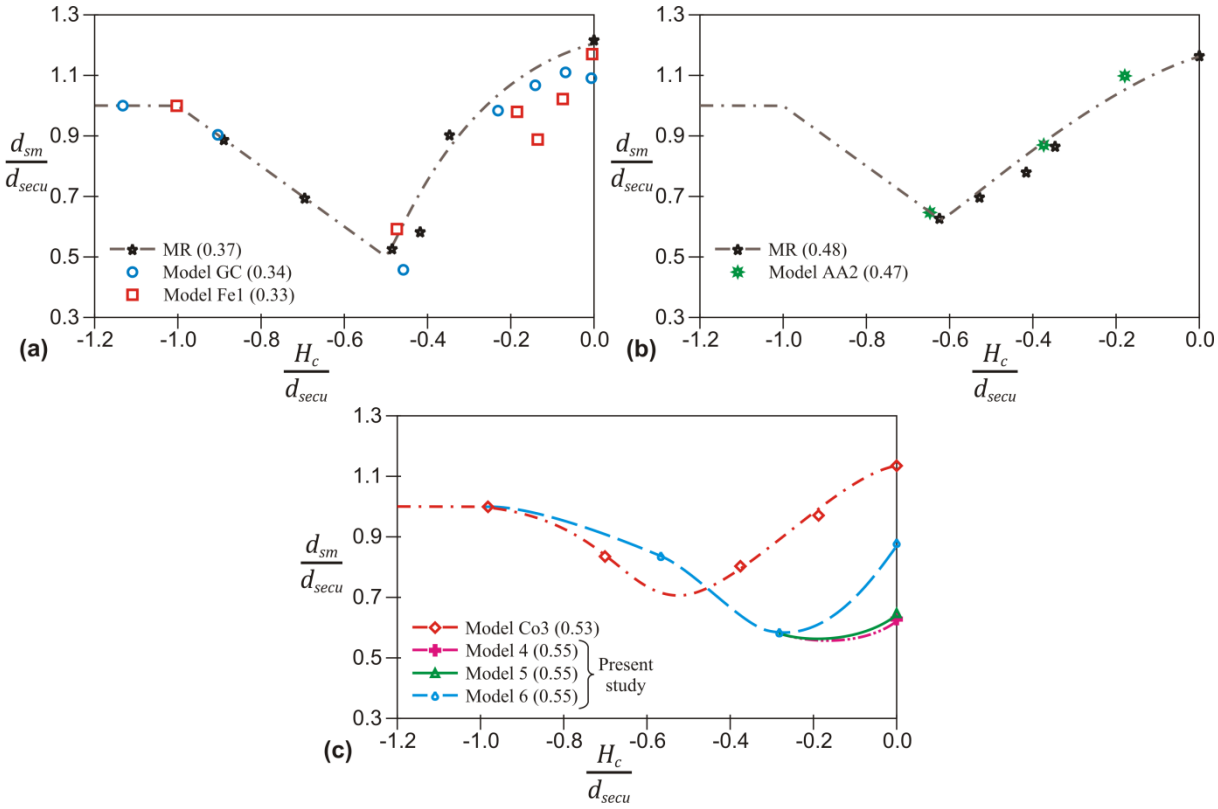

Figure 5.10 – Effect of the relative column width and column/pile-cap shapes on d_{sm}/d_{secu} as function of H_c/d_{secu} for Situation 3

Figure 5.10(b) shows the comparison of d_{sm}/d_{secu} for a complex pier with rectangular column/pile-cap shapes (Model AA2) and a cylindrical column-caisson model (Model MR for $D_c/D_{pc} = 0.48$). The increment on d_{sm} values of Model AA2 relative to Model MR, approximately 8–10% on average, may be associated with the pile-cap shape, since results in rectangular piers reflect higher magnitudes of the flow structure (*e.g.*, downflow, horseshoe vortex, vortices and turbulence intensity) when compared to circular piers, as referred by Dey and Raikar (2007). Figure 5.10(c) displays the comparison of Model Co3 (rectangular column/pile-cap shapes) with Models 4, 5 and 6 of the present study (round-nose rectangular column/pile-cap shapes), where a relevant increase of d_{sm} values is observed in the Model Co3 compared to the other three models for the range $-0.5 < H_c/d_{secu} < 0$. This increment can be associated mainly to geometry definitions of Model Co3, namely: the relative thinner pile cap ($T/d_{secu} \approx 0.37$); the asymmetry of the pile-cap extension lengths ($f_l/f_t = 0.89$); and the rectangular shape of both the column and pile cap.

5.7. CONCLUSIONS

The most important conclusions of this chapter, relative to the experiments performed in this study with Configuration C1, can be summarized as follows:

1. Seven complex pier models, characterized in Table 3.1, were used to quantify the influence of the complex pier position and geometry on the equilibrium scour depth. The experimental results were classified according to three pile-cap situations: (i) Situation 1, characterized by the bottom of the pile cap being above the initial bed level; (ii) Situation 2, characterized by the pile cap being partially buried in the initial bed configuration; and (iii) Situation 3, characterized by the pile cap being initially completely buried in the bed;
2. The equilibrium scour depth, d_{se}, at complex piers is generally influenced by the relative column position (H_c/h), by the relative column width (expressed by D_c/D_{pc} and f_l/f_t), by the relative pile-cap thickness (T/h), by the pile-group configuration and by the shape of the complex pier components (*i.e.*, column, pile cap and piles). The equilibrium scour depth at these piers is also influenced by the effects of flow intensity, flow shallowness and sediment coarseness widely characterized for single piers;
3. The combined effect of D_c/D_{pc} and H_c/h on d_{se} was evaluated for Models 2, 3 and 5. In general, the differences in d_{se} values range from minimal to relevant with decreasing H_c/h ratio, due to the corresponding increasing influence of the column on the scour process. For a specific H_c/h position, the increment in d_{se} values is directly associated with the increment in the column width and also with the corresponding reduction in the pile-cap front and side extension lengths. For the lower relative column-width values, *i.e.*, $D_c/D_{pc} < 0.6$, it could be concluded that the pile cap overhang from the column face plays the role of an obstruction to the downflow adjacent to the column, reducing the vortex system and hence the scour depth. This reduction is most evident in the cases when the top of the pile cap is close to the initial bed level, for which the flow behaviour is similar to collars in single piers. For larger relative column-width values, *i.e.*, $D_c/D_{pc} \geq 0.6$, the influence of the pile cap overhang is negligible;
4. The combined effect of T/h and H_c/h on d_{se} was also evaluated for two sets of complex pier models (*i.e.*, Models 4, 5 and 6 on a set and Models 1 and 2 on another set). In both sets and for Situation 1, the increment in d_{se} values is related to the increment in T/h, while, in Situation 2, the d_{se} behaviour with H_c/h depends not only on T/h ratio but also on the pile-group contribution to the scour process. When the pile cap is completely buried (Situation 3), the effect of T/h in d_{se} showed to be negligible; and
5. The effect of the pile-group configuration (represented by the number of alignments, n) on d_{se} was also assessed. This effect is more evident in Situations 1, in which the pile group is the main component contributing to the scour process, whereas in Situation 2, this effect occurs when the piles are exposed to the flow along the scouring process. In these situations and for the piles separation used in the experimental tests, the increment in the number of alignments (n) of the pile group implies an increase in the scour depth.

On the comparison of the present experimental study with the results of studies performed to date, it was concluded that:

1. In seven out of the thirteen complex pier models analysed in studies from literature (presented in Table 2.2), the tests were carried out for short durations, *i.e.*, least than four days. That fact may lead to relevant inaccuracy on evaluation of the equilibrium scour depth. Additionally, some of the tests performed with the thirteen models may also be slightly reflecting wall and contraction effects; and
2. The experimental data of seven reported models in addition to the data from the present study were used to evaluate the critical relative column position at which the maximum equilibrium scour depth is achieved, $(H_c/T)_{\max}$. The results reveal that $(H_c/T)_{\max}$ decreases with increasing D_c/D_{pc} ratio. For practical applications, the relative position $(H_c/T)_{\max}$ can be obtained through equation (5.2).

6. COMPLEX PIER COMPONENTS CONTRIBUTIONS ON THE EQUILIBRIUM SCOUR DEPTH

6.1. INTRODUCTION

The most commonly used methods to predict the equilibrium scour depth at complex piers, d_{se}, are (1) Auckland method (Coleman, 2005), (2) FDOT method (Sheppard and Renna, 2010) and (3) HEC-18 method (Arneson *et al*., 2012), as presented in section 2.3.6. The last two and most recent methods were developed through quantifying the contribution of each structural pier component to the total scour depth, justifying that these two methods will be retained in the present analysis. The HEC-18 method calculates the total equilibrium scour depth by adding the scour depth assumed to be produced separately by each pier component, as illustrated in Figure 2.34, somehow adopting the superposition concept suggested earlier by Sheppard and Jones (1998). The FDOT method also adopts the superposition concept since the equilibrium scour depth is calculated at one hypothetically equivalent cylindrical pier whose diameter is the sum of the equivalent diameters of the column, the pile cap and the pile group, as shown in Figure 2.36. A key idea to be retained herein is that the HEC-18 and FDOT methods were developed on the basis of experiments performed on isolated components of the complex pier by authors such as Salim and Jones (1996), Sheppard and Jones (1998), Smith (1999) or Jones and Sheppard (2000a). Another important fact is that most of those experiments were of short duration and so do not provide an accurate basis for predicting equilibrium scour depths. More recently, Dey *et al*. (2008), Muto (2008) and Amini *et al.* (2011, 2012, 2014) carried out work on scour at complex piers exploiting the superposition concept, but their work also suffers from being based on experiments with rather short durations.

Local scour experiments performed for isolated components necessarily ignore the interactions and joint effects of the different components of the complex piers on the near-field flow structure, namely the most obvious: (1) the deflection of the downflow generated along the upstream face of the column by pile cap overhang (characterized by f_l and f_t, see Figure 2.21); (2) the interactions of the downflow generated by the upstream face of the pile cap and the vortical structures occurring around the piles; and (3) the interactions of the internal boundary layer created along the bottom face of the pile cap and those vortical structures. Such interactions depend on the position of the base of the column relative to the initial bed level, the pile-cap thickness, the longitudinal projection of the pile cap beyond the front of the pile group (see f_p in Figure 2.21), f_l and f_t lengths, and other geometrical pier characteristic dimensions. Considering the scour at a complex pier to be the sum of the scour at the individual components as if they were in isolation ignores the interaction between the constituent components and hence can lead to inaccurate predictions. Indeed, this is probably the reason why existing methods, based upon the superposition concept, do not properly predict the equilibrium scour depth, as stated by, *e.g*., Ataie-Ashtiani *et al*. (2010) or Ferraro *et al*. (2013).

Since the non-linear interaction between the different components seems to be an important issue, a new approach is attempted in this study to experimentally assess the contribution of each complex pier component to the total equilibrium scour depth. The basic idea behind this new approach can be illustrated with a particular case: for the same approach flow, bed sediment and pier geometry and alignment, the scour depth directly ascribable to the column can be unambiguously evaluated by subtracting the scour depth at an incomplete "pier", without the particular column, from the scour depth at the equivalent complete pier; it is reasonable to assume that, by putting back the column into the incomplete "pier", the scour depth would correspond again to the scour depth at the complete pier. The same applies to the other pier components. Accordingly, the scour depth at three different configurations, defined by three different combinations of complex pier components (see Figure 3.2), was experimentally obtained for each position of the base of the column relative to the initial bed level, as defined by H_c. Those were Configuration C1, corresponding to the complete pier, Configuration C2, without the column, and Configuration C3, without the pile group. Configurations C2 and C3 do not represent real complex piers; instead, they are experimental configurations used to calculate, through subtraction, the contribution of the missing complex pier component to the total scour depth, as follows:

$$d_{sec} = d_{seC1} - d_{seC2} \tag{6.1}$$

$$d_{sepg} = d_{seC1} - d_{seC3} \tag{6.2}$$

$$d_{sepc} = d_{seC1} - d_{sec} - d_{spg} \tag{6.3}$$

where d_{sec}, d_{sepc} and d_{sepg} are, respectively, the equilibrium scour depths associated with the column, the pile cap and the pile group; and d_{seC1}, d_{seC2} and d_{seC3} represent the equilibrium scour depths at Configurations C1, C2 and C3, respectively. From equations (6.1) to (6.3), it is clear that d_{sec} and d_{sepg} can be obtained directly subtracting experimental values, while d_{sepc} requires the previous knowledge of d_{sec} and d_{sepg}, as illustrated in Figure 6.1.

The subtraction approach has some physical limitations. In fact, tests with Configuration C2, *i.e.*, the complex pier without the column, cannot be performed when the top of the pile cap is below the initial bed level. For this reason, the contributions of the column and the pile cap to the local scour depth may only be obtained when the bottom of the column is above the initial bed level. It should, though, be noticed here that the experiments underlying the existing superposition methods also suffer from the same sort of physical limitations: experiments with completely buried isolated pile cap or pile group are also not feasible.

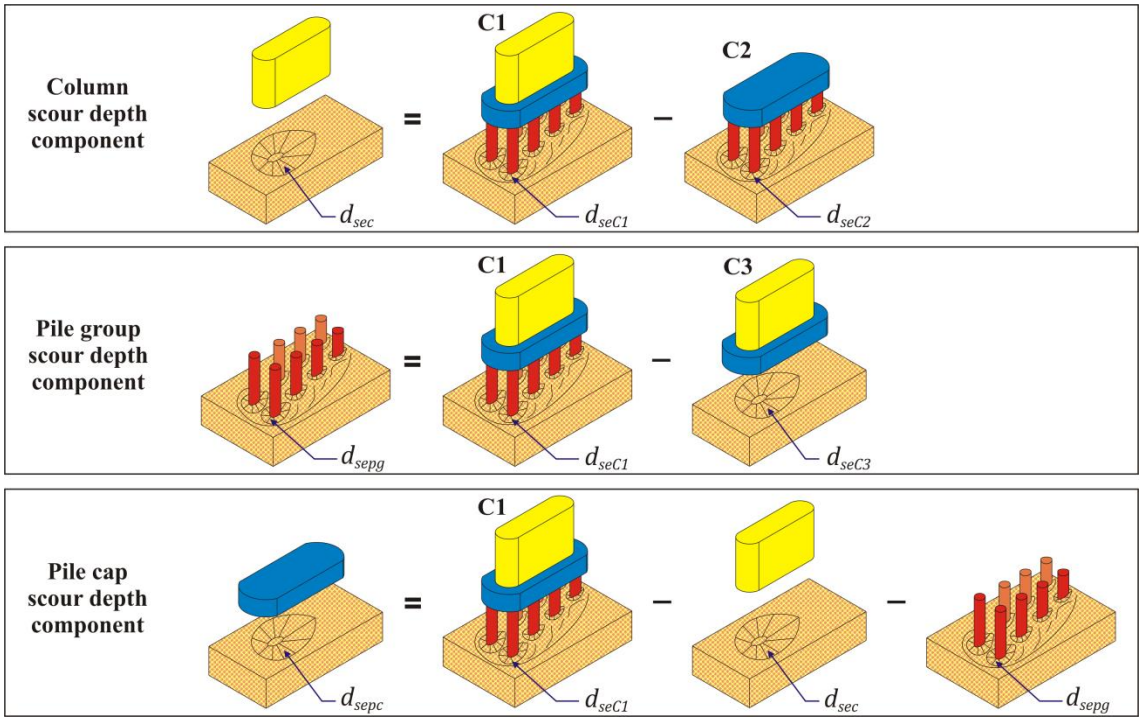

Figure 6.1 – Scheme of the subtraction approach (contribution of the complex pier components on scour depth)

In the present study, it is assumed that the scour depth associated to the column, d_{sec}, the pile group, d_{sepg}, and the pile cap, d_{sepc}, can be assessed by the following expressions included in or inspired by the HEC-18 method (Arneson *et al*., 2012):

$$d_{sec} = K_{hc} d_{secu} \tag{6.4}$$

$$d_{sepg} = K_{hpg} d_{sepgu} \tag{6.5}$$

$$d_{sepc} = K_{hpc} d_{sepcu} \tag{6.6}$$

Here, the factor K_{hc} accounts for the influence of the position of the base of the column, H_c (see Figure 2.21); d_{secu} is the equilibrium scour depth developed at a single pier with the same dimensions as the column; K_{hpg} is the factor accounting for the influence of the position of the top of the pile group, H_{pg} (see Figure 2.21); d_{sepgu} is the equilibrium scour depth developed at an unsubmerged pile group; K_{hpc} is the factor accounting for the influence of the position of the base of the pile cap, H_{pc} (see Figure 2.21); d_{sepcu} is the equilibrium scour depth developed at a single pier with the same dimensions as the pile cap.

A total of 70 tests performed in this study was used to: (1) describe the temporal evolution of the scour depth for Configurations C2 and C3 of the complex pier (section 6.3); (2) estimate the contribution of complex pier components on equilibrium scour depth according to the subtraction approach, by

calculating factors K_{hc}, K_{hpg} and K_{hpc} of equations (6.4) to (6.6) (section 6.4); (3) compare these factors with the corresponding factors obtained by means of tests with isolated components (section 6.5); and (4) compare these factors with the corresponding factors obtained on the basis of the methods based upon the superposition concept, *i.e.*, FDOT and HEC-18.

6.2. EXPERIMENTAL DATA PRESENTATION

From a total of seventy tests performed in this study with the purpose of analysing the contribution of the pier components, thirty-four correspond to Configuration C1 (presented and discussed in Chapter 5), fourteen correspond to Configuration C2 and twenty-two correspond to Configuration C3. Table 6.1 summarizes the relevant characteristic variables of the thirty-six tests performed for Configurations C2 and C3, namely: the relative column position, H_c/h, test duration, t_d, maximum scour depth measured at the end of the tests, d_{sm}, and equilibrium scour depth, d_{se}.

Table 6.1 – Relative column position, test duration, maximum and equilibrium scour depth values for tests with Configurations C2 and C3

Model	Pile-cap position	H_c/h	Configuration C2			Configuration C3		
			t_d (h)	d_{sm} (m)	d_{se} (m)	t_d (h)	d_{sm} (m)	d_{se} (m)
1	D	1.000	428.1	0.141	0.168	571.5	0.051	0.062
	E	0.667	480.4	0.130	0.154			
	F	0.333	458.4	0.105	0.130			
	H	0.050	571.2	0.015	0.035			
2	D	1.000	412.7	0.139	0.156	431.3	0.033	0.039
	E	0.667	431.0	0.122	0.144	478.5	0.071	0.086
	F	0.333	478.9	0.087	0.125	389.3	0.082	0.104
	H	0.050	571.2	0.015	0.035	481.6	0.153	0.172
3	D	1.000	412.7	0.139	0.156	431.3	0.033	0.039
	E	0.667	431.0	0.122	0.144	479.1	0.064	0.078
	F	0.333	478.9	0.087	0.125	526.6	0.085	0.100
	H	0.050	571.2	0.015	0.035	597.5	0.160	0.185
4	D	1.000	428.1	0.141	0.168	571.5	0.051	0.062
	E	0.667	480.4	0.130	0.154	413.6	0.062	0.083
	F	0.333	458.4	0.105	0.130	500.9	0.116	0.129
	G	0.185	481.7	0.083	0.109			
	H	0.050	571.2	0.015	0.035			
5	D	1.000	412.7	0.139	0.156	431.3	0.033	0.039
	E	0.667	431.0	0.122	0.144	480.5	0.051	0.063
	F	0.333	478.9	0.087	0.125	259.8	0.075	0.093
	G	0.185	413.6	0.059	0.078	458.7	0.138	0.156
	H	0.050	571.2	0.015	0.035	671.1	0.095	0.118

Table 6.1 (cont.) – Relative column position, test duration, maximum and equilibrium scour depth values for tests with Configurations C2 and C3

Model	Pile-cap position	H_c/h	Configuration C2			Configuration C3		
			t_d (h)	d_{sm} (m)	d_{se} (m)	t_d (h)	d_{sm} (m)	d_{se} (m)
6	D	1.000	405.8	0.126	0.144			
	E	0.667	259.6	0.104	0.126	501.2	0.040	0.043
	F	0.333	500.7	0.083	0.105	484.6	0.029	0.055
	G	0.185	501.0	0.073	0.100	411.7	0.067	0.125
	H	0.050	571.2	0.015	0.035			
7	N	1.000	166.5	0.135	0.141	288.0	0.000	0.002
	O	0.667	226.0	0.131	0.135	335.8	0.028	0.031
	P	0.320	243.0	0.153	0.158	219.3	0.096	0.119
	Q	0.160	246.2	0.094	0.119	149.0	0.163	0.178
	R	0.000				239.3	0.174	0.184
	S	−0.330				212.1	0.154	0.171

In accordance with the procedures described in section 5.2 (for tests with Configuration C1), the recorded experimental scour depth values of Configurations C2 and C3 were extrapolated to time infinite through equation (5.1) to estimate d_{se}.

Six of the thirty-five tests performed for Configuration C1 are used as reference for the evaluation of the subtraction approach. In four of those only the column was exposed to the flow during the scouring process, corresponding to the case where the top of the pile cap remains buried below the bottom of the scour hole: test M2L1 for Models 1 and 2 (Table 3.2), test M3L1 for Model 3 (Table 3.2), test M6L1 for Models 4 to 6 (Table 3.2) and test M7T1 for Model 7 (Table 3.5). In the two remaining reference tests, only the pile group was exposed to the flow during the scouring process, which corresponds to the case where the bottom of the pile cap is above and out of the water, *i.e.*, test M1A1 for Models 1 to 6 (Table 3.2) and test M7M1 for Model 7 (Table 3.5). The equilibrium scour depth values, d_{se}, obtained for the above mentioned six reference tests (values previously presented on Table 5.1 and Table 5.2) are summarized in Table 6.2 as reference for the analysis in this chapter.

Table 6.2 – Equilibrium scour depths of the reference tests

Test	d_{secu} (m)	Test	d_{secu} (m)	Test	d_{sepgu} (m)
M2L1	0.240	M6L1	0.178	M1A1	0.123
M3L1	0.218	M7T1	0.179	M7M1	0.139

6.3. TEMPORAL EVOLUTION OF THE SCOUR DEPTH (CONFIGURATIONS C2 AND C3)

The temporal evolution of the scour depth at Configuration C1 (*i.e.*, complete complex piers) was analysed and discussed in Chapter 4. In this section, a brief description of the scour depth time evolution in Configurations C2 and C3 is presented and tentatively justified. For this purpose, all the tests carried out with Model 3 are used to characterize the effect of the relative column position, H_c/h, on scour depth time evolution, as illustrated in Figure 6.2. In Configuration C2 (complex pier without

the column), a continuous increment in scour depth values with time evolution is identified from test M3H2 to the test M3D2, *i.e.*, with the increment of H_c/h, as shown in Figure 6.2(a). That is directly associated with the increment in the area exposed to the approach flow, which leads to the development of a larger vortex system and to a deeper scour hole. In test M3H2 (Figure 6.2(a)), the small value of the scour depth achieved is directly associated to a slow scouring rate as a result of a small obstruction area (a portion of the front pile cap face), whereas, in test M3D2 (Figure 6.2(a)), the higher value of the scour depth reached relates to the maximum obstruction of the flow due to the front faces of the (entire) pile cap and of the upstream piles. In Configuration C3 (complex pier without the pile group), a systematic decrease of the scouring rate is observed with the increment of H_c/h (from test M3H3 to test M3D3), as shown in Figure 6.2(b). This effect is mostly associated with the corresponding: (1) decrease of the obstruction area to the approach flow (*i.e.*, reduction of the area of the column exposed to the flow); (2) weakening of the strength of the downflow formed along the upstream face of the column/pile-cap set due to the interaction of that set with the main flow; and (3) attenuation of the influence of the boundary layer, generated below the bottom pile cap face, on the scour hole development. These physical explanations justify the delay in the beginning of the scour process and the low initial scour rate observed in tests M3D3 and M3E3, as shown in Figure 6.2(b). Similar results and relative variations of the temporal evolution of the scour depth with H_c/h for Configurations C2 and C3 as described for Model 3 (Figure 6.2) could be observed for the other six models.

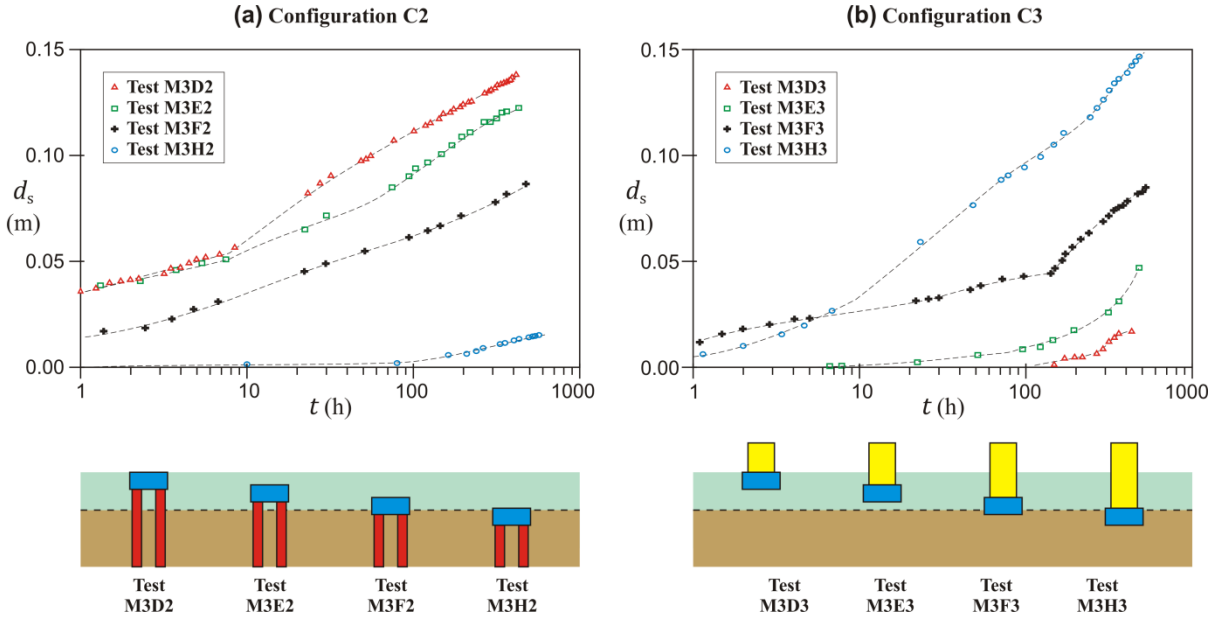

Figure 6.2 – Scour depth time evolution in tests with Model 3 for: (a) Configuration C2 and (b) Configuration C3

In order to compare the temporal evolution of the scour depth in the three configurations, six tests were selected, corresponding to two sets of three tests (each of those tests for a different configuration): one set corresponding to a model with two pile alignments (Model 4 in Position E, see Figure 3.4), the other set corresponding to a model with only one pile alignment (Model 7 in Position Q, see Figure 3.4). Figure 6.3(a) displays the scour depth time evolution and pictures the respective final scour hole at the end of the tests, for the corresponding three tests of Model 4. The scour depth time evolution for Configuration C2 (test M4E2) shows a trend similar to the respective evolution for Configuration C1 (test M4E1) since for this position the pile cap and the pile group are

the main components that contribute to the scour process. In Configuration C3 (test M4E3), the scour depth evolution is characterized by a slower scour rate during the first 200 hours followed by a higher scour rate associated to the main contribution of the pile cap, as shown in Figure 6.3(a). This trend is analogous to that observed in the test M3E3 analysed above in this section. The scour depth time evolution and the respective final scour hole in the three tests of Model 7 selected (Position Q) are presented in Figure 6.3(b). For this position, the scour depth evolution for Configuration C3 (test M7Q3) shows a trend relatively similar to the corresponding evolution for Configuration C1 (test M7Q1). This is due to the fact that in the mentioned position the column and the pile cap are now the main components contributing to the scour process. Furthermore, in this case (with only one pile alignment) the scour rate in Configuration C2 (test M7Q2) is almost half of that obtained for Configuration C1, which means that, for this position, the column considerably influences the scour process.

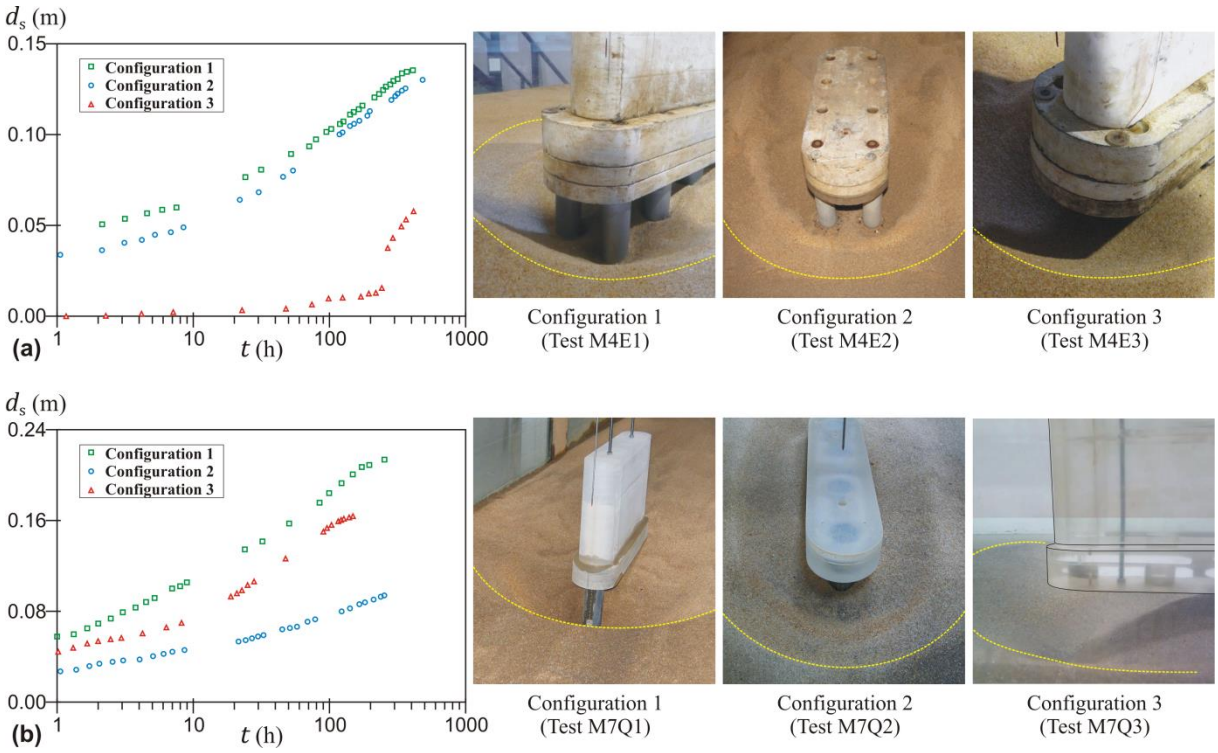

Figure 6.3 – Scour depth time evolution and final scour hole in Configurations C1, C2 and C3 for: (a) Model 4 (Position E) and (b) Model 7 (Position Q)

6.4. CONTRIBUTIONS OF COMPLEX PIER COMPONENTS TO THE EQUILIBRIUM SCOUR DEPTH BY A SUBTRACTION APPROACH

The experimental contributions of the column, pile group and pile cap on the total equilibrium scour depth were calculated through equations (6.1), (6.2) and (6.3), respectively, using the scour depth values reported in Table 5.1 and Table 5.2 for Configuration C1 and in Table 6.1 for Configurations C2 and C3. The relative position of the base of the column, H_c/h, the relative position of the base of the pile cap, H_{pc}/h (equal to the relative position of the top of the pile group, H_{pg}/h), and the

equilibrium scour depths associated to the column, d_{sec}, pile cap, d_{sepc}, and pile group, d_{sepg}, for all vertical positions of the piers' components are summarized in Table 6.3.

Table 6.3 – Equilibrium scour depths associated to each complex pier component

Model	Pile-cap position	$\frac{H_c}{h}$	$\frac{H_{pc}}{h} = \frac{H_{pg}}{h}$	Column d_{se} (m)	Pile cap d_{se} (m)	Pile group d_{se} (m)	Total d_{se} (m)
1	D	1.000	0.400	0.000	0.062	0.106	0.168
	E	0.665	0.065	0.039	-	-	0.193
	F	0.335	-0.265	0.069	-	-	0.199
	H	0.050	-0.550	0.183	-	-	0.218
2	D	1.000	0.550	0.000	0.039	0.117	0.156
	E	0.665	0.215	0.041	0.045	0.099	0.185
	F	0.335	-0.115	0.067	0.037	0.088	0.192
	H	0.050	-0.400	0.154	0.018	0.017	0.189
3	D	1.000	0.550	0.000	0.039	0.117	0.156
	E	0.665	0.215	0.031	0.047	0.097	0.175
	F	0.335	-0.115	0.052	0.048	0.077	0.177
	H	0.050	-0.400	0.140	0.045	-0.010	0.175
4	D	1.000	0.400	0.000	0.062	0.106	0.168
	E	0.665	0.065	0.019	0.064	0.090	0.173
	F	0.335	-0.265	0.030	0.099	0.031	0.160
	G	0.185	-0.415	0.092	-	-	0.201
	H	0.050	-0.550	0.149	-	-	0.184
5	D	1.000	0.550	0.000	0.039	0.117	0.156
	E	0.665	0.215	0.017	0.046	0.098	0.161
	F	0.335	-0.115	0.034	0.059	0.066	0.159
	G	0.185	-0.265	0.090	0.066	0.012	0.168
	H	0.050	-0.400	0.083	0.035	0.000	0.118
6	D	1.000	0.700	0.000			0.144
	E	0.665	0.365	0.015	0.028	0.098	0.141
	F	0.335	0.035	0.031	0.024	0.081	0.136
	G	0.185	-0.115	0.095	0.030	0.070	0.195
	H	0.050	-0.250	0.141	-	-	0.176
7	N	1.000	0.678	0.000	0.002	0.139	0.141
	O	0.667	0.345	0.015	0.016	0.119	0.150
	P	0.322	0.000	0.033	0.089	0.069	0.188
	Q	0.161	-0.161	0.111	0.067	0.052	0.230
	R	0.000	-0.322	-	-	0.004	0.188
	S	−0.333	-0.655	-	-	-0.003	0.168

The non-dimensional factors $K_{hc} = d_{sec}/d_{secu}$, $K_{hpc} = d_{sepc}/d_{sepcu}$ and $K_{hpg} = d_{sepg}/d_{sepgu}$ were calculated through the inversion of equations (6.4) to (6.6); the values of d_{sec}, d_{sepc} and d_{sepg} correspond to those reported in Table 6.3 while the values of d_{secu} and d_{sepgu} are those included in Table 6.2. The values of d_{sepcu} (referring to the pile cap) were obtained through the central predictor suggested by Lança *et al*. (2013b) by assuming the flow intensity factor (K_I) defined by Sheppard *et al*. (2014) and the shape factor (K_S) suggested by Fael *et al*. (2014). This way, d_{sepcu} was calculated as $d_{sepcu} = 0.262$ m for Models 1 to 6 and $d_{sepcu} = 0.214$ m for Model 7. It is assumed that the two flow intensity ratios used in this study, which were $U/U_c \approx 0.80$ for Models 1 to 6 and $U/U_c \approx 0.97$ for Model 7, do not influence the factors K_{hc}, K_{hpc} and K_{hpg} as each pair of the corresponding scour depths values, notably (d_{sec}; d_{secu}), (d_{sepc}; d_{sepcu}) and (d_{sepg}; d_{sepgu}), were measured under the same experimental conditions.

In this section, the contributions relative to the column, pile group and pile cap are presented in the same order as in Figure 6.1 (a, b and c, respectively). Figure 6.4 provides the values of factor K_{hc} as a function of the relative position of the base of the column, H_c/h. As mentioned in section 6.1, the column contribution could only be obtained when the top of the pile cap (base of the column) is above the initial bed level, *i.e.*, $H_c > 0$. In this range, H_c is normalized by the approach flow depth, h, to represent the column suspended in the flow. The figure highlights the systematic increase of K_{hc} as H_c/h decreases, reflecting the increment of the column frontal area exposed to the approach flow above the scour hole as submergence increases, *i.e.*, as H_c/h decreases. The increase of column submergence increases the strength of the associated downflow and vortical structures, leading to stronger scouring. Figure 6.4 reveals that K_{hc} also depends on the ratio of column width to pile-cap width, D_c/D_{pc}, a parameter that represents the shielding effect due to the pile-cap extension lengths (longitudinal and transversal distances of pile cap face out of the column face, f_l and f_t respectively): for the same relative position of the base of the column, higher values of factor K_{hc} were typically obtained for larger D_c/D_{pc} ratios. It should be stressed that the deflection of the downflow generated along the upstream face of the column by the pile cap overhang, interaction ignored in tests with isolated columns, is clearly represented by the influence of parameter D_c/D_{pc} on factor K_{hc}.

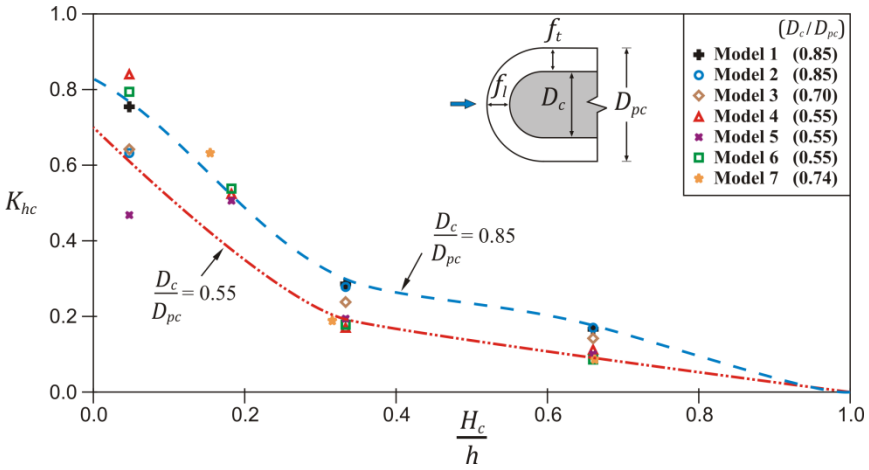

Figure 6.4 – Variation of factor K_{hc} with the relative position of the base of the column

Figure 6.5 shows the variation of K_{hpg} with the relative position of the top of the pile group, H_{pg}/h or (H_{pg}/D_{pc}). In the case where the top of the pile group is above the initial bed level ($H_{pg} \geq 0$), H_{pg} is normalized by the approach flow, h, to represent the pile group submergence in the flow, whereas, in

the case where the top of the pile group is below the initial bed level ($H_{pg} < 0$), H_{pg} is normalized by the pile-cap width, D_{pc}, since D_{pc} mostly embodies the influence of the pile cap on the exposition of the upstream piles to the flow within the scour hole. No data are available for Model 1 because Configuration C3 was not tested. Figure 6.5 shows the decrease of K_{hpg} as H_{pg}/h decreases, for $H_{pg} > 0$. This can be explained by the decrease of the flow obstruction resulting from the corresponding decrease of the frontal area of the upstream piles, which in turn leads to the reduction of the scour depth. The factor K_{hpg} also slightly depends on the relation f_p/D_p; the lower values of K_{hpg} correspond to the higher f_p/D_p ratios, observed in Model 7, where $f_p/D_p = 0.6$. This finding is consistent with the results of Lagasse *et al*. (2010) on scouring at debris-laden piles, according to which the scour depth at the pile face is strongly dependent on the upstream debris length in front of the pile face. The interactions of the downflow generated by the upstream face of the pile cap and the vortical structures occurring around the piles can be captured by the influence of f_p/D_p on the factor K_{hpg}. When the top of the pile group is below the initial bed level, *i.e*., for $H_{pg} < 0$, a similar trend is observed: K_{hpg} decreases as H_{pg}/D_{pc} decreases. In this range, corresponding to situations where the pile cap is partially or completely buried in the bed, the contribution of the pile group to scouring is highly dependent on the joint action of the column and the pile cap on the process. This joint action, captured by the ratio of column width to pile-cap width, D_c/D_{pc}, contributes to the exposition of the upstream piles to the flow inside the scour hole. As D_c/D_{pc} increases, the scour protection resulting from the collar effect inherent to the pile cap (effect due to pier collars used as bridge scour countermeasure) decreases and the scour depth tends to increase as well, as shown in Figure 6.5. The distance from the pile-cap bottom to the initial bed level at which the pile group contributes to the scouring process decreases with decreasing D_c/D_{pc}, as discussed in section 5.3.

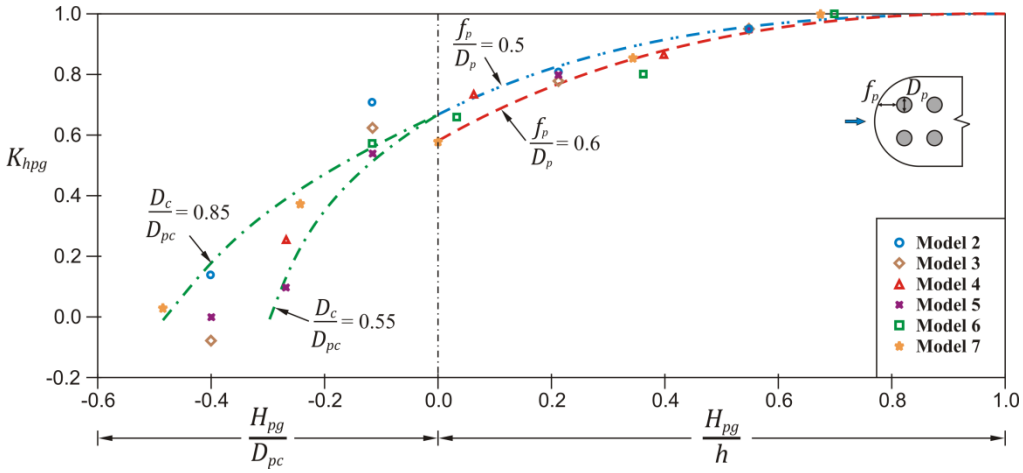

Figure 6.5 – Variation of factor K_{hpg} with the relative position of the top of the pile group

Figure 6.6 provides the variation of K_{hpc} with the relative position of the base of the pile cap, H_{pc}/h or (H_{pc}/T). In the case where the bottom of the pile cap is above the bed level ($H_{pc} \geq 0$), H_{pc} is normalized by the approach flow depth, h, to represent the pile cap suspension in the flow, whereas, in the case where the bottom of the pile cap is below the initial bed level ($H_{pc} < 0$), H_{pc} is normalized by the pile-cap thickness, T, since T defines the lower value of H_{pc} where the pile cap is completely buried in the bed. No data are available for $H_{pc}/T < -1$ due to physical limitation previously identified on the experimental exploitation of Configuration C2 (complex pier without the column). Again, no data on K_{hpc} exist for Model 1, since Configuration C3 was not tested for this model.

From Figure 6.6, it can be concluded that, when the pile cap is partially buried in the bed, *i.e.*, for $H_{pc}/T > -1$, K_{hpc} tends to increase with H_{pc}/T and, except for Model 2, K_{hpc} reaches a maximum in the range $-0.6 \leq H_{pc}/T \leq 0$. This trend can be ascribed to the pile cap protrusion from the undisturbed initial bed since the strength of the downflow generated in the upstream face of the pile cap, as well as of the associated vortical flow structure, increase with H_{pc}/T, leading to deeper scour holes. When the base of the pile cap is above the initial bed level, *i.e.*, for $H_{pc} > 0$, K_{hpc} tends to decrease with H_{pc}/h; this indicates that the effect of the flow structures associated with the pile cap tends to decrease as the pile cap is placed higher in the water column. In other words, the pile cap contributes most scouring when it is close to the initial bed level.

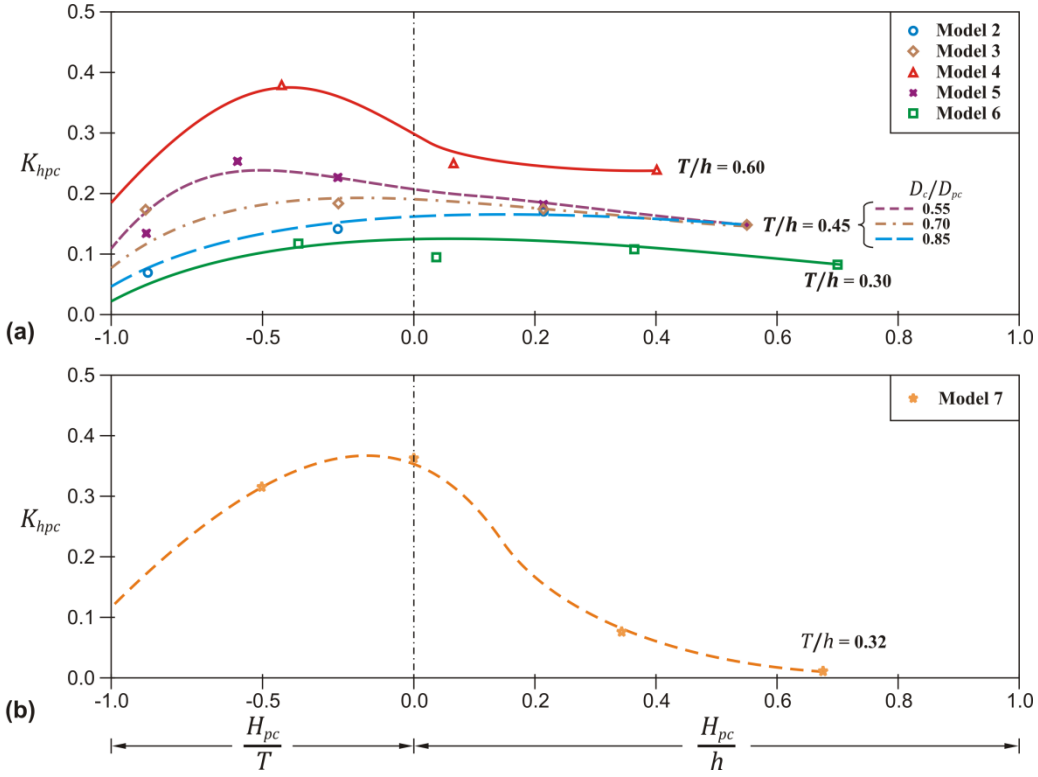

Figure 6.6 – Variation of factor K_{hpc} with the relative position of the base of the pile cap: (a) Models 1 to 6 and (b) Model 7

From the data on Models 2, 3 and 5 (all with $T/h = 0.45$), it can be concluded that the variation of K_{hpc} with the relative position of the base of the pile cap is also dependent of the relative column width, D_c/D_{pc}, as illustrated in Figure 6.6(a). Since Models 4 to 6 only differ in the pile-cap thickness, T, the scouring results at these models clearly indicate that T plays a key role on scouring: the equilibrium scour increases with T/h, corroborating the results of Ferraro *et al.* (2013). For essentially the same value of T/h, for example Model 6 ($T/h = 0.30$, Figure 6.6(a)) and Model 7 ($T/h = 0.32$, Figure 6.6(b)), different values of K_{hpc} arise as a result of different D_c/D_{pc} ratios as well as of different pile-group configurations (characterized by n and f_p, see Table 3.1). When the base of the pile cap is close to the initial bed level, either above or below, the greater contribution of the pile cap for Model 7, where $D_c/D_{pc} = 0.74$, can be explained by (1) the preservation of the downflow jet formed along the upstream face of the column, that is only negligibly affected by the reduced pile-cap overhang and (2) the different interaction of the internal boundary layer created along the surface of

the base of the pile cap with the vortical structures due to the piles. The boundary layer is differently disrupted by the two pile groups, influencing differently the flow acceleration otherwise created underneath the pile cap.

6.5. COMPARISON OF SUBTRACTION AND SUPERPOSITION APPROACHES

6.5.1 EXPERIMENTAL DATA FROM STUDIES WITH ISOLATED COMPONENTS

As previously mentioned, studies on local scouring at isolated components of complex piers were mostly carried out during the last decades with the purpose of characterizing the contribution of each complex pier component on the equilibrium scour depth, d_{se}, following the superposition concept (Sheppard and Jones, 1998). In order to compare the results of the previous section, relative to the contribution of the complex pier components on d_{se} obtained through subtraction (*i.e.*, factors K_{hc}, K_{hpg} and K_{hpc} represented in Figure 6.4 to Figure 6.6, respectively), experimental data from isolated components (superposition concept) were considered. Those included: (a) (Jones and Sheppard, 2000; Amini *et al.*, 2014) for isolated columns; (b) (Jones and Sheppard, 2000; Amini *et al.*, 2011) for isolated pile caps; and (c) (Salim and Jones, 1996; Smith, 1999; Dey *et al.*, 2008; Muto, 2008; Amini *et al.*, 2012) for isolated pile groups. Figure 6.7 shows the geometric characteristics of the three complex pier components.

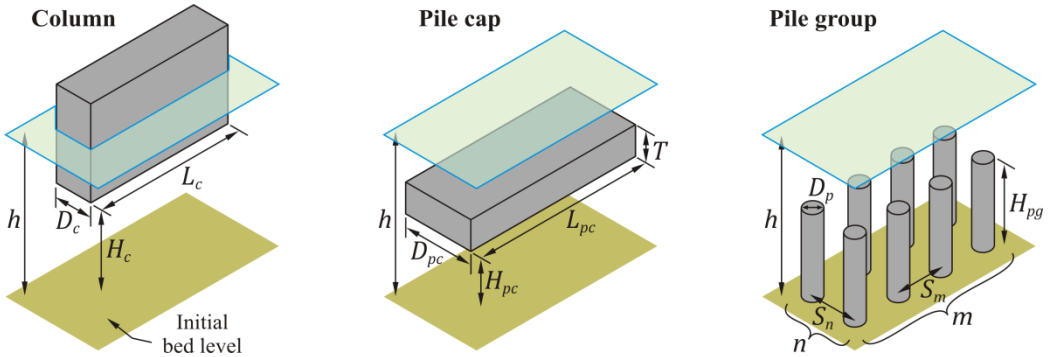

Figure 6.7 – Scheme of the geometry of complex pier components

The values of the most important control variables and non-dimensional parameters characterizing the set of tests with isolated components performed by those researchers are summarized in Table 6.4 for studies with isolated columns, in Table 6.5 for studies with isolated pile caps and in Table 6.6 for studies with isolated pile groups. Each isolated complex pier component model was evaluated for different positions in relation to the initial bed level (Figure 6.7), those referenced by: (1) H_c for isolated columns (distance from the initial bed level to the column bottom surface); (2) H_{pc} for isolated pile caps (distance from the initial bed level to the pile cap bottom surface); and (3) H_{pg} for submerged pile groups (distance from the initial bed level to the top of the pile group). For each model of isolated component the number of tests (each corresponding to one specific position of the component in relation to the initial bed level), the component shape and the test durations, t_d, are also included in Table 6.4, Table 6.5 and Table 6.6.

Table 6.4 – Characteristic control variables and non-dimensional parameters of studies on suspended columns

Study	Model	Shape	Number of tests	D_c (m)	$\frac{h}{D_c}$	$\frac{L_c}{D_c}$	$\frac{U}{U_c}$	$\frac{D_c}{d_{50}}$	t_d (h)
Jones and Sheppard (2000a)	JSc1	R	10	0.152	2.0	NS	≈0.94	152	>46
Amini *et al*. (2014)	Ac1	S	7	0.160	1.5	1.0	0.95	200	24[a]
	Ac2	R	6	0.110	2.2	2.4	0.95	138	24[a]
	Ac3	C	6	0.067	3.6	1.0	0.95	84	24[a]
	Ac4	R	6	0.030	8.0	2.3	0.95	38	24[a]
	Ac5	R	9	0.060	4.0	1.3	0.95	75	24[a]

Note: R = rectangular; S = square; C = circular; NS = not specified.

[a] most of the tests were carried out with durations of 8 hours; nevertheless scour depths were adjusted to a 24 hours duration taking into account that in each model a reference test with duration of 24 hours was performed

Table 6.5 – Characteristic control variables and non-dimensional parameters of studies on suspended pile caps

Study	Model	Shape	Number of tests	D_{pc} (m)	$\frac{h}{D_{pc}}$	$\frac{L_{pc}}{D_{pc}}$	$\frac{U}{U_c}$	$\frac{D_{pc}}{d_{50}}$	$\frac{T}{h}$	t_d (h)
Jones and Sheppard (2000a)	JSpc1	R	6	0.305	1.0	NS	≈0.94	305	0.10	>46
	JSpc2	R	7	0.305	1.0	NS	≈0.94	305	0.20	>46
	JSpc3	R	5	0.305	1.0	NS	≈0.94	305	0.30	>46
	JSpc4	R	6	0.305	1.0	NS	≈0.94	305	0.40	>46
	JSpc5	R	3	0.305	1.0	NS	≈0.94	1694	0.60	>46
	JSpc6	R	3	0.305	1.0	NS	0.92	1694	0.80	>46
Amini *et al*. (2011)	Apc1	S	9	0.200	1.2	1.0	0.95	250	0.13	24[a]
	Apc2	S	9	0.200	1.2	1.0	0.95	250	0.21	24[a]
	Apc3	R	8	0.150	1.6	2.0	0.95	188	0.13	24[a]
	Apc4	R	11	0.177	1.4	1.4	0.95	221	0.46	24[a]
	Apc5	R	10	0.175	1.4	2.1	0.95	219	0.25	24[a]
	Apc6	Ch	7	0.137	1.8	5.5	0.95	171	0.21	24[a]
	Apc7	R	7	0.077	3.1	1.6	0.95	96	0.15	24[a]
	Apc8	R	6	0.123	2.0	2.4	0.95	154	0.31	24[a]

Note: R = rectangular; S = square; C = circular; Ch = chamfered; NS = not specified.

[a] most of the tests were carried out with durations of 8 hours; nevertheless scour depths were adjusted to a 24 hours duration taking into account that in each model a reference test with duration of 24 hours was performed

Table 6.6 – Characteristic control variables and non-dimensional parameters of studies on submerged pile groups

Study	Model	Pile shape	Number of tests	D_p (m)	Array ($n \times m$)	$\frac{S_p}{D_p}$	$\frac{h}{D_p}$	$\frac{U}{U_c}$	$\frac{D_p}{d_{50}}$	t_d (h)
Salim and Jones (1996)	SJ1	S	6	NS	3 × 3	NS	NS	≈1.00	NS	4-24
Smith (1999)	Sm1	S	3	0.032	3 × 8	3.0	≈11.7	≈0.90	169-185	39-96
	Sm2	S	3	0.032	8 × 3	3.0	≈11.7	≈0.90	169-185	58-115
Dey *et al*. (2008)	Dey1	C	9	0.030	1 × 1	NA	8.3	≈0.90	10-37	48
	Dey2	C	9	0.060	1 × 1	NA	4.2	≈0.90	20-74	48
	Dey3	C	16	0.080	1 × 1	NA	3.1	≈0.90	27-99	48
Muto (2008)	Mu1	C	5	0.050	1 × 1	NA	≈1.2	≈0.95	35	NS
Amini *et al*. (2012)	Apg1	C	6	0.060	2 × 2	2.0	4.0	≈0.95	75	24[a]
	Apg2	C	7	0.042	2 × 4	2.0	5.7	≈0.96	53	24[a]
	Apg3	C	7	0.060	3 × 3	2.0	4.0	≈0.97	75	24[a]
	Apg4	C	6	0.042	4 × 4	1.9	5.7	≈0.96	53	24[a]
	Apg5	C	7	0.042	4 × 5	2.0	5.7	≈0.96	53	24[a]

Note: R = rectangular; S = square; C = circular; Ch = chamfered; NS = not specified; NA = not applicable.

[a] most of the tests were carried out with durations of 8 hours; nevertheless scour depths were adjusted to a 24 hours duration taking into account that in each model a reference test with duration of 24 hours was performed

In the calculation of factors $K_{hc} = d_{sec}/d_{secu}$, $K_{hpc} = d_{sepc}/d_{sepcu}$ and $K_{hpg} = d_{sepg}/d_{sepgu}$ for the experimental data with isolated components, the values of the variables d_{sec}, d_{sepc} and d_{sepg} correspond to the maximum scour depth measured in each of the tests performed for each of the isolated component geometries considered (Table 6.4, Table 6.5 and Table 6.6). For the case of pile groups (Table 6.6), the values of the variable d_{sepgu} correspond to the maximum scour depth measured in the tests with unsubmerged pile groups. For the other cases, the values of the variables d_{secu} and d_{sepcu} were obtained through the predictor suggested by Lança *et al*. (2013b) considering a flow intensity factor (K_I) as defined by Sheppard *et al*. (2014) and a shape factor (K_S) as defined by Fael *et al*. (2014). In the calculation of those values, the same geometric configuration of each component (*i.e*., width, length and shape), bed granulometry and flow conditions used in each set of tests were considered.

6.5.2 COMPARISON OF THE CONTRIBUTIONS OF COMPLEX PIER COMPONENTS FROM BOTH APPROACHES

Figure 6.8 refers to the values of the column factor, K_{hc}, obtained through both approaches. This figure is the equivalent to Figure 6.4, now extended to negative values of H_c. In this range, H_c is rendered non-dimensional through d_{secu}. The dashed line is the envelope curve of the literature data. The figure highlights the systematic increase of K_{hc} as H_c/h and H_c/d_{secu} decrease, reflecting the increment of the column frontal area exposed to the flow above or inside the scour hole as submergence increases. More importantly, Figure 6.8 shows that the data obtained in the present study tend to plot above the data from the literature, mostly for $0 < H_c/h < 0.2$. For $H_c/h > 0$, the smaller values of K_{hc} obtained from the data reported by Jones and Sheppard (2000) and Amini *et al*. (2014) can be partly attributed to the short duration of their tests. Independent of this effect, the values of K_{hc}

obtained through subtraction seem physically sounder, in particular, for the relative position of the base of the column $H_c/h = [0.05, 0.18]$. In fact, when the top of the pile cap or the column-bottom approach the initial bed, the scour depth induced by the pile cap as measured for Configuration C2 tends to be comparatively small (see tests M4F2, M4H2 and equivalent for different models). This implies that most of the scour depth at complete complex piers is mostly driven by the column when the top of the pile cap is near to the initial bed. It seems that the excavation power of the downflow, horseshoe vortex and wake vortices directly induced by the pile cap do not add much to the power of the equivalent flow structures created by the column in spite of the protecting collar effect mobilized by the top surface of the pile cap. This explanation deserves to be further investigated through detailed flow mapping.

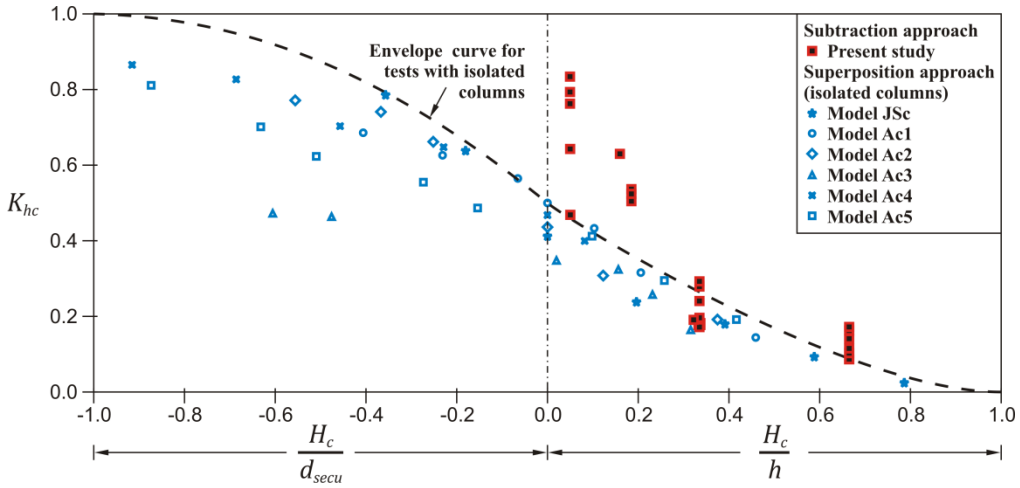

Figure 6.8 – Comparison of K_{hc} obtained through subtraction with K_{hc} obtained from tests with isolated columns

Figure 6.9 shows the values of factor K_{hpc} as a function of the relative position of the base of the pile cap, H_{pc}/h and H_{pc}/T. It compares the results of this study with those of Jones and Sheppard (2000) and Amini *et al.* (2011) for three ranges of the relative pile-cap thickness, T/h: (1) $0.30 \leq T/h \leq 0.32$ in Figure 6.9(a); (2) $0.40 \leq T/h \leq 0.46$ in Figure 6.9(b); and (3) $T/h = 0.60$ in Figure 6.9(c). The data of Jones and Sheppard (2000) cover the range $H_{pc} > 0$, whereas the data by Amini *et al.* (2011) cover practically the same range as the present study. With few exceptions, the present values of K_{hpc} are of the same order of magnitude and follow the same trend as those of Jones and Sheppard (2000), whereas higher values were obtained from the data reported by Amini *et al.* (2011). These discrepancies mostly likely result from the different relative flow depth, h/D_{pc}, values and range covered by the three studies: $h/D_{pc} = [2.0; 1.4]$ in the study of Amini *et al.* (2011), Figure 6.9(a) and Figure 6.9(b), respectively; $h/D_{pc} = 1.0$ in the study of Jones and Sheppard (2000); and $h/D_{pc} = [1.0; 1.5]$ in the present study, Models 1 to 6 and Model 7 respectively. It is worth noting that the maxima values of K_{hpc} are significantly smaller than the maxima K_{hpc}.

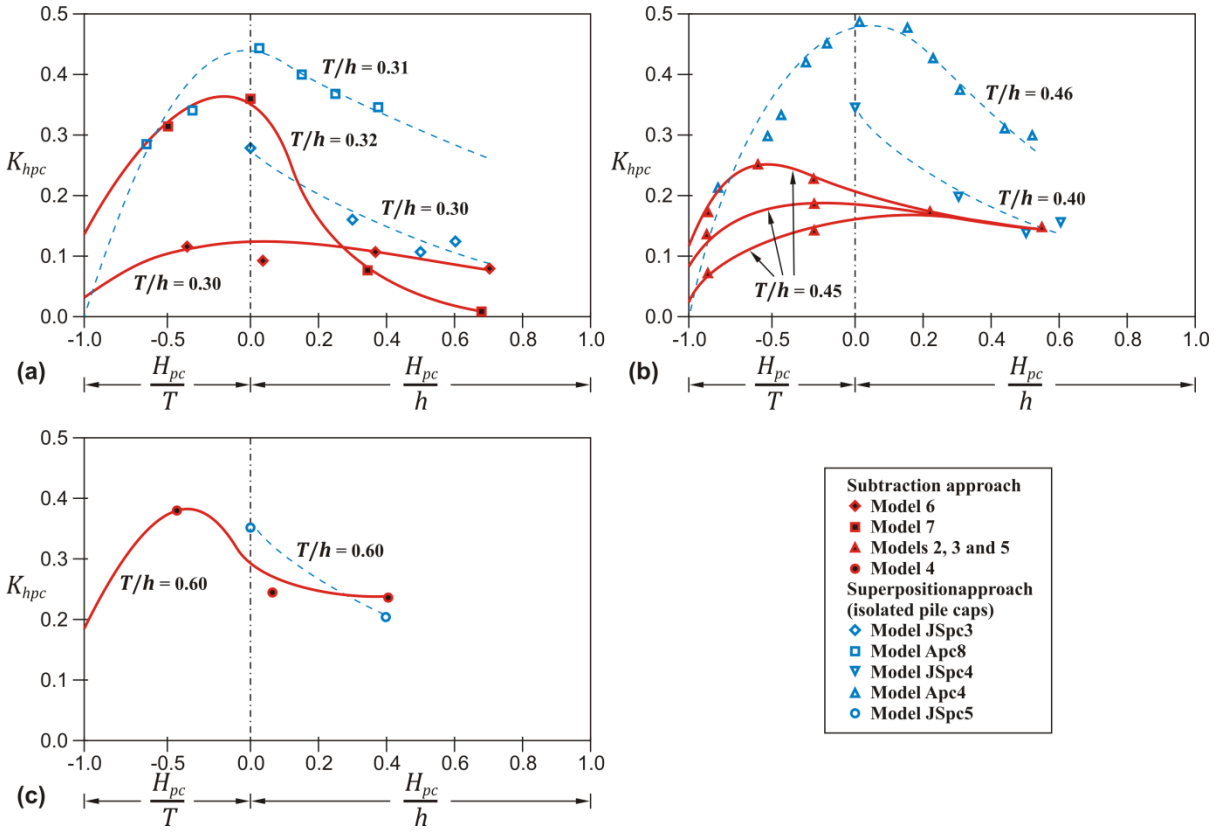

Figure 6.9 – Comparison of K_{hpc} obtained through subtraction with K_{hpc} obtained from tests with isolated pile caps: (a) $T/h \approx 0.30$, (b) $T/h \approx 0.45$ and (c) $T/h \approx 0.60$

The values of the factor K_{hpg} obtained through subtraction and from experimental data on isolated pile groups are plotted in Figure 6.10 as a function of the relative position of the top of the pile group, H_{pg}/h and H_{pg}/D_{pc}, the scaling length depending on whether $H_{pg} < 0$ or $H_{pg} > 0$, as before. The data gathered from the literature include those reported by Salim and Jones (1996), Smith (1999), Dey *et al*. (2008), Muto (2008) and Amini *et al*. (2012).

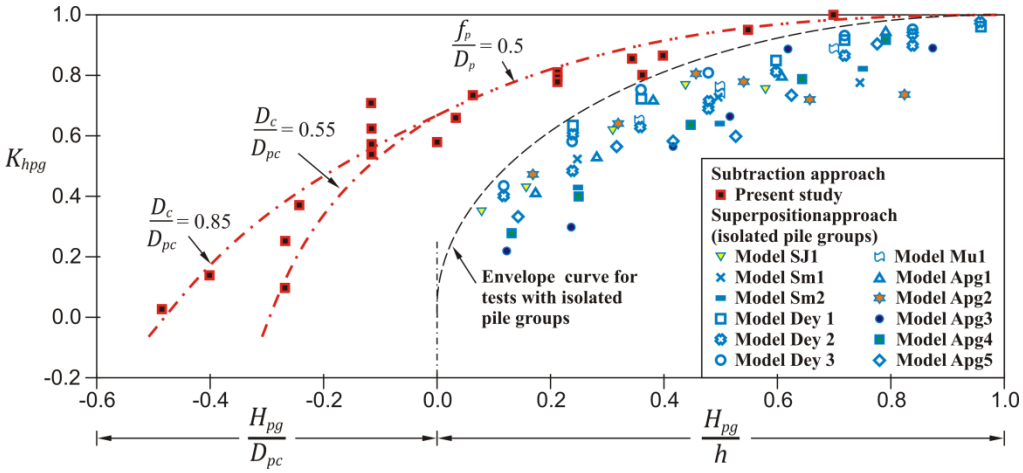

Figure 6.10 – Comparison of K_{hpg} obtained through subtraction with K_{hpg} obtained from tests with pile groups

These literature data are somewhat scattered, possibly due to different pile-group arrangements, to different time effects associated to different durations of the experiments as well as to different relative grain sizes, D_p/d_{50}, as reported in Table 6.6. To reduce uncertainty in the comparison, the literature data are enveloped by a dashed line in Figure 6.10. According to the figure, it can be concluded that the contribution of the pile groups obtained through the subtraction approach leads to values of K_{hpg} clearly larger than those obtained for isolated pile groups. It should be stressed here that the data obtained in this study seem physically more robust. Pile groups cannot trigger scouring when $H_{pg} < 0$ but this does not mean that they do not contribute to the process once they become exposed to the flow, as implied by the results of previous studies. On the contrary, pile groups contribute significantly to scouring even for $H_{pg} < 0$, and this behaviour is captured by the subtraction approach.

6.6. FURTHER DISCUSSION

The contributions of the complex pier components to the equilibrium scour depth discussed in section 6.4 were finally compared with the predictions of methods based on the superposition concept, *i.e.*, FDOT and HEC-18 methods. The comparison focused on the factors K_{hc}, K_{hpc} and K_{hpg}, as shown in Figure 6.11, where the same non-dimensional positions as in Figure 6.8 to Figure 6.10 were adopted. The results obtained for Model 5 are showed in Figure 6.11. From Figure 6.11(a) it can be concluded that the data on the column contribution practically coincide with the prediction curves produced through the FDOT and the HEC-18 methods. Figure 6.11(b) shows that the pile-cap contributions obtained in the present study follow a trend similar to the predictions obtained by means of FDOT and HEC-18 methods when the bottom of the pile cap is above the initial bed level, *i.e.*, for $H_{pc} > 0$. On the contrary, if the pile cap is partially buried in the bed, *i.e.*, for $H_{pc} < 0$, the results obtained through both predictors and the data of the present study are far apart, particularly for HEC-18. The significant overestimation of K_{hpc} by the HEC-18 method can be attributable to the fact that, in this situation ($H_{pc} < 0$), the method considers a pile cap foundation deeper than the expected scour depth (see section 2.3.6.2). Finally, the data on the contribution of the pile groups, as represented by K_{hpg}, follow the same trend as the results obtained through both FDOT and HEC-18 methods but the values are rather different, as shown in Figure 6.11(c). Indeed, the HEC-18 method tends to underestimate the values of K_{hpg} whereas the FDOT method produces conservative values of K_{hpg}. The behaviour of the HEC-18 method is directly associated to the fact that it was derived from the results of isolated pile groups by Salim and Jones (1996), and which are represented by equation (2.59). As mentioned previously, tests with submerged pile groups ignored the interactions of the downflow generated by the upstream face of the pile cap and the vortical structures occurring around the piles, reducing the local scour. The overestimation in the FDOT method can, in turn, be attributed to conservative values for the factor $h_{pg(\max)}$ (see equation (2.83)) used in the contribution of the pile group by Sheppard and Renna (2010). That factor accounts for a limiting water depth at which the flow influences the scouring process around the pile group. It should be mentioned here that none of the two predictors considers the influence of f_p/D_p on the pile-group contribution, while this effect was identified to be important in the present study. Similar results and relative variations of the three factors described in Figure 6.11 – for Model 5 – could be observed for the other six pier models tested in this study.

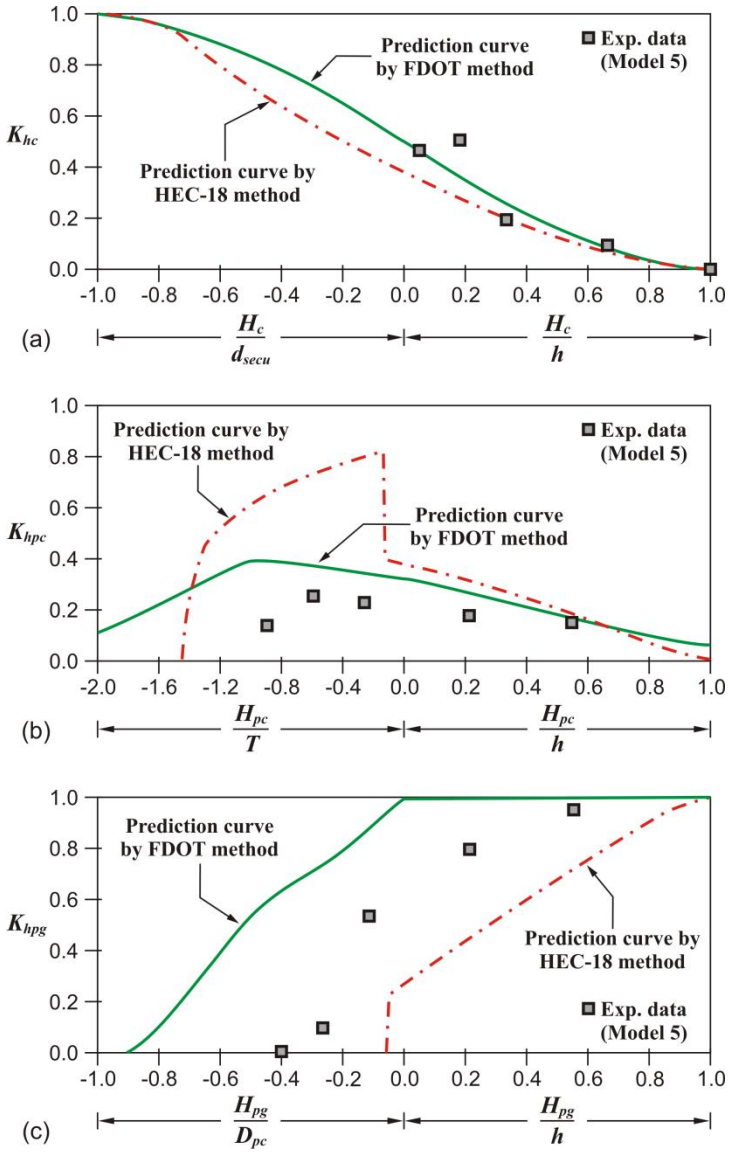

Figure 6.11 – Comparison of factors K_{hc} , K_{hpc} and K_{hpg} obtained by the subtraction concept with the corresponding values predicted by FDOT and HEC-18 methods: (a) variation of factor K_{hc}; (b) variation of factor K_{hpc}; and (c) variation of factor K_{hpg}

6.7. CONCLUSIONS

A new experimental approach to assess the contribution of each component of the complex pier (column, pile cap and pile group) to the total equilibrium local scour depth has been proposed in this chapter. This approach takes account the interactions of the different aspects of the flow field and their impact on the local scour depth since the experimental contribution of a given component is derived by subtracting the scour depth generated at a configuration without that component from the scour depth at the complete complex pier. The most important conclusions of this study can be summarized as follows:

1. The column contribution increases as the position of its base relative to the initial bed level, H_c/h, decreases; it also depends on the ratio of the column-width to the width of the pile cap, D_c/D_{pc}. The subtraction approach provides values of the column contribution larger than those obtained for isolated columns for small values of H_c/h;
2. The largest values of the pile-cap contribution were obtained for pile caps which were partially buried in the bed, where the subtraction approach provides smaller values than experiments with isolated pile caps. Similar to the column contribution, the pile-cap contribution also depends on the ratio D_c/D_{pc};
3. The most marked differences between the data obtained through subtraction and those measured at isolated pier components was identified for the pile groups, where the subtraction approach leads to significantly higher scour values. The pile-group contribution decreases with decreasing the position of its top relative to the initial bed level. When the top of the piles is above the initial bed level, this contribution also depends on the relation f_p/D_p, whereas, when the top of the piles is below the initial bed level, this contribution is highly dependent on D_c/D_{pc};
4. Both the HEC-18 and the FDOT methods seem to properly predict the contributions of the column and the pile cap to the overall scour when these pier components are suspended above the initial bed; both methods, however, over-predict the contribution of the scour depth induced by the pile cap, the over-prediction being particularly marked in the case of HEC-18; the FDOT method produces conservative scour depth values due to the pile group whereas the HEC-18 method tends to underestimate these values.

7. PREDICTION OF EQUILIBRIUM SCOUR DEPTH AROUND COMPLEX PIERS

7.1. INTRODUCTION

Local scour can lead to partial failure or to collapse of bridge piers and decks. The cost of large bridges, with common and/or special complex piers, justifies carrying out an accurate prediction of scour depth, for both economic and safety reasons, which in turn leads to the interest of hydraulic engineers in predicting the equilibrium scour depth, d_{se}. However, it is known that, despite the studies conducted in the past for pile-supported piers, the scour predictors do not reproduce adequately the measured values (*e.g.*, Ferraro *et al*., 2013). This derives from the fact that there are many factors influencing the phenomenon. As mentioned in section 2.1, presently, three methods to predict equilibrium scour depths at common complex piers can be considered as consolidated: the Auckland method (Coleman, 2005), the FDOT method (Sheppard and Renna, 2010) and the HEC-18 method (Arneson *et al*., 2012). According to Ettema *et al*. (2011), the scour depth at special complex piers, characterized by non-conventional column and pile-cap geometries, should be estimated by hydraulic-models and/or numerical models.

The aim of this chapter is to (1) evaluate the performance of the three mentioned methods using part of the tests performed in this study (section 7.2), (2) suggest a new scour predictor, aiming at improving the accuracy of the existing ones (section 7.3) and (3) validate the new predictor using experimental data published in the literature (section 7.4). Within the first objective, the equilibrium scour depths associated with the 48 tests performed with Configuration C1 (*i.e.*, complex pier with the three elements) and presented in section 5.2 are used to evaluate the performance of the three mentioned and most used predictors. Concerning the second objective, the results obtained in Chapters 5 and 6 were considered for the development of a new predictor.

7.2. APPLICABILITY OF AVAILABLE SCOUR DEPTH PREDICTORS

The performance of Auckland (Coleman, 2005), FDOT (Sheppard and Renna, 2010) and HEC-18 (Arneson *et al*., 2012) methods was assessed by comparing the methods' predictions of d_{se} for the present study's 48 tests conditions with the corresponding extrapolated values of the experimental measurements (henceforth referred to as observed equilibrium scour depths). Those extrapolated values correspond to the values summarized in Table 5.1 and Table 5.2. The application of the three predictors was performed as follows:

- In Situation 1 (pile cap above the initial bed level), the Auckland's method K_S factor was estimated by taking into account the pile-group shape. Similarly, the shape of the pile cap and

the shape of the column were used in Situation 2 (pile cap partially buried in the bed) and in Situation 3 (pile cap completely buried in the bed), respectively, and;

- The shape factor for circular piers, *i.e.*, $K_s = 1.0$, was used in the application of the FDOT method, for rounded-nose rectangular columns or pile caps, in accordance with Ferraro *et al*. (2013).

The comparison between observed d_{se} values and the corresponding d_{se} values predicted by the discussed methods is presented in Figure 7.1. The data were separated in three groups, each corresponding to one of the three situations considered (see Chapter 5). In accordance with Ferraro *et al*. (2013), the accuracy of the three methods can be evaluated by the number of results contained within two asymmetric bounds (+30% and −10% with respect to the perfect agreement straight line), *i.e.*, assuming a safety factor of 1.3 (overestimation of 30%) and an economy factor of 0.9 (underestimation of 10%), respectively. It is worth remember that over-prediction of scour depth may lead to excessive costs of the bridge while under-prediction may leads to bridge failure. The same bounds were included in the plots of Figure 7.1.

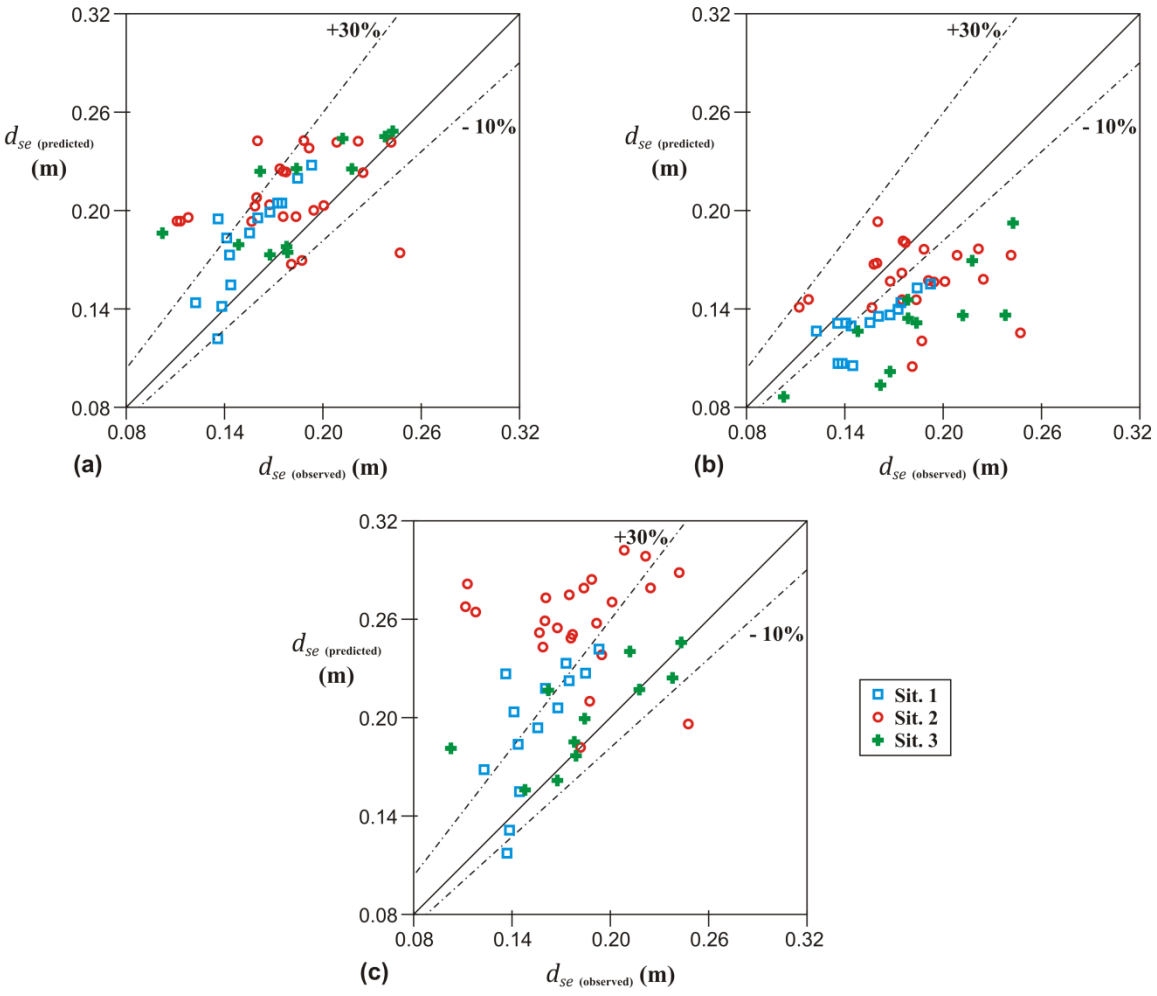

Figure 7.1 – Comparison of observed and predicted equilibrium scour depths, for the methods of: (a) Auckland, (b) HEC-18 and (c) FDOT

The results show that the Auckland method gives the most acceptable predictions of d_{se} for the seven models. In this method 77.1% of the predicted values (37/48) are within the boundaries, as shown in Figure 7.1(a). In general, the HEC-18 method gives underestimated values of d_{se} in the three situations analysed, as most values, in particular 42 out of 48, are below the perfect agreement straight line, as shown in Figure 7.1(b). Only 14 out of 48 predicted values (29.2%) could fit within the boundaries. The FDOT method provides conservative values of d_{se}, the most evident discrepancy being observed in Situation 2, with values above the diagonal and over the upper boundary limit, as shown in Figure 7.1(c). Overall (*i.e.*, for the three situations), 43.8% of the values predicted by this method (21 out of 48) are within the boundaries, with underestimated predictions for only five tests. These results are consistent with those of Ferraro *et al*. (2013).

The explanations for the deviations between observed and predicted equilibrium scour depth values, as shown in Figure 7.1, are several and difficult to isolate in each case. Still it can be advanced that:

- In relation to the HEC-18 method (Arneson *et al*., 2012): (a) not all the local scour mechanisms are accounted for in the factors of equation (2.31), as discussed by Sheppard *et al*. (2011); (b) in accordance with Lança *et al*. (2013a), the method uses inappropriate expressions to calculate the factors to account for the pile spacing, K_{sp}, and the number of piles in line with the flow, K_m, which are required to estimate D_{epg} (see equation (2.60)); and (c) when the pile cap is partially buried in the bed (Situation 2), the method considers that the pile group does not contribute to the scour process (*i.e.*, $d_{sepg} = 0$); however, in most tests performed in the present study for this situation, the pile group was exposed in the scour hole.
- Concerning the Auckland method (Coleman, 2005): (a) the predictor considers that d_{se} is not influenced by the relative sediment size when $D_e/d_{50} > 50$; in fact, recent studies on scouring at single piers show that d_{se} decreases with the increase in D_e/d_{50}, for $D_e/d_{50} > 100$ (see Figure 2.10), condition that occurred in 39 of the 48 tests; (b) factors K_{sp} and K_m used to calculate D_{epg} in the HEC-18 method are also used in this predictor; and (c) for some pile-cap positions in Situation 3, the predictor disregards the potential reduction in the scour depth attributable to the presence of the pile cap in the scour hole.
- Finally, regarding the FDOT method (Sheppard and Renna, 2010), in Situation 2, and for most H_c/h values in Situation 3, in which the top of the pile group is below the initial bed level, the predictor overestimates the values of D_{epg}. This occurs because the method adopts conservative values of factor K_{hpg} in equation (2.82).

7.3. PROPOSAL OF A REVISED PREDICTOR

According to the results presented in the previous section, the three discussed methods do not properly reproduce the scour measurements. The methods based on the assumption of an equivalent diameter of the complex pier, D_e (*i.e.*, Auckland and FDOT) showed the best performance. Therefore, taking into account the analysis performed on that same section, better estimates of the equilibrium scour depth, d_{se}, would require the introduction of some adjustments to their equations. In this regard, a new formulation is suggested to estimate d_{se} at complex piers aligned with the approach flow under clear-water conditions ($0.4 \leq U/U_c \leq 1.0$).

The proposed predictor is based on the assumption that d_{se} may be calculated using an equation fitted to single piers but using an equivalent diameter D_e of the complex pier, as in Auckland and FDOT methods. Since the effects of flow intensity, sediment grading, sediment coarseness and flow

shallowness on the equilibrium scour depth have been extensively studied for single piers (cylindrical shape mostly), the evaluation of scour depth at complex piers is centred in the estimation of the equivalent pier diameter, D_e. In this regard, the corresponding D_e definition shall take into account the different influences of pier geometry on the flow structure and the respective scouring process (in particular, relative pile-cap position, relative column width, and relative pile-cap thickness, among others). This definition is the frame of the equations developed for the suggested predictor, presented below.

In the proposed formulation, the equations suggested by Sheppard *et al*. (2014) and Lança *et al*. (2013b) to predict d_{se} at single piers were integrated and adjusted to the case of complex piers, in which the single cylindrical pier diameter of the original expressions was replaced by the equivalent diameter of the complex pier, thus

$$\frac{d_{se}}{D_e} = 2.6 K_I K_{hDe} K_d \tag{7.1}$$

with

$$K_I = 1.0 - 1.2 \left[ln\left(\frac{U}{U_c}\right)\right]^2 \tag{7.2}$$

$$K_{hDe} = \tanh\left[\left(1.3\frac{h}{D_e}\right)^{0.7}\right] \tag{7.3}$$

$$K_d = \begin{cases} 1 & \text{for} \quad 50 \le D_e/d_{50} \le 100 \\ 0.2 + \dfrac{3.5}{(D_e/d_{50})^{0.32}} & \text{for} \quad D_e/d_{50} > 100 \end{cases} \tag{7.4}$$

The conceptual variation in the equilibrium scour depth, d_{se}, with the column position, H_c, is illustrated in Figure 7.2(a). This representation is based on the corresponding variation observed in the seven models of the present study (see Figure 5.1, Figure 5.5 and Figure 5.6) and in those published in other studies (see Figure 2.28). According to this conceptual variation (Figure 7.2(a)), the d_{se} behaviour changes markedly when the top of the pile cap (H_c): (1) is positioned at $h + T$ (Situation 1), which corresponds to the limit position at which the scour process is still only associated to the pile group; (2) is positioned at H_x (Situation 2), which corresponds to the position at which the maximum scour depth occurs; (3) is positioned at H_b (Situation 3), which corresponds to the position (below the initial bed level) at which the minimum scour depth occurs; and (4) remains below the base of the scour hole (Situation 3), which corresponds to the limit position at which the scour process is only associated to the column. In the latter case, H_c is equal to d_{secu} (equilibrium scour depth for an uniform single pier with the same geometrical definition as the complex pier column), *i.e.*, d_{se} is calculated by equation (7.1), with $D_e = K_{sc} D_c$ where K_{sc} is the column shape factor and D_c is the column width.

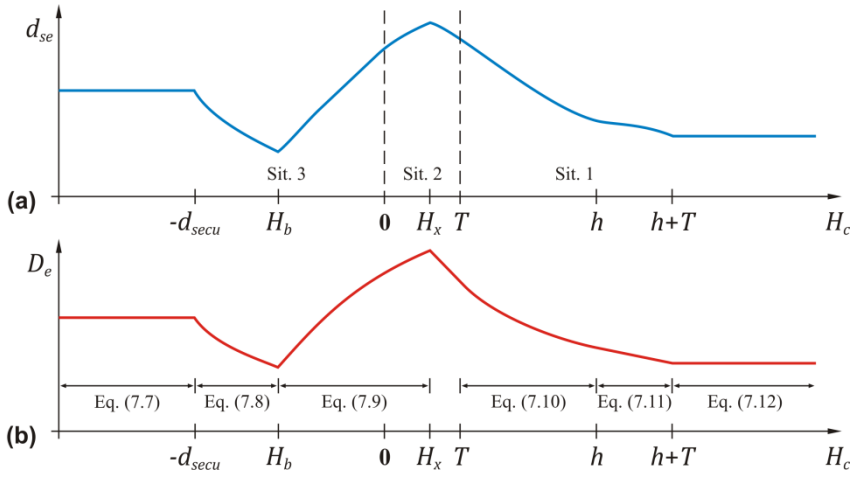

Figure 7.2 – Conceptual variation of: (a) d_{se} with H_c and (b) D_e with H_c

In section 5.6.3, equation (5.2) was suggested to estimate the relation H_x/T, which is rewritten below in terms of H_x, thus

$$H_x = \begin{cases} 0 & \text{for } \dfrac{D_c}{D_{pc}} > 0.65 \\ \dfrac{T\left[0.9 + 0.1\left(\dfrac{f_l}{f_t}\right)^{0.4}\right]\left[0.84 - 3.1\left(\dfrac{D_c}{D_{pc}}\right)^{3.1}\right]}{K_{spc}\left[\tanh\left(\dfrac{h}{D_{pc}}\dfrac{1}{\sqrt{D_c/D_{pc}}}\right)\right]^{0.2}} & \text{for } 0.15 \le \dfrac{D_c}{D_{pc}} \le 0.65 \end{cases} \tag{7.5}$$

As well as in equation (5.2), K_{spc} is the pile-cap shape factor where a value of 1.04 is adopted for rectangular shapes and a value of 1.00 for circular or round-nose rectangular shapes.

Taking into account the results of the present study in Situation 3 (see Figure 5.1, Figure 5.5 and Figure 5.6) and the experimental results on scouring at: (1) complex piers (Coleman, 2005; Ataie-Ashtiani *et al*., 2010; Ferraro *et al*., 2013); and (2) piers founded on caissons (Melville and Raudkivi, 1996; Umeda *et al*., 2010; Lu *et al*., 2011), the following expression was deduced to calculate the top of the pile-cap position H_b at which the minimum scour depth shall occur

$$H_b = \begin{cases} 0 & \text{for } \dfrac{D_c}{D_{pc}} < \dfrac{1}{7} \\ 7.8\left[\left(\dfrac{D_c}{D_{pc}} - \dfrac{1}{7}\right)^{0.91} - 0.98\left(\dfrac{D_c}{D_{pc}} - \dfrac{1}{7}\right)^{0.79}\right] d_{secu} & \text{for } \dfrac{D_c}{D_{pc}} \ge \dfrac{1}{7} \end{cases} \tag{7.6}$$

According to results of the present study, d_{se} varies not only with H_c as outlined in Figure 7.2(a), but also with the relative column width, D_c/D_{pc}, the relative pile-cap thickness, T/h, and the pile-group configuration (expressed by the equivalent width of the pile group, D_{epg}). In accordance with Coleman (2005), the variation in D_e with H_c can be represented by the scheme illustrated in Figure 7.2(b). It is assumed that these variations can be clearly defined for six different ranges of H_c (Figure 7.2(b)): $H_c \le -d_{secu}$; $-d_{secu} < H_c \le H_b$; $H_b < H_c \le H_x$; $H_x < H_c \le h$; $h < H_c \le h + T$, and;

$H_c > h + T$. In these ranges D_e can be estimated by expressions taking into account the discussed relationships (H_c, D_c/D_{pc}, T/h, D_{epg}) and also the width and shape of both the column and the pile cap. These expressions were derived by taking into account mainly the results of the present study (Chapters 5 and 6) and some experimental data available in the literature about scouring at complex piers and other specific pier foundations (Table 7.1). The scouring results for those specific pier foundations (*e.g.*, pile groups, piers founded on caissons, piers with debris raft) can be comparable to the corresponding results at particular pile cap positions of the complex pier.

Table 7.1 – Control variables and non-dimensional parameters for specific pier foundations' studies

Study	Total tests used	U/U_c	D_c/D_{pc}	T/h	h/D_{pc}	t_d (day)
Melville and Dongol (1992)	8	1.00	–	0.09–0.95	1.39–2.91	6.0
Melville and Raudkivi (1996)	6	1.00	0.31–0.82	–	2.47–3.64	1.0
Coleman (2005)	4	0.83–0.85	0.25, 0.53	0.10, 0.24	1.72–5.00	NS
Ataie-Ashtiani *et al*. (2010)	4	0.75–0.81	0.24, 0.47	0.21, 0.28	1.67	1.4–2.3
Umeda *et al*. (2010)	1	0.90	0.60	–	2.94	4.1
Lu *et al*. (2011)	1	0.90	0.71	–	2.91	2.3
Ferraro *et al*. (2013)	2	0.90	0.33	0.50	0.67	11.1–17.1

Note: NS = not specified.

The inversion of equation (7.1) enabled a back calculation of D_e values using the d_{se} values obtained experimentally (from both the present and the literature studies mentioned in this section). Following this procedure, the values of D_e were adjusted by regression taking into account the contribution of each component (column, pile cap and pile group) and the following equations were obtained:

$$D_e = K_{sc} D_c \quad \text{for} \quad H_c \leq -d_{secu} \tag{7.7}$$

$$D_e = K_{sc} D_c \left[1 + \left(\frac{H_c + d_{secu}}{H_b + d_{secu}} \right)^{1.4} \left(1.1 \left(\frac{D_c}{D_{pc}} - \frac{1}{7} \right)^{0.65} - 1 \right) \right] \quad \text{for} \quad -d_{secu} < H_c \leq H_b \tag{7.8}$$

$$D_e = \begin{cases} K_{sc} D_c \left[1.1 \left(\frac{D_c}{D_{pc}} - \frac{1}{7} \right)^{0.65} \right] + D_{epg} K_A + \\ K_{spc} D_{pc} \tanh\left(1.8 \frac{T}{D_c} \right) \sqrt{1 - \frac{H_c}{H_b}} \left[\left(\frac{D_c}{D_{pc}} - \frac{1}{7} \right)^{0.4} - \left(\frac{D_c}{D_{pc}} \right)^{1.3} \right] \end{cases} \quad \text{for } H_b < H_c \leq H_x \tag{7.9}$$

$$D_e = \begin{cases} K_{sc}D_c\left[\frac{3}{4}\left(1-\frac{H_c}{h}\right)^2\sqrt{\frac{D_c}{D_{pc}}}\right] + \\ K_{spc}D_{pc}\left[\left(\frac{9}{14}-\frac{9}{15}\tanh\left(\frac{f_p}{D_p}\right)\right)\left(\left(\frac{T}{h}\right)^{1.2}+\left(\frac{T}{h}\right)^{4.5}\right)e^{\left(-2.2\frac{H_c}{h}\right)}\right] \\ +D_{epg}\left[1-\frac{1}{9}\left(3+\sqrt{\frac{f_p}{D_p}}\right)\left(1-\frac{H_c-T}{h}\right)^{2.3}\right] \end{cases} \quad \text{for } T < H_c \le h \tag{7.10}$$

$$D_e = \begin{cases} K_{spc}D_{pc}\left[\left(\frac{1}{4}-\frac{1}{15}\tanh\left(\frac{f_p}{D_p}\right)\right)\left(\left(\frac{T_*}{h}\right)^{1.2}+\left(\frac{T_*}{h}\right)^{4.5}\right)\right] \\ +D_{epg}\left[1-\frac{1}{9}\left(3+\sqrt{\frac{f_p}{D_p}}\right)\left(\frac{T_*}{h}\right)^{2.3}\right] \end{cases} \quad \text{for } h < H_c \le h+T \tag{7.11}$$

$$D_e = D_{epg} \quad \text{for} \quad H_c \ge h+T \tag{7.12}$$

where K_{sc} = column shape factor; K_{spc} = pile-cap shape factor; K_A = pile group factor; f_p = longitudinal extension length of the pile cap out from the upstream pile front, as outlined in Figure 7.3; $T_* = h-(H_c-T)$ = submerged pile-cap thickness (distance from the bottom of the pile cap to the flow surface). Factor K_A is given by

$$K_A = \frac{2}{3}-\frac{1}{9}\sqrt{\frac{f_p}{D_p}}+\frac{4}{5}\left(\frac{D_c}{D_{pc}}\right)^{-0.7}\left[\frac{H_c-T}{D_{pc}}\right] \tag{7.13}$$

with a minimum for K_A = 0.

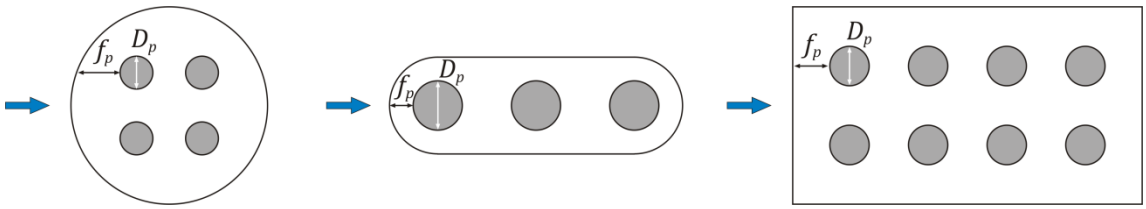

Figure 7.3 – Longitudinal extension length of the pile cap out from the upstream piles front

According to results of Figure 2.14, the column shape factor, K_{sc}, of equations (7.7) to (7.10) can be estimated as

$$K_{sc} = \begin{cases} 1.0 & \text{for cylindrical shapes} \\ 1.2-0.12\tanh\left(\frac{L_c}{D_c}-1\right) & \text{for rectangular square-nose shapes} \\ 1.0-0.17\tanh\left(\frac{L_c}{D_c}-1\right) & \text{for rectangular round-nose shapes} \end{cases} \tag{7.14}$$

where L_c = column length. The pile-cap shape factor, K_{spc}, of equations (7.9) to (7.11) can be estimated by equation (7.14) using L_{pc} and D_{pc} instead of L_c and D_c, respectively, where L_{pc} = pile cap length. The expressions included in equation (7.14) are valid for piers aligned with the approach flow and $L_c/D_c > 1$.

For $H_c \leq -d_{secu}$, in which the top of the pile cap remains buried below the base of the scour hole, equation (7.7) is considered appropriate because only the column is exposed to the flow. When the pile cap is completely buried in the initial bed level and the scour hole no more exposes completely the front face of the pile cap ($-d_{secu} < H_c \leq H_b$), which may be attributable to the physical interference of the top of the pile cap on the scour hole development process, equation (7.8) is suggested. In fact, the experimental results of this study and the studies of Melville and Raudkivi (1996), Ataie-Ashtiani *et al*. (2010), Umeda *et al*. (2010) and Lu *et al*. (2011) were used to derive this equation, which takes into account the decrease in the equivalent diameter from $H_c \leq -d_{secu}$ to $H_c = H_b$. For $H_b < H_c \leq H_x$, which is characterized by the fact that most of the scour process is associated to the column and the pile cap, equation (7.9) is proposed by taking into account: (1) the equivalent diameter D_e at position $H_c = H_b$ calculated in equation (7.8); (2) the maximum scour depth and the corresponding D_e, observed in each complex pier model tested in this study and in those reported in the literature (see section 5.6.3); and (3) the reduction in the pile group contribution to the scour process with decreasing H_c, which is represented by factor K_A through equation (7.13). For $H_x < H_c \leq T$, in which the pile cap is partially buried in the initial bed level, the combined use of equations (7.9) and (7.10), with a linear transition, is suggested. In Situation 1, in which the three elements of the complex pier are exposed to the flow ($T < H_c \leq h$), the use of equation (7.10) is suggested. This equation was based on the results of section 6.4, concerning the pile group contribution to the scour process (see Figure 6.5). This equation also included the effect of the pile cap extension relatively to the front of the upstream piles and which is represented by f_p/D_p (Figure 7.3). For $h < H_c \leq h + T$, in which the pile cap is partially immersed in water, equation (7.11) represents an improvement in the equation suggested by Melville and Dongol (1992), which was adopted in the Auckland method, *i.e*., equation (2.42). In the derivation of equation (7.11) the experimental data of the present study for the column position $H_c = h$ was used, together with the results of the studies performed by Melville and Dongol (1992), Coleman (2005) and Ferraro *et al*. (2013). For $H_c > h + T$, in which the pile cap is out of the flow, equation (7.12) is appropriate, as only the pile group is exposed to the flow. In pile groups aligned with the approach flow, the variable D_{epg} can be estimated by

$$D_{epg} = nD_pK_{spg}K_{spn}K_{spm} \tag{7.15}$$

where K_{spg} = factor to account for the shape of the piles (1.2 for square shapes and 1.0 for circular shapes); K_{spn} = factor to account for the pile spacing width; K_{spm} = factor to account for the pile spacing length. The experimental data obtained by Lança *et al*. (2013a) – corresponding to six pile group configurations defined by $\{n \times m$ = [1×4, 2×4, 3×4, 4×1, 4×2, 4×3]; n = number of alignments; m = number of piles in line with the flow} for different normalized pile spacing, *i.e*., $S_n/D_p = S_m/D_p$ = [1, 2, 3, 4.5, 6] (S_n = pile spacing width; S_m = pile spacing length) – were used to estimate factors K_{spn} and K_{spm}. The inversion of equation (7.1) enabled a back calculation of the values of D_{epg} corresponding to the extrapolated d_{se} values, which are used in equation (7.15) for calculating these two factors. The following two expressions may be used to estimate factors K_{spn} and K_{spm}

$$K_{spn} = 1 - \left(1 - \frac{1}{n}\right) \tanh\left[\left(\frac{S_n}{D_p} - 1\right)^{0.5}\right] \tag{7.16}$$

$$K_{spm} = 1 + \frac{(m-1)^{0.14}}{12.5}\left(\frac{S_m}{D_p} + \frac{m^{1.4}}{6.5}\right)^2 e^{\left(-0.65\frac{S_m}{D_p}\right)} \tag{7.17}$$

If $m > 6$, the value of $m = 6$ should be used in equation (7.17).

7.4. VALIDATION OF THE PROPOSED PREDICTOR

As mentioned in section 2.3.5.1, five studies were identified in the literature, which contained experimental data on scouring at complex piers, under clear-water conditions. From those studies, only tests by Grimaldi and Cardoso (2010) (Model GC, Table 2.2) and Ferraro *et al*. (2013) (Models Fe1 and Fe2, Table 2.2) were reported for long-durations, *i.e*., longer than 7 days, which enables a good estimation of equilibrium scour depth, d_{se}, by extrapolation of scour depth records to infinite (see section 2.3.4). Given that the scour-depth data reported by Grimaldi and Cardoso (2010) and Ferraro *et al*. (2013) were not extrapolated (*i.e*., these studies reported the scour depth measured at the end of the tests), the scour-depth records of those studies were used to calculate d_{se} values by extrapolation similarly to the procedure used for the present study tests (see section 5.2). The experimental data obtained in these two studies above were considered in addition to the data obtained in the present study to validate the suggested predictor.

In the studies selected from literature, all tests were performed with complex pier models aligned with the approach flow under clear-water conditions. Table 2.2 summarizes the flow and sediment characteristics of the corresponding pier models while Figure 2.27 shows the piers' dimensions. In the case of Model Fe2, other than the eleven tests published, two additional tests were considered in the analysis, both having been performed on the relative column positions H_c/h = [0.33, –0.25]. These two tests were carried out by one of the discussed paper authors (Cardoso, A. H., personal communication). It can be concluded that the 10 experimental models considered (7 from the present study and 3 published in the literature) correspond to a wide range of complex pier geometries.

For the validation of the proposed predictor, some additional tests selected from literature were considered: (1) thirty long-duration tests at pile groups, which represent complex piers in which the pile cap is out of the flow (*i.e*., for the range $H_c > h + T$ in Figure 7.2(a)); and (2) sixty-one long-duration tests at single piers, which represent complex piers in which the top of the pile cap remains buried below the base of the scour hole (*i.e*., for the range $H_c \leq -d_{secu}$ in Figure 7.2(a)). All tests selected from literature were performed for piers with cylindrical shapes under clear-water conditions. In the case of pile groups, the tests selected were those in which the array was aligned with the approach flow. Table 7.2 and Table 7.3 summarize the values of the most important control variables and non-dimensional parameters, which characterize the selected tests at single piers and pile groups, respectively. Most equilibrium scour depths included in both tables correspond to values reported by Lança *et al*. (2013a, 2013b), although the others were estimated by extrapolation of the scour-depth records through equation (2.18).

Table 7.2 – Control variables and non-dimensional parameters for single piers' studies with long-duration tests

Study	Total tests	U/U_c	h/D	D/d_{50}	t_d (day)
Ettema (1980)	5	0.95-1.00	4.0-6.0	119-187	8.1-13.1
Sheppard *et al*. (2004)	4	0.85-0.97	0.9-3.9	1143-4155	6.0-24.2
Grimaldi (2005)	2	1.00	2.1-2.8	105-140	6.1-6.2
Simarro *et al*. (2011)	5	0.88-0.94	2.0-2.1	49-93	24.9-45.6
Lança *et al*. (2013b)	45	0.95-1.04	0.5-5.0	58-465	7.0-13.7

Table 7.3 – Control variables and non-dimensional parameters for pile groups' studies with long-duration tests

Study	Array ($n \times m$)	U/U_c	h/D_p	D_p/d_{50}	t_d (day)
Lança *et al*. (2013a)	1x4, 2x4, 3x4 4x1, 4x2, 4x3	≈0.96	4.0	58	6.9-16.2

Figure 7.4 shows the comparison of the scour depths obtained using the predictors associated to Auckland (Coleman, 2005), FDOT (Sheppard and Renna, 2010) and HEC-18 (Arneson *et al*., 2012) methods, and the proposed formulation with the corresponding scour depths observed in the 174 selected tests. Those correspond to (a) 61 tests with single piers, (b) 30 tests with pile groups and (c) 83 tests with complex piers (48 of which performed in this study). In a similar procedure to the one referred to in the previous section, two asymmetric bounds are considered in the comparison, which correspond to +30% and −10% with respect to the perfect agreement straight line. In Figure 7.4, values of equilibrium scour depth, d_{se}, were normalized by the equivalent diameter, D_e, which was evaluated for each test in accordance with the method considered. Thereby, the values of D_e were calculated: in the Auckland method, by equations (2.39) to (2.44); in the FDOT method, by equations (2.65) to (2.98); in the HEC-18 method, by inversion of equation (2.31); in the proposed predictor, by equations (7.7) to (7.12).

According to the results plotted in Figure 7.4, it can be concluded that:

- The suggested formulation describes the d_{se} values for different data sets within deviation ranges smaller than those obtained using the Auckland, the HEC-18 and the FDOT methods, as shown when comparing Figure 7.4(a) with Figure 7.4(b), Figure 7.4(c) and Figure 7.4(d). In the proposed predictor, 86% of the predicted values (149/174) are within the boundaries, as shown in Figure 7.4(a);
- Almost a third of the scour depth predictions obtained with the FDOT method are outside the chosen deviation bounds (56/174), as shown in Figure 7.4(b). Most of the predictions that are in overestimation correspond to tests at complex piers (particularly in Situation 2) while most of the predictions that are in underestimation correspond to tests at single piers.
- Almost a third of the scour depth predictions obtained with the Auckland method are also outside the chosen deviation bounds (58/174), as shown in Figure 7.4(c). The distribution of those (58) predicted values is approximately uniform in all three types of tests (*i.e*., tests at single piers, pile groups and complex piers); and
- Most of the scour depth predictions obtained by HEC-18 method are outside the chosen deviation bounds (142/174), as shown in Figure 7.4(d). Part of those is in underestimation.

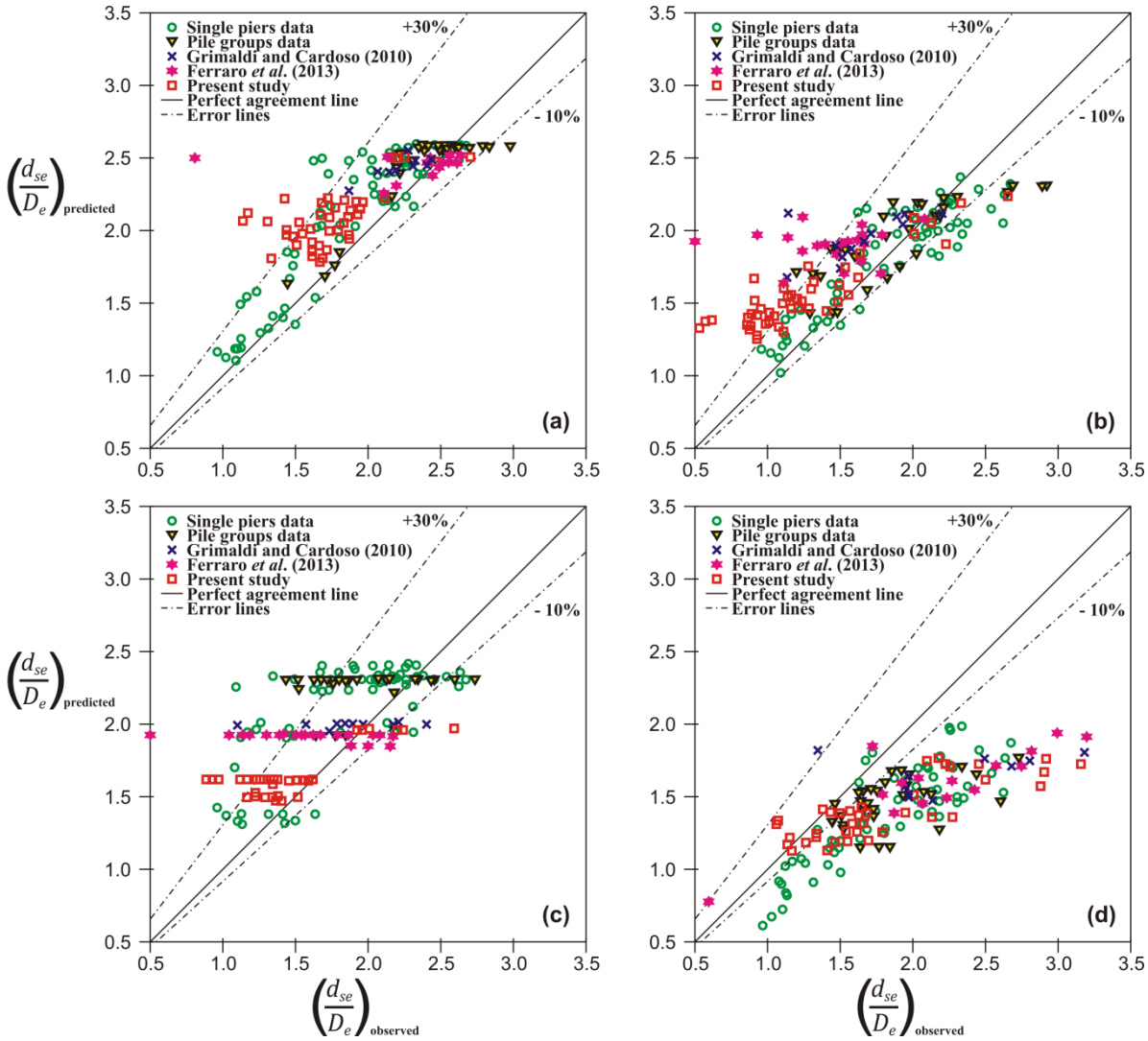

Figure 7.4 – Predicted versus observed scour depths at complex piers by: (a) suggested formulation, (b) FDOT predictor, (c) Auckland predictor and (d) HEC-18 predictor

Figure 7.5 shows the results of the variation in the observed d_{se} values, with the relative column position, H_c/h, for the three complex pier models from literature. Figure 7.5(a) corresponds to the results of the pier model by Grimaldi and Cardoso (2010) (*i.e.*, Model GC), although Figure 7.5(b) corresponds to the results of the pier models by Ferraro *et al.* (2013) (*i.e.*, Models Fe1 and Fe2). Figure 7.5 also includes the d_{se} variation with H_c/h, estimated by the suggested formulation and represented by dashed lines. It is evident that the proposed predictor properly reproduces the trend of the observed data in the three discussed pier models.

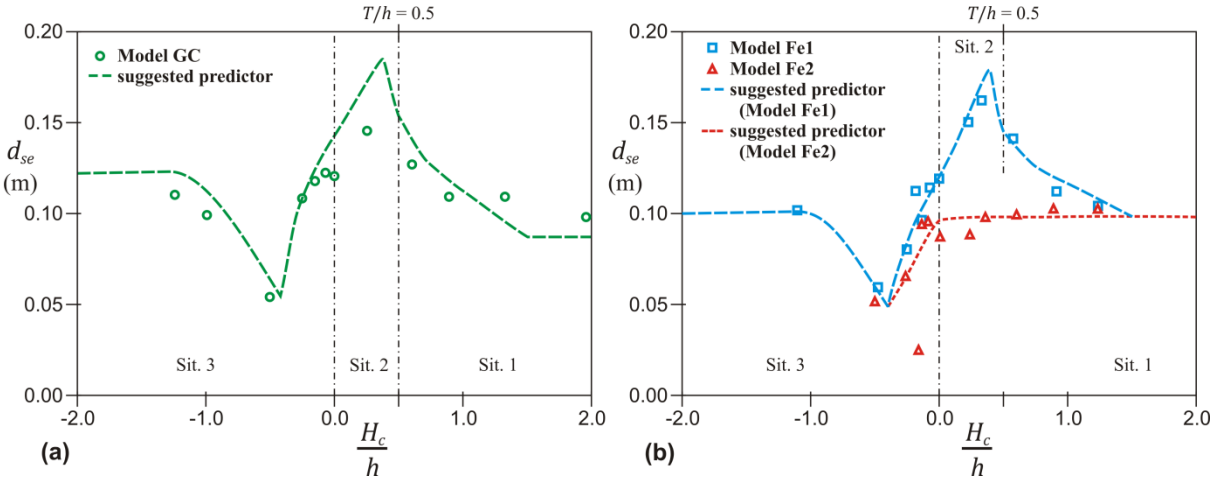

Figure 7.5 – Equilibrium scour depths as a function of column position with: (a) model by Grimaldi and Cardoso (2010) and (b) models by Ferraro *et al*. (2013)

7.5. CONCLUSIONS

From the previous discussion, the following important conclusions can be drawn:

1. Experimental data obtained through forty-eight of the tests performed in this study, with seven different complex pier models, were used to evaluate the performance of three methods to predict d_{se} at complex piers, *i.e*., Auckland (Coleman, 2005), FDOT (Sheppard and Renna, 2010) and HEC-18 (Arneson *et al*., 2012). For the purpose of graphical comparison, two asymmetric bounds were considered, which correspond to a safety factor of 1.3 (allowing an overestimation of 30%) and to an economic factor of 0.9 (allowing an underestimation of 10%), being concluded that: (i) the HEC-18 predictor systematically tends to underestimate d_{se} values in the three analysed situations of the pile-cap position; (ii) the FDOT predictor gives conservative values of d_{se}, the most evident discrepancy being observed in Situation 2; and (iii) the Auckland predictor gives more acceptable values of d_{se}. The deviations in the predictions from the three methods seem to be associated with the inadequacy of the expressions to determine some of the variables used in the calculation of d_{se};
2. A new formulation to predict d_{se} at complex piers is suggested, *i.e*., equations (7.1) to (7.17). Thirty-five long-duration tests reported in literature, with three other different complex pier models, were used to validate the proposed predictor. From the comparison of the Auckland, the FDOT and the HEC-18 methods with the new predictor, it can be concluded that the proposed formulation gives estimations of d_{se}, which represents an acceptable compromise between safety and economy, given that 77% of the predicted values (27/35) are scattered around the line of perfect agreement within the boundaries. Other ninety-one long duration tests reported in literature for single piers and pile groups, which represent particular positions of complex piers relatively to the initial bed level, were also considered in the validation of the suggested predictor. In that case, the proposed formulation provides good estimations of d_{se}, in which 94% of the values (86/91) are scattered around the line of perfect agreement within the boundaries.

8. CONCLUSIONS AND FUTURE RESEARCH

8.1. CONCLUSIONS

8.1.1 GENERAL APPROACH

The present study included an extensive research to systematically map equilibrium scour at common complex piers. These piers are consisted of a column founded on a pile cap supported by an array of piles (see Figure 1.2(b)). An experimental campaign of eighty-four long-duration laboratory tests was performed with seven pier models, aligned with the approach flow under clear-water conditions, to understand and characterize local scour around complex piers. The components of the seven piers (see Figure 3.1) were designed and built with common shapes, *i.e.*, rectangular round-nosed for column and pile cap and cylindrical for piles. Three different configurations of the complex pier models were considered in those eighty-four tests: complete complex pier (Configuration C1); complex pier without the column (Configuration C2); and complex pier without the pile group (Configuration C3) (see Figure 3.2). Each of the seven models was tested for a variety of pile-cap positions relatively to the initial bed level, as shown in Figure 3.4. The experimental results were classified according to three pile-cap situations: (1) Situation 1, characterized by the bottom of the pile cap being above the initial bed level; (2) Situation 2, characterized by the pile cap being partially buried in the initial bed configuration; and (3) Situation 3, characterized by the pile cap being initially completely buried in the bed.

Forty-eight out of the total number of tests were performed with the Configuration C1 (*i.e.*, complete complex pier) in order to: (1) quantify the influence of the complex pier position and geometry on the temporal evolution of the scour depth (results and discussion presented in Chapter 4); (2) quantify the influence of the complex pier position and geometry on the equilibrium scour depth (results and discussion presented in Chapter 5); and (3) evaluate the performance of three methods used to predict the equilibrium scour depth at complex piers (results and discussion presented in Chapter 7). Furthermore, seventy out of the total number of tests performed were used to quantify the contribution of the complex pier components on the total equilibrium scour depth (results and discussion presented in Chapter 6). From these seventy tests, thirty-five correspond to Configuration C1, thirteen correspond to Configuration C2 and twenty-two correspond to Configuration C3.

The contribution of this study may be resumed on the following main achievements:

8.1.2 TEMPORAL EVOLUTION OF THE SCOUR DEPTH AT COMPLEX PIERS

In terms of the temporal evolution of scour depth at complex piers, it was concluded that:

1. The temporal evolution of scour depth at complex piers is generally influenced by the relative column position (H_c/h), by the relative column width (D_c/D_{pc}), by the relative pile-cap thickness (T/h) and by the pile-group configuration. The different stages in the scour depth time evolution are associated with the number of structural elements of the complex pier that are exposed to the flow inside the scour hole developed along the scouring process.

2. In Situation 1, the pile group is the main component to contribute to the scour process, while, in Situation 2, most of the scour process is associated to the column and the pile cap. In Situation 3, the column is the main component to contribute to the scour process.

3. The criterion established to stop the tests by Melville and Chiew (1999) for single piers, also commonly used in complex piers, was evaluated. This criterion seems to no longer have such a good performance when more than one component of the complex pier is exposed to the flow in the scour hole. In general, the application of this criterion would imply much smaller experiment running times than those required for the different scouring phases (*e.g.*, the different stages presented in sections 4.2 and 4.3 for the complex pier models considered on the experimental study carried out). Equation (4.1), based on Sheppard *et al*. (2011), can be used to estimate the time recommended to stop the tests with complex piers.

8.1.3 EFFECTS OF COMPLEX PIER GEOMETRY ON THE EQUILIBRIUM SCOUR DEPTH

Concerning the characterization of the effect of complex pier geometry on the equilibrium scour depth, it was concluded that:

1. The equilibrium scour depth, d_{se}, at complex piers is generally influenced by the relative column position (H_c/h), by the relative column width (expressed by D_c/D_{pc} and f_l/f_t), by the relative pile-cap thickness (T/h), by the pile-group configuration and by the shape of the complex pier components (*i.e.*, column, pile cap and piles). The equilibrium scour depth at these piers is also influenced by the effects of flow intensity, flow shallowness and sediment coarseness widely characterized for single piers.

2. The combined effect of D_c/D_{pc} and H_c/h on d_{se} was evaluated for Models 2, 3 and 5. In general, the differences in d_{se} values range from minimal to relevant with decreasing H_c/h ratio, due to the corresponding increasing influence of the column on the scour process. For a specific H_c/h position, the increment in d_{se} values is directly associated with the increment in the column width and also with the corresponding reduction of the pile-cap front and side extension lengths. For the lower relative column-width values, *i.e.*, $D_c/D_{pc} < 0.6$, it could be concluded that the pile cap overhang from the column face plays the role of an obstruction to the downflow adjacent to the column, reducing the vortex system and hence the scour depth. This reduction is most evident in the cases when the top of the pile cap is close to the initial bed level, for which the flow behaviour is similar to collars in single piers. For larger relative column-width values, *i.e.*, $D_c/D_{pc} \geq 0.6$, the influence of the pile cap overhang is negligible.

3. The combined effect of T/h and H_c/h on d_{se} was also evaluated for two sets of complex pier models (*i.e.*, Models 4, 5 and 6 on a set and Models 1 and 2 on another set). In both sets and for Situation 1, the increment in d_{se} values is related to the increment in T/h, while, in Situation 2, the d_{se} behaviour with H_c/h depends not only on T/h ratio but also on the pile-group contribution to the scour process. When the pile cap is completely buried (Situation 3), the effect of T/h in d_{se} showed to be negligible.

4. The effect of the pile-group configuration (represented by the number of alignments, n) on d_{se} was also assessed. This effect is more evident in Situations 1, in which the pile group is the main component contributing to the scour process whereas in Situation 2, this effect occurs when the piles are exposed to the flow along the scouring process. In these situations and for the piles separation used in the experimental tests, the increment in the number of alignments (n) of the pile group implies an increase in the scour depth.

5. In seven out of the thirteen complex pier models analysed in studies from literature (presented in Table 2.2), the tests were carried out for short durations, *i.e.*, least than four days. That fact may lead to relevant inaccuracy on evaluation of the equilibrium scour depth. Additionally, some of the tests performed with the thirteen models may also be slightly reflecting wall and contraction effects.

6. The experimental data of seven reported models in addition to the data from the present study were used to evaluate the critical relative column position at which the maximum equilibrium scour depth is achieved, $(H_c/T)_{\max}$. The results reveal that $(H_c/T)_{\max}$ decreases with increasing D_c/D_{pc} ratio. For practical applications, the relative position $(H_c/T)_{\max}$ can be obtained through equation (5.2).

8.1.4 COMPLEX PIER COMPONENTS CONTRIBUTION ON THE EQUILIBRIUM SCOUR DEPTH

Concerning the contribution of the complex pier components on local scour depth:

1. A new, physically sounder approach to assess the contribution of complex piers' components on scouring was presented and discussed in this work. According to this new approach, the scour depth due to a given component is calculated by subtracting the scour depth due to the two other pier components from the scour depth corresponding to the complete complex pier, this way keeping the prevailing interactions between the pier components. Those interactions refer to: (i) the deflection of the downflow generated along the upstream face of the column by the pile cap overhang and (ii) the interaction of the downflow generated in the pile cap front and lower faces with the flow structure around the upstream piles. This approach can be considered as an appropriate alternative to estimate the complex pier components' contributions on the total equilibrium scour depth.

2. The column contribution increases as the position of its base relative to the initial bed level, H_c/h, decreases; it also depends on the ratio of the column-width to the width of the pile cap,

D_c/D_{pc}. The subtraction approach provides values of the column contribution larger than those obtained for isolated columns for small values of H_c/h. The largest values of the pile-cap contribution were obtained for pile caps which were partially buried in the bed, where the subtraction approach provides smaller values than experiments with isolated pile caps. Similar to the column contribution, the pile-cap contribution also depends on the ratio D_c/D_{pc}. The most marked differences between the data obtained through subtraction and those measured at isolated pier components was identified for the pile groups, where the subtraction approach leads to significantly higher scour values. The pile-group contribution decreases with decreasing the position of its top relative to the initial bed level. When the top of the piles is above the initial bed level, this contribution also depends on the relation f_p/D_p, whereas, when the top of the piles is below the initial bed level, this contribution is highly dependent on D_c/D_{pc};

3. Both the HEC-18 and the FDOT methods seem to properly predict the contributions of the column and the pile cap to the overall scour when these pier components are suspended above the initial bed; both methods, however, over-predict the contribution of the scour depth induced by the pile cap, the over-prediction being particularly marked in the case of HEC-18; the FDOT method produces conservative scour depth values due to the pile group whereas the HEC-18 method tends to underestimate these values.

8.1.5 PREDICTION OF EQUILIBRIUM SCOUR DEPTH AROUND COMPLEX PIERS

On the assessment of the three available methods used to predict the equilibrium scour depth at complex piers:

1. Experimental data obtained in this study, *i.e.*, the forty-eight tests performed with Configuration C1 (complete pier), were used to evaluate the performance of three methods to predict the equilibrium scour depth at complex piers, Auckland, FDOT and HEC-18. For the purpose of graphical comparison, two asymmetric bounds were considered, which correspond to a safety factor of 1.3 and to an economic factor of 0.9, being concluded that: (i) the HEC-18 predictor systematically tends to underestimate the equilibrium scour depth values in the three analysed situations of the pile-cap position; (ii) the FDOT predictor gives conservative values of the equilibrium scour depth, the most evident discrepancy being observed in Situation 2; and (iii) the Auckland predictor gives more acceptable values of the equilibrium scour depth. The deviations in the predictions from the three methods seem to be associated with the inadequacy of the expressions to determine some of the variables used in the calculation of the equilibrium scour depth.

2. A new formulation to predict the equilibrium scour depth at complex piers, based on the experimental results of the ninety-two tests performed in the present study as well as in scouring results reported in literature, is suggested, *i.e.*, equations (7.1) to (7.17). Thirty-five long-duration tests reported in literature, with three other different complex pier models, were used to validate the proposed predictor. From the comparison of the Auckland FDOT and HEC-18 methods with the new predictor, it can be concluded that the proposed formulation gives estimations of the equilibrium scour depth, which represents an acceptable compromise between safety and economy, given that 77% of the predicted values (27/35) are scattered

around the line of perfect agreement within the boundaries. Other ninety-one long duration tests reported in literature for single piers and pile groups, which represent particular positions of complex piers relatively to the initial bed level, were also considered in the validation of the suggested predictor. In that case, the proposed formulation provides good estimations of the equilibrium scour depth, in which 94% of the values (86/91) are scattered around the line of perfect agreement within the boundaries.

8.2. FUTURE RESEARCH

The present experimental campaign included exclusively tests with piers aligned with the approach flow under clear-water conditions. In order to complement the knowledge obtained from the study concerning local scour at complex piers, with common geometries, the following tasks are suggested for future research:

1. Characterization of the skew angle effect on the equilibrium scour depth:
   - For several authors, the effect of skew angle on the equilibrium scour depth at complex piers is treated as if these piers behaved the same way as single piers, which has never been confirmed and deserves further investigation;
   - This characterization may be performed through: (a) systematic laboratory measurements of the scour depth at skewed complex piers until the near-equilibrium is reached for different pile-cap positions relatively to the initial bed level (*i.e.*, for the three mentioned situations); and (b) comparison of the experimental outputs with those obtained at the same complex pier aligned with the flow. The results of these tests may be used to include a new factor in equations (7.8) to (7.12), expressions that incorporate the suggested predictor; and
   - In the estimation of the new factor to reflects the pier alignment effect, the scouring results included in Figure 2.17 for single skewed piers and the scouring results obtained by Lança *et al*. (2013a) in tests with skewed pile groups should also be considered since these two set of tests correspond to particular positions of the complex pier, *i.e.*, where the top of the pile cap remains buried below the base of the scour hole and where the pile cap is out of the flow, respectively.

2. Characterization of the effect of shape of complex pier components on the equilibrium scour depth:
   - The influence of the pier shape has been studied by several authors particularly for single piers (Figure 2.14) being essential to study this effect of shape of the three components of the complex pier on the equilibrium scour depth since enormous combinations of column, pile cap and pile group geometries are possible;
   - In the case where at least two of the three complex pier components are exposed to the flow, this characterization may be performed by comparison of the experimental scour depths obtained in any of the seven complex pier models studied in this work with those obtained at the same complex pier configuration with different shapes of each component of the complex pier;

- In the case where the pile cap is out of the flow (*i.e.*, only the pile group exposed to the flow), it may be recommended to carry out long-duration tests with square piles since most of the tests available in the literature were performed with cylindrical piles (e.g., Figure 2.31). That experimental data may be used to improve equations (7.15) to (7.17), expressions that incorporate the suggested predictor; and
- In the case where the top of the pile cap remains buried below the base of the scour hole (*i.e.*, only the column exposed to the flow), it may be recommended to extend the data reported in this topic (Figure 2.14) through long-duration tests with columns of different shapes and relations L_c/D_c (L_c = column length; D_c = column width). That experimental data may be used to improve equations (7.1) to (7.4), expressions that incorporate also the suggested predictor.

3. Characterization of the flow field around complex piers:
   - As mentioned in Chapter 2, few studies were found in the literature on the characterization of the flow structure around complex piers in contrast with the wider advance in singe piers. It is important to explore further the behaviour of the flow structures around complex piers as a step towards the improvement of the suggested formulation to predict equilibrium scour depths;
   - This characterization may be performed through experimental measurements in hydraulic-models and/or numerical modelling. In both cases, it is recommended to feature the flow field for different positions of the complex pier relatively to the initial bed level (e.g., pile cap above the bed level, pile cap partially buried and completely buried in the bed). Additionally, the measurements/computer-simulations may be performed for different stages of the scouring process, e.g., initial phase (flatbed), principal phase (at approximately 50% of the equilibrium scour depth) and equilibrium phase. The experimental measurements in hydraulic-models will also be of utmost value for the calibration and validation of the numerical models; and
   - For the flow field characterization with hydraulic-models, it is recommended that the complex pier model is built with transparent Perspex in order to facilitate the use of different measurement techniques: Particle Image Velocimetry (PIV), Acoustic Doppler Velocimetry (ADV), Acoustic Doppler Velocity Profilers (ADVP) and Laser Doppler Velocimetry (LDV). Some of these techniques were widely used for single piers (see section 2.2.1). Since there are no studies on the numerical modelling of the flow field around complex piers, it is recommended to evaluate the different computer-simulations techniques used for single piers in order to select the appropriate techniques that can be used in the case of the complex piers. These techniques include (see section 2.2.1): Large-Eddy Simulation (LES), Reynolds-Averaged Navier–Stokes (RANS), Detached-Eddy Simulation (DES) or hybrid RANS-LES.

REFERENCES

Ahmed, F. and Rajaratnam, N. (1997). *The three-dimensional turbulent boundary layer flow around bridge piers*. Journal of Hydraulic Research, 35 (2), 209 – 224.

Ahmed, F. and Rajaratnam, N. (1998). *Flow around bridge piers*. Journal of Hydraulic Engineering, 124 (3), 288 – 300.

Alabi, P.D. (2006). *Time development of local scour at a bridge pier fitted with a collar*. Master's degree thesis, Univ. of Saskatchewan, Saskatoon, Saskatchewan, Canada.

Amini, A., Melville, B.W. and Ali, T.M. (2014). *Local scour at piled bridge piers including an examination of the superposition method*. Canadian Journal of Civil Engineering, 41 (5), 461 – 471.

Amini, A., Melville, B.W., Ali, T.M. and Ghazali, A.H. (2012). *Clear-water local scour around pile groups in shallow-water flow*. Journal of Hydraulic Engineering, 138 (2), 177 – 185.

Amini, S.A., Mohammad, T.A., Aziz, A.A., Ghazali, A.H. and Huat, B.B.K. (2011). *A local scour prediction method for pile caps in complex piers*. Water Management, 164 (2), 73 – 80.

Arneson, L.A., Zevenbergen, L.W., Lagasse, P.F. and Clopper, P.E. (2012). *Evaluating scour at bridges (HEC-18)*. Technical Rep. No. FHWA (Federal Highway Administration) HIF-12-003, Washington, DC.

Ataie-Ashtiani, B. and Aslani-Kordkandi, A. (2012). *Flow field around side-by-side piers with and without a scour hole*. European Journal of Mechanics - B/Fluids, 36, 152 - 166.

Ataie-Ashtiani, B. and Beheshti, A.A. (2006). *Experimental investigation of clear-water local scour at pile groups*. Journal of Hydraulic Engineering, 132 (10), 1100 - 1104.

Ataie-Ashtiani, B., Baratian-Ghorghi, Z. and Beheshti, A. A. (2010). *Experimental investigation of clear-water local scour of compound piers*. Journal of Hydraulic Engineering, 136 (6), 343 – 351.

Baker, R.E. (1986). *Local scour at bridge piers in non-uniform sediment*. Report Nº 402, School of Engineering, The University of Auckland, Auckland, New Zeland.

Barkdoll, B.B. (2000). *Time scale for local scour at bridge piers*. Journal of Hydraulic Engineering, 126 (10), 793 - 794.

Beheshti, A.A. and Ataie-Ashtiani, B. (2010). *Experimental study of three-dimensional flow field around a complex bridge pier*. Journal of Engineering Mechanics, 136 (2), 143 – 154.

Bertoldi, D.A. and Jones, J.S. (1998). *Time to scour experiments as an indirect measure of stream power around bridge piers*. Proceedings of the International Water Resource Engineering Conference, Memphis, Tennessee, 264 - 269.

Breusers, H.N.C. and Raudkivi, A.J. (1991). *Scouring*. IAHR Hydraulic Structures Design Manual. A. A. Balkema, Rotterdam, Netherlands.

Breusers, H.N.C., Nicollet, G. and Shen, H.W. (1977). *Local scour around cylindrical piers*. Journal of Hydraulic Research, 15 (3), 211 - 252.

Cardoso, A.H. (1982). *Canal de inclinação variável* (in Portuguese). Proc. 62/32/3, National Laboratory for Civil Engineering, Lisbon, Portugal.

Chabert, J. and Engeldinger, P. (1956). *Etude des affouillements autour des piles des ponts*. Laboratoire d'Hydraulique, Chatou, France.

Chang, W-Y., Constantinescu, G., Lien, H-C., Tsai, W-F., Lai, J-S. and Loh, C-H. (2013). *Flow structure around bridge piers of varying geometrical complexity*. Journal of Hydraulic Engineering, 139 (8), 812 – 826.

Chang, Y.W., Constantinescu, G., Miyawaki, S., Tsai, W.F. and Lien, H.C. (2010). The flow and turbulence structure at a rectangular bridge pier with a low angle of attack. Proceedings of River Flow 2010, Germany, 681 – 689.

Chee, R.K.W. (1982). *Live-bed scour at bridge piers*. Report No. 290, University of Auckland, School of Engineering, New Zealand.

Chiew, Y.M. (1984). *Local scour at bridge piers: Report No. 355*. University of Auckland, School of Engineering, New Zealand.

Chiew, Y.M. and Melville, B.W. (1987). *Local scour around bridge piers*. Journal of Hydraulic Research, 25 (1), 15 - 26.

Coleman, S.E. (2005). *Clearwater local scour at complex piers*. Journal of Hydraulic Engineering, 131 (4), 330 - 334.

Coleman, S.E., Lauchlan, C.S. and Melville, B.W. (2003). *Clear-water scour development at bridge abutments*. Journal of Hydraulic Research, 41 (5), 521 - 531.

Couto, L.T. and Cardoso, A.H. (2001). *Erosões localizadas junto de encontros e de pilares de pontes, Parte II - Da situação de referência à prática* (in Portuguese). Recursos Hídricos, 22 (1), 75 - 86.

Dargahi, B. (1989). *The turbulent flow field around a circular cylinder*. Experiments in Fluids, 8, 1 - 12.

Dargahi, B. (1990). *Controlling mechanism of local scouring*. Journal of Hydraulic Engineering, 116 (10), 1197 - 1214.

Dey, S. and Raikar, R.V. (2007). *Characteristics of horseshoe vortex in developing scour holes at piers*. Journal of Hydraulic Engineering, 133 (4), 399 - 413.

Dey, S., Raikar, R.V. and Roy, A. (2008). *Scour at submerged cylindrical obstacles under steady flow*. Journal of Hydraulic Engineering, 134 (1), 105 – 109.

Diab, R. (2011). *Experimental Investigation on Scouring around Piers of different Shape and Alignment in Gravel*. Dr.-Ing. Thesis, Darmstadt University of Technology, Germany.

Diab, R., Link, O. and Zanke, U. (2009). *Experimental investigation of 3D flow field around square pier*. Proceedings of 33rd IAHR Congress: Water Engineering for a Sustainable Environment, Vancouver, Canada.

Diab, R., Zanke, U. and Link, O. (2010). *3D turbulent flow field at square pier in a gravel scour hole*. Proceedings of River Flow 2010, Germany, 691 - 697.

Dietz, J.W. (1972). *Construction of long piers at oblique currents: Illustrated by the BAB-Main Bridge Eddersheim*. Report No. 31, Mitteilungsblatt der Bundersanstalt fur Wasserbau.

Elliott, K.R. and Baker, C.J. (1985). *Effect of pier spacing on scour around bridge piers*. Journal of Hydraulic Engineering, 111 (7), 1105 - 1109.

Ettema, R. (1976). *Influence of bed gradation on local scour: Report No. 124*. University of Auckland, School of Engineering, New Zealand.

Ettema, R. (1980). *Scour at bridge piers: Report No. 216*. University of Auckland, School of Engineering, New Zealand.

Ettema, R., Constantinescu, G. and Melville, B. (2011). *Evaluation of bridge scour research: pier scour process and predictions*. National Cooperative Highway Research Program 24-27(01), Transportation Research Board, Washington, DC.

Ettema, R., Kirkil, G. and Muste, M. (2006). *Similitude of large-scale turbulence in experiments on local scour at cylinders*. Journal of Hydraulic Engineering, 132 (1), 33 - 40.

Ettema, R., Melville, B.W. and Barkdole, B. (1998a). Scale effect in pier-scour experiments. Journal of Hydraulic Engineering, 124 (6), 639 - 642.

Ettema, R., Mostafa, E.A., Melville, B.W. and Yassin, A.A. (1998b). *Local scour at skewed bridge piers*. Journal of Hydraulic Engineering, 124 (7), 756 - 759.

Fael, C., Lança, R. and Cardoso, A. (2014). *Pier shape and alignment effects on local scour*. Proc. Small scale morphological evolution of coastal, estuarine and rivers systems Conference, Nantes.

Ferraro, D., Tafarojnoruz, A., Gaudio, R. and Cardoso, A.H. (2013). *Effects of pile cap thickness on the maximum scour depth at a complex pier*. Journal of Hydraulic Engineering, 139 (5), 482 – 491.

Franzetti, S., Larcan, E. and Mignosa, P. (1982). *Influence of tests duration on the evaluation of ultimate scour around circular piers*. International Conference on the Hydraulic Modelling of Civil Engineering Structures, Coventry, England.

Graf, W.H. (1995). *Load scour around piers*. Annual Rep., Laboratoire de Recherches Hydrauliques, École Polytechnique Fédérale de Lausanne, Lausanne, Switzerland.

Graf, W.H. and Istiarto, I. (2002). *Flow pattern in the scour hole around a cylinder*. Journal of Hydraulic Research, 40 (1), 13 - 20.

Grimaldi, C. (2005). *Non-conventional countermeasures against local scouring at bridge abutments*. Ph.D. dissertation, Universitá della Calabria, Cocenza, Italy.

Grimaldi, C. and Cardoso, A.H. (2010). *Methods for local scour depth estimation at complex bridge piers*. Proceedings of 1st IAHR European Division Congress, Edinburgh, UK.

Grimaldi, C., Gaudio, R., Calomino, F., and Cardoso, A. (2009). *Control of scour at bridge piers by a downstream bed sill*. Journal of Hydraulic Engineering, 135 (1), 13 – 21.

Hannah, C.R. (1978). *Scour at pile groups*. Report Nº 78-3, Department of Civil Engineering, University of Canterbury, Christchurch, New Zealand.

Jain, S.C. and Fischer, E.E. (1979). *Scour around bridge piers at high Froude numbers*. Report No. FHWA-RD-79-104, Federal Highway Administration, U.S. Department of Transportation, Washington, D.C., U.S.A.

Jones, J.S. (1989). *Laboratory studies of the effects of footings and pile groups on bridge pier scour*. Proceedings of Bridge Scour Symposium, Rep. No. FHWA-RD-90-035, Subcommittee on Sedimentation, Interagency Advisory Committee on Water Data, Federal Highway Administration, Washington, DC, 340–359.

Jones, J.S. and Sheppard, D.M. (2000a). *Local scour at complex pier geometries*. Proceedings of World Environmental and Water Resources Congress 2000, USA, May.

Jones, J.S. and Sheppard, D.M. (2000b). *Scour at wide bridge piers*. Proceedings for the 2000 Water Resources Engineering Conference, Minneapolis, USA.

Jones, J.S., Kilgore, R.T. and Mistichelli, M.P. (1992). *Effects of footing location on bridge pier scour*. Journal of Hydraulic Engineering, 118 (2), 280 – 289.

Khosronejad, A., Kang, S. and Sotiropoulos, F. (2012). *Experimental and computational investigation of local scour around bridge piers*. Advances in Water Resources, 37 (2012), 73 – 85.

Kirkil, G., Constantinescu, S.G. and Ettema, R. (2008). *Coherent structures in the flow field around a circular cylinder with scour hole*. Journal of Hydraulic Engineering, 134 (5), 572 - 587.

Kirkil, G., Constantinescu, S.G. and Ettema, R. (2009). *Detached eddy simulation investigation of turbulence at a circular pier with scour hole*. Journal of Hydraulic Engineering, 135 (11), 888 - 901.

Kothyari, U.C., and Kumar, A. (2012). *Temporal variation of scour around circular compound piers*. Journal of Hydraulic Engineering, 138 (11), 945 - 957.

Kothyari, U.C., Hager, W.H. and Oliveto, G. (2007). *Generalized approach for clear-water scour at bridge foundation elements*. Journal of Hydraulic Engineering, 133 (11), 1229 - 1240.

Kumar, A. and Kothyari, U.C. (2012). *Three-dimensional flow characteristics within the scour hole around circular uniform and compound piers*. Journal of Hydraulic Engineering, 138 (5), 420 – 429.

Kumar, A., Kothyari, U.C. and Ranga Raju, K.G. (2012). *Flow structure and scour around circular compound bridge piers e A review*. Journal of Hydro-environment Research, 6 (4), 251 – 265.

Lagasse, P.F., Zevenbergen, L.W. and Clopper, P.E. (2010). *Impacts of debris on bridge pier scour*. Proceedings of International Conference on Scour and Erosion 2010, USA, 854 - 863.

Lança, R. (2013). *Clear-water scour at single piers and pile groups*. PhD thesis, University of Beira Interior. Covilhã, Portugal.

Lança, R., Fael, C. and Cardoso, A. (2010). *Assessing equilibrium clear water scour around single cylindrical piers*. Proceedings of River Flow 2010, Germany.

Lança, R., Fael, C. and Cardoso, A. (2011). *Effect of relative sediment size on clear-water equilibrium scour depth at single cylindrical piers*. Proceedings of the 34th IAHR World Congress, Brisbane, Australia.

Lança, R., Fael, C., Maia, R., Pêgo, J. and Cardoso, A. (2013a). *Clear-water scour at pile groups*. Journal of Hydraulic Engineering, 139 (10), 1089 – 1098.

Lança, R., Fael, C., Maia, R., Pêgo, J. and Cardoso, A. (2013b). *Clear-water scour at comparatively large cylindrical piers*. Journal of Hydraulic Engineering, 139 (11), 1117 – 1125.

Lança, R., Simarro, G., Fael, C. M. S. and Cardoso, A. (2015). *Effect of viscosity on the equilibrium scour depth at single cylindrical piers*. Journal of Hydraulic Engineering, 10.1061/(ASCE)HY.1943-7900.0001102, 06015022.

Laursen, E.M. and Toch, A. (1956). *Scour around bridge piers and abutments*. Bulletin Nº. 4, Iowa Highway Research Board, Ames, IA, USA.

Lee, S.O. and Sturm. T.W. (2009). *Effect of sediment size scaling on physical modelling of bridge pier scour*. Journal of Hydraulic Engineering, 135 (10), 793 - 802.

Link, O., Pfleger, F. and Zanke, U. (2008). *Characteristics of developing scour-holes at a sand-embedded cylinder*. Proceedings of International Journal of Sediment Research, 23 (3), 258 - 266.

López, G., Teixeira, L., Ortega-Sánchez, M. and Simarro, G. (2014). *Estimating final scour depth under clear-water flood waves*. Journal of Hydraulic Engineering, 140 (3), 328 – 332.

Lu, J.-Y., Shi, Z.-Z., Hong, J.-H., Lee, J.-J. and Raikar, R.V. (2011). *Temporal variation of scour depth at nonuniform cylindrical piers*. Journal of Hydraulic Engineering, 137 (1), 45 - 56.

Martín-Vide, J.P., Hidalgo, C. and Bateman, A. (1998). *Local scour at piled bridge foundations*. Journal of Hydraulic Engineering, 124 (4), 439 - 444.

Mashahir, M.B., Zarrati, A.R. and Rezayi, M.J. (2004). *Time development of scouring around a bridge pier protected by collar*. Proceedings of 2nd International Conference on Scour and Erosion, Singapore.

Melville, B. (2008). *The physics of local scour at bridge piers.* Proceedings of International Conference on Scour and Erosion 2008, 28 - 40.

Melville, B., Coleman, S. and Priestley, S. (2006). *Local scour at complex piers*. Proceedings of World Environmental and Water Resources Congress 2006, USA, May.

Melville, B.W. (1975). *Local scour at bridge sites: Report no. 117*. University of Auckland, School of Engineering, New Zealand.

Melville, B.W. (1984). *Live-bed scour at bridge piers*. Journal of Hydraulic Engineering, 110 (9), 1234 - 1247.

Melville, B.W. (1997). *Pier and abutment scour – an integrated approach*. Journal of Hydraulic Engineering, 132 (2), 125 - 136.

Melville, B.W. and Chiew, Y.M. (1999). *Time scale for local scour at bridge piers*. Journal of Hydraulic Engineering, 125 (1), 59 - 65.

Melville, B.W. and Coleman, S.E. (2000). *Bridge Scour*. Water Resources Publications, LLC, Colorado, USA.

Melville, B.W. and Dongol, D.M. (1992). *Bridge pier scour with debris accumulation*. Journal of Hydraulic Engineering, 118 (9), 1306 - 1310.

Melville, B.W. and Raudkivi, A.J. (1977). *Flow characteristics in local scour at bridge piers*. Journal of Hydraulic Research, 15 (4), 373 - 380.

Melville, B.W. and Raudkivi, A.J. (1996). *Effect of foundation geometry on bridge pier scour*. Journal of Hydraulic Engineering, 122 (4), 203 - 209.

Melville, B.W. and Sutherland, A.J. (1988). *Design method for local scour at bridge piers*. Journal of Hydraulic Engineering, 114 (10), 1210 - 1226.

Modjeski, R. (1922). *Bridges old and new*. Journal of the Franklin Institute, 194 (3), 291 – 327.

Moreno, M., Couto, L. and Maia, R. (2012a). *Evolução temporal da profundidade de erosão localizada junto de pilares complexos* (in Portuguese). Proceedings of 11º Congresso da Água, Porto, Portugal, 6-8 February.

Moreno, M., Couto, L. and Maia, R. (2012c). *Evolución temporal de la profundidad de erosión local junto de pilas de puentes de geometría compleja* (in Spanish). Proceedings of XXV Congreso Latinoamericano de Hidráulica, San José, Costa Rica, 9-12 September.

Moreno, M., Couto, L., Maia, R. and Cardoso, A. (2014b). *Erosões localizadas em pilares complexos de pontes: desempenho de modelos de previsão existentes* (in Portuguese). Revista Recursos Hídricos 35 (1), 5 - 22.

Moreno, M., Maia, R. and Couto, L. (2015b). *Effects of relative column width and pile cap elevation on local scour depth around complex piers*. Journal of Hydraulic Engineering, 10.1061/(ASCE)HY.1943-7900.000108, 04015051.

Moreno, M., Maia, R. and Couto, L. (2016a). *Prediction of equilibrium local scour depth at complex bridge piers*. Journal of Hydraulic Engineering. 10.1061/(ASCE)HY.1943-7900.0001153, 04016045.

Moreno, M., Maia, R., Couto, L. and Cardoso, A. (2012b). *Evaluation of local scour depth around complex bridge piers*. Proceedings of River Flow 2012, San José, Costa Rica, 5-7 September.

Moreno, M., Maia, R., Couto, L. and Cardoso, A. (2014a). *Contribution of complex pier components on local scour depth*. Proceedings of 3rd IAHR Europe Congress, Porto, Portugal, 14-16 April.

Moreno, M., Maia, R., Couto, L. and Cardoso, A. (2016b). *Subtraction approach to experimentally assess the contribution of the complex pier components to the local scour depth*. Manuscript submitted for publication to Journal of Hydraulic Engineering.

Moreno, M., Maia, R., Pêgo, J.P., Couto, L. and Cardoso, A.H. (2014c). *Contribuição das componentes de um pilar complexo na profundidade de erosão localizada* (in Portuguese). Proceedings of 9 Jornadas de Hidráulica, Recursos Hídricos e Ambiente do Departamento de Engenharia Civil da FEUP, Porto, Portugal, 31 October.

Moreno, M., Muralha, A., Couto, L., Maia, R. and Cardoso, A.H. (2015a). *Influence of column width on the equilibrium scour depth at a complex pier*. Proceedings of 36th IAHR World Congress, The Hague, The Netherlands, 28 June – 3 July.

Morton, B.R. and Evans-Lopez, J.L. (1986). *Horseshoe vortices and bridge pier erosion*. Proceedings 5th Australasian Fluid Mechanics Conference, Auckland, New Zealand, 256 - 259.

Mostafa, E.A. (1994). *Scour around skewed bridge piers*. PhD Thesis, Alejandria University, Alejandria, Egypt.

Movahedi, N., Dehghani, A.A., Aarabi, M.J. and Zahiri, A.R. (2013). *Temporal evolution of local scour depth around side-by-side piers*. Journal of Civil Engineering and Urbanism, 3 (3), 82 – 86.

Muñoz, E.E., Núñez, F. and Mohammadi, J. (2009). *Investigation of common causes of bridge collapse in Colombia*. Practice Periodical on Structural Design and Construction, 14 (4), 194 - 200.

Muto, Y. (2008). *Local scour around a submerged cylindrical pier*. Proceedings of International Conference on Scour and Erosion 2008, 180 - 185.

Muzzammil, M. and Gangadhariah, T. (2003). *The mean characteristics of horseshoe vortex at a cylindrical pier*. Journal of Hydraulic Research, 41 (3), 285 - 297.

Neil, C.R. (1967). *Mean velocity criterion for scour of coarse uniform bed material*. Proceedings of XII IAHR Congress, Fort Collins, Colorado, USA.

Nicollet, G., and Ramette, M. (1971). *Deformation des lits alluvionnaires affouillements autour des piles de ponts cylindriques*, Direction des Etudes et Recherches (EDF), Chatou, France (in French).

Nogueira, H.I.S, Franca, M.J. and Ferreira, R.M.L. (2008). *Caracterização laboratorial do escoamento turbulento a montante de um cilindro colocado verticalmente em fundo de areia* (in Portuguese). Revista de Recursos Hídricos 29 (2), 27 - 40.

Oliveto G. and Hager, W.H. (2002). *Temporal evolution of clear-water pier and abutment scour*. Journal of Hydraulic Engineering, 128 (4), 811 - 820.

Oliveto G. and Hager, W.H. (2005). *Further results to time-dependent local scour at bridge elements*, Journal of Hydraulic Engineering, 131 (2), 97 - 105.

Pagliara, S. and Carnacina, I. (2011). *Influence of wood accumulation on bridge pier scour*. Journal of Hydraulic Engineering, 137 (1), 254 - 261.

Parola, A.C., Mahavadi, S.K., Brown, B.M. and El-Khoury, A. (1996). *Effects of rectangular foundation geometry on local pier scour*. Journal of Hydraulic Engineering, 122 (1), 35 – 40.

Pritsivelis, A. (1999). *Local sediment scour at large circular piles*. M.Sc. Thesis, Florida University, Gainesville, FL.

Radice, A. and Tran, C. K. (2012). *Study of sediment motion in scour hole of a circular pier*. Journal of Hydraulic Research, 50 (1), 44 – 51.

Raikar, R.V. and Dey, S. (2008). *Kinematics of horseshoe vortex development in an evolving scour hole at a square cylinder*. Journal of Hydraulic Research, 46 (2), 247 - 264.

Rao, S.K., Sumner, D. and Balachandar, R. (2004). *A visualization study of fluid-structure interaction between a circular cylinder and a channel bed*. Journal of Visualization, 7 (3), 187-199.

Raudkivi, A.J. (1986). Functional trends of scour at bridge piers. Journal of Hydraulic Engineering, 112 (1), 1 - 13.

Raudkivi, A.J. and Ettema, R. (1977). *Effect of sediment gradation on clear-water scour*. Journal of the Hydraulics Division, 103 (HY10), 1209 - 1213.

Raudkivi, A.J. and Ettema, R. (1983). *Clear-water scour at cylindrical piers*. Journal of Hydraulic Engineering, 109 (3), 339-350.

Raudkivi, A.J. and Sutherland, A.J. (1981). *Scour at bridge crossings*. Road Research unit Bulletin 54, National Roads Board, Wellington, New Zeland.

Richardson, E.V. and Davis, S.R. (1995). *Evaluating scour at bridges*. Third edition. Publication No. FHWA IP 90-017, Hydraulic Engineering Circular No. 18. National Highway Institute, U. S. Department of Transportation, Federal Highway Administration.

Richardson, E.V. and Davis, S.R. (2001). *Evaluating scour at bridges*. Fourth edition. Publication No. FHWA NHI 01-001, Hydraulic Engineering Circular No. 18. National Highway Institute, U. S. Department of Transportation, Federal Highway Administration.

Richardson, E.V., Harrison, L.J., Richardson J.R. and Davis, S.R. (1993). *Evaluating scour at bridges*. Publication FHWA-IP-90-017, Federal Highway Administration, US Department of Transportation, Washington, D.C.

Sadeque, M.A.F., Rajaratnam, N. and Loewen, M.R. (2008). *Flow around cylinders in open channels*. Journal of Engineering Mechanics, 134 (1), 60 - 71.

Salim, M. and Jones, J.S. (1996). *Scour around exposed pile foundations*. Proceedings of the American Society of Civil Engineers "North American Water and Environment Congress 96", Anaheim (U.S.).

Shen, H.W., Schneider, V.R. and Karaki, S.S. (1966). *Mechanics of local scour*. Publication No. CER 66-HWS-VRS-SK22, Colorado State University, Fort Collins, CO.

Shen, H.W., Schneider, V.R. and Karaki, S.S. (1969). *Local scour around bridge piers*. Journal of the Hydraulics Division, 95 (6), 1919 - 1940.

Sheppard, D.M. (1999). *Conditions of maximum local scour*. Proceedings of Stream Stability and Scour at Highway Bridges, E. V. Richardson and P. F. Lagasse, eds., Reston, Va.

Sheppard, D.M. (2003). *Large scale and live bed local pier scour experiments*. Final report BB-473. Florida Department of Transportation.

Sheppard, D.M. and Glasser, T. (2004). *Sediment scour at piers with complex geometries*. Proc. 2nd International conference on Scour and Erosion, World Scientific, Singapore.

Sheppard, D.M. and Jones, J.S. (1998). *Scour at complex pier geometries*. Compendium of scour papers from ASCE Water Resources Conferences, Eds. E.V. Richardson and P.F. Lagasse, ASCE, New York.

Sheppard, D.M. and Miller, W. (2006). *Live-bed local pier scour experiments*. Journal of Hydraulic Engineering, 132 (7), 635 - 642.

Sheppard, D.M. and Renna, R. (2010). *Florida bridge scour manual*. Florida Department of Transportation, Tallahassee.

Sheppard, D.M., Demir, H. and Melville, B. (2011). *Scour at wide piers and long skewed piers*. National Cooperative Highway Research Program Rep. 682, Transportation Research Board, Washington, DC.

Sheppard, D.M., Melville, B. and Demir, H. (2014). *Evaluation of existing equations for local scour at bridge piers*. Journal of Hydraulic Engineering, 140 (1), 14 – 23.

Sheppard, D.M., Mufeed, O. and Glasser, T. (2004). *Large scale clear-water local pier scour experiments*. Journal of Hydraulic Engineering, 130 (10), 957 - 963.

Sheppard, D.M., Mufeed, O., Pritsivelis, A. and Glasser, T. (2000). *Clearwater local scour experiments in a large flume*. Proceedings of the Water Resources Engineering Conference, Mineapolis, USA.

Simarro, G., Fael, C., and Cardoso, A. (2011). *Estimating equilibrium scour depth at cylindrical piers in experimental studies*. Journal of Hydraulic Engineering, 137 (9), 1089–1093.

Smith, W.L. (1999). *Local structure-induced sediment scour at pile groups*. M.Sc. Thesis, Florida University, Gainesville, FL.

Sousa, A.M. (2007). *Erosão localizada junto a pilares cilíndricos complexos* (in Portuguese). M.Sc. Thesis, Instituto Superior Técnico, Lisbon, Portugal.

Sumer, B. M. and Fredsøe, J. (2002). *The Mechanics of Scour in the Marine Environment*. Advanced Series on Ocean Engineering. World Scientific Publishing Co. Pte. Ltd., Singapore.

Sumer, B.M., Christiansen, N. and Fredsøe, J. (1992). *Time scale of scour around a vertical pile*. Proceedings of 2nd International Offshore and Polar Engineering Conference, San Francisco.

Tison, L.J. (1940). *Erosion autour des piles de ponts en riviere*. Annales des Travaux Publics de Belgique, 41 (6), 813 - 817.

Umeda, S., Yamazaki, T. and Yuhi, M. (2010). *An experimental study of scour process and sediment transport around a bridge pier with foundation*. Proceedings of International Conference on Scour and Erosion 2010, 66 - 75.

Unger, J. and Hager, W.H. (2007). *Down-flow and horseshoe vortex characteristics of sediment embedded bridge piers*. Experiments in Fluids, 42, 1 - 19.

Usera, G., Chreties, Ch., Medina, M., Simarro, G. and Teixeira, L. (2010). *Avances en la modelación numérica del fenómeno de socavación local en pilas* (in Spanish). Proceedings of XXV Congreso Latinoamericano de Hidráulica, San José, Costa Rica, 9-12 September.

Veerappadevaru, G. Gangadharaiah, T. and Jagadeesh, T.R. (2011). *Vortex scouring process around bridge pier with a caisson*. Journal of Hydraulic Research, 49 (3), 378 – 383.

Veerappadevaru, G. Gangadharaiah, T. and Jagadeesh, T.R. (2011). *Temporal variation of vortex scour process around caisson piers*. Journal of Hydraulic Research, 50 (2), 200 – 207.

Yalin, M.S. (1971). *Theory of Hydraulic Models*. MacMillan Civil Engineering Hydraulics, Macmillan Publishers Limited.

Zhao, G. and Sheppard, D.M. (1999). *The effect of flow skew angle on sediment scour near pile groups*. Stream Stability and Scour at Highway Bridges, 377 - 391.

Zhao, W. and Huhe, A. (2006). *Large-eddy simulation of three-dimensional turbulent flow around a circular pier*. Journal of Hydrodinamics, 18 (6), 765 - 772

APPENDIX: EXPERIMENTAL DATA

	Pages
Tests with Configuration C1	**157 to 204**
Tests with Configuration C2	**205 to 218**
Tests with Configuration C3	**219 to 240**

Test M1A1

d_{50}	h	U	U_c	U/U_c	B/D_{pc}	B/h	h/D_{pc}
0.086 mm	0.20 m	0.258 m/s	0.322 m/s	0.80	10.0	10.0	1.0

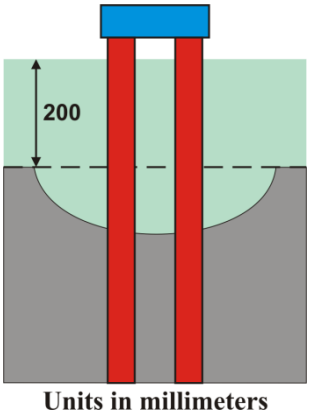

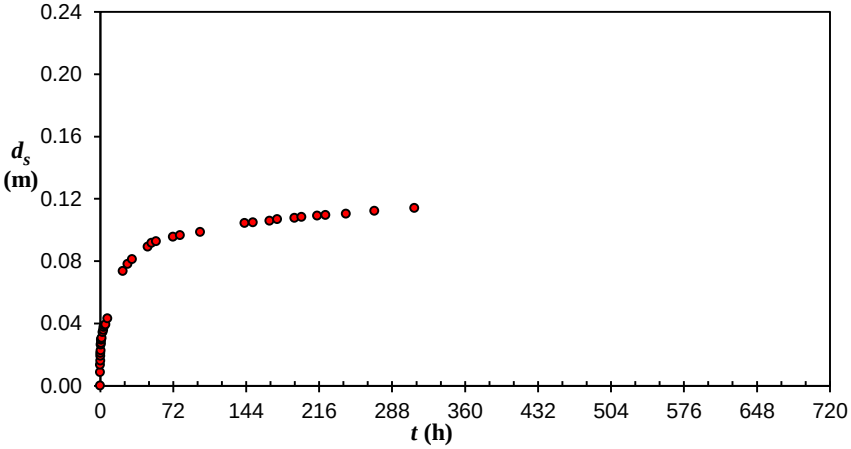

Scour depth measurements in the test M1A1

t_d (h)	d_{sm} (m)		t_d (h)	d_{sm} (m)		t_d (h)	d_{sm} (m)		t_d (h)	d_{sm} (m)
0.00	0.0000		1.25	0.0298		31.45	0.0811		174.83	0.1068
0.05	0.0086		1.50	0.0307		46.97	0.0892		191.78	0.1077
0.10	0.0134		2.40	0.0343		50.85	0.0917		198.83	0.1083
0.20	0.0160		3.00	0.0357		55.32	0.0926		214.25	0.1090
0.30	0.0192		3.58	0.0377		71.87	0.0955		222.38	0.1095
0.40	0.0210		4.28	0.0386		78.88	0.0966		242.68	0.1104
0.50	0.0227		5.47	0.0393		98.78	0.0987		270.58	0.1121
0.67	0.0263		7.15	0.0431		142.60	0.1044		310.00	0.1139
0.83	0.0274		22.33	0.0736		150.87	0.1048			
1.00	0.0294		26.95	0.0780		167.20	0.1057			

Test M1D1

d_{50}	h	U	U_c	U/U_c	B/D_{pc}	B/h	h/D_{pc}
0.086 mm	0.20 m	0.258 m/s	0.322 m/s	0.80	10.0	10.0	1.0

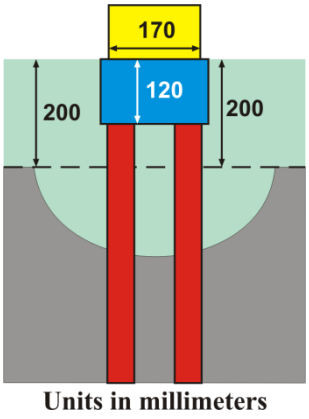

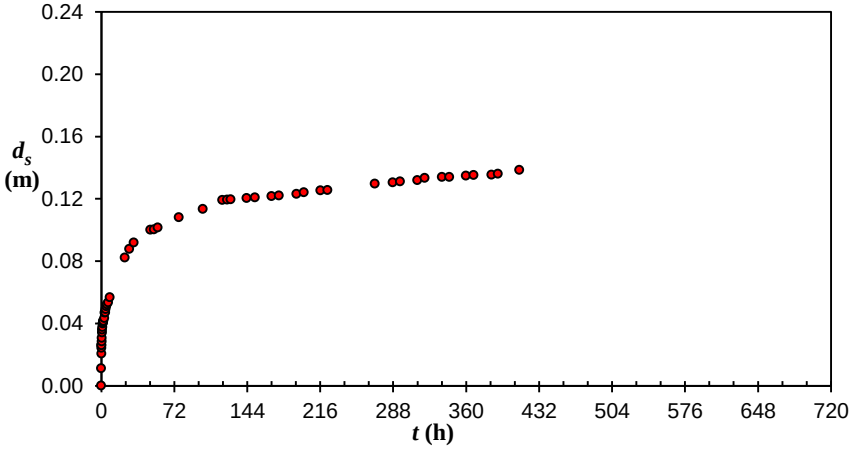

Scour depth measurements in the test M1D1

t_d (h)	d_{sm} (m)	t_d (h)	d_{sm} (m)	t_d (h)	d_{sm} (m)	t_d (h)	d_{sm} (m)
0.00	0.0000	2.25	0.0416	55.83	0.1014	270.12	0.1296
0.07	0.0111	3.20	0.0433	76.70	0.1080	287.72	0.1304
0.15	0.0205	3.50	0.0468	100.40	0.1133	295.05	0.1311
0.23	0.0243	4.00	0.0471	119.58	0.1191	312.05	0.1319
0.32	0.0261	4.50	0.0491	124.22	0.1194	319.32	0.1334
0.40	0.0258	5.00	0.0509	127.75	0.1195	336.28	0.1340
0.50	0.0283	5.68	0.0521	143.52	0.1204	343.52	0.1339
0.67	0.0307	6.87	0.0534	151.62	0.1208	359.83	0.1347
0.83	0.0341	8.47	0.0567	168.10	0.1217	367.58	0.1351
1.00	0.0359	23.30	0.0822	175.28	0.1221	385.17	0.1353
1.25	0.0375	27.58	0.0878	192.75	0.1230	391.42	0.1360
1.50	0.0398	32.12	0.0919	199.83	0.1241	412.67	0.1385
1.75	0.0405	48.67	0.1000	216.25	0.1252		
2.00	0.0413	52.17	0.1003	223.42	0.1255		

Test M1E1

d_{50}	h	U	U_c	U/U_c	B/D_{pc}	B/h	h/D_{pc}
0.086 mm	0.20 m	0.258 m/s	0.322 m/s	0.80	10.0	10.0	1.0

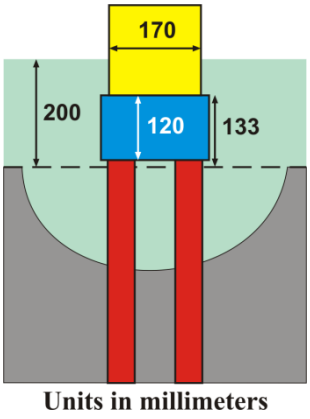

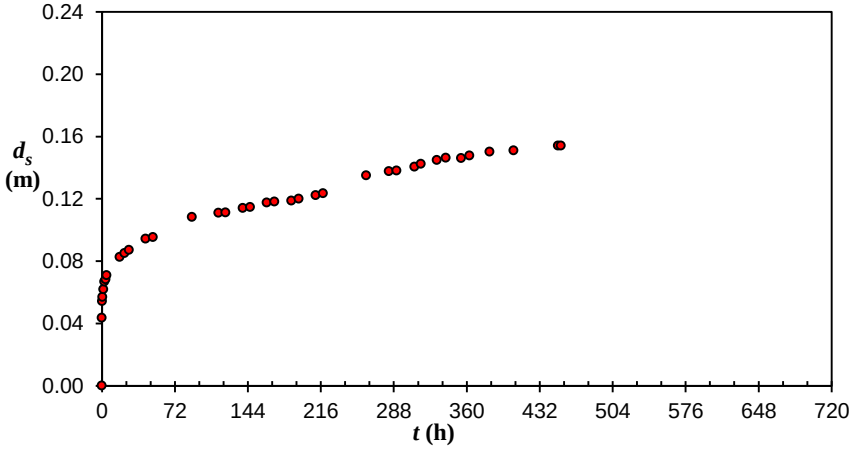

Scour depth measurements in the test M1E1

t_d (h)	d_{sm} (m)	t_d (h)	d_{sm} (m)	t_d (h)	d_{sm} (m)	t_d (h)	d_{sm} (m)
0.00	0.0000	26.65	0.0871	187.20	0.1188	339.28	0.1462
0.10	0.0435	43.13	0.0943	194.42	0.1199	354.65	0.1460
0.30	0.0542	50.58	0.0954	210.92	0.1222	362.70	0.1477
0.67	0.0570	88.78	0.1083	218.23	0.1234	382.53	0.1501
1.55	0.0619	115.00	0.1110	260.98	0.1349	406.47	0.1510
2.42	0.0668	122.05	0.1111	283.22	0.1376	450.08	0.1541
3.58	0.0683	138.97	0.1140	290.98	0.1380	452.92	0.1540
4.78	0.0708	146.22	0.1146	308.60	0.1405		
17.48	0.0826	162.90	0.1175	314.75	0.1423		
22.20	0.0850	170.43	0.1182	330.73	0.1449		

Test M1F1

d_{50}	h	U	U_c	U/U_c	B/D_{pc}	B/h	h/D_{pc}
0.086 mm	0.20 m	0.258 m/s	0.322 m/s	0.80	10.0	10.0	1.0

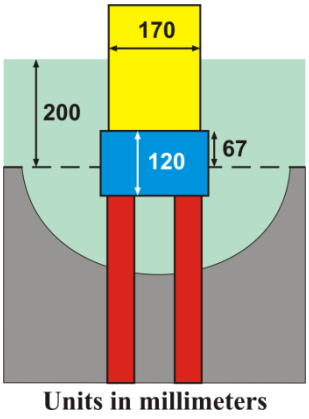

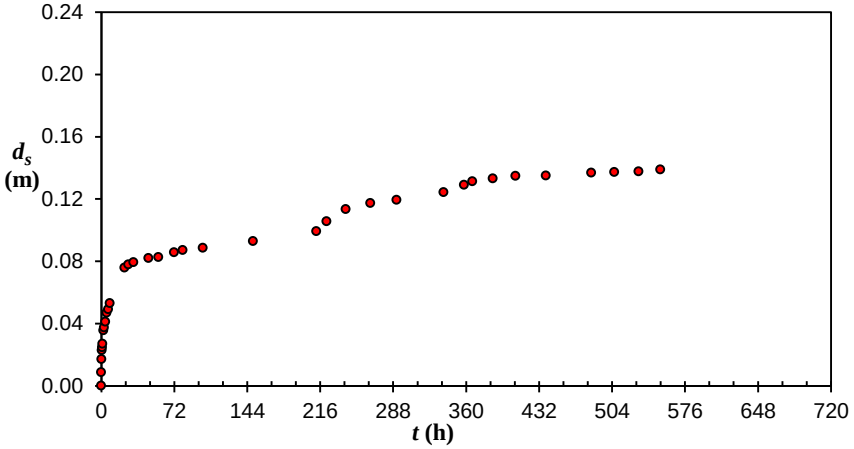

Scour depth measurements in the test M1F1

t_d (h)	d_{sm} (m)	t_d (h)	d_{sm} (m)	t_d (h)	d_{sm} (m)	t_d (h)	d_{sm} (m)
0.00	0.0000	5.42	0.0468	80.45	0.0872	366.18	0.1312
0.07	0.0087	6.87	0.0491	100.17	0.0885	386.30	0.1331
0.23	0.0170	8.38	0.0530	149.78	0.0928	408.77	0.1347
0.43	0.0229	22.83	0.0758	212.23	0.0993	438.95	0.1349
0.78	0.0246	26.85	0.0778	222.40	0.1056	483.48	0.1368
1.13	0.0269	31.88	0.0793	241.40	0.1134	506.22	0.1372
2.10	0.0355	46.53	0.0820	265.47	0.1173	530.43	0.1377
2.92	0.0373	56.33	0.0826	291.50	0.1194	551.80	0.1389
4.10	0.0411	71.80	0.0857	337.90	0.1243	358.07	0.1290

Test M1H1

d_{50}	h	U	U_c	U/U_c	B/D_{pc}	B/h	h/D_{pc}
0.086 mm	0.20 m	0.258 m/s	0.322 m/s	0.80	10.0	10.0	1.0

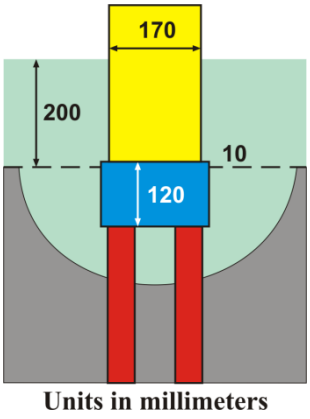

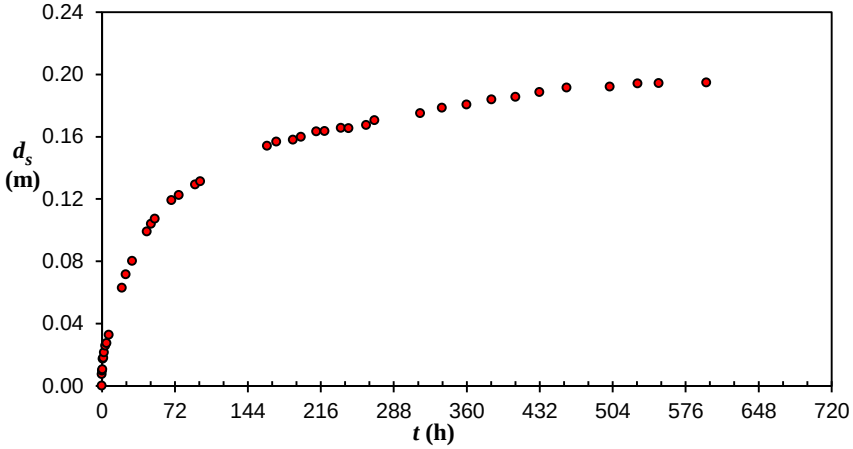

Scour depth measurements in the test M1H1

t_d (h)	d_{sm} (m)		t_d (h)	d_{sm} (m)		t_d (h)	d_{sm} (m)		t_d (h)	d_{sm} (m)
0.00	0.0000		23.72	0.0715		188.50	0.1580		384.62	0.1838
0.10	0.0074		29.80	0.0802		196.37	0.1599		408.27	0.1854
0.28	0.0097		44.43	0.0991		211.63	0.1632		431.72	0.1886
0.53	0.0105		48.63	0.1040		219.83	0.1636		458.73	0.1915
1.00	0.0173		52.42	0.1073		236.05	0.1655		501.22	0.1921
1.55	0.0178		68.73	0.1192		243.63	0.1654		528.70	0.1940
2.27	0.0214		75.88	0.1224		260.78	0.1675		549.58	0.1943
3.50	0.0256		92.05	0.1293		269.20	0.1704		596.68	0.1947
4.63	0.0273		97.20	0.1312		314.03	0.1751			
6.75	0.0326		163.07	0.1541		335.72	0.1784			
19.70	0.0628		172.25	0.1567		359.88	0.1806			

Test M1I1

d_{50}	h	U	U_c	U/U_c	B/D_{pc}	B/h	h/D_{pc}
0.086 mm	0.20 m	0.258 m/s	0.322 m/s	0.80	10.0	10.0	1.0

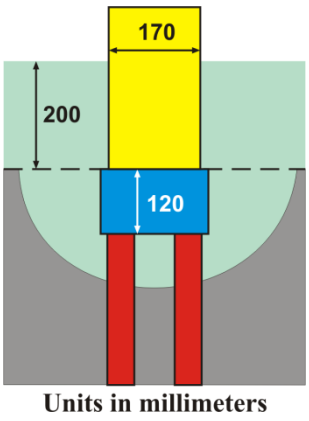

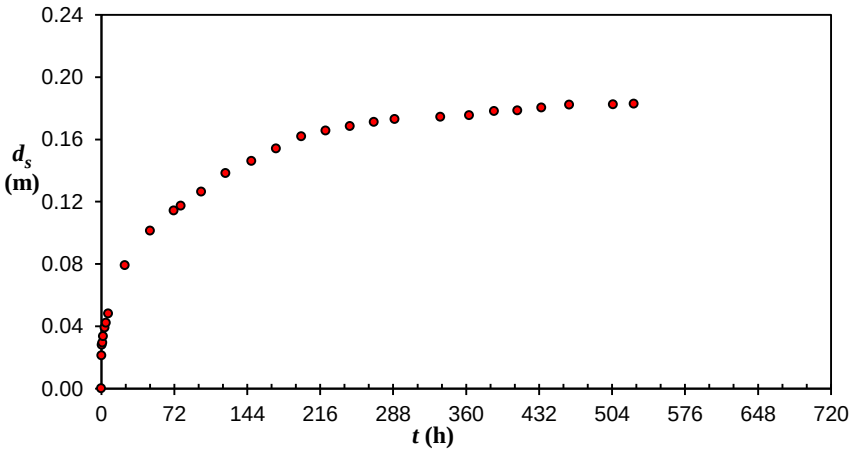

Scour depth measurements in the test M1I1

t_d (h)	d_{sm} (m)		t_d (h)	d_{sm} (m)		t_d (h)	d_{sm} (m)		t_d (h)	d_{sm} (m)
0.00	0.0000		23.35	0.0790		197.50	0.1618		410.58	0.1784
0.18	0.0211		48.25	0.1012		221.55	0.1655		434.48	0.1803
0.48	0.0279		71.42	0.1143		245.53	0.1685		461.82	0.1822
1.07	0.0294		78.42	0.1172		269.15	0.1711		505.05	0.1824
2.00	0.0335		98.83	0.1264		289.50	0.1730		525.48	0.1828
3.28	0.0391		122.57	0.1382		334.63	0.1744			
4.65	0.0422		148.12	0.1460		363.23	0.1754			
6.78	0.0480		172.58	0.1541		387.78	0.1781			

Test M2E1

d_{50}	h	U	U_c	U/U_c	B/D_{pc}	B/h	h/D_{pc}
0.086 mm	0.20 m	0.258 m/s	0.322 m/s	0.80	10.0	10.0	1.0

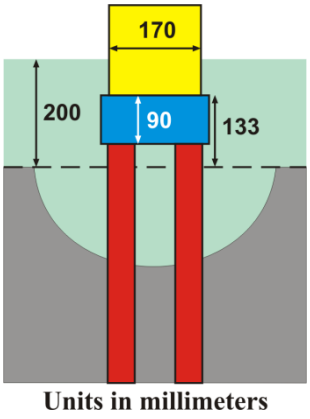

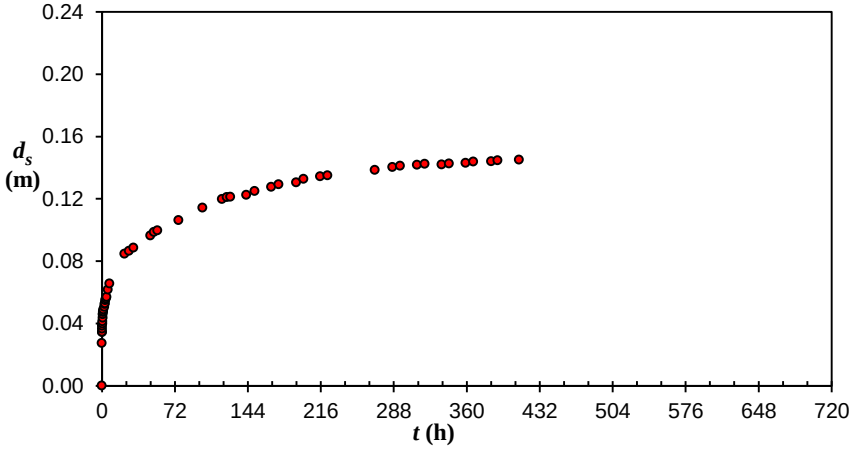

Scour depth measurements in the test M2E1

t_d (h)	d_{sm} (m)		t_d (h)	d_{sm} (m)		t_d (h)	d_{sm} (m)		t_d (h)	d_{sm} (m)
0.00	0.0000		2.35	0.0505		55.00	0.0996		222.60	0.1349
0.08	0.0273		2.72	0.0524		75.73	0.1063		269.43	0.1385
0.17	0.0344		3.00	0.0529		99.38	0.1142		286.85	0.1403
0.25	0.0345		3.50	0.0548		118.68	0.1198		294.35	0.1411
0.33	0.0366		4.03	0.0559		123.35	0.1209		311.17	0.1417
0.42	0.0384		4.80	0.0569		126.93	0.1212		318.62	0.1423
0.50	0.0398		6.02	0.0616		142.68	0.1225		335.42	0.1420
0.67	0.0412		7.55	0.0655		150.77	0.1249		342.68	0.1426
0.83	0.0435		22.43	0.0847		167.17	0.1276		358.95	0.1429
1.00	0.0459		26.75	0.0865		174.42	0.1293		366.72	0.1437
1.17	0.0473		31.28	0.0886		191.83	0.1305		384.33	0.1440
1.33	0.0477		47.77	0.0963		198.97	0.1327		390.55	0.1446
1.57	0.0489		51.33	0.0987		215.40	0.1344		411.72	0.1450

Test M2F1

d_{50}	h	U	U_c	U/U_c	B/D_{pc}	B/h	h/D_{pc}
0.086 mm	0.20 m	0.258 m/s	0.322 m/s	0.80	10.0	10.0	1.0

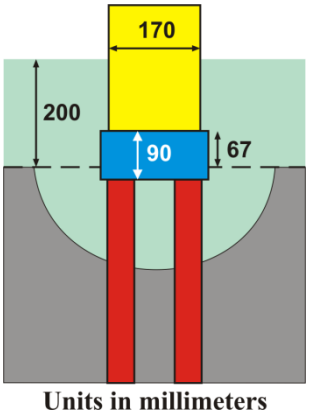

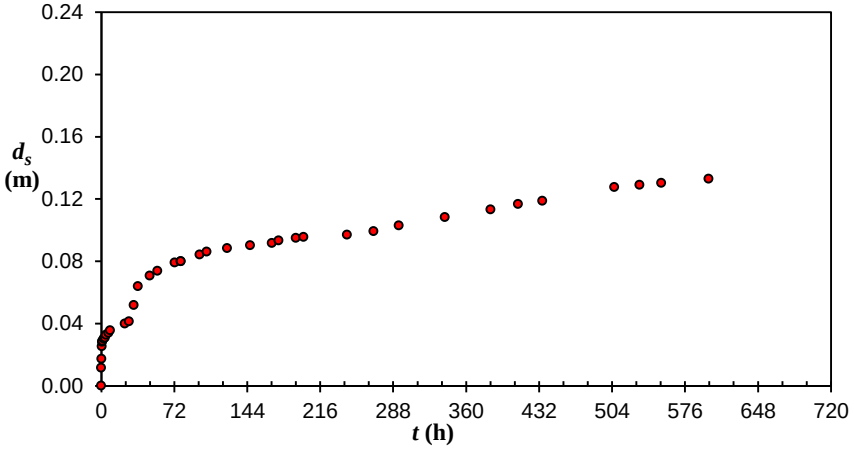

Scour depth measurements in the test M2F1

t_d (h)	d_{sm} (m)	t_d (h)	d_{sm} (m)	t_d (h)	d_{sm} (m)	t_d (h)	d_{sm} (m)
0.00	0.0000	8.88	0.0355	97.27	0.0843	293.73	0.1029
0.10	0.0115	23.22	0.0398	104.22	0.0860	339.08	0.1083
0.23	0.0173	27.25	0.0414	124.25	0.0883	384.28	0.1132
0.45	0.0252	32.15	0.0518	147.12	0.0901	411.28	0.1166
0.77	0.0282	36.20	0.0638	168.38	0.0917	435.33	0.1187
1.08	0.0288	47.83	0.0706	175.07	0.0933	506.35	0.1276
2.42	0.0302	55.42	0.0737	192.20	0.0949	531.35	0.1289
3.67	0.0308	72.48	0.0790	199.70	0.0956	552.60	0.1303
4.78	0.0327	78.57	0.0799	242.55	0.0969	599.42	0.1328
7.10	0.0339	78.57	0.0799	268.77	0.0992		

Test M2H1

d_{50}	h	U	U_c	U/U_c	B/D_{pc}	B/h	h/D_{pc}
0.086 mm	0.20 m	0.258 m/s	0.322 m/s	0.80	10.0	10.0	1.0

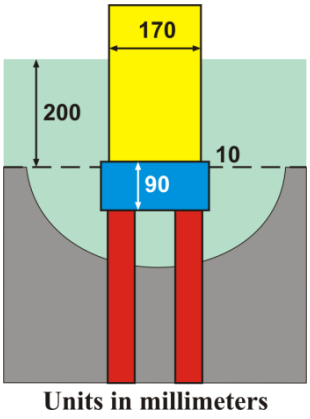

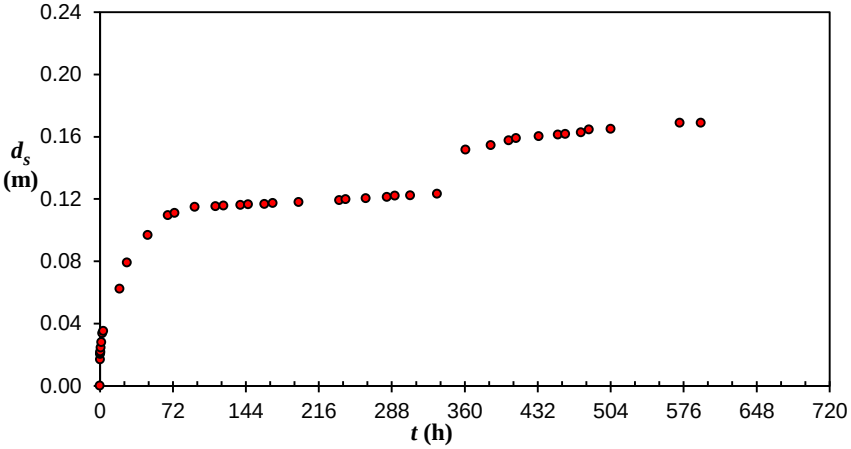

Scour depth measurements in the test M2H1

t_d (h)	d_{sm} (m)		t_d (h)	d_{sm} (m)		t_d (h)	d_{sm} (m)		t_d (h)	d_{sm} (m)
0.00	0.0000		47.40	0.0967		236.30	0.1191		433.07	0.1603
0.12	0.0168		67.17	0.1094		242.53	0.1197		451.97	0.1612
0.28	0.0204		73.87	0.1110		262.55	0.1203		459.47	0.1617
0.50	0.0211		93.67	0.1149		283.40	0.1212		474.83	0.1626
0.67	0.0220		114.25	0.1152		291.18	0.1221		482.80	0.1645
1.00	0.0244		121.97	0.1156		306.20	0.1223		504.17	0.1649
1.63	0.0279		138.75	0.1160		332.78	0.1232		572.23	0.1688
2.43	0.0336		146.45	0.1164		361.03	0.1515		593.00	0.1689
3.32	0.0352		162.43	0.1167		385.75	0.1544			
19.67	0.0623		170.50	0.1172		403.40	0.1575			
26.87	0.0791		196.22	0.1180		410.58	0.1589			

Test M2I1

d_{50}	h	U	U_c	U/U_c	B/D_{pc}	B/h	h/D_{pc}
0.086 mm	0.20 m	0.258 m/s	0.322 m/s	0.80	10.0	10.0	1.0

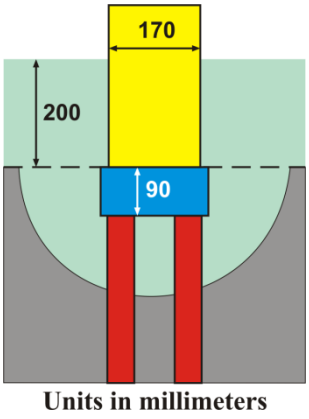

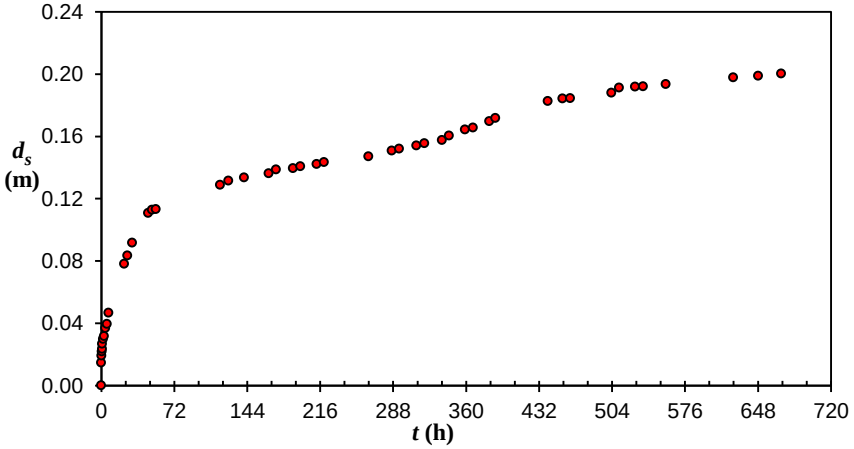

Scour depth measurements in the test M2I1

t_d (h)	d_{sm} (m)	t_d (h)	d_{sm} (m)	t_d (h)	d_{sm} (m)	t_d (h)	d_{sm} (m)
0.00	0.0000	25.88	0.0835	212.67	0.1422	388.83	0.1718
0.10	0.0145	30.50	0.0917	220.00	0.1433	440.62	0.1825
0.25	0.0191	46.18	0.1108	263.77	0.1471	455.08	0.1843
0.50	0.0217	50.22	0.1127	286.85	0.1507	462.75	0.1845
0.75	0.0235	54.03	0.1132	293.92	0.1519	503.63	0.1879
1.00	0.0267	117.30	0.1287	311.12	0.1540	511.08	0.1912
1.82	0.0298	125.43	0.1314	318.77	0.1555	526.97	0.1919
2.78	0.0316	141.13	0.1335	336.22	0.1576	534.87	0.1921
4.00	0.0368	165.18	0.1361	343.10	0.1604	557.12	0.1934
5.48	0.0394	172.50	0.1387	358.85	0.1643	623.70	0.1978
7.08	0.0466	189.25	0.1395	366.75	0.1656	648.32	0.1988
22.63	0.0781	196.42	0.1408	382.93	0.1697	670.88	0.2003

Test M2J1

d_{50}	h	U	U_c	U/U_c	B/D_{pc}	B/h	h/D_{pc}
0.086 mm	0.20 m	0.258 m/s	0.322 m/s	0.80	10.0	10.0	1.0

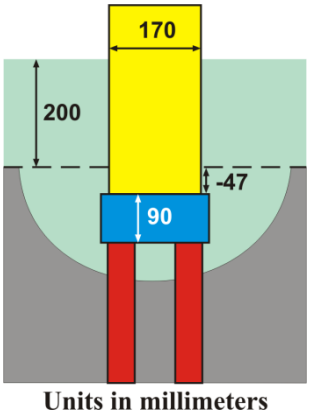

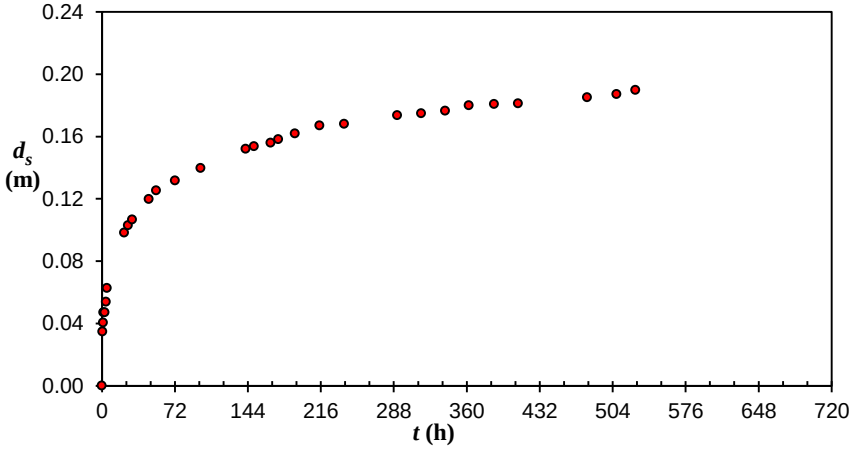

Scour depth measurements in the test M2J1

t_d (h)	d_{sm} (m)		t_d (h)	d_{sm} (m)		t_d (h)	d_{sm} (m)		t_d (h)	d_{sm} (m)
0.00	0.0000		25.95	0.1029		166.47	0.1560		362.22	0.1800
0.50	0.0348		29.98	0.1066		174.03	0.1581		386.93	0.1807
1.10	0.0404		46.43	0.1197		190.53	0.1619		410.62	0.1811
1.50	0.0470		53.68	0.1253		214.68	0.1669		479.00	0.1851
2.68	0.0470		72.13	0.1317		239.10	0.1680		507.97	0.1872
4.05	0.0539		97.55	0.1396		291.57	0.1736		526.60	0.1898
4.93	0.0626		141.82	0.1519		315.18	0.1747			
21.90	0.0981		150.05	0.1536		338.68	0.1765			

Test M2K1

d_{50}	h	U	U_c	U/U_c	B/D_{pc}	B/h	h/D_{pc}
0.086 mm	0.20 m	0.258 m/s	0.322 m/s	0.80	10.0	10.0	1.0

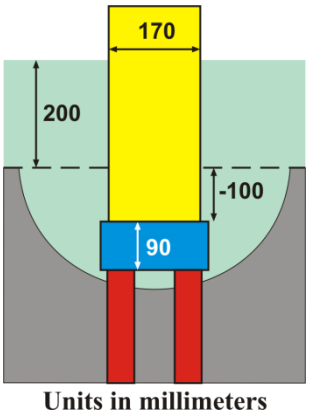

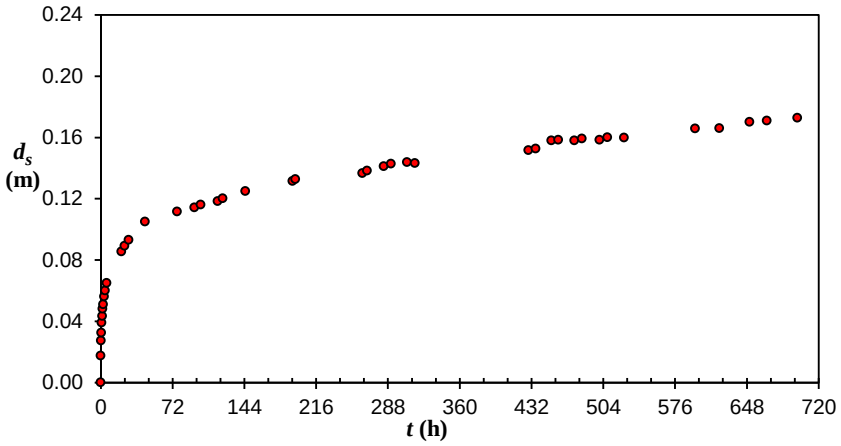

Scour depth measurements in the test M2K1

t_d (h)	d_{sm} (m)	t_d (h)	d_{sm} (m)	t_d (h)	d_{sm} (m)	t_d (h)	d_{sm} (m)
0.00	0.0000	52.35	0.1085	355.10	0.1462	698.77	0.1728
0.10	0.0175	76.77	0.1116	363.62	0.1479	761.45	0.1755
0.30	0.0273	93.90	0.1143	429.07	0.1516	787.05	0.1780
0.60	0.0324	100.40	0.1160	436.37	0.1527	818.93	0.1787
1.00	0.0391	117.22	0.1183	452.20	0.1580	843.55	0.1808
1.50	0.0434	122.50	0.1202	458.93	0.1584	865.77	0.1826
1.90	0.0480	145.02	0.1249	475.15	0.1580	932.68	0.1884
2.48	0.0510	192.42	0.1315	482.72	0.1592	955.63	0.1917
3.30	0.0560	195.27	0.1327	500.42	0.1584	979.87	0.1919
4.38	0.0600	262.57	0.1365	508.28	0.1601	1004.05	0.1935
5.82	0.0650	267.18	0.1383	524.83	0.1597	1011.85	0.1944
20.77	0.0855	283.92	0.1412	596.35	0.1657	1029.23	0.1958
23.92	0.0892	291.08	0.1428	620.60	0.1660	1035.58	0.1960
27.90	0.0931	307.25	0.1437	650.77	0.1701	1099.97	0.1978
44.43	0.1050	315.15	0.1431	668.03	0.1709	1125.82	0.1987

Test M2L1

d_{50}	h	U	U_c	U/U_c	B/D_{pc}	B/h	h/D_{pc}
0.086 mm	0.20 m	0.258 m/s	0.322 m/s	0.80	10.0	10.0	1.0

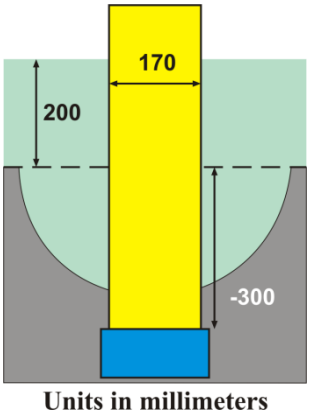

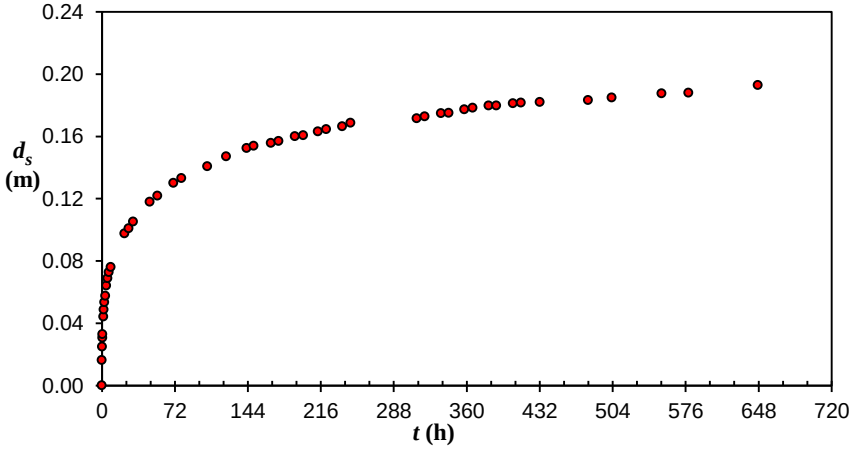

Scour depth measurements in the test M2L1

t_d (h)	d_{sm} (m)	t_d (h)	d_{sm} (m)	t_d (h)	d_{sm} (m)	t_d (h)	d_{sm} (m)
0.00	0.0000	8.80	0.0760	166.75	0.1557	357.62	0.1773
0.10	0.0163	22.32	0.0976	174.47	0.1569	365.83	0.1782
0.25	0.0248	26.50	0.1009	190.67	0.1600	381.65	0.1797
0.43	0.0307	30.85	0.1052	198.68	0.1606	389.20	0.1798
0.58	0.0329	47.13	0.1179	213.37	0.1630	405.70	0.1812
1.42	0.0442	54.85	0.1218	221.45	0.1646	413.45	0.1815
1.93	0.0487	70.67	0.1301	237.33	0.1664	432.17	0.1819
2.53	0.0534	78.50	0.1330	245.30	0.1687	479.92	0.1833
3.37	0.0575	103.95	0.1408	310.63	0.1715	503.13	0.1848
4.47	0.0640	122.67	0.1471	318.57	0.1728	552.37	0.1875
5.58	0.0688	142.88	0.1525	334.58	0.1747	578.78	0.1880
6.92	0.0727	149.87	0.1538	342.42	0.1749	647.45	0.1929

Test M3E1

d_{50}	h	U	U_c	U/U_c	B/D_{pc}	B/h	h/D_{pc}
0.086 mm	0.20 m	0.258 m/s	0.322 m/s	0.80	10.0	10.0	1.0

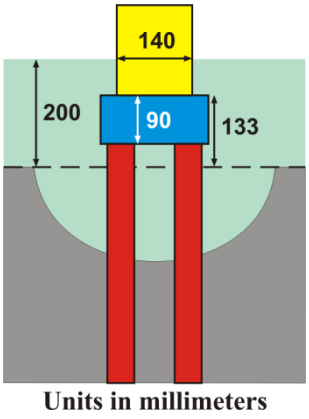

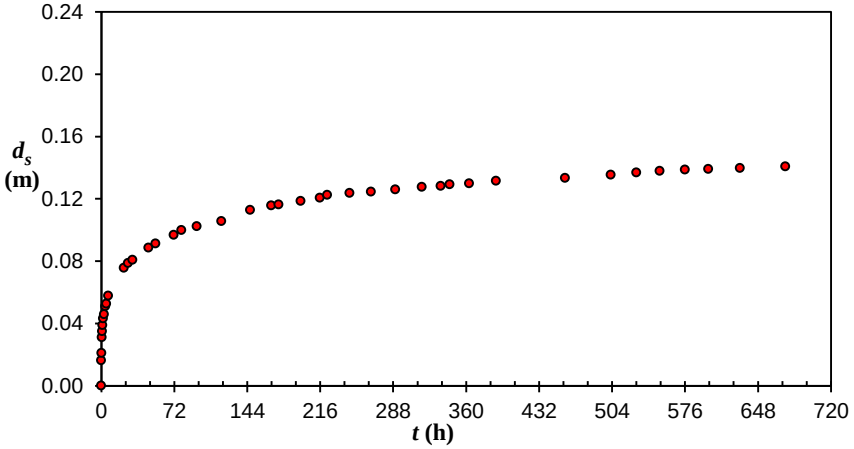

Scour depth measurements in the test M3E1

t_d (h)	d_{sm} (m)	t_d (h)	d_{sm} (m)	t_d (h)	d_{sm} (m)	t_d (h)	d_{sm} (m)
0.00	0.0000	22.43	0.0755	174.92	0.1163	389.53	0.1315
0.10	0.0162	26.53	0.0787	196.78	0.1185	457.77	0.1334
0.28	0.0210	31.00	0.0808	215.62	0.1206	502.85	0.1354
0.60	0.0311	46.57	0.0886	223.15	0.1224	527.98	0.1367
0.85	0.0349	53.57	0.0913	245.23	0.1236	551.22	0.1378
1.18	0.0388	71.58	0.0967	266.15	0.1244	575.98	0.1386
2.00	0.0432	79.03	0.0999	290.20	0.1260	599.18	0.1390
2.77	0.0459	94.18	0.1022	316.50	0.1276	630.17	0.1397
3.98	0.0510	118.43	0.1056	335.03	0.1282	674.98	0.1408
5.15	0.0525	147.07	0.1128	343.73	0.1293		
7.00	0.0578	167.87	0.1157	363.07	0.1298		

Test M3F1

d_{50}	h	U	U_c	U/U_c	B/D_{pc}	B/h	h/D_{pc}
0.086 mm	0.20 m	0.258 m/s	0.322 m/s	0.80	10.0	10.0	1.0

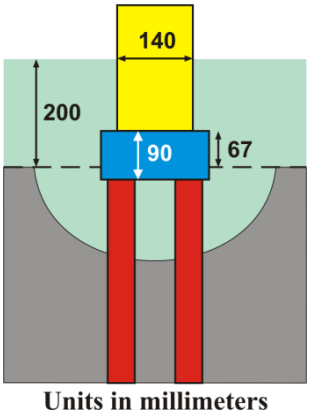

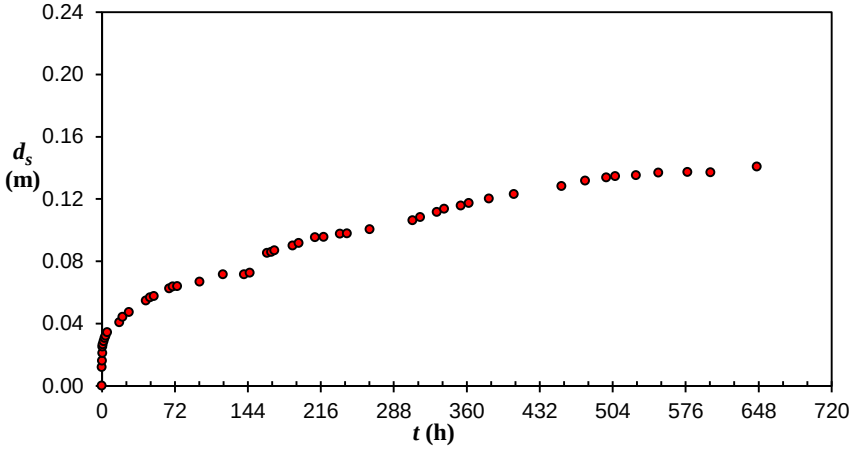

Scour depth measurements in the test M3F1

t_d (h)	d_{sm} (m)		t_d (h)	d_{sm} (m)		t_d (h)	d_{sm} (m)		t_d (h)	d_{sm} (m)
0.00	0.0000		43.38	0.0546		188.33	0.0899		382.03	0.1202
0.10	0.0120		47.62	0.0567		194.20	0.0917		406.58	0.1230
0.30	0.0160		51.32	0.0576		210.40	0.0954		453.70	0.1281
0.50	0.0210		66.55	0.0625		219.03	0.0956		476.87	0.1316
0.73	0.0250		70.05	0.0636		235.02	0.0975		497.68	0.1337
1.00	0.0265		74.32	0.0638		241.88	0.0978		506.78	0.1346
1.80	0.0286		96.42	0.0668		264.47	0.1004		527.03	0.1351
2.82	0.0307		119.45	0.0714		306.77	0.1063		549.35	0.1369
3.83	0.0321		140.28	0.0714		314.12	0.1082		577.82	0.1373
5.17	0.0344		146.10	0.0726		330.47	0.1116		600.67	0.1371
17.15	0.0406		162.97	0.0853		337.95	0.1135		646.32	0.1406
20.50	0.0441		167.02	0.0858		354.15	0.1157			
26.78	0.0472		170.20	0.0869		362.13	0.1172			

Test M3H1

d_{50}	h	U	U_c	U/U_c	B/D_{pc}	B/h	h/D_{pc}
0.086 mm	0.20 m	0.258 m/s	0.322 m/s	0.80	10.0	10.0	1.0

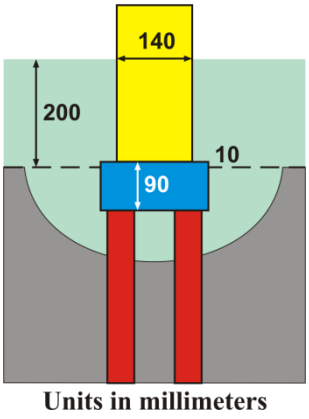

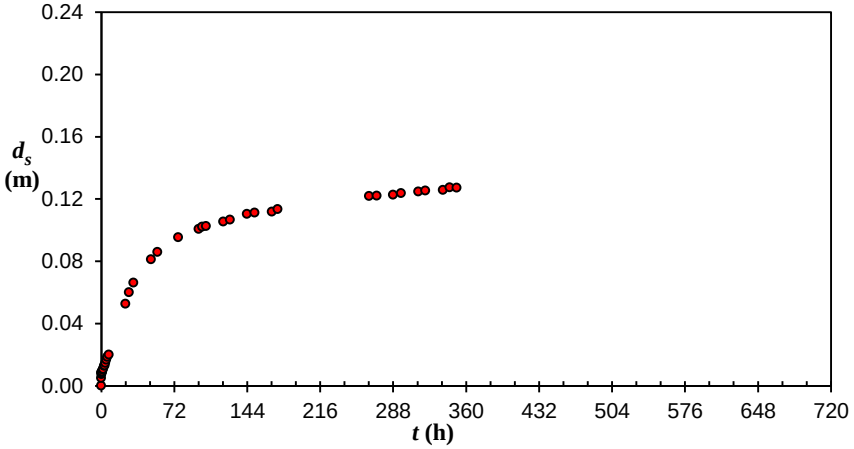

Scour depth measurements in the test M3H1

t_d (h)	d_{sm} (m)	t_d (h)	d_{sm} (m)	t_d (h)	d_{sm} (m)	t_d (h)	d_{sm} (m)
0.00	0.0000	2.85	0.0127	55.55	0.0859	174.22	0.1134
0.08	0.0050	3.52	0.0130	75.85	0.0954	264.32	0.1218
0.17	0.0074	3.98	0.0147	96.08	0.1006	271.77	0.1220
0.25	0.0083	4.93	0.0167	99.72	0.1020	288.13	0.1227
0.38	0.0087	6.03	0.0185	103.58	0.1024	295.88	0.1236
0.53	0.0085	7.67	0.0200	120.58	0.1053	312.80	0.1247
0.72	0.0089	24.08	0.0525	127.23	0.1066	319.92	0.1252
0.97	0.0090	27.40	0.0599	143.93	0.1104	337.27	0.1257
1.38	0.0102	31.87	0.0662	151.47	0.1112	344.00	0.1273
1.83	0.0108	49.27	0.0811	168.57	0.1118	350.80	0.1271

Test M3I1

d_{50}	h	U	U_c	U/U_c	B/D_{pc}	B/h	h/D_{pc}
0.086 mm	0.20 m	0.258 m/s	0.322 m/s	0.80	10.0	10.0	1.0

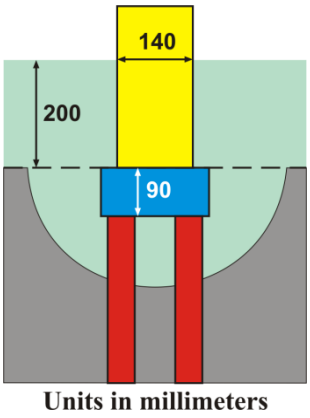

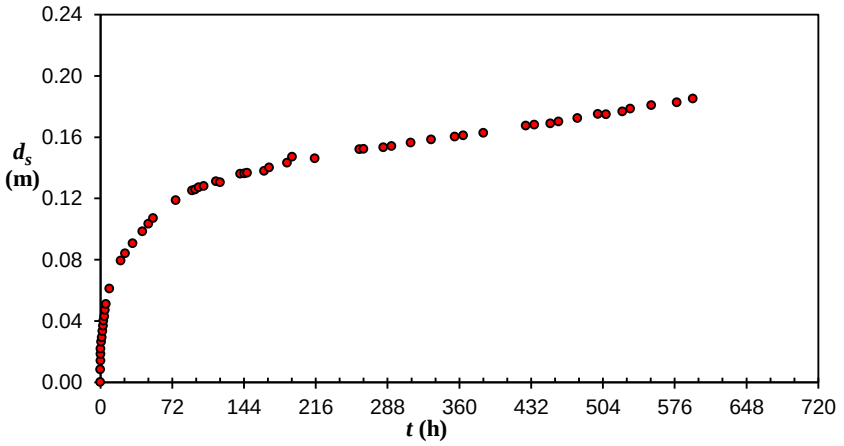

Scour depth measurements in the test M3I1

t_d (h)	d_{sm} (m)	t_d (h)	d_{sm} (m)	t_d (h)	d_{sm} (m)	t_d (h)	d_{sm} (m)
0.00	0.0000	9.08	0.0610	140.43	0.1360	355.65	0.1603
0.08	0.0082	20.35	0.0793	144.48	0.1362	363.90	0.1611
0.17	0.0140	24.85	0.0841	147.15	0.1365	384.28	0.1626
0.25	0.0182	32.37	0.0906	164.48	0.1379	426.95	0.1674
0.42	0.0218	42.35	0.0984	169.22	0.1401	435.47	0.1680
0.88	0.0264	48.20	0.1034	187.23	0.1431	451.33	0.1689
1.45	0.0292	52.88	0.1071	192.43	0.1470	459.57	0.1701
2.03	0.0332	75.67	0.1188	215.12	0.1461	478.67	0.1723
2.68	0.0368	91.93	0.1251	259.97	0.1519	499.13	0.1751
3.12	0.0400	95.13	0.1258	263.93	0.1523	507.43	0.1748
4.08	0.0430	98.65	0.1272	283.87	0.1533	523.83	0.1767
4.62	0.0470	103.65	0.1279	292.13	0.1540	531.60	0.1785
5.62	0.0510	116.18	0.1311	311.20	0.1563	552.72	0.1808
6.53	0.0526	120.22	0.1305	331.95	0.1584	578.17	0.1826
8.05	0.0586	124.10	0.1331	339.55	0.1592	594.27	0.1850

Test M3J1

d_{50}	h	U	U_c	U/U_c	B/D_{pc}	B/h	h/D_{pc}
0.086 mm	0.20 m	0.258 m/s	0.322 m/s	0.80	10.0	10.0	1.0

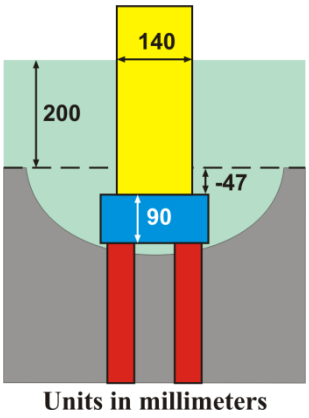

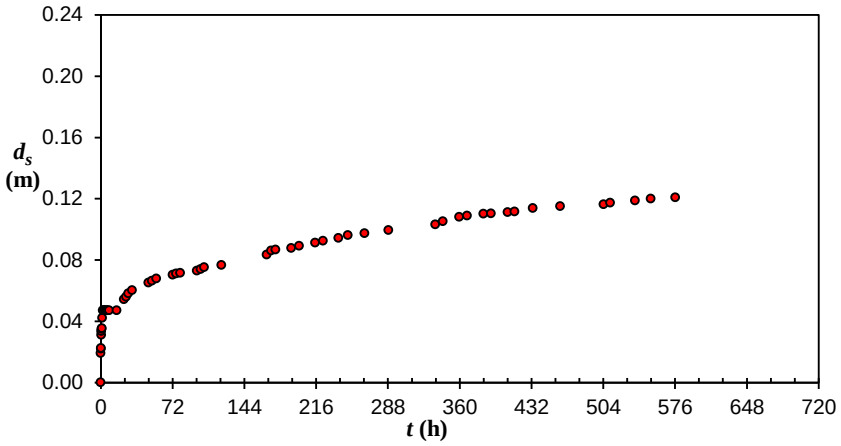

Scour depth measurements in the test M3J1

t_d (h)	d_{sm} (m)	t_d (h)	d_{sm} (m)	t_d (h)	d_{sm} (m)	t_d (h)	d_{sm} (m)
0.00	0.0000	8.58	0.0470	121.10	0.0766	367.43	0.1089
0.03	0.0191	16.00	0.0470	166.43	0.0835	383.88	0.1102
0.12	0.0220	23.20	0.0543	170.92	0.0861	391.42	0.1104
0.32	0.0225	25.45	0.0559	175.45	0.0866	408.15	0.1111
0.50	0.0311	27.63	0.0582	191.03	0.0878	415.30	0.1116
0.70	0.0335	31.55	0.0601	198.93	0.0891	433.47	0.1137
0.95	0.0350	48.03	0.0652	214.98	0.0912	460.78	0.1151
1.20	0.0354	51.48	0.0664	223.13	0.0924	504.33	0.1162
1.63	0.0421	55.83	0.0678	238.38	0.0942	511.17	0.1173
2.20	0.0470	72.20	0.0702	248.00	0.0962	535.95	0.1187
3.00	0.0470	75.83	0.0711	264.68	0.0973	551.75	0.1199
3.67	0.0470	79.67	0.0714	288.70	0.0994	576.28	0.1208
4.75	0.0470	96.50	0.0729	335.75	0.1031		
5.87	0.0470	100.38	0.0739	343.30	0.1052		
7.33	0.0470	103.72	0.0751	359.70	0.1080		

Test M3K1

d_{50}	h	U	U_c	U/U_c	B/D_{pc}	B/h	h/D_{pc}
0.086 mm	0.20 m	0.258 m/s	0.322 m/s	0.80	10.0	10.0	1.0

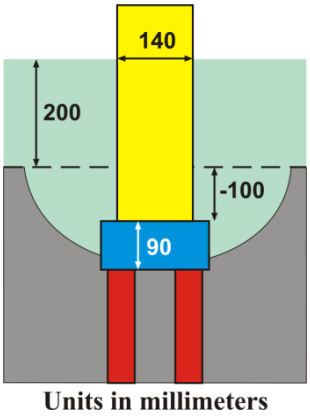

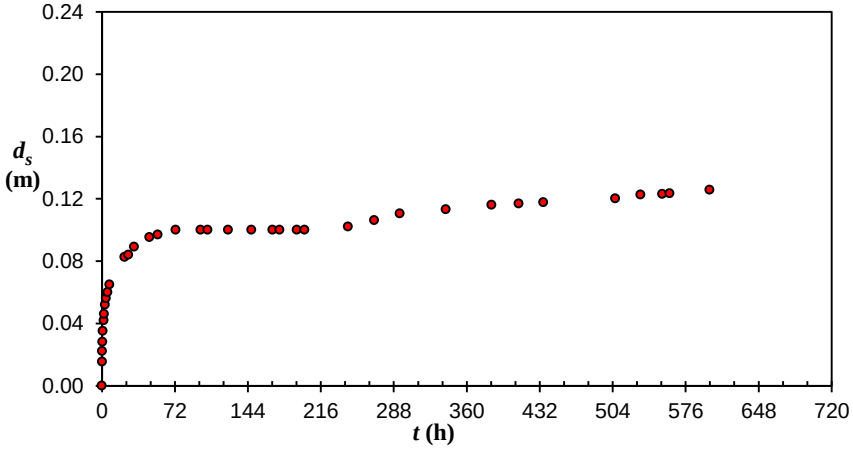

Scour depth measurements in the test M3K1

t_d (h)	d_{sm} (m)		t_d (h)	d_{sm} (m)		t_d (h)	d_{sm} (m)		t_d (h)	d_{sm} (m)
0.00	0.0000		7.50	0.0649		147.45	0.1000		411.47	0.1169
0.12	0.0155		22.20	0.0826		168.58	0.1000		435.63	0.1178
0.30	0.0221		26.25	0.0840		175.42	0.1000		506.67	0.1202
0.53	0.0282		31.75	0.0891		192.35	0.1000		531.48	0.1226
0.83	0.0351		47.00	0.0953		200.00	0.1000		552.87	0.1231
1.70	0.0420		55.17	0.0970		242.87	0.1020		560.13	0.1234
2.25	0.0460		72.80	0.1000		268.80	0.1061		599.60	0.1258
3.17	0.0520		97.53	0.1000		294.05	0.1105			
4.12	0.0560		104.40	0.1000		339.30	0.1131			
5.62	0.0600		124.58	0.1000		384.58	0.1160			

Test M3L1

d_{50}	h	U	U_c	U/U_c	B/D_{pc}	B/h	h/D_{pc}
0.086 mm	0.20 m	0.258 m/s	0.322 m/s	0.80	10.0	10.0	1.0

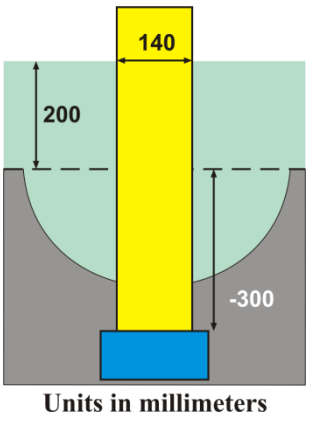

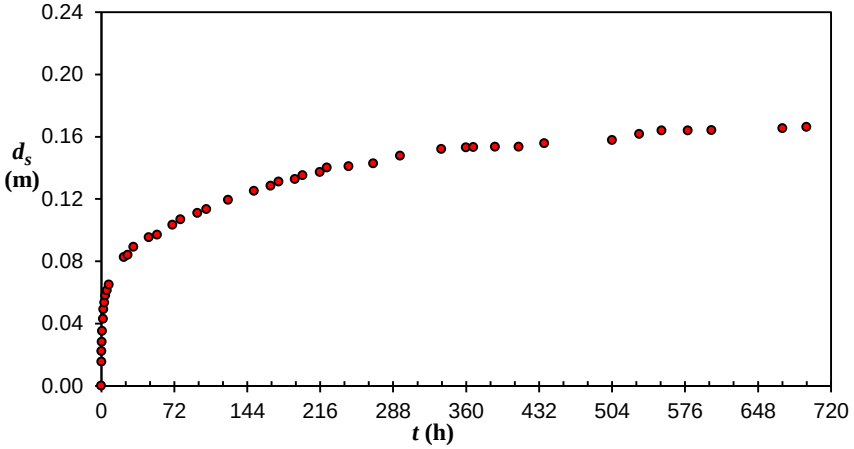

Scour depth measurements in the test M3L1

t_d (h)	d_{sm} (m)	t_d (h)	d_{sm} (m)	t_d (h)	d_{sm} (m)	t_d (h)	d_{sm} (m)
0.00	0.0000	22.20	0.0826	167.30	0.1283	367.30	0.1533
0.12	0.0155	26.25	0.0840	175.13	0.1310	388.70	0.1535
0.30	0.0221	31.75	0.0891	191.25	0.1327	412.07	0.1535
0.53	0.0282	47.00	0.0953	198.87	0.1351	437.28	0.1557
0.83	0.0351	55.17	0.0970	215.67	0.1372	504.22	0.1578
1.70	0.0430	70.33	0.1034	222.60	0.1401	530.95	0.1617
2.25	0.0491	78.05	0.1069	244.02	0.1410	552.92	0.1639
3.17	0.0535	95.02	0.1110	268.37	0.1427	578.77	0.1640
4.12	0.0580	103.68	0.1134	294.87	0.1477	602.25	0.1642
5.62	0.0612	125.08	0.1193	335.57	0.1520	672.33	0.1654
7.50	0.0649	150.82	0.1251	359.83	0.1531	696.08	0.1661

Test M4E1

d_{50}	h	U	U_c	U/U_c	B/D_{pc}	B/h	h/D_{pc}
0.086 mm	0.20 m	0.258 m/s	0.322 m/s	0.80	10.0	10.0	1.0

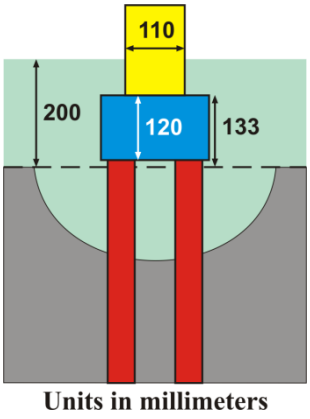

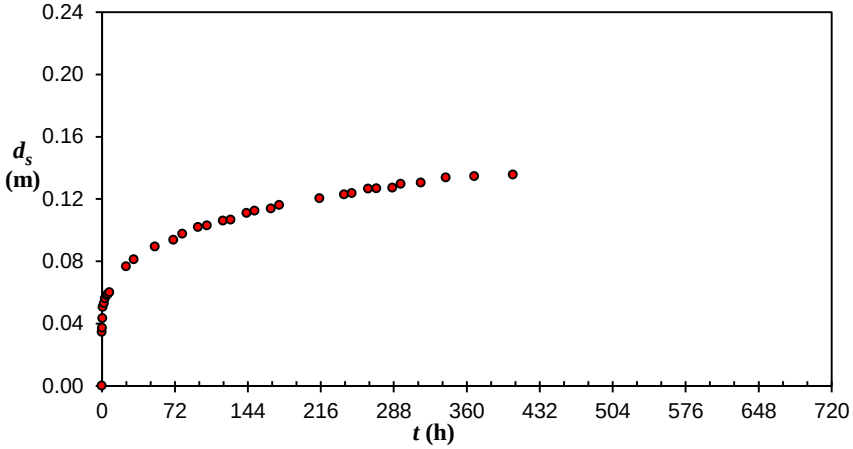

Scour depth measurements in the test M4E1

t_d (h)	d_{sm} (m)		t_d (h)	d_{sm} (m)		t_d (h)	d_{sm} (m)		t_d (h)	d_{sm} (m)
0.00	0.0000		7.53	0.0600		127.13	0.1066		270.88	0.1268
0.10	0.0346		24.05	0.0767		142.90	0.1110		286.65	0.1272
0.28	0.0372		31.40	0.0811		150.83	0.1125		294.98	0.1296
0.55	0.0434		52.33	0.0893		166.95	0.1138		314.95	0.1304
1.02	0.0505		70.75	0.0937		175.00	0.1161		339.58	0.1338
2.17	0.0531		79.33	0.0975		214.92	0.1204		367.58	0.1346
3.20	0.0560		94.82	0.1018		239.05	0.1228		405.80	0.1355
4.57	0.0581		103.65	0.1029		246.82	0.1236			
5.88	0.0588		119.55	0.1060		262.90	0.1266			

Test M4F1

d_{50}	h	U	U_c	U/U_c	B/D_{pc}	B/h	h/D_{pc}
0.086 mm	0.20 m	0.258 m/s	0.322 m/s	0.80	10.0	10.0	1.0

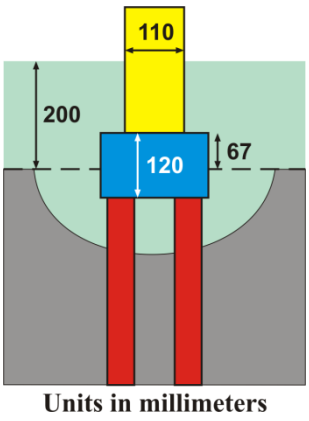

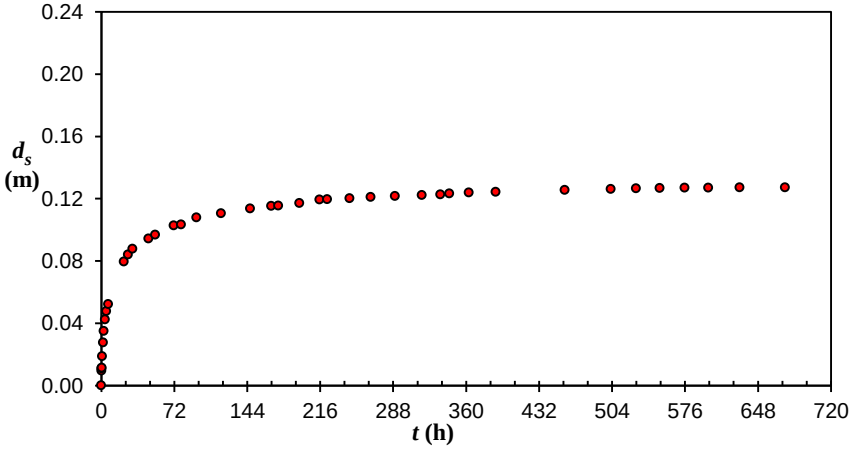

Scour depth measurements in the test M4F1

t_d (h)	d_{sm} (m)	t_d (h)	d_{sm} (m)	t_d (h)	d_{sm} (m)	t_d (h)	d_{sm} (m)
0.00	0.0000	26.43	0.0840	195.58	0.1170	457.55	0.1256
0.12	0.0094	30.92	0.0877	215.42	0.1194	502.75	0.1262
0.27	0.0110	46.50	0.0943	223.05	0.1196	527.78	0.1266
0.50	0.0114	53.38	0.0968	245.00	0.1202	551.12	0.1267
1.00	0.0187	71.53	0.1028	266.05	0.1210	575.72	0.1269
1.92	0.0276	78.85	0.1034	290.00	0.1216	599.08	0.1269
2.53	0.0349	94.08	0.1079	316.38	0.1222	629.90	0.1272
3.68	0.0424	118.25	0.1106	334.80	0.1227	674.92	0.1272
4.95	0.0477	146.85	0.1136	343.67	0.1233		
7.00	0.0522	167.77	0.1152	362.83	0.1238		
22.25	0.0794	174.73	0.1155	389.42	0.1242		

Test M4G1

d_{50}	h	U	U_c	U/U_c	B/D_{pc}	B/h	h/D_{pc}
0.086 mm	0.20 m	0.258 m/s	0.322 m/s	0.80	10.0	10.0	1.0

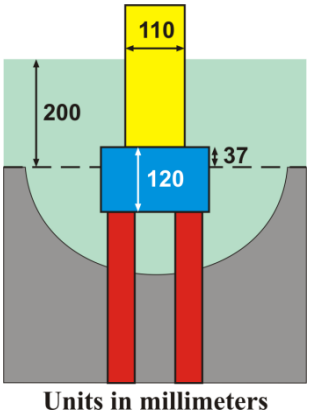

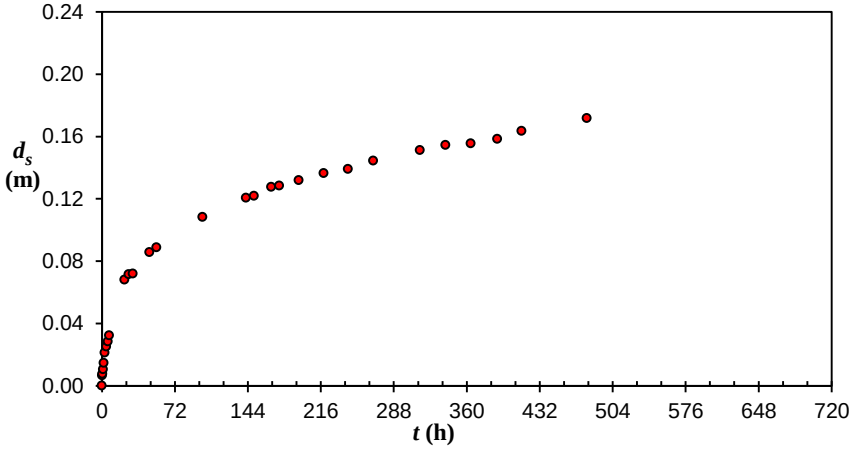

Scour depth measurements in the test M4G1

t_d (h)	d_{sm} (m)		t_d (h)	d_{sm} (m)		t_d (h)	d_{sm} (m)		t_d (h)	d_{sm} (m)
0.00	0.0000		7.23	0.0323		150.25	0.1219		339.27	0.1545
0.13	0.0065		22.47	0.0679		167.15	0.1275		363.97	0.1554
0.50	0.0076		26.38	0.0715		175.02	0.1284		390.32	0.1583
1.13	0.0104		30.62	0.0720		194.18	0.1319		414.27	0.1635
1.97	0.0145		47.07	0.0856		218.90	0.1364		478.47	0.1717
2.82	0.0211		53.92	0.0888		242.93	0.1390			
4.30	0.0250		99.28	0.1082		267.97	0.1445			
5.82	0.0284		142.35	0.1205		313.87	0.1511			

Test M4H1

d_{50}	h	U	U_c	U/U_c	B/D_{pc}	B/h	h/D_{pc}
0.086 mm	0.20 m	0.258 m/s	0.322 m/s	0.80	10.0	10.0	1.0

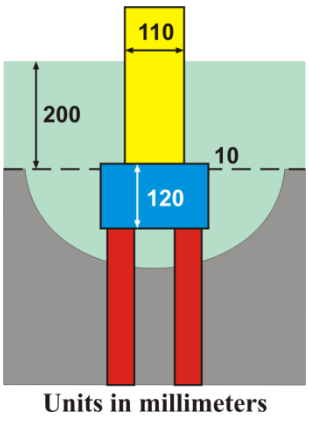

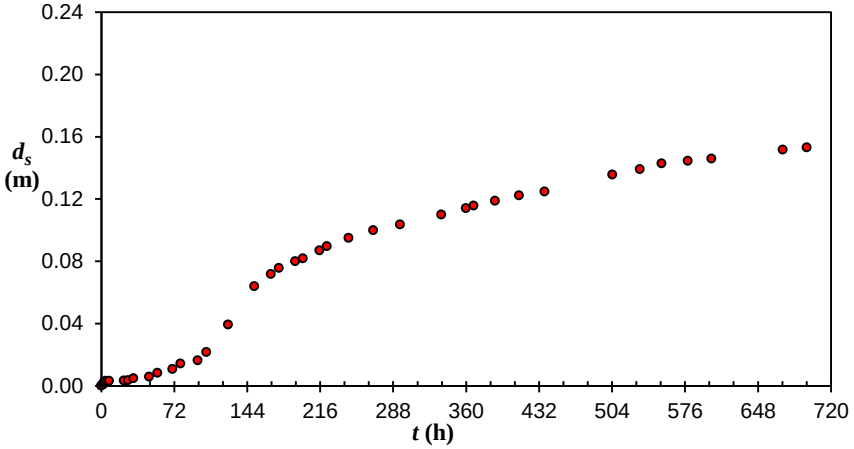

Scour depth measurements in the test M4H1

t_d (h)	d_{sm} (m)	t_d (h)	d_{sm} (m)	t_d (h)	d_{sm} (m)	t_d (h)	d_{sm} (m)
0.00	0.0000	47.17	0.0057	191.35	0.0800	388.80	0.1188
1.80	0.0007	55.35	0.0082	199.05	0.0817	412.17	0.1223
2.42	0.0021	70.40	0.0107	215.53	0.0868	437.53	0.1247
3.27	0.0025	78.23	0.0141	222.77	0.0895	504.28	0.1355
4.28	0.0030	95.10	0.0163	244.10	0.0949	531.43	0.1391
5.67	0.0029	103.85	0.0215	268.57	0.0998	553.02	0.1428
7.72	0.0031	125.18	0.0392	294.95	0.1035	579.02	0.1445
22.30	0.0033	151.05	0.0638	335.75	0.1098	602.33	0.1459
26.43	0.0035	167.38	0.0717	359.87	0.1140	672.52	0.1515
31.83	0.0048	175.32	0.0755	367.47	0.1157	696.17	0.1531

Test M4I1

d_{50}	h	U	U_c	U/U_c	B/D_{pc}	B/h	h/D_{pc}
0.086 mm	0.20 m	0.258 m/s	0.322 m/s	0.80	10.0	10.0	1.0

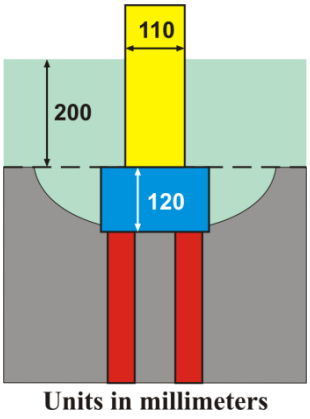

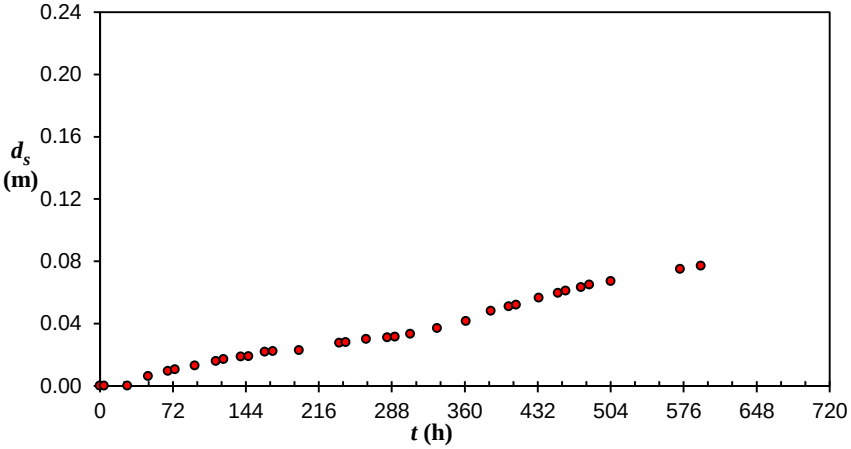

Scour depth measurements in the test M4I1

t_d (h)	d_{sm} (m)		t_d (h)	d_{sm} (m)		t_d (h)	d_{sm} (m)		t_d (h)	d_{sm} (m)
0.00	0.0000		138.95	0.0188		291.30	0.0314		459.67	0.0610
4.00	0.0000		146.58	0.0190		306.43	0.0333		474.93	0.0633
27.00	0.0000		162.67	0.0218		332.92	0.0369		483.00	0.0650
47.62	0.0062		170.63	0.0221		361.25	0.0415		504.25	0.0672
67.28	0.0094		196.42	0.0228		385.83	0.0481		572.50	0.0749
74.08	0.0105		236.38	0.0275		403.62	0.0509		593.00	0.0770
93.78	0.0130		242.53	0.0280		410.72	0.0520			
114.47	0.0159		262.67	0.0301		433.28	0.0565			
122.08	0.0170		283.60	0.0310		452.00	0.0596			

Test M5D1

d_{50}	h	U	U_c	U/U_c	B/D_{pc}	B/h	h/D_{pc}
0.086 mm	0.20 m	0.258 m/s	0.322 m/s	0.80	10.0	10.0	1.0

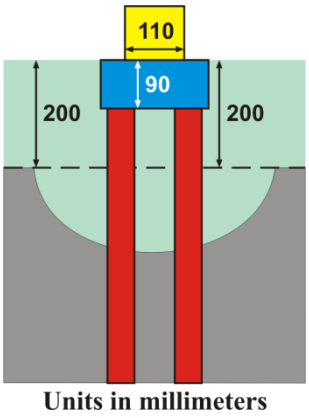

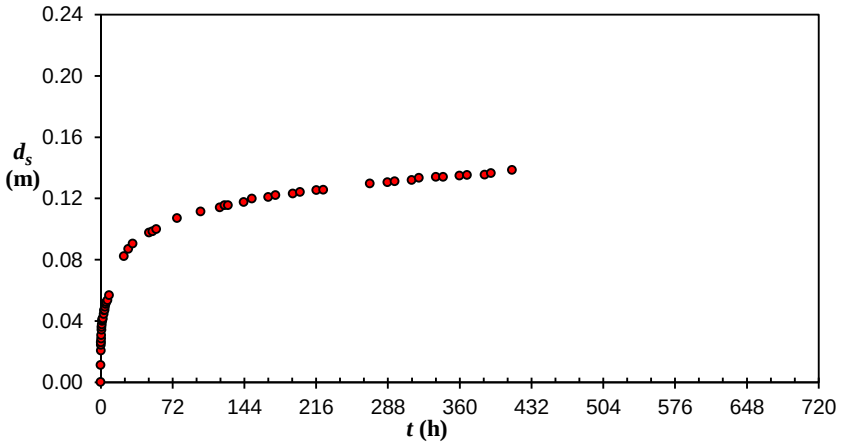

Scour depth measurements in the test M5D1

t_d (h)	d_{sm} (m)	t_d (h)	d_{sm} (m)	t_d (h)	d_{sm} (m)	t_d (h)	d_{sm} (m)
0.00	0.0000	2.25	0.0416	55.83	0.0998	270.12	0.1296
0.07	0.0111	3.20	0.0443	76.70	0.1070	287.72	0.1304
0.15	0.0205	3.50	0.0468	100.40	0.1113	295.05	0.1311
0.23	0.0243	4.00	0.0471	119.58	0.1141	312.05	0.1319
0.32	0.0261	4.50	0.0491	124.22	0.1154	319.32	0.1334
0.40	0.0258	5.00	0.0509	127.75	0.1155	336.28	0.1340
0.50	0.0283	5.68	0.0521	143.52	0.1174	343.52	0.1339
0.67	0.0307	6.87	0.0534	151.62	0.1198	359.83	0.1347
0.83	0.0341	8.47	0.0567	168.10	0.1207	367.58	0.1351
1.00	0.0359	23.30	0.0822	175.28	0.1221	385.17	0.1353
1.25	0.0375	27.58	0.0868	192.75	0.1230	391.42	0.1364
1.50	0.0398	32.12	0.0904	199.83	0.1241	412.67	0.1385
1.75	0.0405	48.67	0.0975	216.25	0.1252		
2.00	0.0413	52.17	0.0983	223.42	0.1255		

Test M5E1

d_{50}	h	U	U_c	U/U_c	B/D_{pc}	B/h	h/D_{pc}
0.086 mm	0.20 m	0.258 m/s	0.322 m/s	0.80	10.0	10.0	1.0

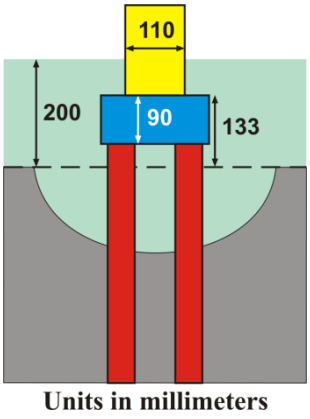

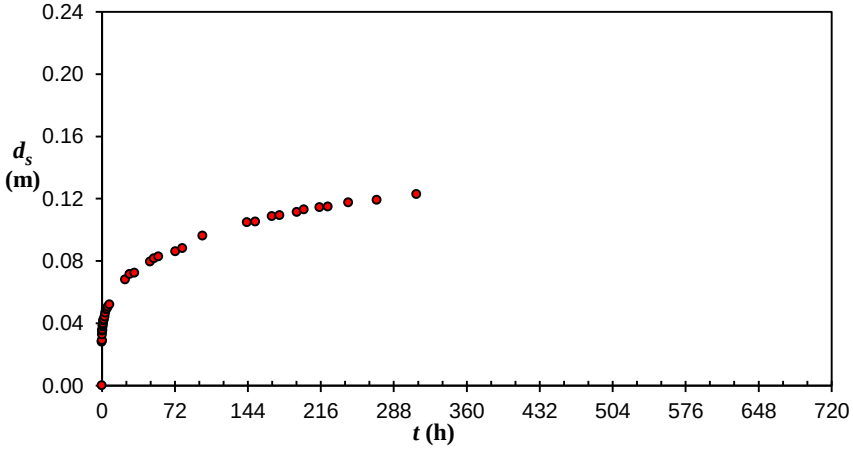

Scour depth measurements in the test M5E1

t_d (h)	d_{sm} (m)	t_d (h)	d_{sm} (m)	t_d (h)	d_{sm} (m)	t_d (h)	d_{sm} (m)
0.00	0.0000	1.25	0.0398	22.90	0.0681	151.42	0.1052
0.05	0.0280	1.50	0.0418	27.55	0.0714	167.75	0.1086
0.10	0.0286	1.75	0.0420	32.00	0.0724	175.38	0.1093
0.20	0.0289	2.00	0.0424	47.55	0.0795	192.37	0.1113
0.30	0.0326	2.95	0.0441	51.40	0.0816	199.25	0.1130
0.40	0.0351	3.52	0.0467	55.85	0.0828	214.83	0.1144
0.50	0.0354	4.17	0.0488	72.43	0.0860	222.92	0.1149
0.67	0.0358	4.85	0.0493	79.45	0.0881	243.33	0.1175
0.83	0.0378	6.00	0.0505	99.37	0.0962	271.13	0.1192
1.00	0.0389	7.62	0.0520	143.18	0.1047	310.55	0.1228

Test M5F1

d_{50}	h	U	U_c	U/U_c	B/D_{pc}	B/h	h/D_{pc}
0.086 mm	0.20 m	0.258 m/s	0.322 m/s	0.80	10.0	10.0	1.0

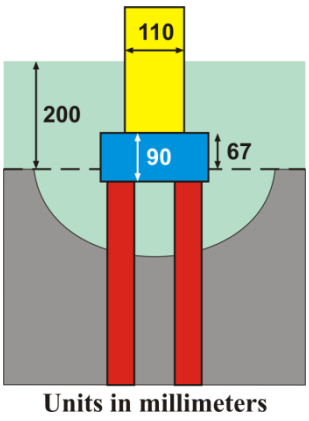

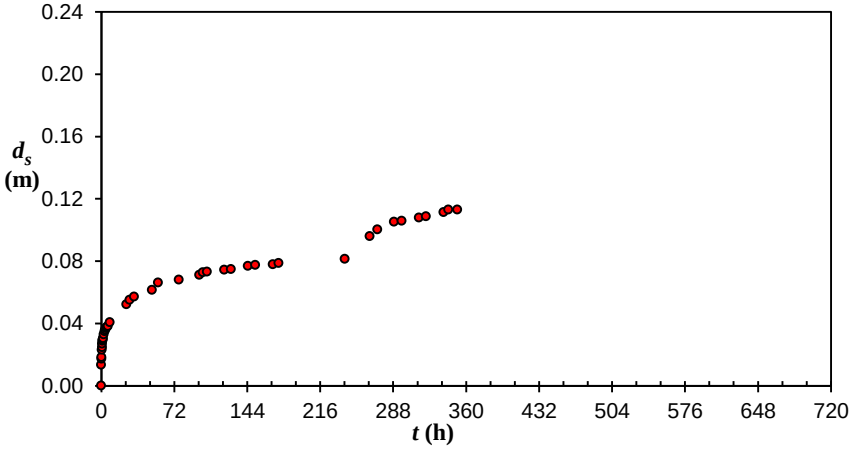

Scour depth measurements in the test M5F1

t_d (h)	d_{sm} (m)	t_d (h)	d_{sm} (m)	t_d (h)	d_{sm} (m)	t_d (h)	d_{sm} (m)
0.00	0.0000	3.57	0.0349	76.60	0.0680	265.00	0.0960
0.08	0.0134	4.13	0.0360	96.80	0.0711	272.47	0.1003
0.25	0.0173	4.62	0.0370	100.43	0.0728	288.87	0.1051
0.42	0.0183	5.60	0.0376	104.30	0.0731	296.58	0.1057
0.67	0.0230	6.72	0.0382	121.30	0.0744	313.50	0.1079
0.83	0.0246	8.35	0.0407	127.90	0.0748	320.63	0.1086
1.00	0.0270	24.83	0.0521	144.68	0.0768	337.95	0.1113
1.33	0.0288	28.10	0.0550	152.15	0.0774	342.73	0.1129
1.67	0.0296	32.57	0.0572	169.23	0.0779	351.43	0.1130
2.00	0.0305	50.05	0.0614	174.95	0.0786		
2.50	0.0328	56.23	0.0661	240.23	0.0813		

Test M5G1

d_{50}	h	U	U_c	U/U_c	B/D_{pc}	B/h	h/D_{pc}
0.086 mm	0.20 m	0.258 m/s	0.322 m/s	0.80	10.0	10.0	1.0

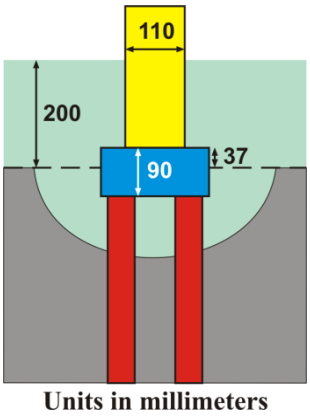

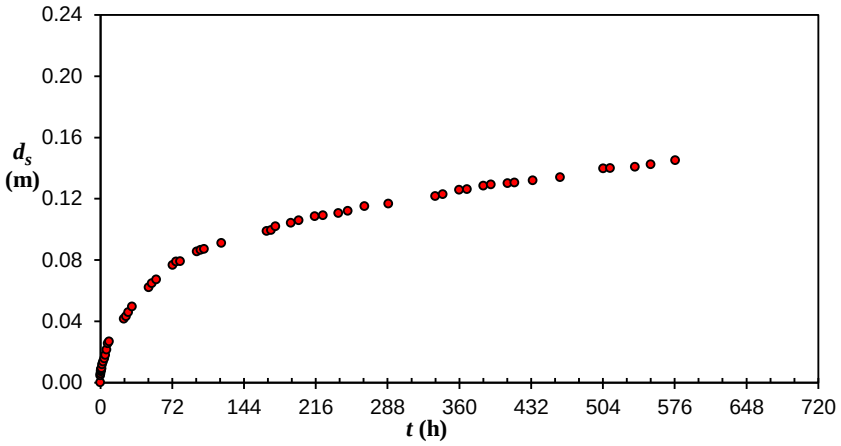

Scour depth measurements in the test M5G1

t_d (h)	d_{sm} (m)	t_d (h)	d_{sm} (m)	t_d (h)	d_{sm} (m)	t_d (h)	d_{sm} (m)
0.00	0.0000	8.75	0.0267	121.45	0.0910	360.07	0.1257
0.10	0.0045	23.58	0.0415	166.83	0.0988	367.75	0.1261
0.32	0.0057	25.78	0.0432	171.23	0.0995	384.18	0.1283
0.45	0.0072	28.00	0.0458	175.78	0.1018	391.75	0.1291
0.65	0.0078	31.87	0.0495	191.30	0.1042	408.50	0.1300
0.85	0.0085	48.50	0.0621	199.10	0.1058	415.58	0.1304
1.08	0.0089	51.63	0.0648	215.02	0.1084	433.78	0.1318
1.33	0.0093	56.17	0.0671	223.45	0.1090	461.10	0.1339
2.00	0.0118	72.55	0.0766	238.72	0.1105	504.45	0.1396
2.95	0.0135	76.10	0.0788	248.28	0.1120	511.53	0.1398
4.00	0.0156	79.97	0.0791	265.02	0.1151	536.28	0.1408
5.00	0.0178	96.80	0.0854	288.98	0.1166	552.08	0.1423
6.17	0.0214	100.67	0.0864	336.10	0.1217	576.60	0.1450
7.65	0.0254	104.00	0.0871	343.42	0.1229		

Test M5H1

d_{50}	h	U	U_c	U/U_c	B/D_{pc}	B/h	h/D_{pc}
0.086 mm	0.20 m	0.258 m/s	0.322 m/s	0.80	10.0	10.0	1.0

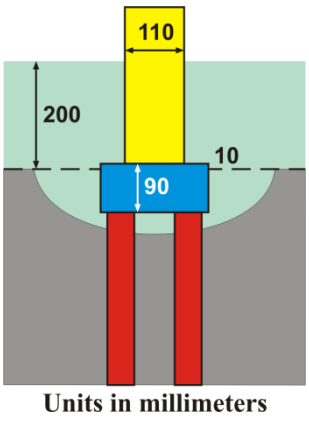

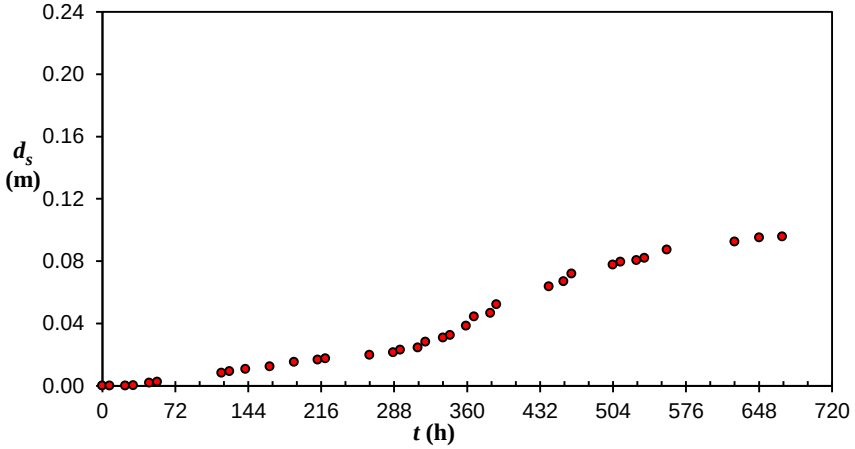

Scour depth measurements in the test M5H1

t_d (h)	d_{sm} (m)	t_d (h)	d_{sm} (m)	t_d (h)	d_{sm} (m)	t_d (h)	d_{sm} (m)
0.00	0.0000	165.32	0.0123	336.40	0.0308	503.68	0.0776
7.17	0.0000	189.33	0.0152	343.17	0.0325	511.28	0.0796
22.80	0.0000	212.63	0.0166	359.03	0.0384	527.07	0.0805
30.63	0.0002	220.22	0.0174	366.75	0.0443	535.05	0.0820
46.37	0.0019	263.82	0.0198	383.08	0.0467	557.15	0.0873
54.12	0.0024	287.07	0.0214	389.10	0.0521	623.97	0.0925
117.50	0.0083	294.00	0.0231	440.82	0.0636	648.32	0.0951
125.43	0.0092	311.47	0.0244	455.15	0.0669	671.07	0.0957
141.20	0.0108	318.83	0.0281	463.02	0.0720		

Test M5I1

d_{50}	h	U	U_c	U/U_c	B/D_{pc}	B/h	h/D_{pc}
0.086 mm	0.20 m	0.258 m/s	0.322 m/s	0.80	10.0	10.0	1.0

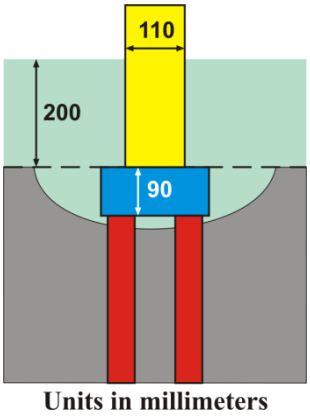

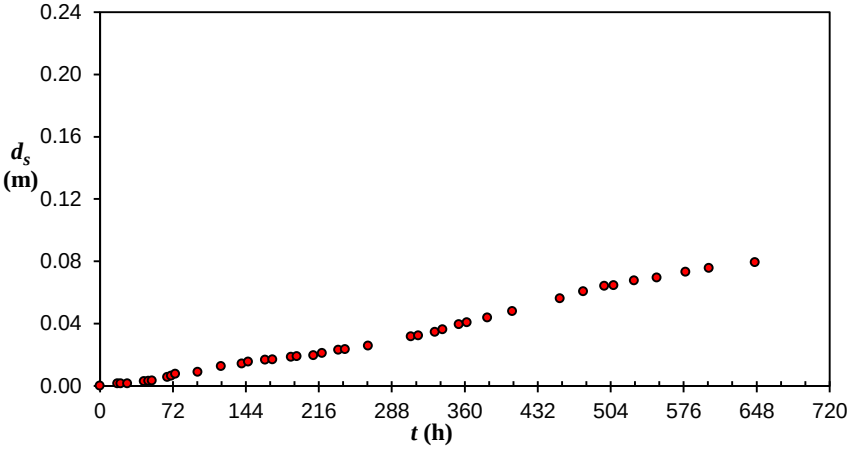

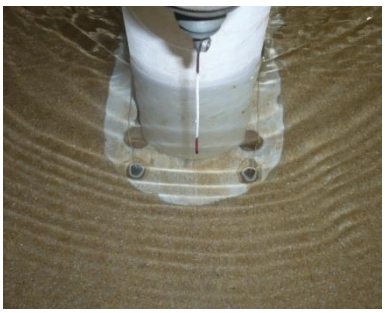

Scour depth measurements in the test M5I1

t_d (h)	d_{sm} (m)	t_d (h)	d_{sm} (m)	t_d (h)	d_{sm} (m)	t_d (h)	d_{sm} (m)
0.00	0.0000	96.60	0.0088	235.28	0.0230	406.97	0.0478
17.42	0.0015	119.67	0.0125	242.08	0.0235	453.92	0.0561
20.58	0.0015	140.17	0.0141	264.67	0.0256	477.08	0.0607
27.00	0.0015	146.28	0.0155	306.97	0.0316	497.75	0.0641
43.58	0.0028	163.17	0.0166	314.33	0.0322	506.97	0.0646
47.83	0.0032	170.37	0.0168	330.67	0.0346	527.25	0.0675
51.52	0.0034	188.52	0.0184	338.15	0.0361	549.53	0.0694
66.67	0.0055	194.42	0.0190	354.33	0.0394	577.87	0.0732
70.33	0.0063	210.58	0.0196	362.22	0.0406	600.88	0.0755
74.50	0.0076	219.33	0.0209	382.25	0.0437	646.50	0.0792

Test M6D1

d_{50}	h	U	U_c	U/U_c	B/D_{pc}	B/h	h/D_{pc}
0.086 mm	0.20 m	0.258 m/s	0.322 m/s	0.80	10.0	10.0	1.0

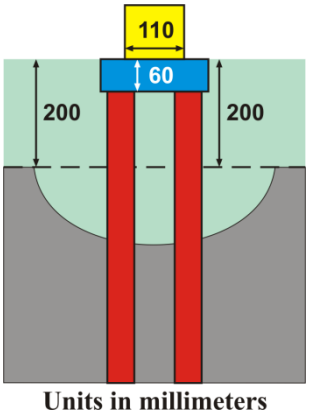

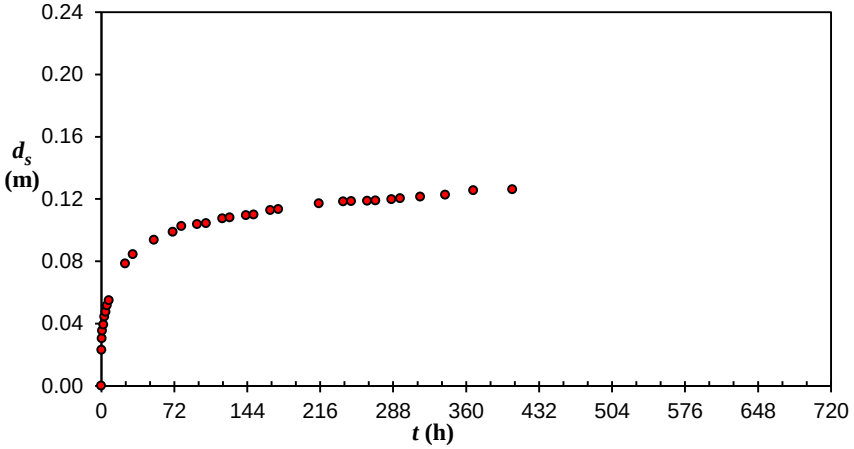

Scour depth measurements in the test M6D1

t_d (h)	d_{sm} (m)		t_d (h)	d_{sm} (m)		t_d (h)	d_{sm} (m)		t_d (h)	d_{sm} (m)
0.00	0.0000		23.72	0.0785		142.80	0.1095		286.38	0.1197
0.20	0.0230		31.23	0.0845		150.58	0.1099		294.83	0.1204
0.50	0.0304		52.05	0.0936		166.78	0.1127		314.67	0.1213
0.95	0.0354		70.60	0.0988		174.77	0.1133		339.47	0.1227
2.02	0.0393		79.08	0.1024		214.83	0.1171		367.32	0.1255
2.97	0.0444		94.70	0.1037		238.78	0.1184		405.77	0.1261
4.42	0.0475		103.42	0.1044		246.67	0.1186			
5.63	0.0515		119.42	0.1075		262.60	0.1187			
7.40	0.0549		126.90	0.1081		270.75	0.1189			

Test M6E1

d_{50}	h	U	U_c	U/U_c	B/D_{pc}	B/h	h/D_{pc}
0.086 mm	0.20 m	0.258 m/s	0.322 m/s	0.80	10.0	10.0	1.0

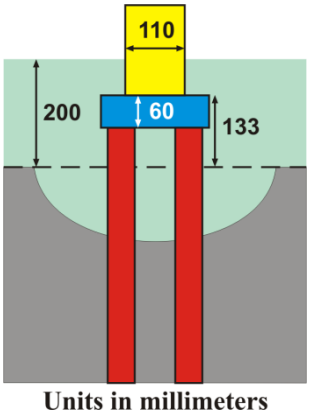

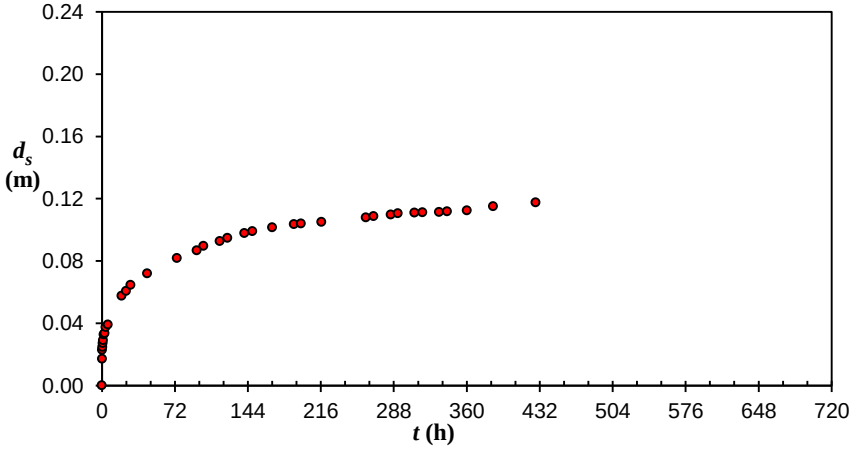

Scour depth measurements in the test M6E1

t_d (h)	d_{sm} (m)		t_d (h)	d_{sm} (m)		t_d (h)	d_{sm} (m)		t_d (h)	d_{sm} (m)
0.00	0.0000		5.98	0.0391		123.92	0.0947		285.05	0.1097
0.13	0.0171		19.55	0.0575		140.75	0.0978		292.00	0.1106
0.33	0.0229		24.00	0.0607		148.55	0.0990		308.42	0.1109
0.58	0.0247		28.33	0.0646		168.22	0.1015		316.30	0.1112
0.87	0.0271		44.72	0.0719		189.45	0.1036		332.80	0.1113
1.28	0.0289		73.95	0.0817		196.40	0.1040		340.60	0.1117
1.87	0.0326		93.57	0.0866		216.80	0.1050		360.38	0.1124
2.77	0.0335		100.20	0.0896		260.67	0.1079		386.23	0.1151
3.77	0.0373		116.50	0.0927		268.00	0.1087		428.20	0.1175

Test M6F1

d_{50}	h	U	U_c	U/U_c	B/D_{pc}	B/h	h/D_{pc}
0.086 mm	0.20 m	0.258 m/s	0.322 m/s	0.80	10.0	10.0	1.0

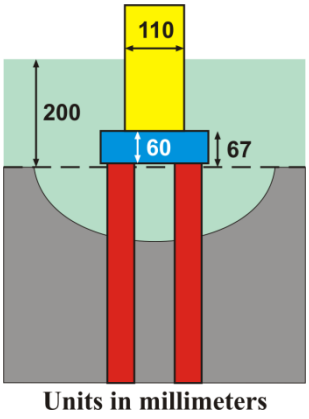

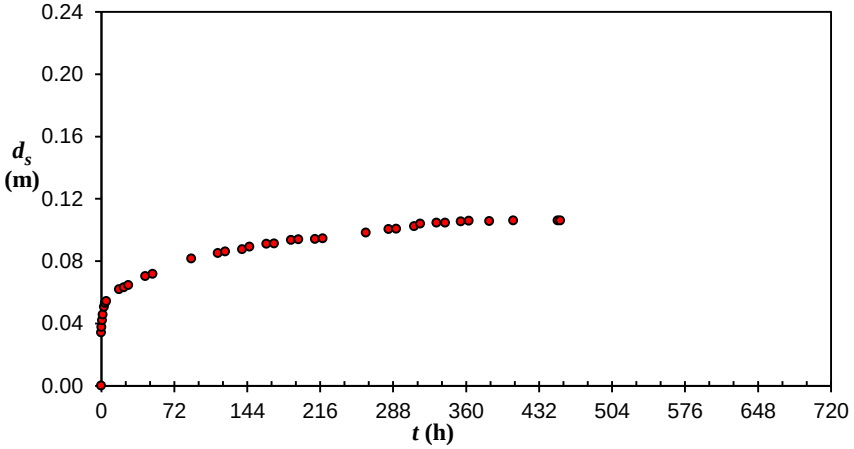

Scour depth measurements in the test M6F1

t_d (h)	d_{sm} (m)	t_d (h)	d_{sm} (m)	t_d (h)	d_{sm} (m)	t_d (h)	d_{sm} (m)
0.00	0.0000	26.78	0.0645	187.33	0.0934	339.42	0.1045
0.10	0.0341	43.40	0.0703	194.70	0.0938	354.93	0.1054
0.32	0.0375	50.75	0.0717	211.07	0.0940	362.83	0.1058
0.90	0.0419	89.05	0.0816	218.50	0.0945	382.82	0.1056
1.63	0.0456	115.10	0.0851	261.12	0.0981	406.60	0.1060
2.65	0.0505	122.32	0.0860	283.47	0.1005	450.33	0.1060
3.73	0.0530	139.20	0.0875	291.07	0.1007	452.98	0.1060
5.03	0.0542	146.50	0.0892	308.88	0.1022		
17.65	0.0619	162.93	0.0909	314.87	0.1039		
22.47	0.0631	170.72	0.0912	330.98	0.1046		

Test M6G1

d_{50}	h	U	U_c	U/U_c	B/D_{pc}	B/h	h/D_{pc}
0.086 mm	0.20 m	0.258 m/s	0.322 m/s	0.80	10.0	10.0	1.0

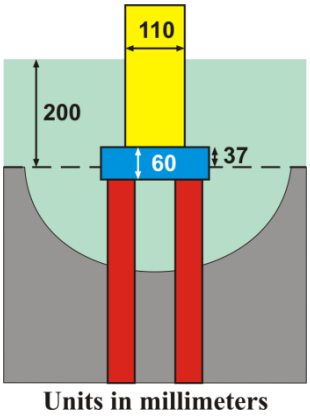

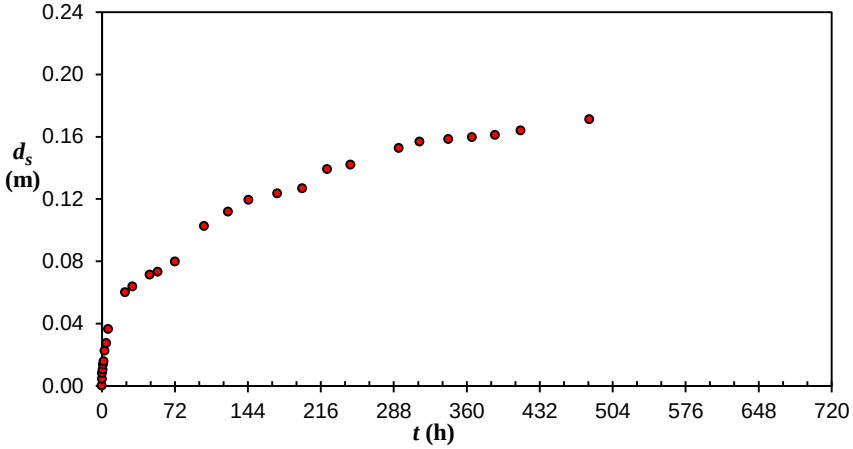

Scour depth measurements in the test M6G1

t_d (h)	d_{sm} (m)		t_d (h)	d_{sm} (m)		t_d (h)	d_{sm} (m)		t_d (h)	d_{sm} (m)
0.00	0.0000		4.33	0.0274		101.02	0.1025		293.10	0.1526
0.17	0.0044		6.37	0.0363		124.45	0.1117		313.70	0.1567
0.33	0.0081		23.00	0.0599		144.67	0.1194		341.82	0.1584
0.75	0.0102		30.17	0.0637		173.18	0.1235		365.43	0.1595
1.25	0.0135		47.33	0.0712		197.90	0.1267		388.10	0.1610
1.87	0.0156		55.22	0.0731		222.30	0.1390		413.22	0.1639
2.82	0.0225		72.30	0.0797		245.30	0.1419		481.05	0.1711

Test M6H1

d_{50}	h	U	U_c	U/U_c	B/D_{pc}	B/h	h/D_{pc}
0.086 mm	0.20 m	0.258 m/s	0.322 m/s	0.80	10.0	10.0	1.0

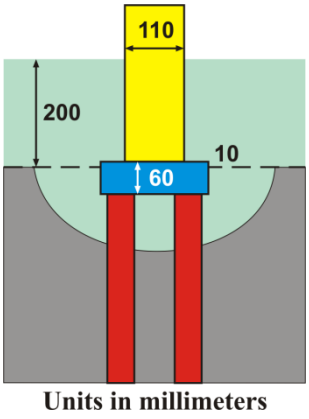

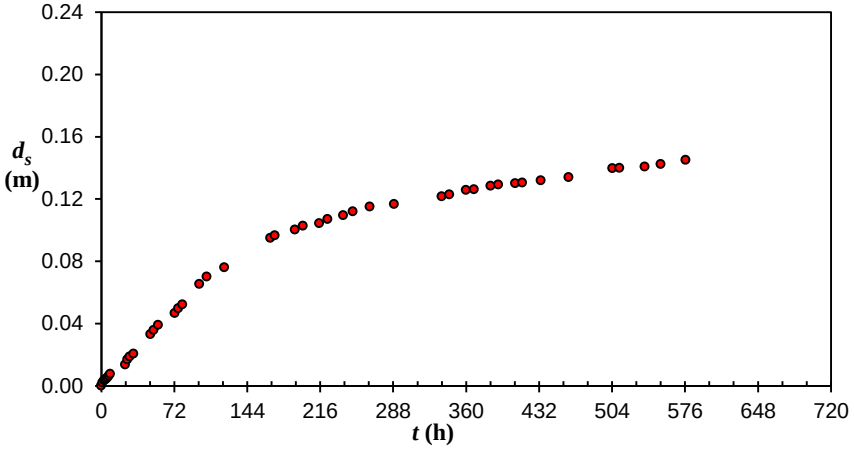

Scour depth measurements in the test M6H1

t_d (h)	d_{sm} (m)	t_d (h)	d_{sm} (m)	t_d (h)	d_{sm} (m)	t_d (h)	d_{sm} (m)
0.00	0.0000	48.50	0.0331	199.10	0.1028	391.75	0.1291
1.08	0.0020	51.63	0.0358	215.02	0.1044	408.50	0.1300
2.95	0.0035	56.17	0.0391	223.45	0.1070	415.58	0.1304
4.00	0.0039	72.55	0.0466	238.72	0.1095	433.78	0.1318
5.00	0.0045	76.10	0.0498	248.28	0.1120	461.10	0.1339
6.17	0.0054	79.97	0.0521	265.02	0.1151	504.45	0.1396
7.65	0.0064	96.80	0.0654	288.98	0.1166	511.53	0.1398
8.75	0.0077	104.00	0.0701	336.10	0.1217	536.28	0.1408
23.58	0.0135	121.45	0.0760	343.42	0.1229	552.08	0.1423
25.78	0.0169	166.83	0.0948	360.07	0.1257	576.60	0.1450
28.00	0.0188	171.23	0.0965	367.75	0.1261		
31.87	0.0205	191.30	0.1002	384.18	0.1283		

Test M6I1

d_{50}	h	U	U_c	U/U_c	B/D_{pc}	B/h	h/D_{pc}
0.086 mm	0.20 m	0.258 m/s	0.322 m/s	0.80	10.0	10.0	1.0

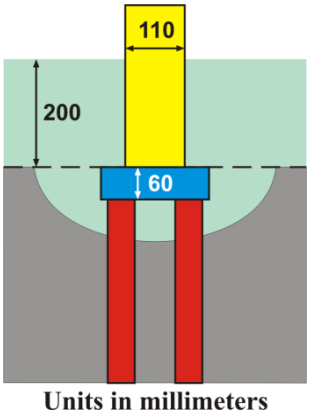

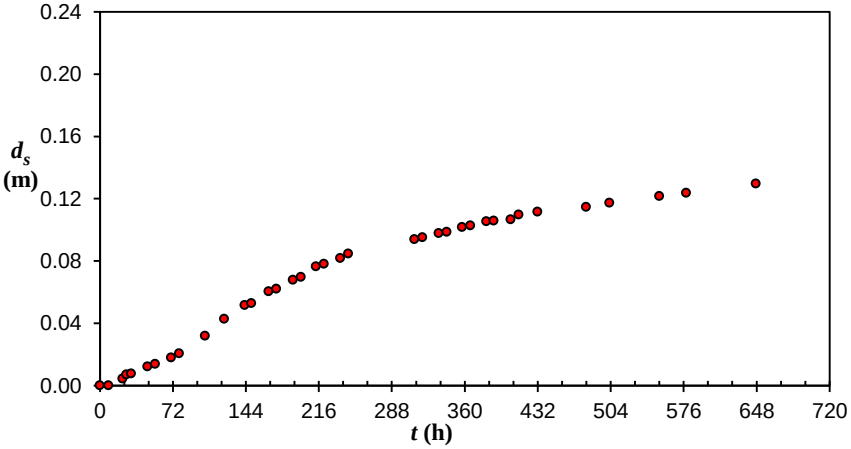

Scour depth measurements in the test M6I1

t_d (h)	d_{sm} (m)		t_d (h)	d_{sm} (m)		t_d (h)	d_{sm} (m)		t_d (h)	d_{sm} (m)
0.00	0.0000		122.60	0.0428		244.98	0.0847		413.28	0.1096
8.55	0.0000		142.78	0.0515		310.48	0.0938		431.92	0.1115
22.22	0.0043		149.62	0.0528		318.33	0.0952		479.73	0.1147
26.18	0.0069		166.60	0.0605		334.42	0.0978		502.88	0.1173
30.73	0.0077		174.20	0.0621		342.18	0.0986		552.12	0.1217
46.83	0.0122		190.57	0.0678		357.38	0.1017		578.52	0.1236
54.58	0.0137		198.42	0.0697		365.67	0.1027		647.37	0.1297
70.43	0.0178		213.22	0.0765		381.37	0.1054			
78.33	0.0205		221.20	0.0780		388.62	0.1057			
103.70	0.0319		237.17	0.0817		405.45	0.1067			

Test M6J1

d_{50}	h	U	U_c	U/U_c	B/D_{pc}	B/h	h/D_{pc}
0.086 mm	0.20 m	0.258 m/s	0.322 m/s	0.80	10.0	10.0	1.0

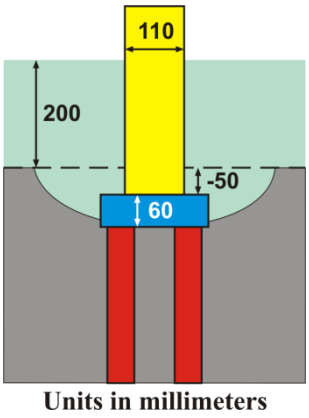

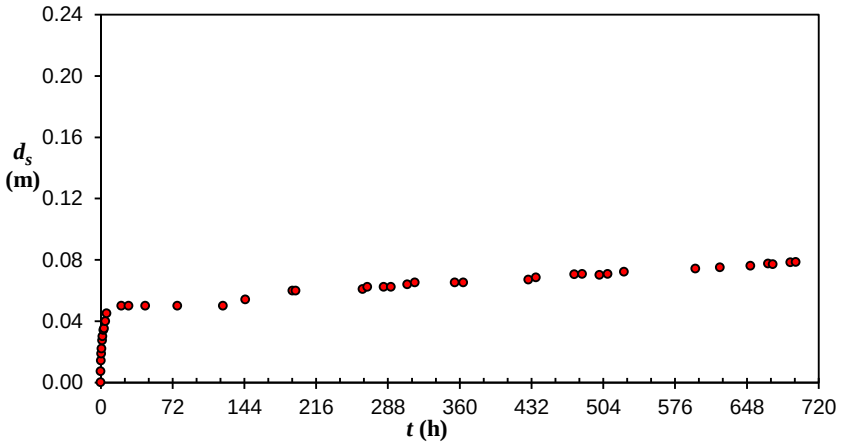

Scour depth measurements in the test M6J1

t_d (h)	d_{sm} (m)	t_d (h)	d_{sm} (m)	t_d (h)	d_{sm} (m)	t_d (h)	d_{sm} (m)
0.00	0.0000	100.50	0.0500	452.22	0.0682	792.80	0.0811
0.10	0.0073	122.58	0.0500	459.13	0.0683	796.48	0.0829
0.30	0.0141	145.20	0.0541	475.23	0.0705	812.50	0.0825
0.60	0.0188	192.45	0.0597	482.92	0.0706	817.07	0.0820
1.00	0.0219	195.47	0.0598	500.45	0.0701	838.07	0.0831
1.50	0.0274	262.77	0.0608	508.48	0.0707	843.65	0.0834
2.00	0.0300	267.40	0.0622	524.90	0.0721	865.87	0.0835
2.72	0.0341	284.00	0.0622	596.57	0.0741	932.88	0.0849
3.50	0.0352	291.30	0.0622	621.30	0.0750	962.78	0.0863
4.57	0.0398	307.47	0.0638	651.80	0.0760	988.47	0.0872
6.05	0.0450	315.20	0.0651	669.37	0.0774	1004.15	0.0875
20.75	0.0500	355.33	0.0651	674.30	0.0771	1012.08	0.0870
28.00	0.0500	363.82	0.0652	691.97	0.0783	1035.78	0.0882
44.67	0.0500	429.15	0.0670	697.15	0.0785	1100.05	0.0886
76.82	0.0500	436.57	0.0684	767.68	0.0801	1126.02	0.0888

Test M6K1

d_{50}	h	U	U_c	U/U_c	B/D_{pc}	B/h	h/D_{pc}
0.086 mm	0.20 m	0.258 m/s	0.322 m/s	0.80	10.0	10.0	1.0

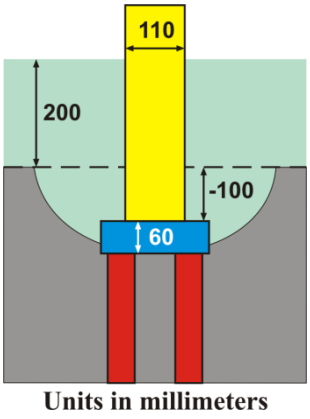

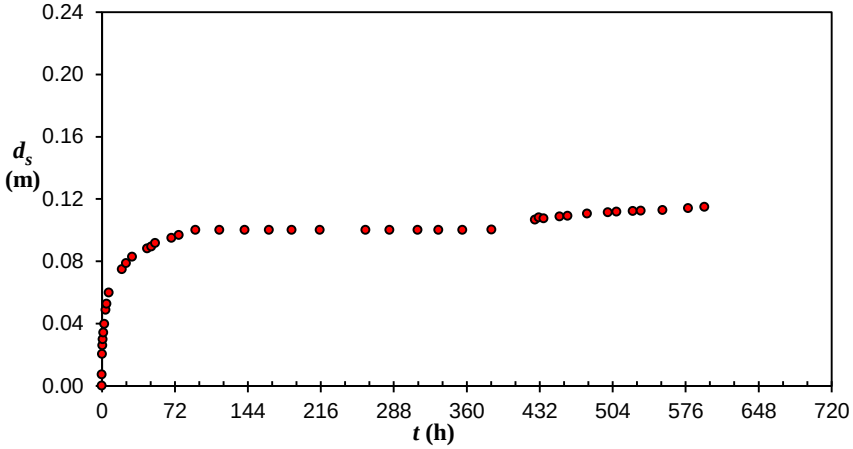

Scour depth measurements in the test M6K1

t_d (h)	d_{sm} (m)	t_d (h)	d_{sm} (m)	t_d (h)	d_{sm} (m)	t_d (h)	d_{sm} (m)
0.00	0.0000	23.98	0.0786	187.50	0.1000	451.63	0.1087
0.10	0.0073	29.92	0.0828	215.22	0.1000	459.72	0.1090
0.32	0.0204	44.68	0.0882	260.10	0.1000	479.00	0.1105
0.53	0.0259	48.75	0.0893	284.03	0.1000	499.45	0.1114
1.00	0.0299	52.63	0.0917	311.52	0.1000	507.77	0.1118
1.50	0.0341	68.80	0.0950	332.28	0.1001	524.15	0.1121
2.38	0.0397	76.10	0.0968	355.98	0.1000	531.88	0.1123
3.70	0.0486	92.33	0.1000	384.58	0.1003	553.27	0.1128
4.75	0.0526	116.20	0.1000	427.32	0.1067	578.47	0.1139
6.97	0.0598	140.83	0.1000	431.32	0.1080	594.62	0.1148
19.77	0.0747	164.90	0.1000	436.00	0.1074		

Test M6L1

d_{50}	h	U	U_c	U/U_c	B/D_{pc}	B/h	h/D_{pc}
0.086 mm	0.20 m	0.258 m/s	0.322 m/s	0.80	10.0	10.0	1.0

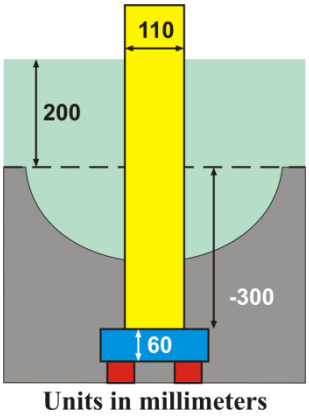

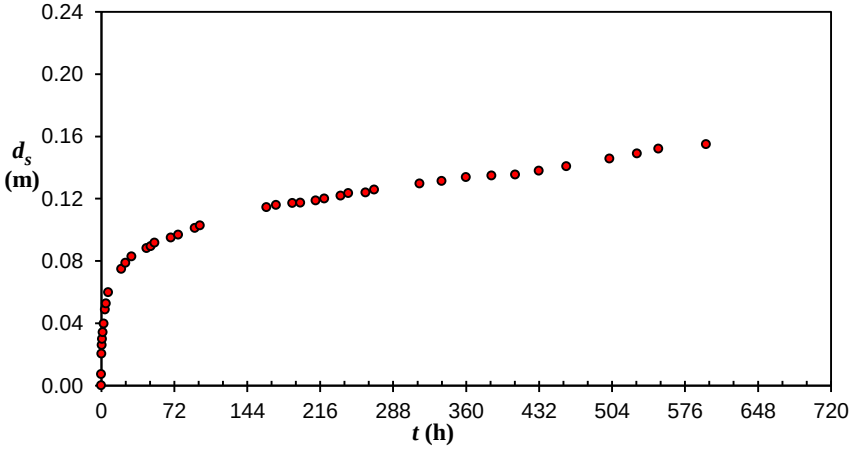

Scour depth measurements in the test M6L1

t_d (h)	d_{sm} (m)	t_d (h)	d_{sm} (m)	t_d (h)	d_{sm} (m)	t_d (h)	d_{sm} (m)
0.00	0.0000	23.98	0.0786	188.60	0.1170	385.07	0.1347
0.10	0.0073	29.92	0.0828	196.60	0.1173	408.50	0.1354
0.32	0.0204	44.68	0.0882	211.72	0.1188	431.97	0.1378
0.53	0.0259	48.75	0.0893	220.05	0.1200	458.85	0.1408
1.00	0.0299	52.63	0.0917	236.15	0.1219	501.50	0.1457
1.50	0.0341	68.80	0.0950	243.83	0.1235	528.67	0.1489
2.38	0.0397	76.10	0.0968	260.85	0.1238	549.92	0.1519
3.70	0.0486	92.33	0.1010	269.43	0.1257	596.80	0.1549
4.75	0.0526	97.40	0.1027	314.12	0.1296		
6.97	0.0598	163.15	0.1144	335.92	0.1312		
19.77	0.0747	172.47	0.1158	359.95	0.1338		

Test M7M1

d_{50}	h	U	U_c	U/U_c	B/D_{pc}	B/h	h/D_{pc}
0.086 mm	0.18 m	0.315 m/s	0.322 m/s	0.80	8.3	5.6	1.5

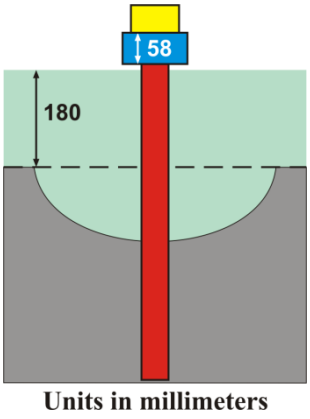

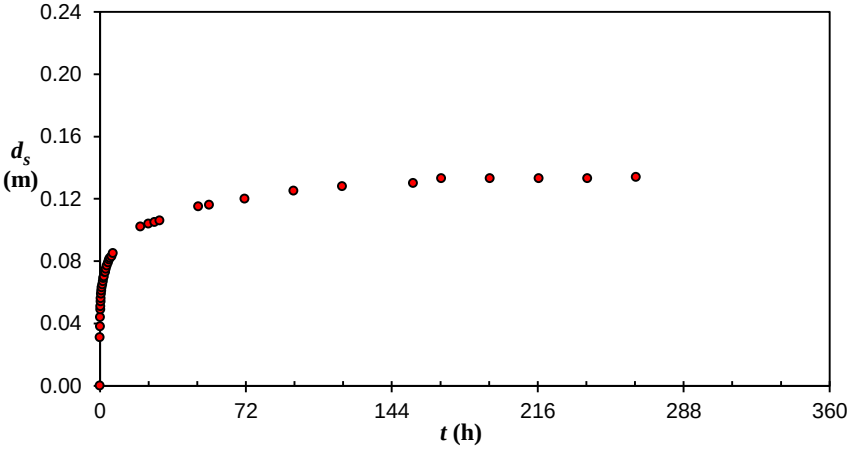

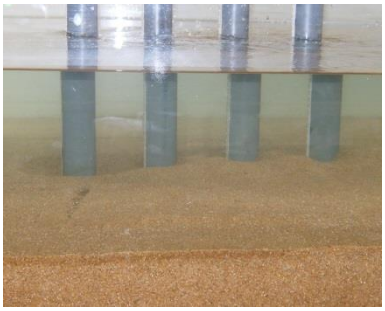

Scour depth measurements in the test M7M1

t_d (h)	d_{sm} (m)		t_d (h)	d_{sm} (m)		t_d (h)	d_{sm} (m)		t_d (h)	d_{sm} (m)
0.00	0.0000		1.00	0.0630		4.50	0.0810		71.50	0.1200
0.03	0.0310		1.25	0.0650		5.00	0.0820		95.50	0.1250
0.08	0.0380		1.50	0.0670		5.75	0.0830		119.50	0.1280
0.17	0.0440		1.75	0.0690		6.50	0.0850		154.50	0.1300
0.25	0.0490		2.00	0.0700		20.00	0.1020		168.50	0.1330
0.33	0.0510		2.33	0.0730		24.00	0.1040		192.50	0.1330
0.42	0.0540		2.67	0.0730		27.00	0.1050		216.50	0.1330
0.50	0.0560		3.00	0.0750		29.50	0.1060		240.50	0.1330
0.67	0.0590		3.50	0.0770		48.50	0.1150		264.50	0.1340
0.83	0.0610		4.00	0.0790		54.00	0.1160			

Test M7N1

d_{50}	h	U	U_c	U/U_c	B/D_{pc}	B/h	h/D_{pc}
0.086 mm	0.18 m	0.315 m/s	0.322 m/s	0.80	8.3	5.6	1.5

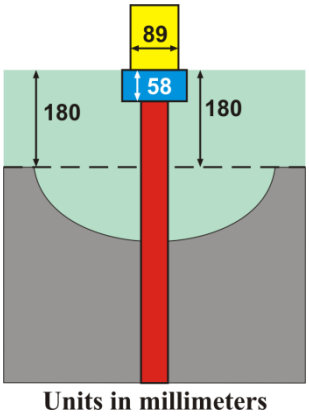

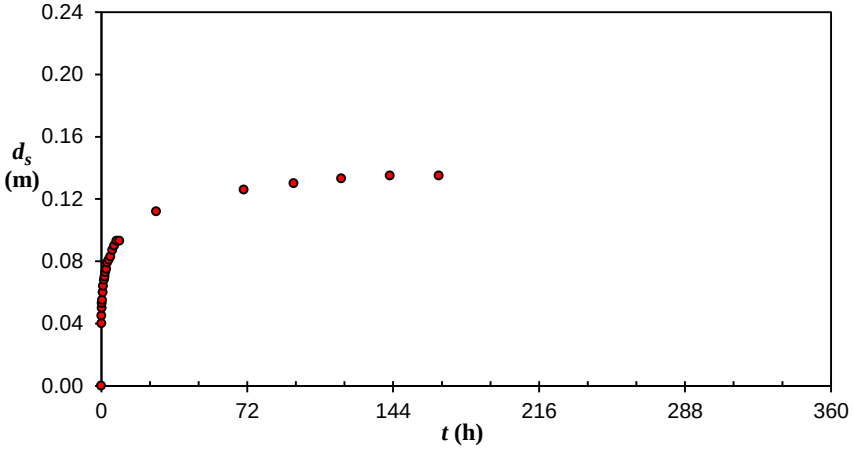

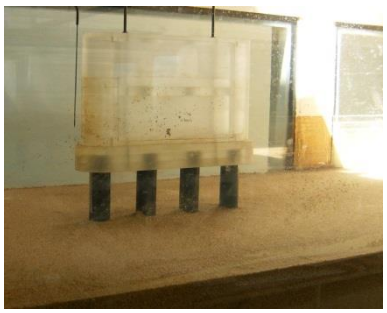

Scour depth measurements in the test M7N1

t_d (h)	d_{sm} (m)		t_d (h)	d_{sm} (m)		t_d (h)	d_{sm} (m)		t_d (h)	d_{sm} (m)
0.00	0.0000		1.00	0.0640		4.50	0.0830		95.00	0.1300
0.08	0.0400		1.33	0.0680		5.50	0.0870		118.50	0.1330
0.17	0.0450		1.67	0.0700		6.50	0.0900		142.50	0.1350
0.25	0.0500		2.00	0.0730		7.50	0.0930		166.50	0.1350
0.33	0.0530		2.50	0.0750		9.00	0.0930			
0.50	0.0550		3.00	0.0790		27.13	0.1120			
0.75	0.0600		3.75	0.0810		70.33	0.1260			

Test M7O1

d_{50}	h	U	U_c	U/U_c	B/D_{pc}	B/h	h/D_{pc}
0.086 mm	0.18 m	0.315 m/s	0.322 m/s	0.80	8.3	5.6	1.5

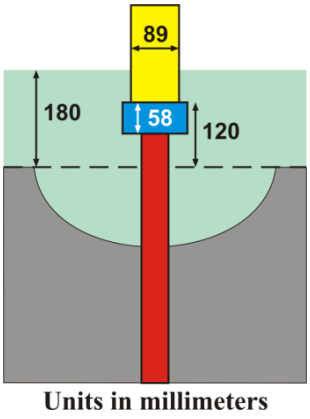

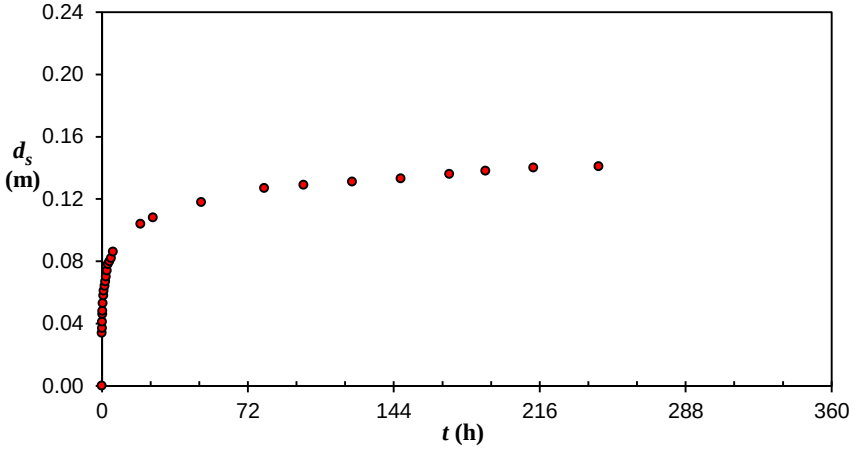

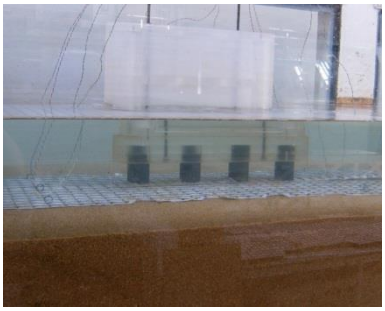

Scour depth measurements in the test M7O1

t_d (h)	d_{sm} (m)		t_d (h)	d_{sm} (m)		t_d (h)	d_{sm} (m)		t_d (h)	d_{sm} (m)
0.00	0.0000		0.75	0.0580		3.75	0.0800		99.50	0.1290
0.03	0.0340		1.00	0.0610		4.50	0.0820		123.50	0.1310
0.08	0.0370		1.33	0.0640		5.50	0.0860		147.50	0.1330
0.17	0.0410		1.67	0.0670		19.00	0.1040		171.50	0.1360
0.25	0.0460		2.00	0.0700		25.17	0.1080		189.33	0.1380
0.33	0.0480		2.50	0.0740		49.00	0.1180		213.00	0.1400
0.50	0.0530		3.00	0.0780		80.17	0.1270		245.17	0.1410

Test M7P1

d_{50}	h	U	U_c	U/U_c	B/D_{pc}	B/h	h/D_{pc}
0.086 mm	0.18 m	0.315 m/s	0.322 m/s	0.80	8.3	5.6	1.5

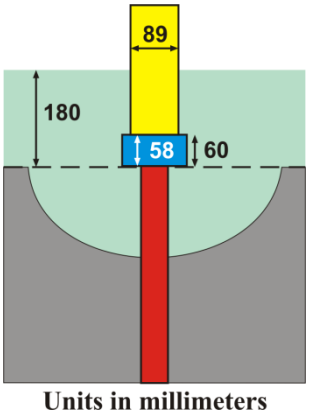

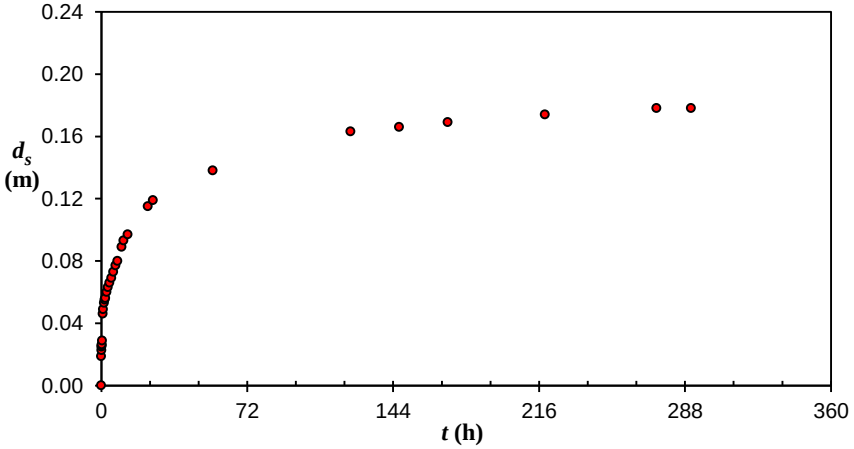

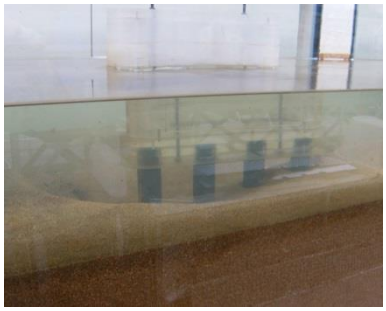

Scour depth measurements in the test M7P1

t_d (h)	d_{sm} (m)		t_d (h)	d_{sm} (m)		t_d (h)	d_{sm} (m)		t_d (h)	d_{sm} (m)
0.00	0.0000		1.00	0.0490		6.00	0.0730		55.00	0.1380
0.05	0.0188		1.33	0.0530		7.00	0.0770		123.00	0.1630
0.08	0.0227		1.67	0.0550		8.00	0.0800		147.00	0.1660
0.17	0.0248		2.00	0.0560		10.00	0.0890		171.00	0.1690
0.25	0.0257		2.67	0.0600		11.00	0.0930		219.00	0.1740
0.33	0.0264		3.33	0.0630		13.00	0.0970		274.00	0.1780
0.50	0.0288		4.00	0.0660		23.00	0.1150		291.00	0.1780
0.75	0.0460		5.00	0.0690		25.50	0.1190			

Test M7Q1

d_{50}	h	U	U_c	U/U_c	B/D_{pc}	B/h	h/D_{pc}
0.086 mm	0.18 m	0.315 m/s	0.322 m/s	0.80	8.3	5.6	1.5

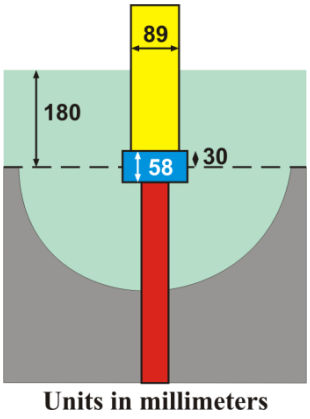

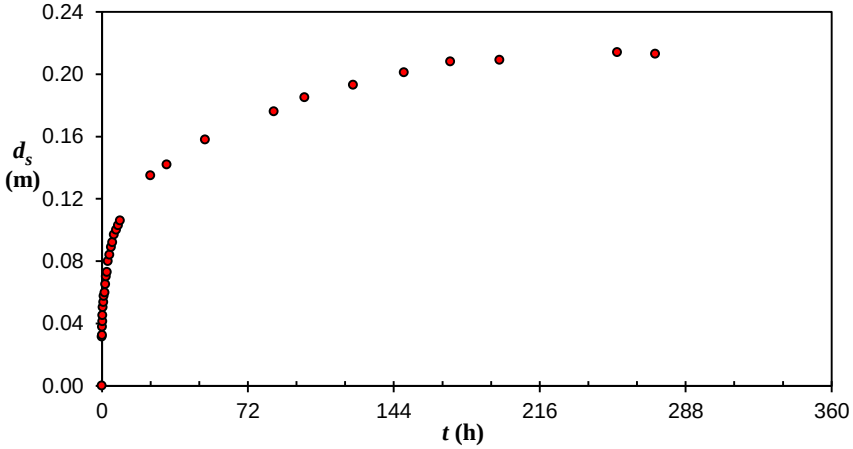

Scour depth measurements in the test M7Q1

t_d (h)	d_{sm} (m)		t_d (h)	d_{sm} (m)		t_d (h)	d_{sm} (m)		t_d (h)	d_{sm} (m)
0.00	0.0000		1.00	0.0575		5.25	0.0920		84.83	0.1760
0.03	0.0314		1.33	0.0597		6.00	0.0970		100.00	0.1850
0.08	0.0325		1.67	0.0652		7.00	0.1000		124.00	0.1930
0.17	0.0378		2.00	0.0700		8.00	0.1030		149.00	0.2010
0.25	0.0412		2.50	0.0730		9.00	0.1060		172.00	0.2080
0.33	0.0451		3.00	0.0800		24.00	0.1350		196.17	0.2090
0.50	0.0504		3.75	0.0840		32.00	0.1420		254.33	0.2140
0.75	0.0536		4.50	0.0890		51.00	0.1580		273.00	0.2130

Test M7R1

d_{50}	h	U	U_c	U/U_c	B/D_{pc}	B/h	h/D_{pc}
0.086 mm	0.18 m	0.315 m/s	0.322 m/s	0.80	8.3	5.6	1.5

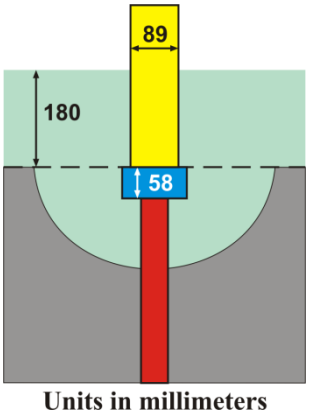

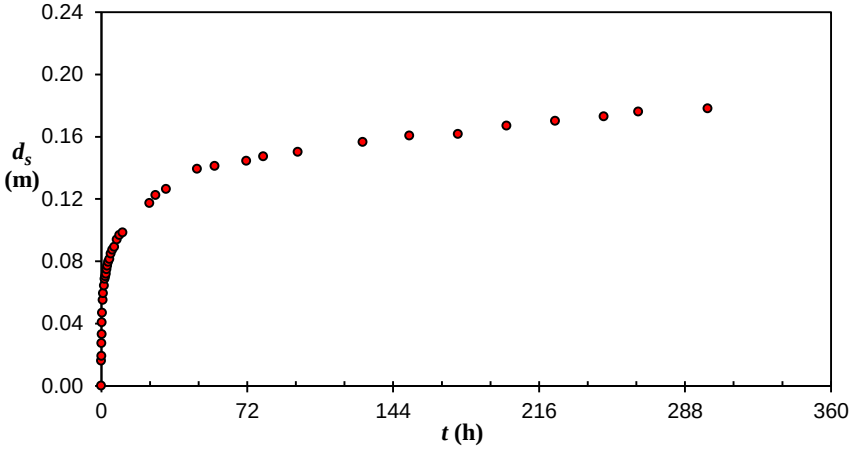

Scour depth measurements in the test M7R1

t_d (h)	d_{sm} (m)	t_d (h)	d_{sm} (m)	t_d (h)	d_{sm} (m)	t_d (h)	d_{sm} (m)
0.00	0.0000	1.67	0.0687	7.75	0.0939	97.00	0.1501
0.03	0.0160	2.00	0.0702	9.00	0.0968	129.00	0.1566
0.08	0.0191	2.33	0.0720	10.50	0.0984	152.00	0.1606
0.17	0.0274	2.67	0.0747	23.75	0.1172	176.00	0.1617
0.25	0.0330	3.00	0.0770	26.75	0.1224	200.00	0.1670
0.33	0.0406	3.50	0.0794	32.00	0.1263	224.00	0.1700
0.50	0.0469	4.00	0.0813	47.33	0.1393	248.00	0.1730
0.75	0.0551	4.75	0.0849	56.00	0.1411	265.00	0.1760
1.00	0.0594	5.50	0.0874	71.67	0.1445	299.22	0.1780
1.33	0.0642	6.50	0.0891	80.00	0.1473		

Test M7S1

d_{50}	h	U	U_c	U/U_c	B/D_{pc}	B/h	h/D_{pc}
0.086 mm	0.18 m	0.315 m/s	0.322 m/s	0.80	8.3	5.6	1.5

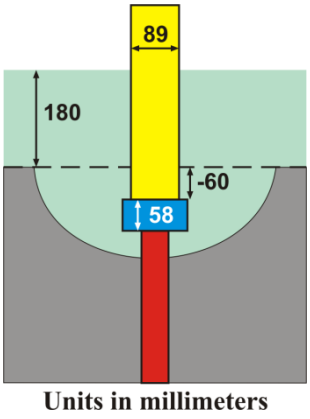

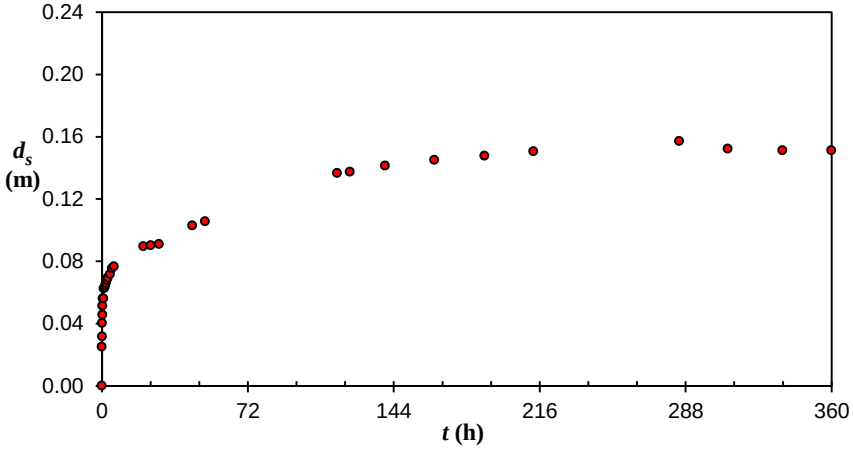

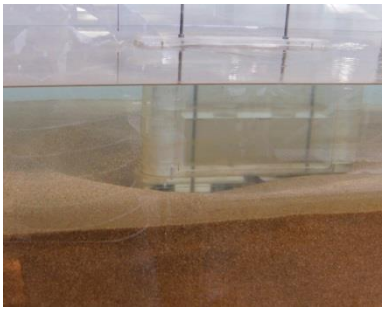

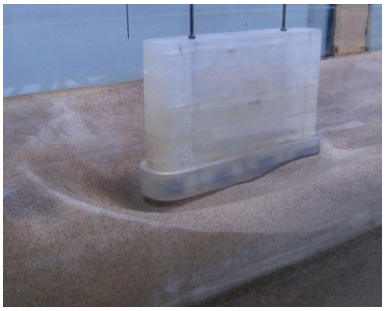

Scour depth measurements in the test M7S1

t_d (h)	d_{sm} (m)		t_d (h)	d_{sm} (m)		t_d (h)	d_{sm} (m)		t_d (h)	d_{sm} (m)
0.00	0.0000		1.00	0.0624		6.00	0.0766		139.67	0.1413
0.05	0.0250		1.33	0.0631		20.50	0.0896		164.00	0.1450
0.08	0.0316		1.67	0.0646		24.07	0.0901		188.73	0.1476
0.17	0.0403		2.00	0.0660		28.15	0.0909		212.95	0.1505
0.25	0.0457		2.50	0.0678		44.57	0.1030		284.90	0.1571
0.33	0.0514		3.00	0.0694		50.90	0.1056		308.90	0.1521
0.50	0.0561		4.00	0.0716		116.07	0.1366		335.90	0.1512
0.75	0.0561		5.00	0.0753		122.33	0.1375		359.90	0.1511

Test M7T1

d_{50}	h	U	U_c	U/U_c	B/D_{pc}	B/h	h/D_{pc}
0.086 mm	0.18 m	0.315 m/s	0.322 m/s	0.80	8.3	5.6	1.5

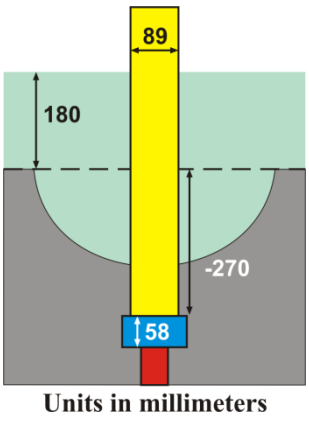

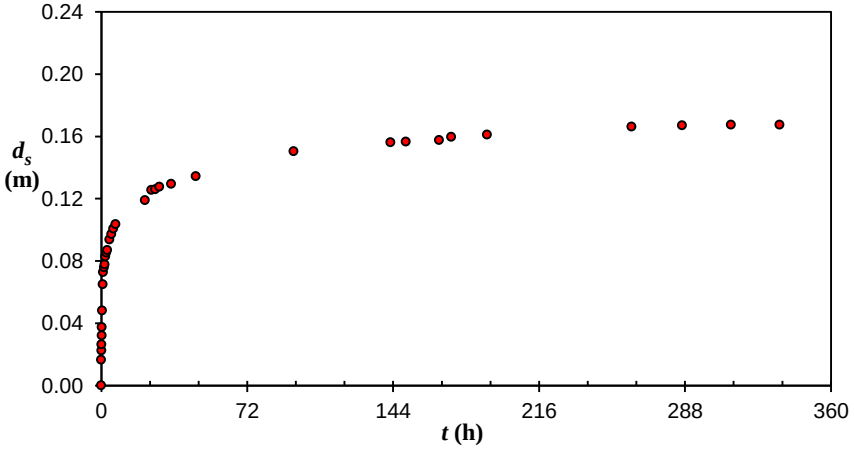

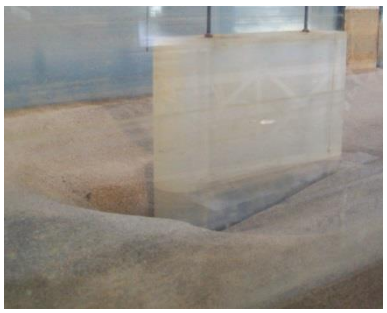

Scour depth measurements in the test M7T1

t_d (h)	d_{sm} (m)		t_d (h)	d_{sm} (m)		t_d (h)	d_{sm} (m)		t_d (h)	d_{sm} (m)
0.00	0.0000		1.33	0.0759		21.67	0.1189		166.67	0.1576
0.05	0.0164		1.67	0.0777		24.67	0.1256		172.67	0.1596
0.08	0.0224		2.00	0.0827		26.67	0.1260		190.33	0.1611
0.17	0.0263		2.50	0.0852		28.67	0.1275		261.67	0.1662
0.25	0.0320		3.00	0.0869		34.50	0.1294		286.67	0.1669
0.33	0.0373		4.00	0.0937		46.67	0.1343		310.67	0.1673
0.50	0.0480		5.00	0.0972		94.92	0.1503		334.67	0.1674
0.75	0.0650		6.00	0.1006		142.67	0.1562			
1.00	0.0727		7.00	0.1036		150.33	0.1565			

Test M4E2

d_{50}	h	U	U_c	U/U_c	B/D_{pc}	B/h	h/D_{pc}
0.086 mm	0.20 m	0.258 m/s	0.322 m/s	0.80	10.0	10.0	1.0

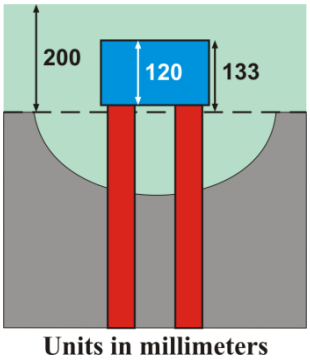

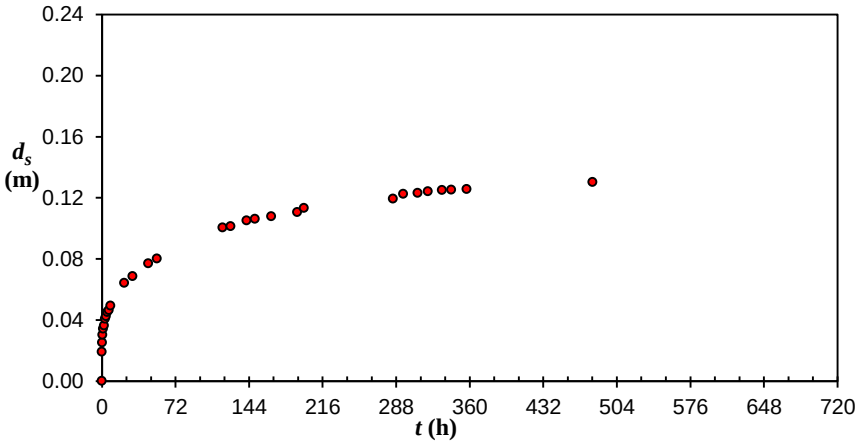

Scour depth measurements in the test M4E2

t_d (h)	d_{sm} (m)		t_d (h)	d_{sm} (m)		t_d (h)	d_{sm} (m)		t_d (h)	d_{sm} (m)
0.00	0.0000		5.25	0.0451		125.95	0.1013		309.07	0.1231
0.10	0.0192		6.85	0.0464		141.72	0.1050		319.18	0.1242
0.32	0.0251		8.45	0.0492		149.98	0.1061		332.97	0.1250
0.58	0.0302		21.83	0.0641		165.78	0.1079		342.07	0.1253
1.05	0.0342		30.07	0.0686		191.08	0.1105		357.07	0.1257
2.13	0.0364		45.40	0.0770		197.73	0.1132		480.37	0.1302
3.12	0.0408		53.98	0.0802		284.92	0.1193			
4.17	0.0423		118.13	0.1004		294.87	0.1224			

Test M4F2

d_{50}	h	U	U_c	U/U_c	B/D_{pc}	B/h	h/D_{pc}
0.086 mm	0.20 m	0.258 m/s	0.322 m/s	0.80	10.0	10.0	1.0

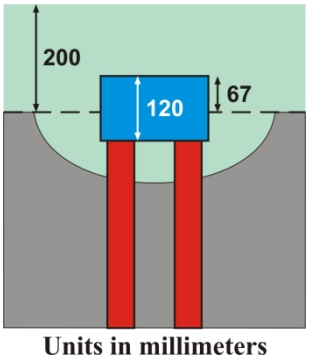

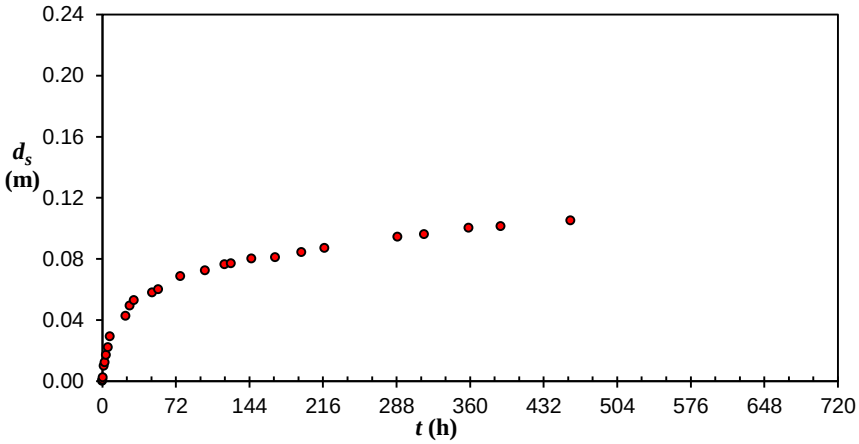

Scour depth measurements in the test M4F2

t_d (h)	d_{sm} (m)		t_d (h)	d_{sm} (m)		t_d (h)	d_{sm} (m)		t_d (h)	d_{sm} (m)
0.00	0.0000		7.62	0.0291		100.63	0.0724		289.22	0.0944
0.25	0.0008		22.75	0.0425		119.75	0.0763		314.95	0.0961
0.55	0.0023		26.92	0.0492		126.10	0.0769		358.53	0.1002
1.63	0.0099		31.05	0.0528		145.93	0.0801		389.88	0.1013
2.42	0.0122		48.87	0.0579		169.25	0.0810		458.35	0.1051
3.78	0.0170		54.85	0.0600		194.93	0.0844			
5.52	0.0221		76.57	0.0686		217.63	0.0871			

Test M4G2

d_{50}	h	U	U_c	U/U_c	B/D_{pc}	B/h	h/D_{pc}
0.086 mm	0.20 m	0.258 m/s	0.322 m/s	0.80	10.0	10.0	1.0

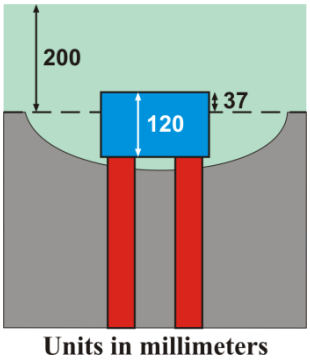

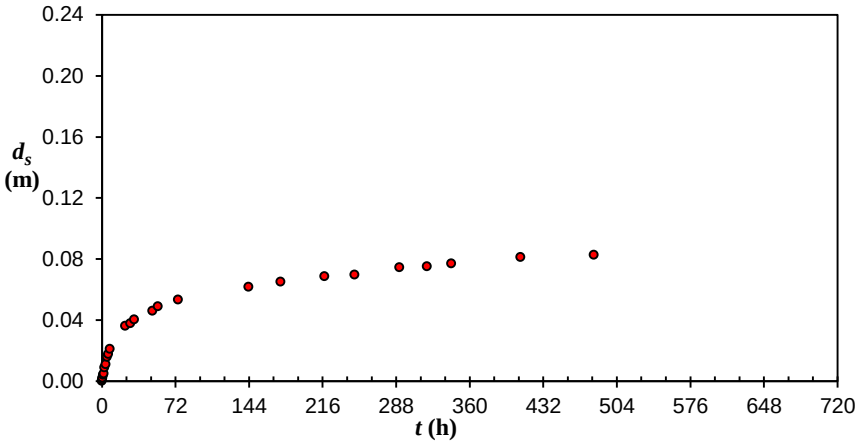

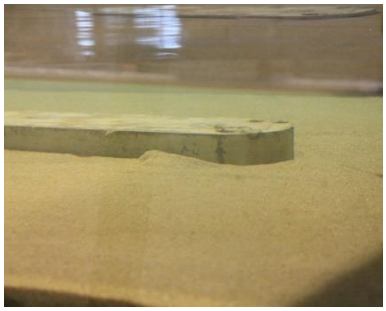

Scour depth measurements in the test M4G2

t_d (h)	d_{sm} (m)		t_d (h)	d_{sm} (m)		t_d (h)	d_{sm} (m)		t_d (h)	d_{sm} (m)
0.00	0.0000		4.98	0.0158		54.75	0.0488		318.37	0.0750
0.27	0.0010		6.32	0.0177		74.55	0.0532		342.08	0.0769
0.62	0.0021		7.82	0.0209		143.63	0.0617		409.88	0.0811
1.12	0.0040		22.85	0.0360		174.83	0.0650		481.70	0.0827
1.85	0.0049		27.87	0.0378		217.92	0.0686			
2.58	0.0088		31.52	0.0403		247.23	0.0696			
3.65	0.0109		49.55	0.0460		291.30	0.0744			

Test M4H2

d_{50}	h	U	U_c	U/U_c	B/D_{pc}	B/h	h/D_{pc}
0.086 mm	0.20 m	0.258 m/s	0.322 m/s	0.80	10.0	10.0	1.0

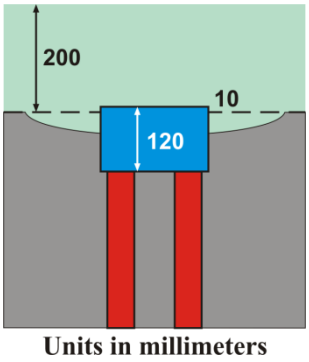

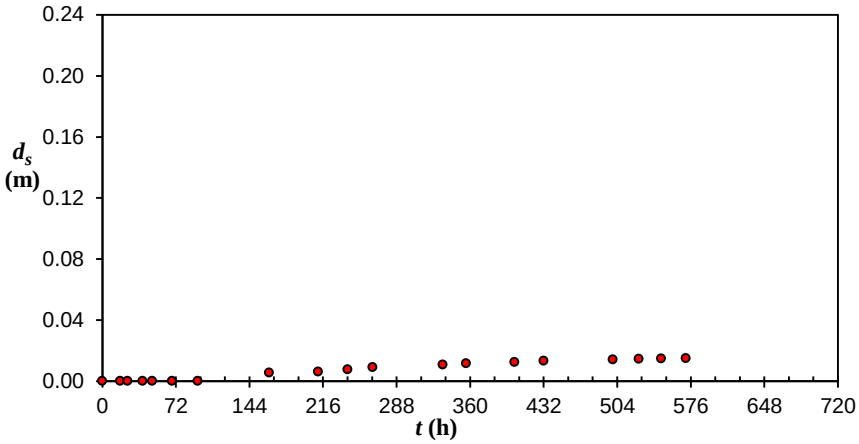

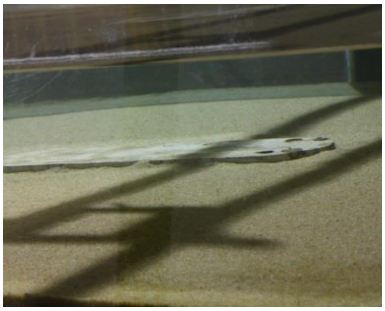

Scour depth measurements in the test M4H2

t_d (h)	d_{sm} (m)		t_d (h)	d_{sm} (m)		t_d (h)	d_{sm} (m)		t_d (h)	d_{sm} (m)
0.00	0.0000		68.27	0.0000		264.52	0.0090		499.82	0.0140
17.63	0.0000		93.42	0.0000		333.40	0.0108		525.10	0.0145
24.60	0.0000		163.23	0.0055		356.25	0.0116		547.23	0.0147
39.50	0.0000		211.15	0.0061		403.42	0.0125		571.20	0.0150
48.77	0.0000		240.28	0.0075		432.10	0.0133			

Test M5E2

d_{50}	h	U	U_c	U/U_c	B/D_{pc}	B/h	h/D_{pc}
0.086 mm	0.20 m	0.258 m/s	0.322 m/s	0.80	10.0	10.0	1.0

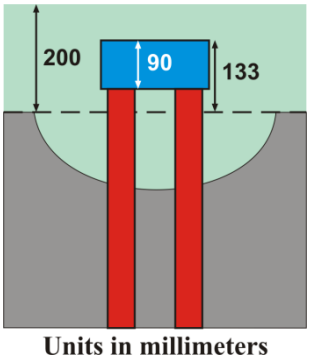

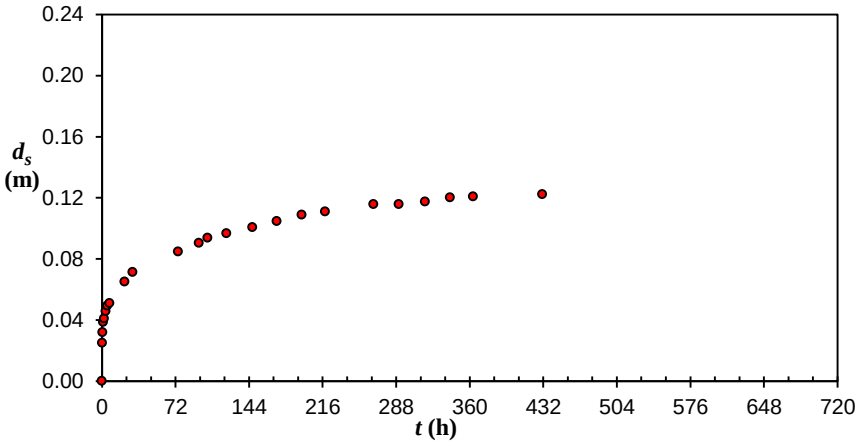

Scour depth measurements in the test M5E2

t_d (h)	d_{sm} (m)		t_d (h)	d_{sm} (m)		t_d (h)	d_{sm} (m)		t_d (h)	d_{sm} (m)
0.00	0.0000		5.37	0.0492		103.50	0.0938		265.75	0.1157
0.17	0.0249		7.48	0.0509		121.83	0.0966		290.62	0.1158
0.50	0.0318		22.28	0.0651		147.45	0.1006		316.45	0.1174
1.32	0.0386		30.15	0.0714		171.05	0.1047		340.70	0.1202
2.28	0.0409		74.57	0.0848		195.75	0.1088		363.35	0.1208
3.75	0.0458		94.95	0.0904		218.50	0.1109		431.00	0.1223

Test M5F2

d_{50}	h	U	U_c	U/U_c	B/D_{pc}	B/h	h/D_{pc}
0.086 mm	0.20 m	0.258 m/s	0.322 m/s	0.80	10.0	10.0	1.0

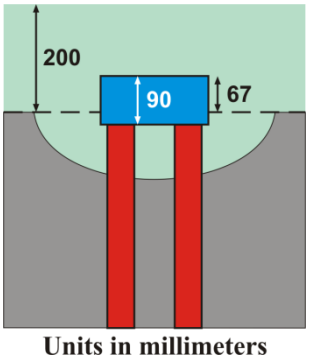

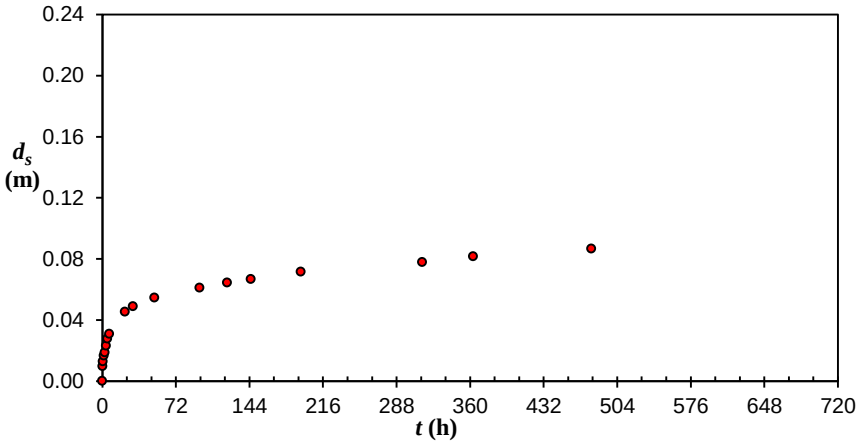

Scour depth measurements in the test M5F2

t_d (h)	d_{sm} (m)		t_d (h)	d_{sm} (m)		t_d (h)	d_{sm} (m)		t_d (h)	d_{sm} (m)
0.00	0.0000		3.57	0.0230		51.22	0.0545		313.20	0.0778
0.17	0.0097		4.82	0.0276		95.37	0.0611		363.00	0.0816
0.43	0.0128		6.72	0.0308		122.38	0.0644		478.92	0.0867
1.38	0.0166		22.27	0.0453		145.35	0.0668			
2.47	0.0187		29.93	0.0488		194.50	0.0715			

Test M5G2

d_{50}	h	U	U_c	U/U_c	B/D_{pc}	B/h	h/D_{pc}
0.086 mm	0.20 m	0.258 m/s	0.322 m/s	0.80	10.0	10.0	1.0

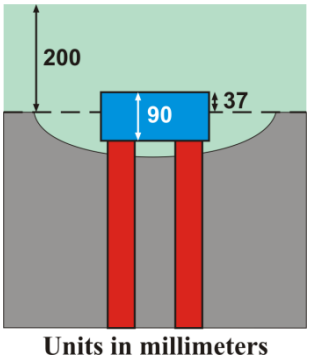

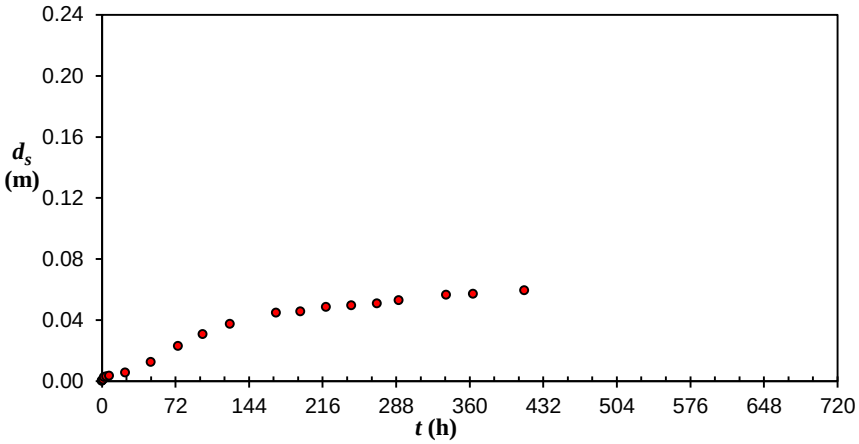

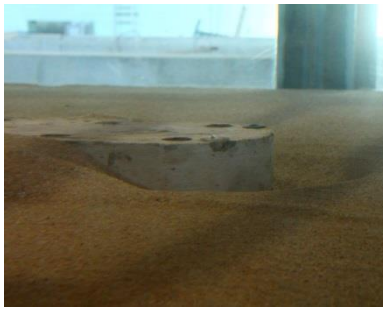

Scour depth measurements in the test M5G2

t_d (h)	d_{sm} (m)		t_d (h)	d_{sm} (m)		t_d (h)	d_{sm} (m)		t_d (h)	d_{sm} (m)
0.00	0.0000		7.13	0.0034		125.43	0.0373		269.27	0.0507
0.25	0.0003		22.85	0.0054		170.47	0.0447		290.70	0.0529
1.28	0.0009		47.98	0.0125		194.47	0.0455		337.00	0.0564
2.23	0.0025		74.50	0.0228		219.30	0.0484		363.38	0.0570
4.30	0.0029		98.70	0.0306		244.18	0.0495		413.63	0.0594

Test M6E2

d_{50}	h	U	U_c	U/U_c	B/D_{pc}	B/h	h/D_{pc}
0.086 mm	0.20 m	0.258 m/s	0.322 m/s	0.80	10.0	10.0	1.0

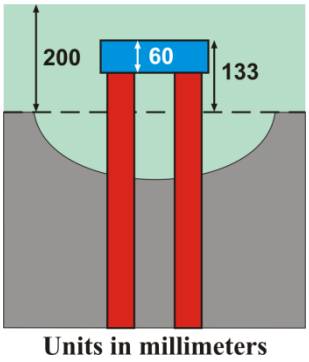

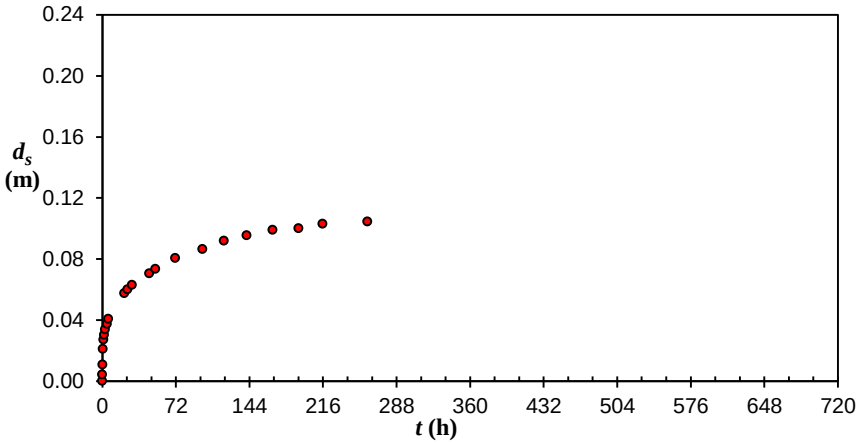

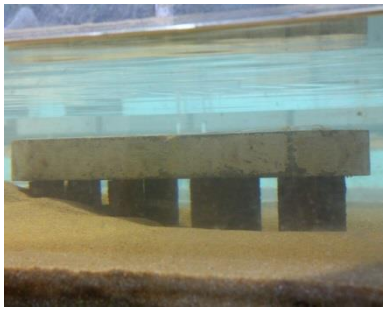

Scour depth measurements in the test M6E2

t_d (h)	d_{sm} (m)		t_d (h)	d_{sm} (m)		t_d (h)	d_{sm} (m)		t_d (h)	d_{sm} (m)
0.00	0.0000		2.92	0.0338		45.97	0.0704		166.72	0.0989
0.10	0.0042		4.57	0.0373		51.98	0.0735		192.23	0.1001
0.28	0.0108		6.05	0.0407		71.45	0.0806		215.70	0.1030
0.65	0.0210		21.48	0.0574		98.20	0.0864		259.57	0.1044
1.13	0.0271		24.73	0.0601		119.00	0.0919			
1.73	0.0302		29.10	0.0629		141.50	0.0954			

Test M6F2

d_{50}	h	U	U_c	U/U_c	B/D_{pc}	B/h	h/D_{pc}
0.086 mm	0.20 m	0.258 m/s	0.322 m/s	0.80	10.0	10.0	1.0

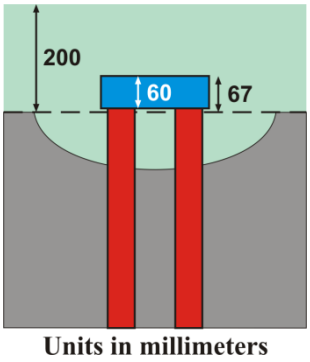

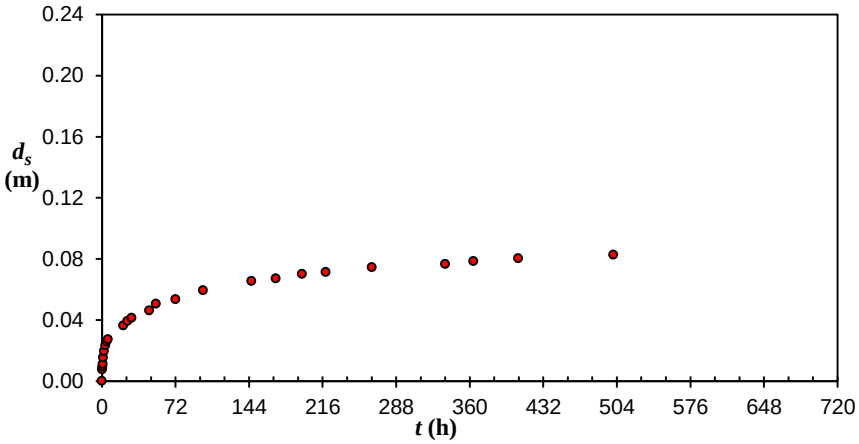

Scour depth measurements in the test M6F2

t_d (h)	d_{sm} (m)		t_d (h)	d_{sm} (m)		t_d (h)	d_{sm} (m)		t_d (h)	d_{sm} (m)
0.00	0.0000		4.73	0.0258		72.08	0.0536		336.05	0.0766
0.23	0.0075		5.80	0.0273		99.18	0.0594		363.67	0.0784
0.48	0.0094		20.88	0.0364		146.32	0.0654		407.47	0.0804
0.85	0.0112		25.08	0.0392		170.23	0.0672		500.72	0.0826
1.33	0.0154		29.02	0.0414		196.02	0.0700			
2.18	0.0195		46.30	0.0462		219.13	0.0714			
3.40	0.0232		53.05	0.0505		264.37	0.0745			

Test M6G2

d_{50}	h	U	U_c	U/U_c	B/D_{pc}	B/h	h/D_{pc}
0.086 mm	0.20 m	0.258 m/s	0.322 m/s	0.80	10.0	10.0	1.0

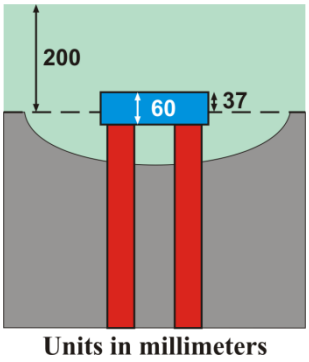

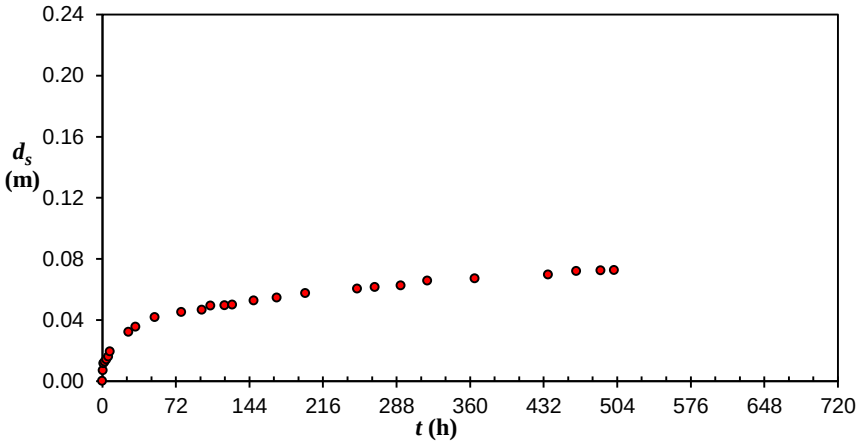

Scour depth measurements in the test M6G2

t_d (h)	d_{sm} (m)		t_d (h)	d_{sm} (m)		t_d (h)	d_{sm} (m)		t_d (h)	d_{sm} (m)
0.00	0.0000		25.57	0.0322		127.37	0.0499		318.30	0.0657
0.60	0.0070		32.50	0.0355		148.22	0.0526		364.70	0.0672
1.35	0.0115		51.25	0.0418		170.77	0.0545		436.42	0.0697
2.52	0.0126		77.37	0.0452		198.60	0.0575		463.93	0.0720
4.07	0.0140		97.33	0.0465		249.45	0.0604		487.87	0.0724
6.02	0.0159		105.85	0.0493		266.93	0.0615		500.97	0.0726
7.47	0.0193		119.78	0.0495		292.32	0.0626			

Test M7O2

d_{50}	h	U	U_c	U/U_c	B/D_{pc}	B/h	h/D_{pc}
0.086 mm	0.18 m	0.315 m/s	0.322 m/s	0.80	8.3	5.6	1.5

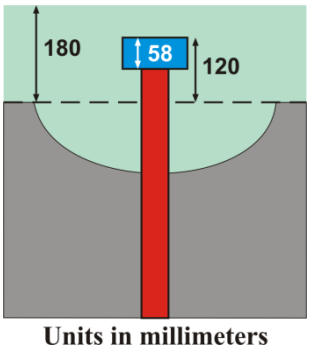

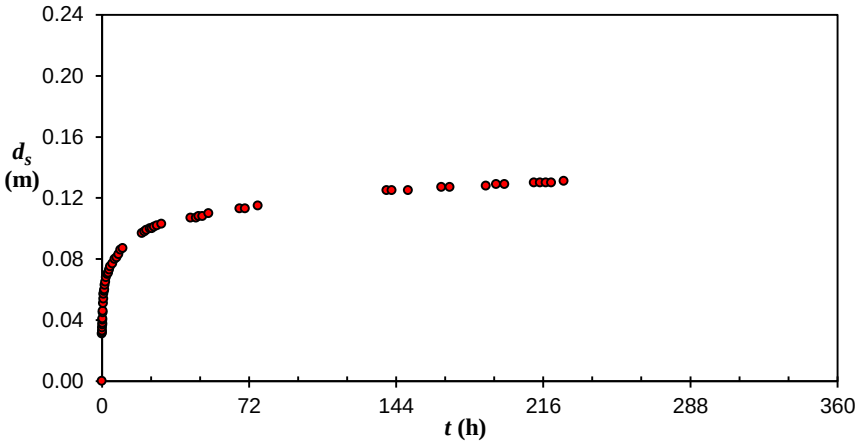

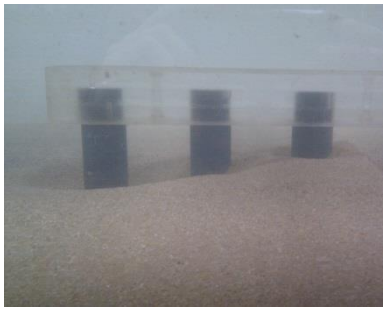

Scour depth measurements in the test M7O2

t_d (h)	d_{sm} (m)	t_d (h)	d_{sm} (m)	t_d (h)	d_{sm} (m)	t_d (h)	d_{sm} (m)
0.00	0.0000	1.17	0.0600	20.75	0.0980	139.37	0.1250
0.05	0.0310	1.33	0.0630	21.75	0.0990	141.92	0.1250
0.08	0.0320	1.75	0.0650	23.43	0.1000	149.83	0.1250
0.13	0.0330	2.08	0.0680	24.47	0.1000	166.17	0.1270
0.17	0.0350	2.58	0.0700	25.50	0.1010	170.25	0.1270
0.22	0.0370	3.08	0.0710	26.92	0.1020	188.00	0.1280
0.25	0.0380	3.58	0.0730	29.07	0.1030	193.00	0.1290
0.30	0.0400	4.08	0.0750	43.42	0.1070	197.00	0.1290
0.33	0.0410	5.08	0.0770	46.05	0.1070	211.50	0.1300
0.42	0.0450	6.22	0.0800	47.33	0.1080	214.50	0.1300
0.50	0.0460	7.17	0.0810	49.20	0.1080	217.33	0.1300
0.58	0.0510	8.08	0.0830	52.18	0.1100	220.00	0.1300
0.75	0.0540	9.08	0.0860	67.45	0.1130	226.00	0.1310
0.83	0.0570	10.13	0.0870	70.12	0.1130		
1.00	0.0590	19.50	0.0970	76.27	0.1150		

Test M7P2

d_{50}	h	U	U_c	U/U_c	B/D_{pc}	B/h	h/D_{pc}
0.086 mm	0.18 m	0.315 m/s	0.322 m/s	0.80	8.3	5.6	1.5

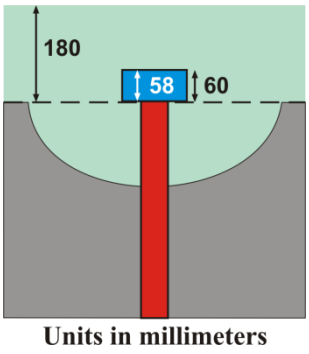

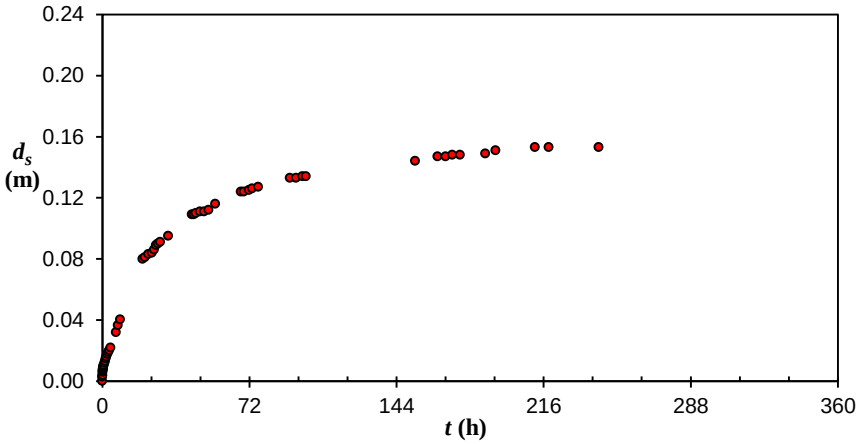

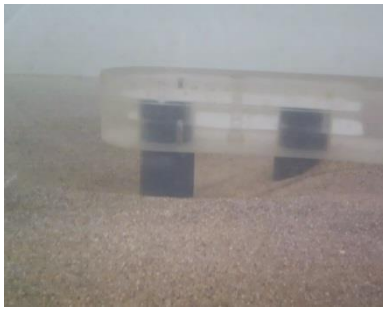

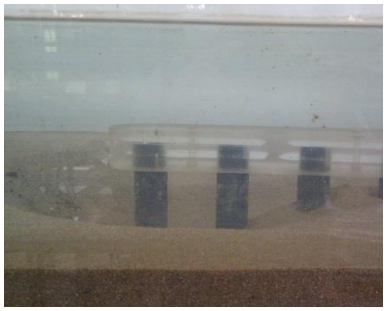

Scour depth measurements in the test M7P2

t_d (h)	d_{sm} (m)	t_d (h)	d_{sm} (m)	t_d (h)	d_{sm} (m)	t_d (h)	d_{sm} (m)
0.00	0.0000	3.00	0.0188	32.28	0.0950	94.83	0.1330
0.05	0.0028	3.50	0.0201	43.83	0.1090	98.00	0.1340
0.08	0.0038	4.00	0.0219	44.83	0.1090	99.67	0.1340
0.17	0.0058	6.67	0.0319	45.83	0.1100	153.17	0.1440
0.25	0.0069	7.70	0.0365	47.78	0.1110	164.17	0.1470
0.33	0.0078	8.72	0.0402	49.83	0.1110	168.00	0.1470
0.42	0.0082	19.70	0.0800	52.03	0.1120	171.33	0.1480
0.50	0.0095	20.83	0.0810	55.33	0.1160	175.03	0.1480
0.75	0.0104	22.50	0.0830	67.83	0.1240	187.57	0.1490
1.00	0.0118	24.28	0.0840	69.33	0.1240	192.50	0.1510
1.33	0.0131	25.32	0.0860	71.83	0.1250	211.73	0.1530
1.67	0.0148	26.28	0.0890	73.33	0.1260	218.50	0.1530
2.00	0.0160	27.30	0.0900	76.33	0.1270	243.03	0.1530
2.50	0.0176	28.28	0.0910	91.78	0.1330		

Test M7Q2

d_{50}	h	U	U_c	U/U_c	B/D_{pc}	B/h	h/D_{pc}
0.086 mm	0.18 m	0.315 m/s	0.322 m/s	0.80	8.3	5.6	1.5

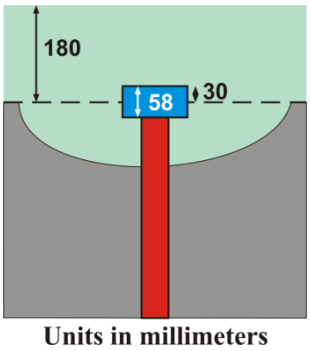

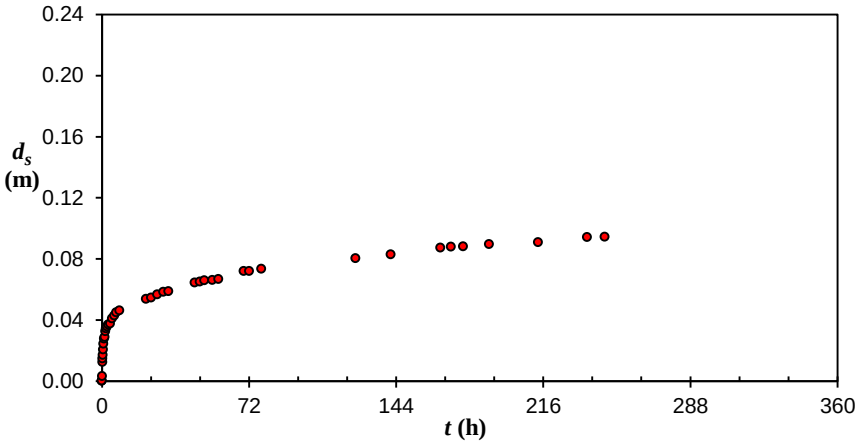

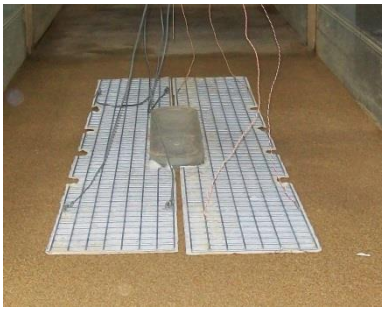

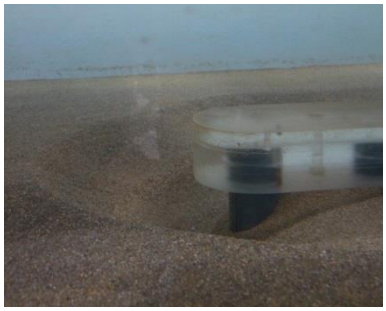

Scour depth measurements in the test M7Q2

t_d (h)	d_{sm} (m)		t_d (h)	d_{sm} (m)		t_d (h)	d_{sm} (m)		t_d (h)	d_{sm} (m)
0.00	0.0000		2.05	0.0345		30.08	0.0583		141.42	0.0829
0.05	0.0002		2.55	0.0357		32.58	0.0588		165.75	0.0873
0.13	0.0032		3.05	0.0370		45.42	0.0643		170.92	0.0879
0.22	0.0125		4.05	0.0375		47.92	0.0650		176.82	0.0881
0.30	0.0146		5.05	0.0410		50.08	0.0659		189.58	0.0895
0.38	0.0170		6.05	0.0427		54.08	0.0661		213.58	0.0909
0.55	0.0206		7.05	0.0450		56.98	0.0668		237.58	0.0942
0.80	0.0243		8.58	0.0461		69.42	0.0719		246.17	0.0944
1.05	0.0277		21.58	0.0537		72.08	0.0720			
1.38	0.0287		24.08	0.0546		78.08	0.0734			
1.72	0.0326		27.08	0.0566		124.08	0.0804			

Test M7R2

d_{50}	h	U	U_c	U/U_c	B/D_{pc}	B/h	h/D_{pc}
0.086 mm	0.18 m	0.315 m/s	0.322 m/s	0.80	8.3	5.6	1.5

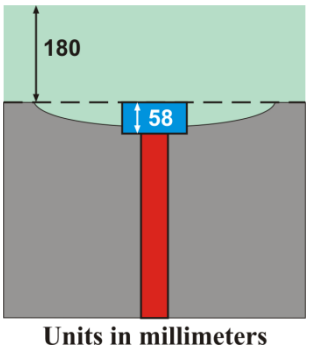

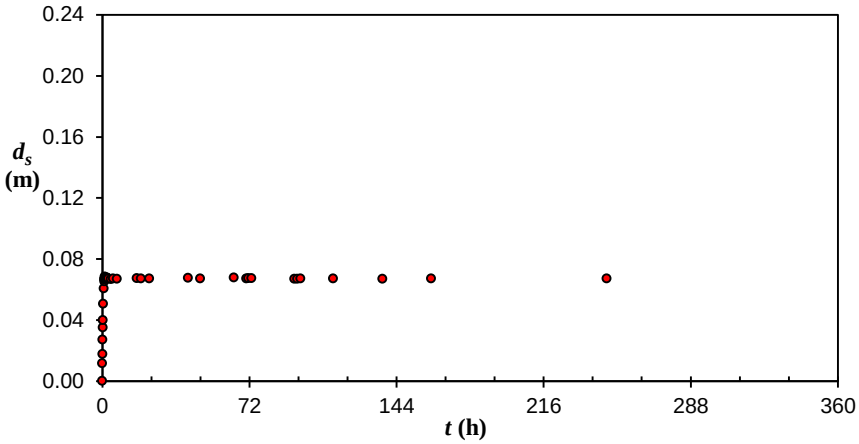

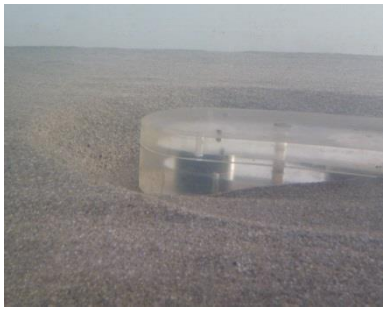

Scour depth measurements in the test M7R2

t_d (h)	d_{sm} (m)	t_d (h)	d_{sm} (m)	t_d (h)	d_{sm} (m)	t_d (h)	d_{sm} (m)
0.00	0.0000	1.08	0.0667	4.23	0.0668	71.48	0.0673
0.05	0.0115	1.17	0.0673	5.23	0.0671	72.98	0.0674
0.08	0.0177	1.25	0.0684	7.23	0.0670	93.98	0.0669
0.17	0.0271	1.33	0.0677	16.98	0.0673	95.48	0.0669
0.25	0.0351	1.50	0.0676	18.98	0.0672	96.98	0.0672
0.33	0.0398	1.75	0.0674	22.98	0.0671	112.98	0.0671
0.50	0.0506	2.00	0.0675	41.98	0.0675	137.23	0.0670
0.75	0.0607	2.33	0.0677	47.98	0.0672	160.98	0.0672
1.00	0.0653	2.67	0.0673	64.48	0.0677	246.98	0.0671
1.05	0.0665	3.00	0.0672	70.48	0.0671		

Test M2E3

d_{50}	h	U	U_c	U/U_c	B/D_{pc}	B/h	h/D_{pc}
0.086 mm	0.20 m	0.258 m/s	0.322 m/s	0.80	10.0	10.0	1.0

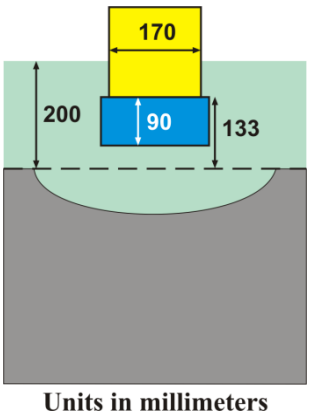

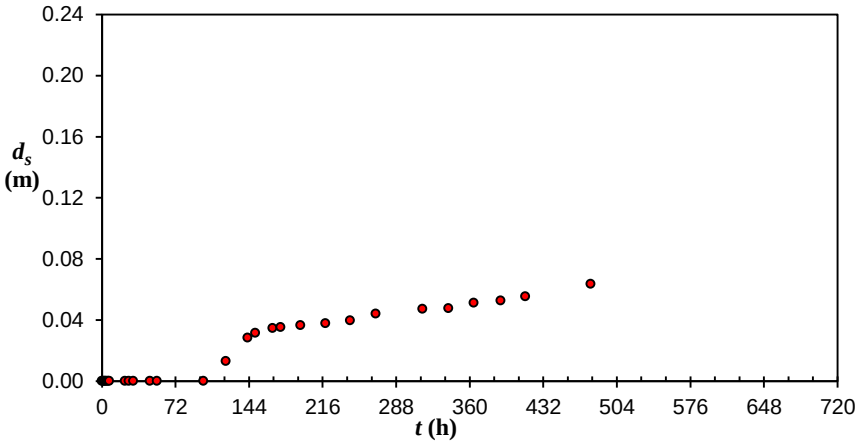

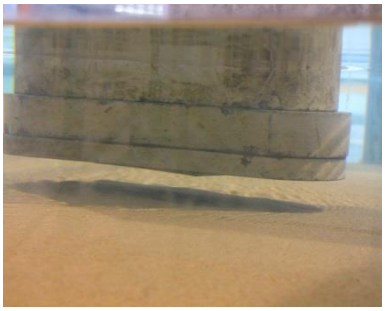

Scour depth measurements in the test M2E3

t_d (h)	d_{sm} (m)		t_d (h)	d_{sm} (m)		t_d (h)	d_{sm} (m)		t_d (h)	d_{sm} (m)
0.00	0.0000		22.55	0.0000		142.50	0.0283		267.97	0.0440
1.00	0.0000		26.40	0.0000		150.25	0.0314		313.93	0.0471
2.00	0.0000		30.68	0.0000		167.23	0.0347		339.28	0.0476
3.00	0.0000		47.07	0.0000		175.00	0.0353		364.03	0.0512
4.28	0.0000		54.00	0.0000		194.27	0.0366		390.30	0.0527
5.92	0.0000		99.28	0.0000		218.90	0.0377		414.35	0.0554
7.25	0.0000		121.38	0.0131		243.00	0.0397		478.50	0.0636

Test M2F3

d_{50}	h	U	U_c	U/U_c	B/D_{pc}	B/h	h/D_{pc}
0.086 mm	0.20 m	0.258 m/s	0.322 m/s	0.80	10.0	10.0	1.0

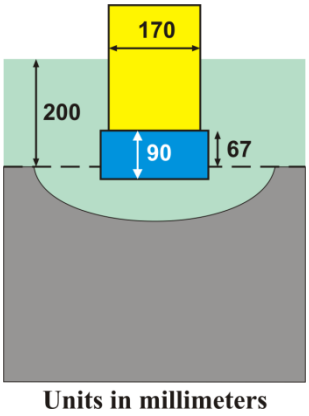

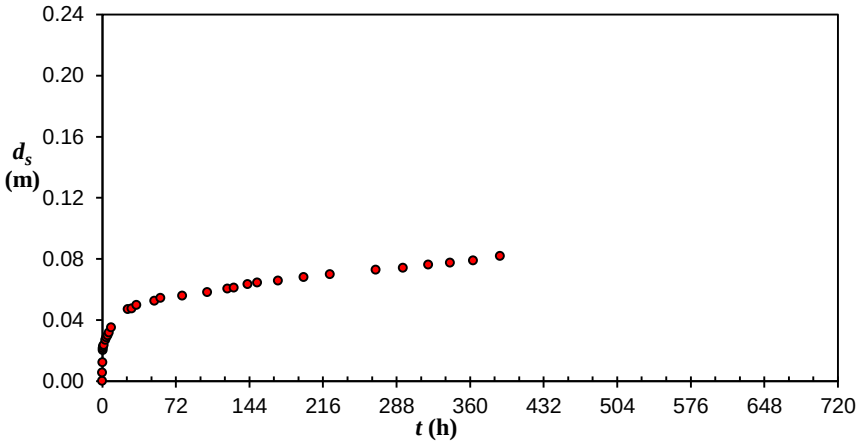

Scour depth measurements in the test M2F3

t_d (h)	d_{sm} (m)	t_d (h)	d_{sm} (m)	t_d (h)	d_{sm} (m)	t_d (h)	d_{sm} (m)
0.00	0.0000	3.90	0.0285	57.15	0.0544	197.23	0.0679
0.10	0.0054	5.23	0.0297	78.45	0.0558	223.02	0.0699
0.25	0.0121	6.50	0.0316	102.68	0.0581	267.62	0.0728
0.45	0.0202	8.60	0.0350	122.40	0.0604	294.28	0.0741
0.65	0.0215	25.07	0.0469	128.75	0.0611	319.20	0.0761
1.02	0.0226	28.77	0.0474	142.45	0.0634	340.40	0.0773
1.63	0.0235	33.53	0.0497	151.68	0.0645	363.05	0.0788
3.03	0.0269	51.05	0.0525	172.00	0.0657	389.33	0.0819

Test M2H3

d_{50}	h	U	U_c	U/U_c	B/D_{pc}	B/h	h/D_{pc}
0.086 mm	0.20 m	0.258 m/s	0.322 m/s	0.80	10.0	10.0	1.0

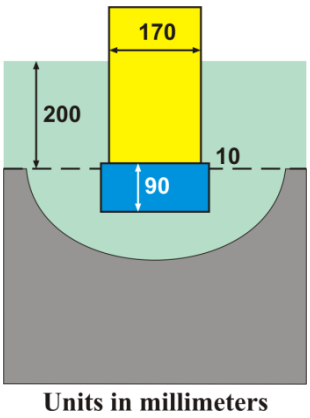

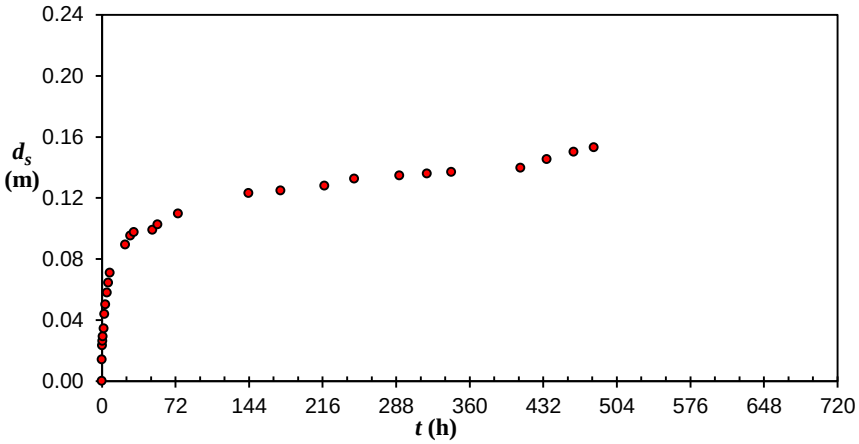

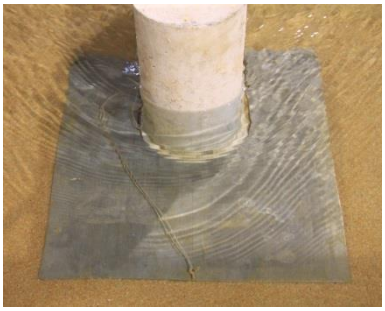

Scour depth measurements in the test M2H3

t_d (h)	d_{sm} (m)		t_d (h)	d_{sm} (m)		t_d (h)	d_{sm} (m)		t_d (h)	d_{sm} (m)
0.00	0.0000		3.52	0.0502		49.48	0.0989		291.27	0.1347
0.10	0.0141		4.90	0.0578		54.62	0.1026		318.22	0.1358
0.30	0.0232		6.18	0.0644		74.48	0.1097		342.02	0.1370
0.55	0.0263		7.73	0.0709		143.48	0.1232		409.73	0.1396
1.00	0.0291		22.72	0.0893		174.77	0.1248		435.58	0.1454
1.70	0.0345		27.82	0.0952		217.87	0.1280		461.88	0.1501
2.50	0.0439		31.38	0.0976		247.10	0.1325		481.60	0.1530

Test M3E3

d_{50}	h	U	U_c	U/U_c	B/D_{pc}	B/h	h/D_{pc}
0.086 mm	0.20 m	0.258 m/s	0.322 m/s	0.80	10.0	10.0	1.0

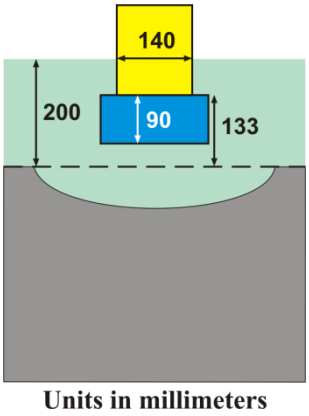

Units in millimeters

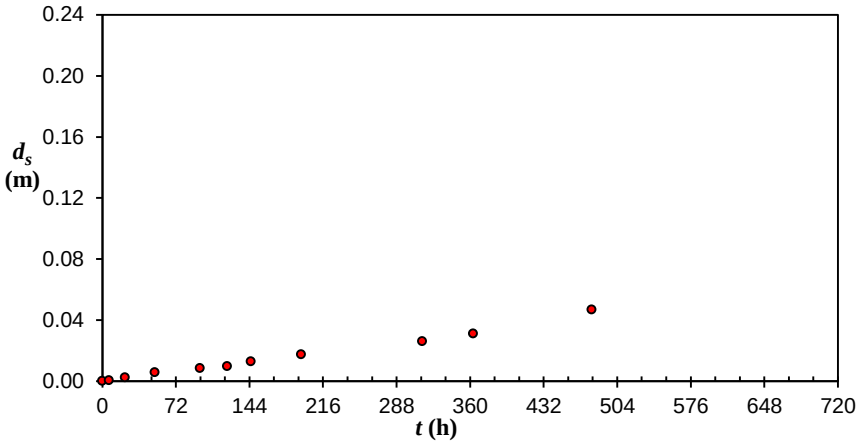

Scour depth measurements in the test M3E3

t_d (h)	d_{sm} (m)		t_d (h)	d_{sm} (m)		t_d (h)	d_{sm} (m)		t_d (h)	d_{sm} (m)
0.00	0.0000		51.25	0.0057		145.47	0.0128		363.05	0.0311
6.63	0.0004		95.50	0.0085		194.55	0.0175		479.13	0.0468
22.28	0.0023		122.35	0.0097		313.35	0.0260			

Test M3F3

d_{50}	h	U	U_c	U/U_c	B/D_{pc}	B/h	h/D_{pc}
0.086 mm	0.20 m	0.258 m/s	0.322 m/s	0.80	10.0	10.0	1.0

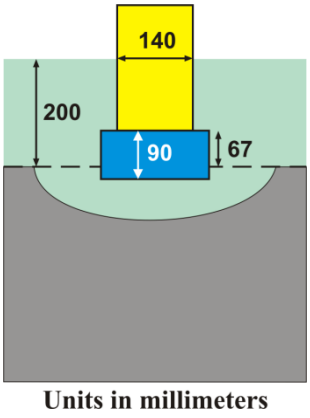

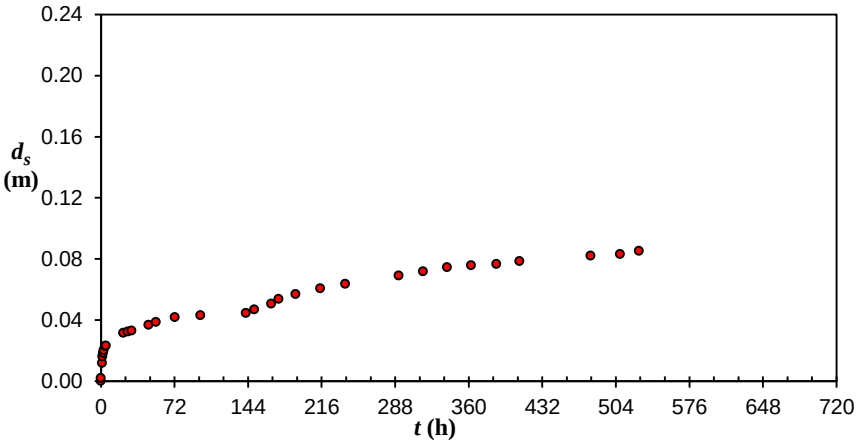

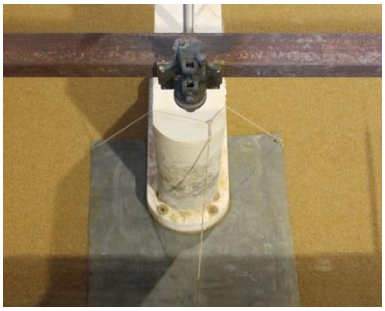

Scour depth measurements in the test M3F3

t_d (h)	d_{sm} (m)		t_d (h)	d_{sm} (m)		t_d (h)	d_{sm} (m)		t_d (h)	d_{sm} (m)
0.00	0.0000		21.90	0.0314		150.17	0.0468		338.87	0.0744
0.10	0.0020		26.17	0.0323		166.68	0.0506		362.32	0.0758
1.10	0.0118		30.08	0.0330		174.12	0.0537		387.13	0.0765
1.50	0.0159		46.65	0.0367		190.75	0.0568		409.67	0.0785
2.00	0.0182		53.80	0.0386		214.78	0.0606		479.45	0.0820
2.88	0.0201		72.33	0.0417		239.33	0.0636		508.15	0.0831
4.08	0.0228		97.58	0.0431		291.45	0.0690		526.62	0.0852
5.03	0.0231		142.03	0.0445		315.37	0.0717			

Test M3H3

d_{50}	h	U	U_c	U/U_c	B/D_{pc}	B/h	h/D_{pc}
0.086 mm	0.20 m	0.258 m/s	0.322 m/s	0.80	10.0	10.0	1.0

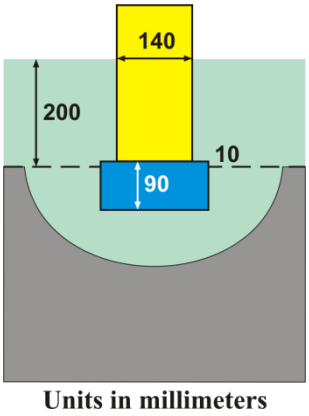

Units in millimeters

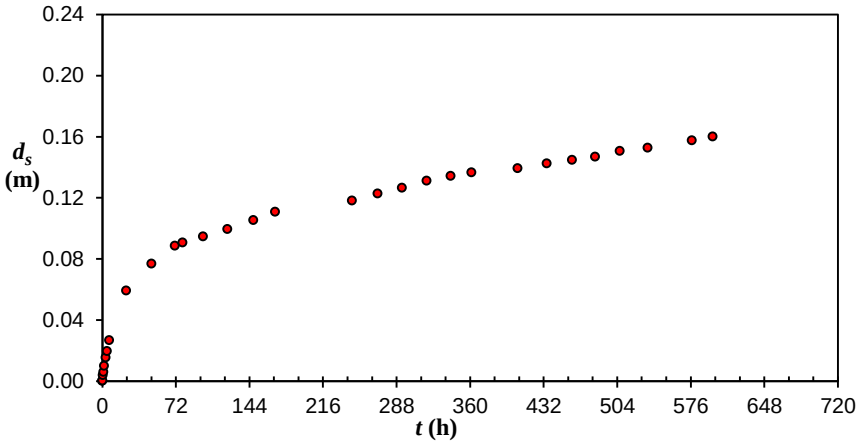

Scour depth measurements in the test M3H3

t_d (h)	d_{sm} (m)	t_d (h)	d_{sm} (m)	t_d (h)	d_{sm} (m)	t_d (h)	d_{sm} (m)
0.00	0.0000	23.35	0.0591	244.57	0.1181	459.87	0.1447
0.15	0.0002	48.37	0.0767	269.60	0.1226	482.57	0.1469
0.50	0.0037	71.27	0.0886	293.57	0.1265	506.68	0.1506
1.15	0.0060	78.50	0.0907	317.63	0.1310	533.82	0.1527
1.98	0.0099	98.82	0.0946	341.17	0.1343	577.13	0.1576
3.42	0.0154	122.67	0.0995	361.62	0.1366	597.53	0.1600
4.67	0.0196	148.10	0.1052	406.75	0.1392		
6.87	0.0267	169.27	0.1107	435.25	0.1425		

Test M4D3

d_{50}	h	U	U_c	U/U_c	B/D_{pc}	B/h	h/D_{pc}
0.086 mm	0.20 m	0.258 m/s	0.322 m/s	0.80	10.0	10.0	1.0

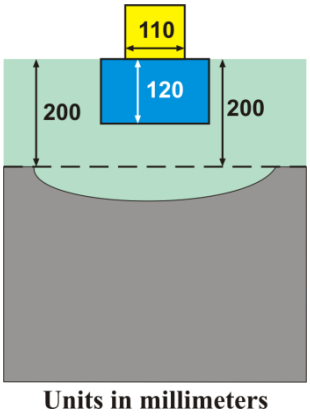

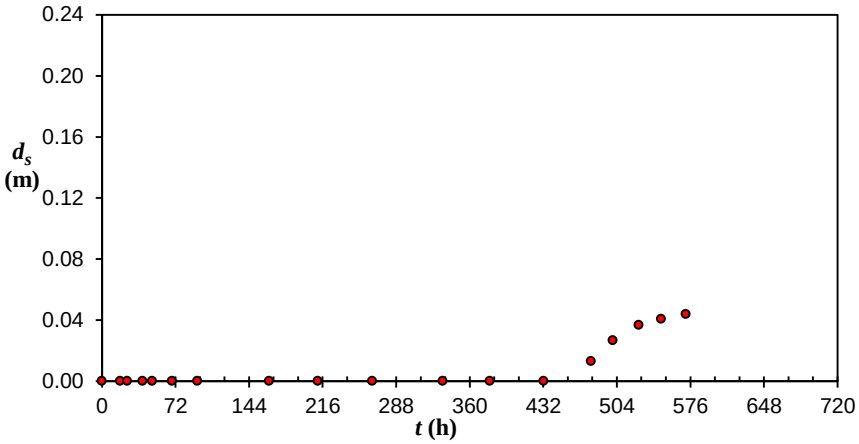

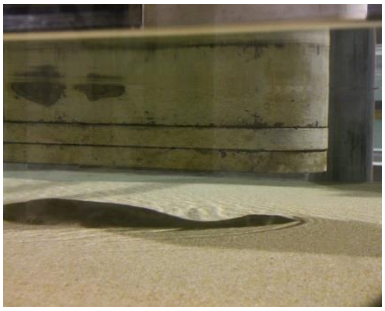

Scour depth measurements in the test M4D3

t_d (h)	d_{sm} (m)		t_d (h)	d_{sm} (m)		t_d (h)	d_{sm} (m)		t_d (h)	d_{sm} (m)
0.00	0.0000		68.50	0.0000		333.55	0.0000		525.37	0.0367
17.87	0.0000		93.30	0.0000		379.58	0.0000		547.37	0.0408
24.83	0.0000		163.50	0.0000		432.33	0.0000		571.48	0.0439
39.65	0.0000		211.32	0.0000		478.87	0.0131			
49.03	0.0000		264.72	0.0000		499.95	0.0266			

Test M4E3

d_{50}	h	U	U_c	U/U_c	B/D_{pc}	B/h	h/D_{pc}
0.086 mm	0.20 m	0.258 m/s	0.322 m/s	0.80	10.0	10.0	1.0

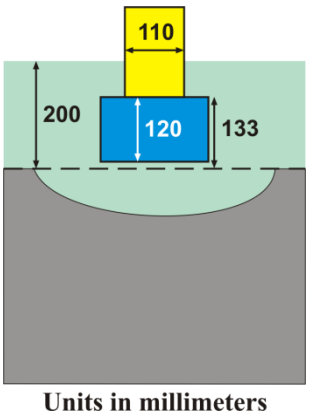

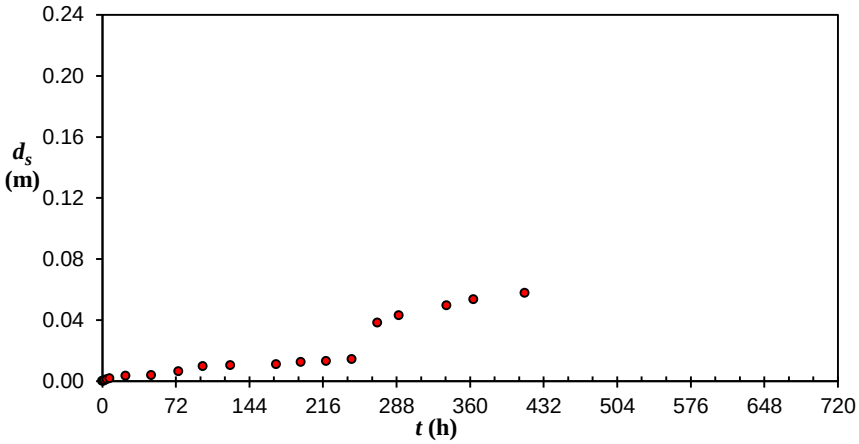

Scour depth measurements in the test M4E3

t_d (h)	d_{sm} (m)		t_d (h)	d_{sm} (m)		t_d (h)	d_{sm} (m)		t_d (h)	d_{sm} (m)
0.00	0.0000		22.85	0.0033		170.37	0.0109		290.37	0.0430
1.17	0.0001		47.87	0.0038		194.47	0.0123		337.02	0.0496
2.28	0.0005		74.52	0.0063		219.20	0.0130		363.30	0.0534
4.18	0.0010		98.53	0.0096		244.25	0.0143		413.58	0.0576
7.13	0.0016		125.42	0.0102		269.17	0.0381			

Test M4F3

d_{50}	h	U	U_c	U/U_c	B/D_{pc}	B/h	h/D_{pc}
0.086 mm	0.20 m	0.258 m/s	0.322 m/s	0.80	10.0	10.0	1.0

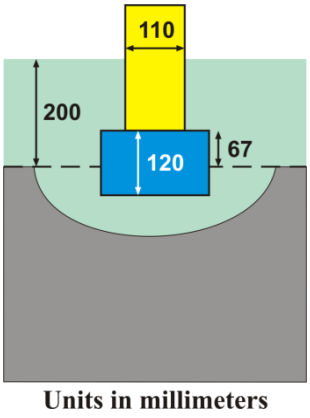

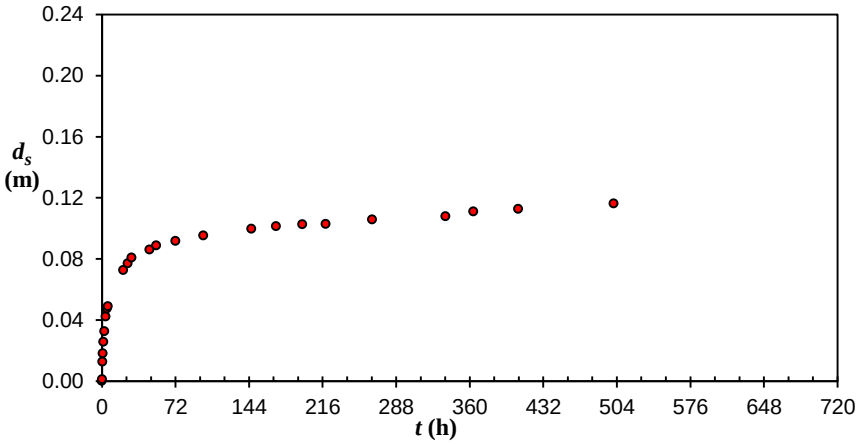

Scour depth measurements in the test M4F3

t_d (h)	d_{sm} (m)		t_d (h)	d_{sm} (m)		t_d (h)	d_{sm} (m)		t_d (h)	d_{sm} (m)
0.00	0.0000		4.90	0.0475		72.18	0.0916		336.38	0.1078
0.12	0.0011		6.03	0.0488		99.45	0.0952		363.80	0.1109
0.55	0.0126		21.00	0.0726		146.48	0.0996		407.62	0.1126
1.00	0.0180		25.32	0.0770		170.47	0.1014		500.92	0.1161
1.58	0.0256		29.17	0.0807		196.17	0.1025			
2.33	0.0326		46.53	0.0861		219.23	0.1028			
3.63	0.0422		53.18	0.0887		264.52	0.1058			

Test M5D3

d_{50}	h	U	U_c	U/U_c	B/D_{pc}	B/h	h/D_{pc}
0.086 mm	0.20 m	0.258 m/s	0.322 m/s	0.80	10.0	10.0	1.0

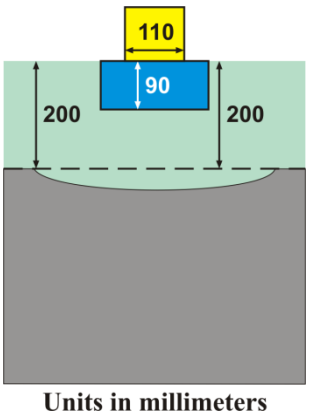

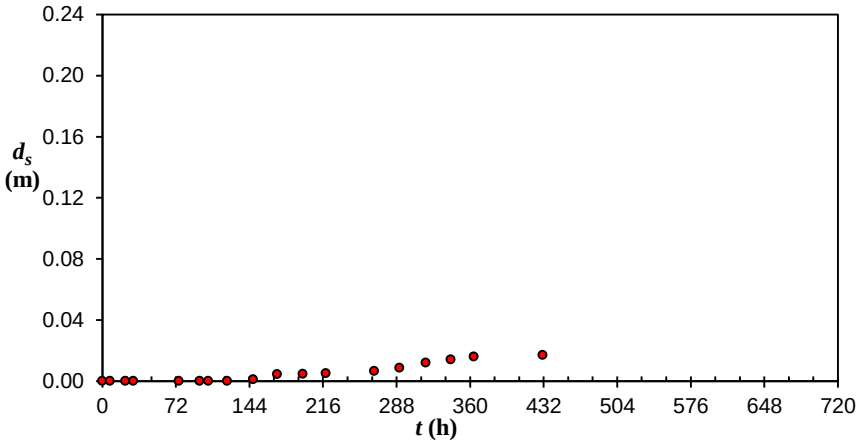

Scour depth measurements in the test M5D3

t_d (h)	d_{sm} (m)		t_d (h)	d_{sm} (m)		t_d (h)	d_{sm} (m)		t_d (h)	d_{sm} (m)
0.00	0.0000		95.32	0.0000		196.10	0.0047		341.07	0.0140
7.35	0.0000		103.77	0.0000		218.68	0.0051		363.63	0.0160
22.52	0.0000		122.27	0.0000		266.12	0.0066		431.27	0.0170
30.52	0.0000		147.70	0.0010		290.90	0.0087			
74.77	0.0000		171.25	0.0044		316.70	0.0119			

Test M5E3

d_{50}	h	U	U_c	U/U_c	B/D_{pc}	B/h	h/D_{pc}
0.086 mm	0.20 m	0.258 m/s	0.322 m/s	0.80	10.0	10.0	1.0

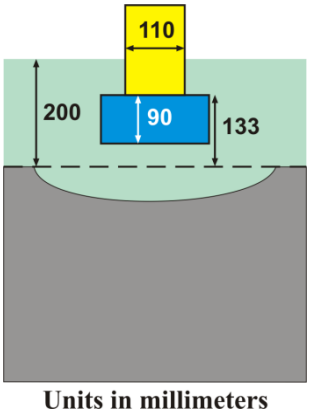

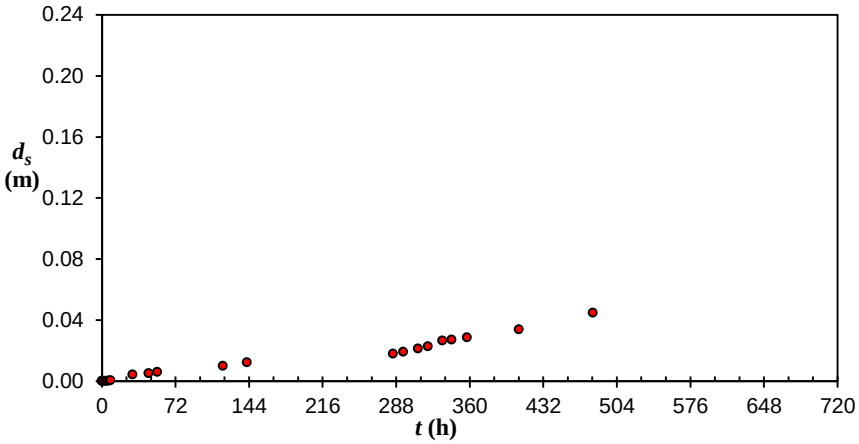

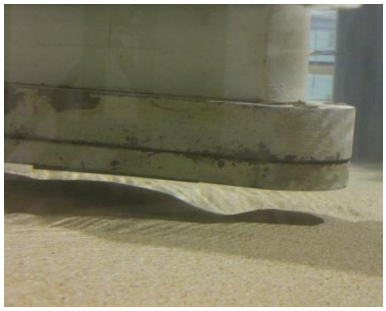

Scour depth measurements in the test M5E3

t_d (h)	d_{sm} (m)		t_d (h)	d_{sm} (m)		t_d (h)	d_{sm} (m)		t_d (h)	d_{sm} (m)
0.00	0.0000		8.55	0.0004		285.12	0.0179		357.30	0.0286
0.32	0.0000		30.17	0.0042		295.02	0.0191		408.13	0.0338
1.13	0.0000		45.68	0.0050		309.30	0.0213		480.52	0.0447
3.28	0.0000		54.10	0.0059		319.27	0.0226			
5.35	0.0000		118.42	0.0098		333.20	0.0264			
7.05	0.0002		141.90	0.0121		342.28	0.0270			

Test M5F3

d_{50}	h	U	U_c	U/U_c	B/D_{pc}	B/h	h/D_{pc}
0.086 mm	0.20 m	0.258 m/s	0.322 m/s	0.80	10.0	10.0	1.0

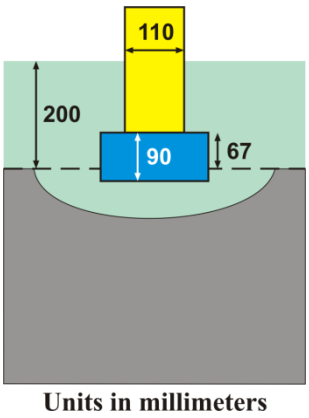

Units in millimeters

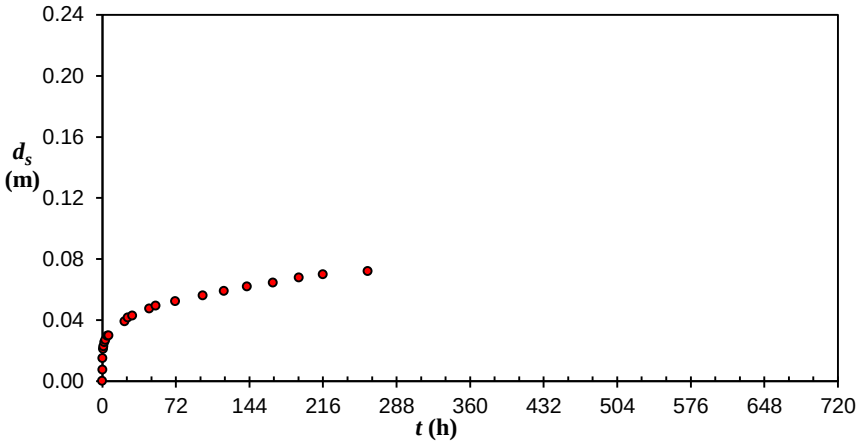

Scour depth measurements in the test M5F3

t_d (h)	d_{sm} (m)		t_d (h)	d_{sm} (m)		t_d (h)	d_{sm} (m)		t_d (h)	d_{sm} (m)
0.00	0.0000		3.08	0.0268		46.13	0.0474		166.98	0.0644
0.13	0.0073		4.82	0.0296		52.22	0.0494		192.42	0.0677
0.38	0.0149		6.22	0.0299		71.60	0.0522		215.95	0.0698
0.80	0.0210		21.77	0.0391		98.33	0.0560		259.82	0.0719
1.30	0.0226		24.90	0.0416		119.23	0.0590			
2.00	0.0254		29.37	0.0429		141.67	0.0618			

Test M5G3

d_{50}	h	U	U_c	U/U_c	B/D_{pc}	B/h	h/D_{pc}
0.086 mm	0.20 m	0.258 m/s	0.322 m/s	0.80	10.0	10.0	1.0

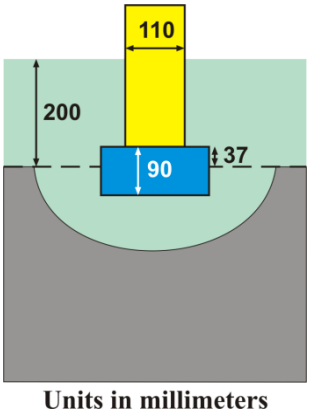

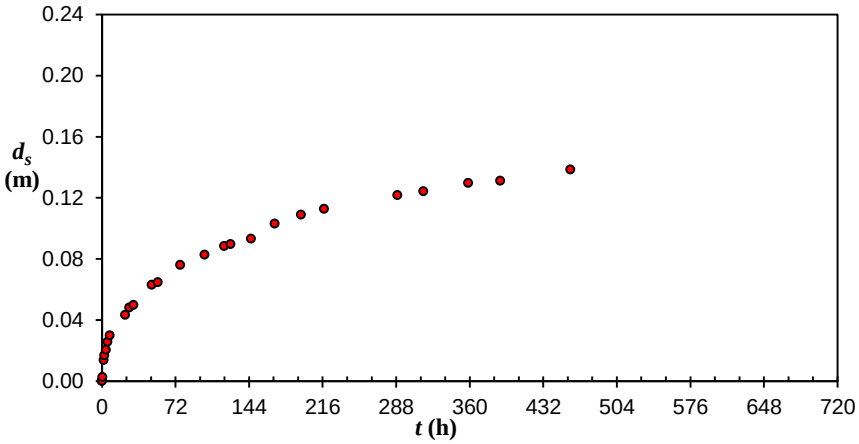

Scour depth measurements in the test M5G3

t_d (h)	d_{sm} (m)		t_d (h)	d_{sm} (m)		t_d (h)	d_{sm} (m)		t_d (h)	d_{sm} (m)
0.00	0.0000		7.73	0.0299		100.65	0.0827		289.37	0.1217
0.22	0.0000		22.77	0.0432		119.87	0.0882		314.93	0.1241
0.57	0.0026		27.07	0.0480		126.12	0.0895		358.67	0.1296
1.78	0.0137		31.07	0.0497		146.10	0.0932		389.92	0.1310
2.43	0.0167		49.02	0.0629		169.38	0.1029		458.68	0.1384
3.90	0.0203		54.88	0.0647		194.85	0.1088			
5.57	0.0256		76.73	0.0760		217.63	0.1126			

Test M6E3

d_{50}	h	U	U_c	U/U_c	B/D_{pc}	B/h	h/D_{pc}
0.086 mm	0.20 m	0.258 m/s	0.322 m/s	0.80	10.0	10.0	1.0

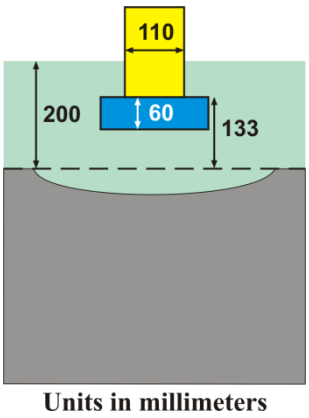

Units in millimeters

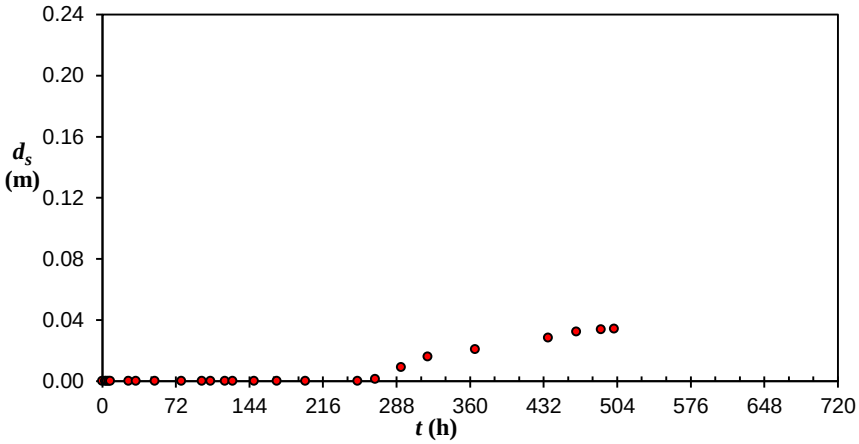

Scour depth measurements in the test M6E3

t_d (h)	d_{sm} (m)	t_d (h)	d_{sm} (m)	t_d (h)	d_{sm} (m)	t_d (h)	d_{sm} (m)
0.00	0.0000	51.38	0.0000	170.93	0.0000	436.57	0.0283
2.68	0.0000	77.53	0.0000	198.85	0.0000	464.17	0.0323
4.33	0.0000	97.60	0.0000	249.72	0.0000	488.03	0.0338
6.22	0.0000	106.05	0.0000	267.10	0.0013	501.18	0.0342
7.75	0.0000	120.03	0.0000	292.57	0.0091		
25.72	0.0000	127.58	0.0000	318.47	0.0159		
32.77	0.0000	148.48	0.0000	364.95	0.0208		

Test M6F3

d_{50}	h	U	U_c	U/U_c	B/D_{pc}	B/h	h/D_{pc}
0.086 mm	0.20 m	0.258 m/s	0.322 m/s	0.80	10.0	10.0	1.0

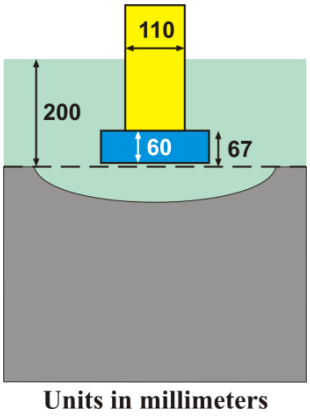

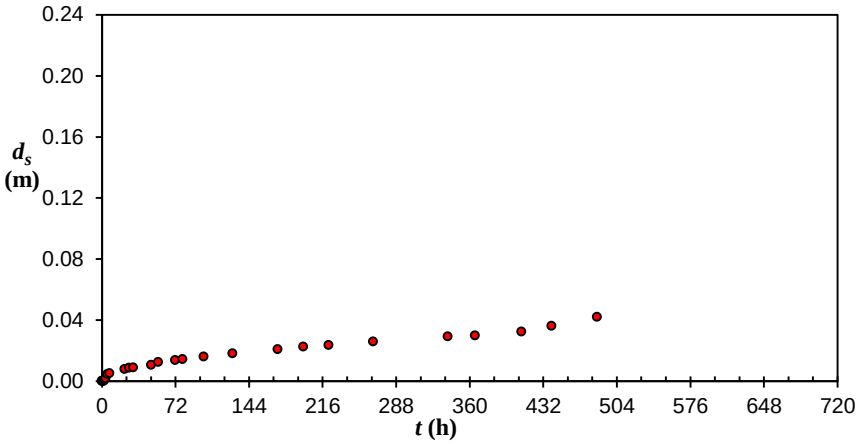

Scour depth measurements in the test M6F3

t_d (h)	d_{sm} (m)		t_d (h)	d_{sm} (m)		t_d (h)	d_{sm} (m)		t_d (h)	d_{sm} (m)
0.00	0.0000		5.13	0.0044		71.73	0.0136		265.63	0.0259
0.17	0.0000		7.38	0.0051		79.05	0.0142		338.47	0.0291
0.58	0.0000		22.37	0.0077		99.80	0.0159		365.18	0.0299
0.83	0.0000		26.52	0.0086		127.88	0.0180		410.88	0.0324
1.88	0.0000		30.63	0.0089		172.22	0.0207		440.10	0.0361
2.67	0.0009		48.17	0.0106		197.10	0.0225		484.63	0.0420
3.78	0.0016		55.08	0.0124		222.05	0.0236			

Test M6G3

d_{50}	h	U	U_c	U/U_c	B/D_{pc}	B/h	h/D_{pc}
0.086 mm	0.20 m	0.258 m/s	0.322 m/s	0.80	10.0	10.0	1.0

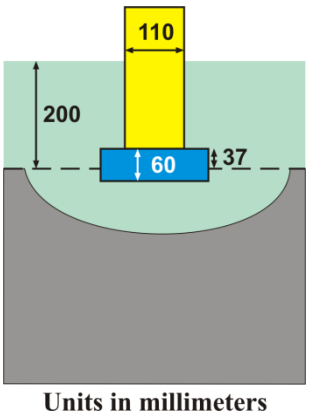

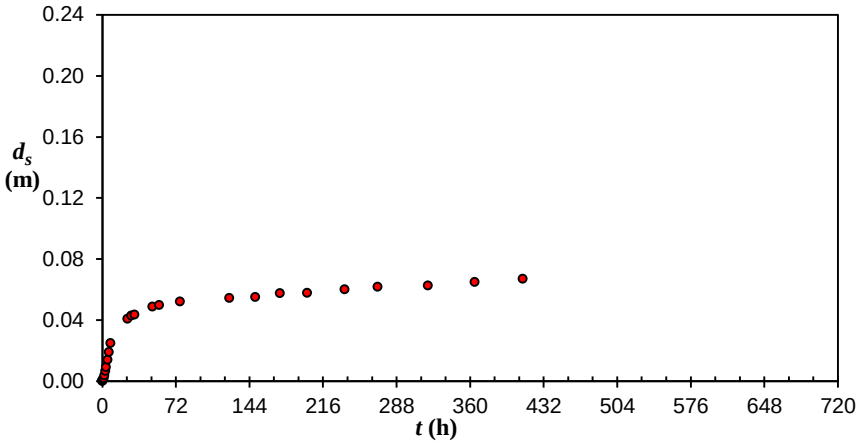

Scour depth measurements in the test M6G3

t_d (h)	d_{sm} (m)		t_d (h)	d_{sm} (m)		t_d (h)	d_{sm} (m)		t_d (h)	d_{sm} (m)
0.00	0.0000		2.97	0.0065		31.63	0.0434		200.52	0.0577
0.22	0.0000		3.87	0.0090		49.15	0.0487		237.38	0.0600
0.35	0.0004		5.43	0.0138		55.80	0.0497		269.72	0.0617
0.63	0.0006		6.68	0.0190		76.22	0.0520		318.85	0.0626
1.00	0.0010		8.22	0.0247		124.53	0.0544		364.55	0.0648
1.63	0.0018		24.67	0.0406		149.83	0.0550		411.72	0.0670
2.28	0.0036		28.47	0.0427		173.90	0.0575			

Test M7N3

d_{50}	h	U	U_c	U/U_c	B/D_{pc}	B/h	h/D_{pc}
0.086 mm	0.18 m	0.315 m/s	0.322 m/s	0.80	8.3	5.6	1.5

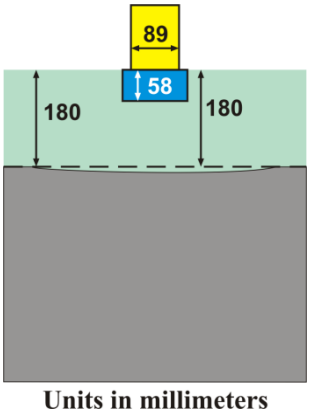

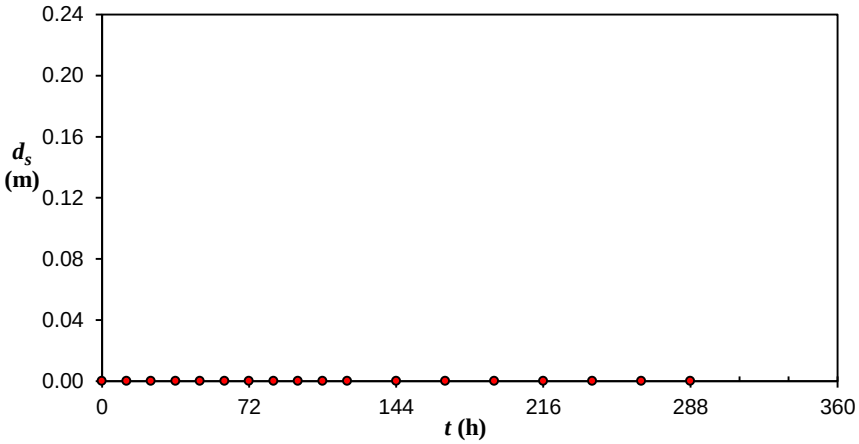

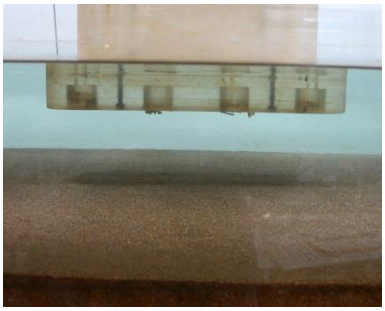

Scour depth measurements in the test M7N3

t_d (h)	d_{sm} (m)		t_d (h)	d_{sm} (m)		t_d (h)	d_{sm} (m)		t_d (h)	d_{sm} (m)
0.00	0.0000		60.00	0.0000		120.00	0.0000		240.00	0.0000
12.00	0.0000		72.00	0.0000		144.00	0.0000		264.00	0.0000
24.00	0.0000		84.00	0.0000		168.00	0.0000		288.00	0.0000
36.00	0.0000		96.00	0.0000		192.00	0.0000			
48.00	0.0000		108.00	0.0000		216.00	0.0000			

Test M7O3

d_{50}	h	U	U_c	U/U_c	B/D_{pc}	B/h	h/D_{pc}
0.086 mm	0.18 m	0.315 m/s	0.322 m/s	0.80	8.3	5.6	1.5

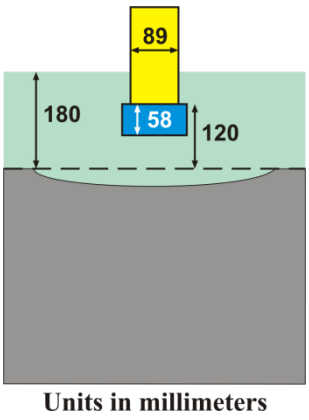

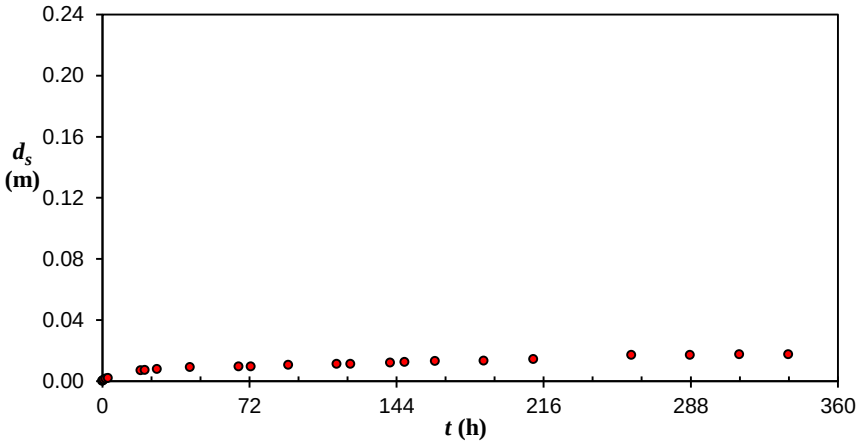

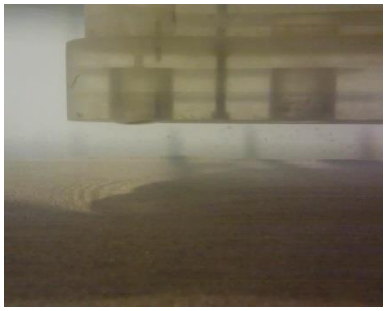

Scour depth measurements in the test M7O3

t_d (h)	d_{sm} (m)		t_d (h)	d_{sm} (m)		t_d (h)	d_{sm} (m)		t_d (h)	d_{sm} (m)
0.00	0.0000		20.75	0.0072		114.75	0.0111		211.00	0.0142
0.25	0.0003		26.75	0.0078		121.50	0.0112		258.92	0.0170
0.75	0.0008		42.92	0.0090		141.00	0.0120		287.75	0.0171
1.75	0.0014		66.75	0.0094		148.00	0.0123		311.75	0.0174
2.75	0.0019		72.75	0.0095		162.93	0.0130		335.75	0.0175
18.75	0.0069		91.00	0.0105		186.75	0.0132			

Test M7P3

d_{50}	h	U	U_c	U/U_c	B/D_{pc}	B/h	h/D_{pc}
0.086 mm	0.18 m	0.315 m/s	0.322 m/s	0.80	8.3	5.6	1.5

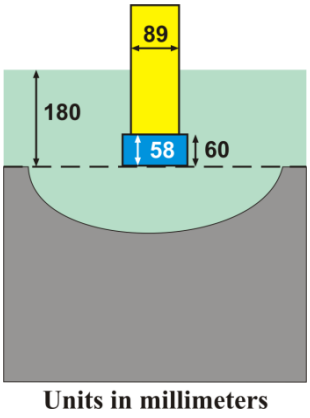

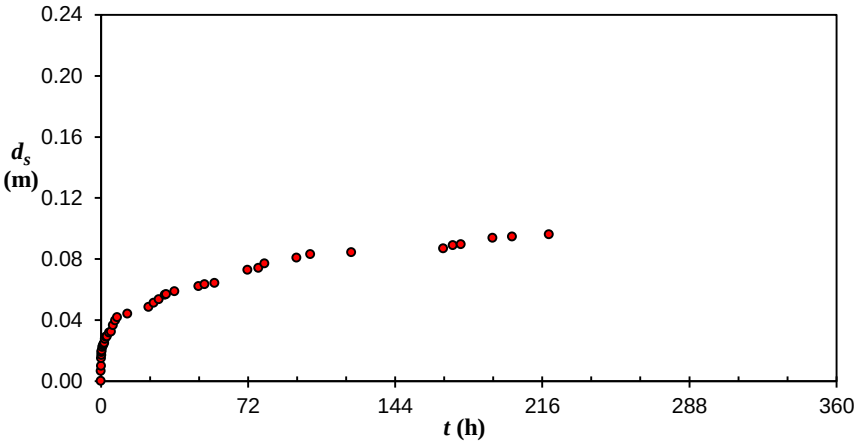

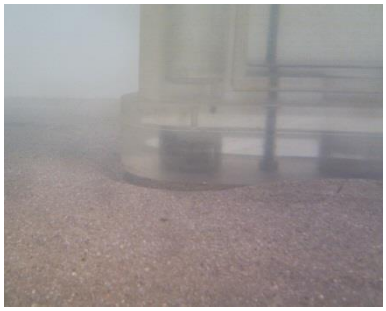

Scour depth measurements in the test M7P3

t_d (h)	d_{sm} (m)	t_d (h)	d_{sm} (m)	t_d (h)	d_{sm} (m)	t_d (h)	d_{sm} (m)
0.00	0.0000	2.00	0.0275	28.30	0.0534	102.55	0.0831
0.05	0.0065	2.50	0.0289	31.30	0.0565	122.55	0.0843
0.08	0.0099	3.00	0.0292	31.97	0.0569	167.55	0.0869
0.17	0.0149	4.00	0.0317	35.97	0.0588	172.30	0.0889
0.25	0.0170	5.00	0.0323	47.80	0.0620	176.22	0.0895
0.33	0.0190	6.00	0.0365	50.80	0.0633	191.80	0.0938
0.50	0.0199	7.00	0.0397	55.63	0.0642	201.22	0.0946
0.75	0.0222	8.00	0.0417	71.80	0.0727	219.30	0.0961
1.00	0.0233	13.00	0.0441	77.13	0.0741		
1.33	0.0241	23.30	0.0484	80.13	0.0770		
1.67	0.0249	25.80	0.0511	95.80	0.0808		

Test M7Q3

d_{50}	h	U	U_c	U/U_c	B/D_{pc}	B/h	h/D_{pc}
0.086 mm	0.18 m	0.315 m/s	0.322 m/s	0.80	8.3	5.6	1.5

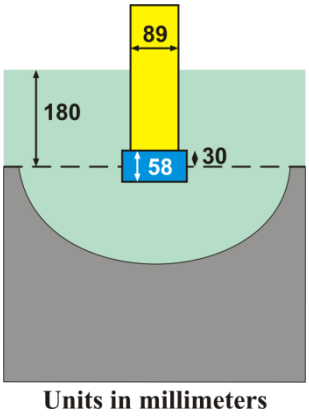

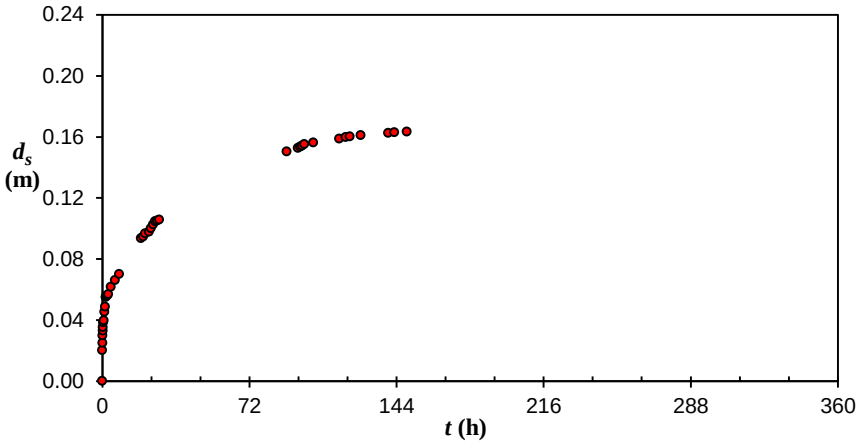

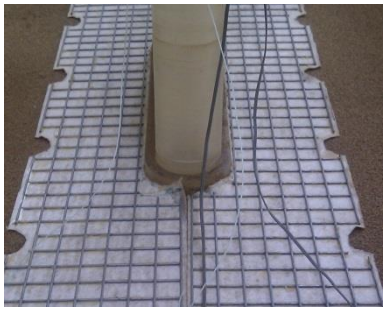

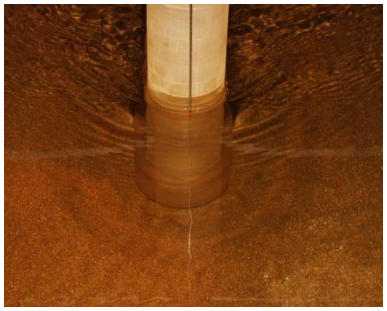

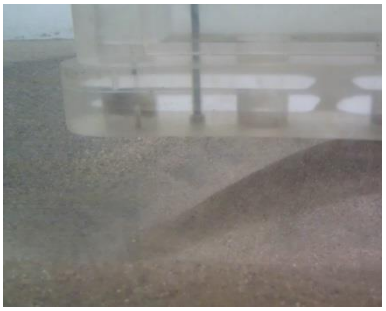

Scour depth measurements in the test M7Q3

t_d (h)	d_{sm} (m)	t_d (h)	d_{sm} (m)	t_d (h)	d_{sm} (m)	t_d (h)	d_{sm} (m)
0.00	0.0000	1.67	0.0550	22.83	0.0978	98.83	0.1553
0.05	0.0202	2.00	0.0556	23.83	0.1001	103.35	0.1563
0.08	0.0250	2.50	0.0560	24.83	0.1025	116.02	0.1588
0.17	0.0299	3.00	0.0568	25.83	0.1046	119.18	0.1599
0.25	0.0330	4.27	0.0616	26.83	0.1050	121.18	0.1603
0.33	0.0352	6.27	0.0661	27.83	0.1058	126.52	0.1610
0.50	0.0385	8.27	0.0701	90.33	0.1503	140.02	0.1626
0.75	0.0396	19.00	0.0935	95.83	0.1527	143.02	0.1629
1.00	0.0453	20.00	0.0945	96.83	0.1536	149.02	0.1633
1.33	0.0486	21.00	0.0966	97.83	0.1542		

Test M7R3

d_{50}	h	U	U_c	U/U_c	B/D_{pc}	B/h	h/D_{pc}
0.086 mm	0.18 m	0.315 m/s	0.322 m/s	0.80	8.3	5.6	1.5

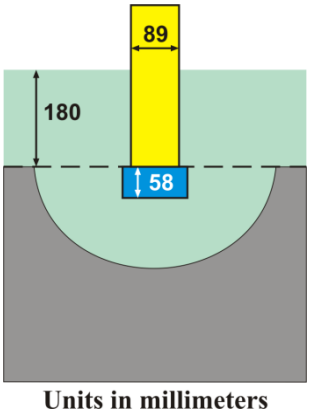

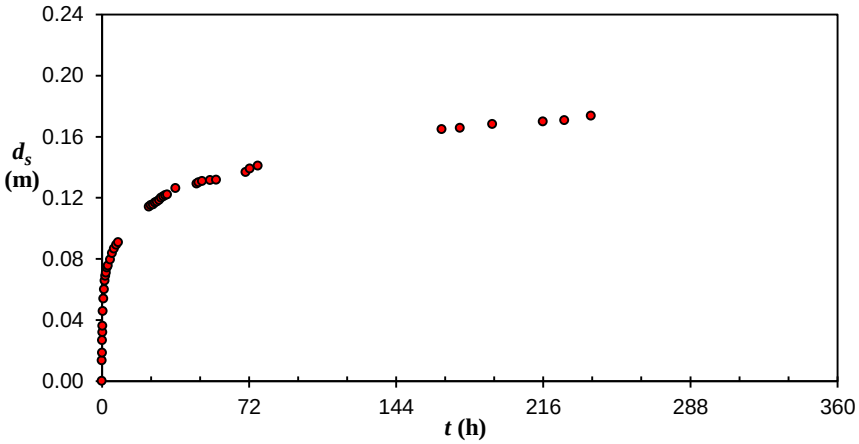

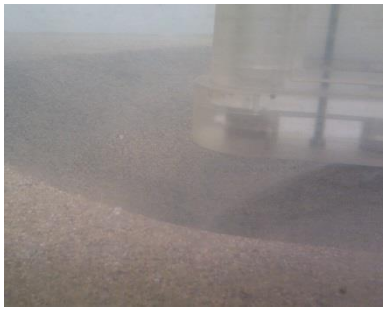

Scour depth measurements in the test M7R3

t_d (h)	d_{sm} (m)	t_d (h)	d_{sm} (m)	t_d (h)	d_{sm} (m)	t_d (h)	d_{sm} (m)
0.00	0.0000	2.00	0.0709	26.00	0.1169	53.00	0.1315
0.05	0.0135	2.50	0.0743	27.00	0.1175	56.00	0.1317
0.08	0.0185	3.00	0.0755	28.00	0.1186	70.33	0.1367
0.17	0.0266	4.00	0.0794	29.00	0.1200	72.33	0.1390
0.25	0.0318	5.00	0.0837	30.00	0.1209	76.33	0.1410
0.33	0.0361	6.00	0.0867	31.00	0.1217	166.33	0.1649
0.50	0.0457	7.00	0.0892	32.00	0.1221	175.33	0.1657
0.75	0.0539	8.00	0.0909	36.00	0.1263	191.08	0.1683
1.00	0.0601	23.00	0.1141	46.33	0.1292	215.83	0.1699
1.33	0.0656	24.00	0.1152	47.33	0.1300	226.33	0.1707
1.67	0.0689	25.00	0.1156	49.00	0.1308	239.33	0.1737

Test M7S3

d_{50}	h	U	U_c	U/U_c	B/D_{pc}	B/h	h/D_{pc}
0.086 mm	0.18 m	0.315 m/s	0.322 m/s	0.80	8.3	5.6	1.5

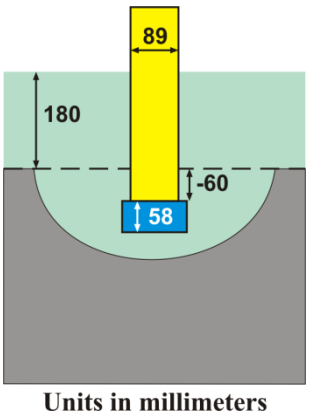

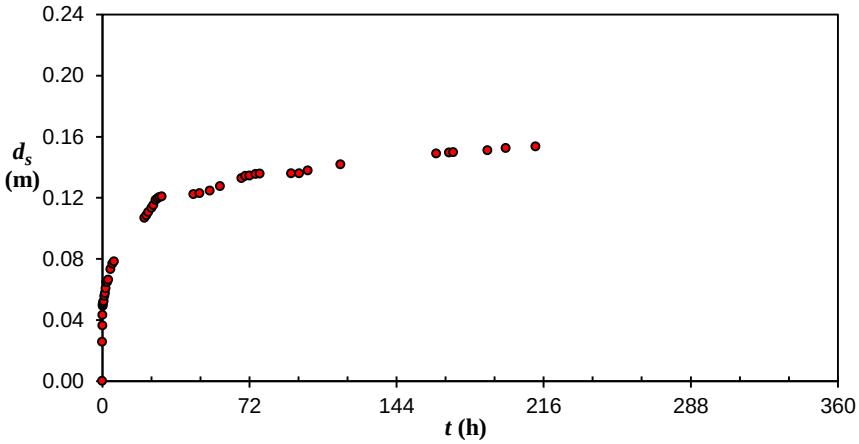

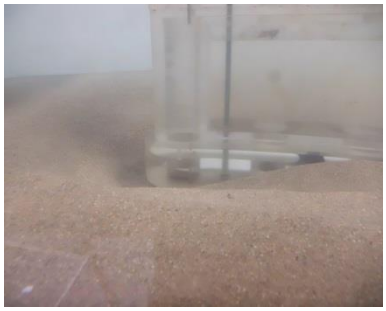

Scour depth measurements in the test M7S3

t_d (h)	d_{sm} (m)	t_d (h)	d_{sm} (m)	t_d (h)	d_{sm} (m)	t_d (h)	d_{sm} (m)
0.00	0.0000	2.50	0.0648	28.10	0.1203	96.47	0.1358
0.05	0.0256	3.00	0.0662	29.10	0.1208	100.68	0.1377
0.08	0.0364	4.00	0.0732	44.60	0.1223	116.68	0.1417
0.17	0.0432	5.00	0.0768	47.60	0.1229	163.43	0.1489
0.25	0.0490	5.83	0.0782	52.60	0.1245	169.77	0.1495
0.33	0.0501	20.60	0.1068	57.60	0.1275	171.77	0.1497
0.50	0.0514	21.60	0.1084	68.10	0.1328	188.60	0.1509
0.75	0.0523	22.60	0.1105	70.10	0.1343	197.60	0.1525
1.00	0.0555	24.10	0.1133	72.10	0.1345	212.10	0.1536
1.33	0.0574	25.10	0.1151	75.10	0.1355		
1.67	0.0606	26.10	0.1184	77.10	0.1357		
2.00	0.0646	27.10	0.1195	92.47	0.1359		